Molecular and Cellular Analysis of Topography-Induced Mechanotransduction

Laura Elizabeth McNamara
BSc. (Hons).

Submitted in fulfilment of the requirements for the
Degree of Doctor of Philosophy (Ph.D.)

Centre for Cell Engineering
Division of Infection and Immunity
Faculty of Biomedical and Life Sciences
University of Glasgow
Glasgow, G12 8QQ
United Kingdom

June 2010

Thesis Abstract

Mechanotransduction is the process by which cells convert mechanical stimuli into an adaptive gene- and protein-level response, via signalling cascades or direct physical effects of the cytoskeleton on the nucleus, and appropriate mechanosignalling is crucial for tissue development and function. Most techniques currently used to study cellular mechanoresponses are relatively damaging to the cells. In contrast, topographically structured substrates, such as microgrooves, have great potential for use as non-invasive mechanostimuli.

In this study, quartz microgrooved substrata (2 μm depth x 25 μm pitch) were used as platforms for the confinement and alignment of cells. A multi-layered approach was adopted to begin to integrate the changes induced by the topographical mechanostimulus at the chromosome, small RNA, transcript, protein and structural levels. Cytoskeletal reorganisation and subnuclear effects were observed using high-resolution confocal 3D reconstructions. Nucleoli appeared aligned along the long axis of the cells and extended in the z-direction on the topography, and the frequency of nucleoskeletal lamin B and A/C tubule-like structures (which probably support the nucleus and act as nucleocytoplasmic transport conduits for nucleic acids and small molecules) was reduced in cells on microgrooves. Alterations in nucleoli and tubules were suggestive of effects on protein synthesis, particularly if rRNA production or transport was affected. A microarray study highlighted a number of logical classes of differentially abundant transcripts between cells on microgrooved substrata and planar controls, and particularly interestingly, suggested that levels of various small untranslated RNAs (such as small nucleolar RNAs) were modulated in cells on the topography. Examination of the band positions of differentially expressed genes, in combination with Fluorescence *In situ* Hybridisation analysis, suggested that mechanical repositioning of Ch 1 may contribute to down-regulation of gene expression on this chromosome in cells on microgrooves. In contrast, the gene up-regulation on Ch 19 was consistent with more localised sub-chromosomal effects, such as looping out of particular loci. Using fluorescence two-dimensional difference gel electrophoresis, several differentially abundant proteins were identified, including nucleophosmin, which is involved in maintenance of nucleolar morphology, and PCNA, which associates with lamin B and is required for DNA replication. Together, the results provide insight into multiple facets of topography-induced mechanotransduction, which should contribute to understanding of mechanotransduction and cell-material interactions.

Contents

Supplementary Material: Complete gene list from the microarray study discussed in Chapter 3, included on CD in the print version of the thesis, and as an additional file in the electronic version of the thesis.

List of Figures

List of Tables

Presentations

Presentations made by the candidate relating to research in this thesis.

McNamara, L.E., Burchmore, R., Riehle, M.O., and Dalby, M.J. How Cella Got Her Groove Back: Topography as a Non-Invasive Mechanostimulus. Poster at the Science, Engineering and Technology (SET) for BRITAIN Event 2010 (House of Commons, London, UK).

McNamara, L.E., Burchmore, R., Riehle, M.O., and Dalby, M.J. Mechanotransduction In Response To A Topographical Mechanostimulus: Chromosome, mRNA, Protein and Whole-Cell Analyses. Oral at the Tissue and Cell Engineering Society (TCES) Conference 2009 (Glasgow, UK).

McNamara, L.E., Riehle, M.O., Burchmore, R., and Dalby, M.J. Mechanotransduction: A Study of Chromosome, mRNA, Protein and Whole-Cell Effects Using Topography as a Non-Invasive Mechanoinducer. Poster at the European Science Foundation-European Molecular Biology Organisation Conference on Biological Surfaces and Interfaces 2009 (Sant Feliu de Guixols, Spain).

McNamara, L.E., Burchmore, R., Riehle, M.O., and Dalby, M.J. Topography- Induced Mechanotransduction: 3D Confocal and Proteomic Study. Oral at the Tissue and Cell Engineering Society Conference 2008 (Nottingham).

McNamara, L.E., Riehle, M.O., Burchmore, R., and Dalby, M.J. Proteomic and Microscopic Analysis of Mechanotransduction in Cell Guidance. Poster at the World Biomaterials Congress 2008 (Amsterdam, The Netherlands).

McNamara, L.E., Riehle, M.O., Burchmore, R., and Dalby, M.J. Mechanotransduction in Three Dimensions (3D): Cyto- and Nucleoskeletal Effects of a Grooved Topography. Poster at the British Society for Cell and Developmental Biology Conference 2008 (Warwick, UK).

McNamara, L.E., Riehle, M.O., Dalby, M.J., and Burchmore, R. Topographically-Induced Cell Morphologies: A Proteomic Approach. Poster at the Tissue Engineering and Regenerative Medicine International Society European Chapter (TERMIS-EU) Conference 2007 (London, UK).

Publications

Publications authored by the candidate relating to the work in this thesis (papers marked with an asterisk * are particularly related to the thesis).

McNamara, L.E., Dalby, M.J., Riehle, M.O., and Burchmore, R. Fluorescence two-dimensional difference gel electrophoresis for biomaterial applications. J. R. Soc. Interface **7** (2010) S107-118. (Review). *

McNamara, L.E., Riehle, M.O., Burchmore, R. and Dalby, M.J. Diamond nanocrystal size affects osteoblastic responses. Nanomedicine **4** (2009) 613-17. (Short Review).

McNamara, L.E., Riehle, M.O., Burchmore, R., and Dalby, M.J. Dynamic cell alignment on switchable topography. Nanomedicine **3** (2008) 411-14. (Short Review).

McNamara, L.E., McMurray, R.J., Biggs, M.J.P., Kantawong, F., Oreffo, R.O.C.O. and Dalby, M.J. Nanotopographical control of stem cell differentiation. Submitted. (Review). *

McNamara, L.E., McMurray, R.J., Dalby, M.J., and Tsimbouri, P. Nanostructured surfaces and cell behaviour. Chapter in Comprehensive Biomaterials. Elsevier. In press. (Book Chapter). *

McNamara, L.E., Kantawong, F.A., Dalby, M.J., Riehle, M.O., Jayawardena, K., and Burchmore, R. Preventing and troubleshooting artifacts in saturation labelled 2D-fluorescence difference gel electrophoresis (DiGE) (Review/Research Article; manuscript in preparation). *

Brydone, A.S., Dalby, M.J., Meek, R.M.D., and McNamara, L.E. Extracellular matrix deposition and remodelling on a grooved topography. (Research Article; manuscript in preparation).

Distinctions

Distinctions received by the candidate relating to the research presented in this thesis.

SET for BRITAIN

Selected to present at the Science, Engineering and Technology for Britain (SET for BRITAIN) event (House of Commons, London, UK) - 2010

Scottish International Education Trust Travel Grant

Awarded a £950 travel grant to present research at the European Science Foundation-European Molecular Biology Organisation (ESF-EMBO) conference on Biological Surfaces and Interfaces (Sant Feliu de Guixols, Spain) - 2009

London Materials Society

Shortlisted for the London Materials Society June Wilson Prize - 2009

Acknowledgments

I would particularly like to thank my family for their unwavering support and encouragement during this Ph.D. You have always been there for me, and I am really grateful. This thesis is dedicated to the memory of my grandpa, Michael McNamara, who was a lovely man and firm believer in the value of education.

I would like to thank my supervisors, Drs. Matt Dalby, Mathis Riehle and Richard Burchmore, for their excellent support, expertise, constructive criticism, and for giving me the freedom to explore new ideas. You made a great tripod! I really value all the advice you have given me over the years, especially during the 'knitting' of this thesis. Thanks for all the cake, pub trips, lunches and lab outings, which were always a highlight.

I thank my principle assessor, Dr. Andy Pitt, for his stimulating questions, sense of humour and friendly encouragement. Thanks are also due to my final year co-assessor, Dr. Julia Douglas, and my PG assessors, Dr. John Coote and Prof. Sylke Muller, for their contributions.

I have been fortunate to be able to draw on the expertise and assistance of many people during the project. I am very grateful to Drs. Fahsai Kantawong and Jay Jayawardena for their fantastic assistance with the challenging world of DiGE, and Drs. Richard Burchmore and Karl Burgess for their help with MS. Thank you to Andy Hart, Carol-Anne Smith, Anne McIntosh and Dr. Graham Hamilton for their wonderful technical support, and Kate for maintaining the washroom stocks. I am grateful to Dr. Abhay Andar for fabricating a microgrooved Si substrate, and Sara MacFarlane for fabricating the quartz substrates that were vital in this thesis. I thank Dr. Norbert Klauke for his generosity with the confocal microscope. I am very grateful to Dr. Jing Wang for the excellent microarray work she performed on this project, and for letting me participate in it. Thanks are also due to Dr. Pawel Herzyk for performing the microarray statistical analysis, and for taking the time to involve me in the process. Thanks to Dr. Stephen Yarwood, Rebecca Bird and David Henderson for their advice on siRNA, and to Lewis Ross and Dr. Thomas Endlein for IT-related help. Thank you to Dr. Jos Broers (University of Maastricht, Netherlands) for provision of GFP-tagged constructs, Dr. Chris Gribbon (University of Bath) for suggesting some useful papers, and Prof. Geoff Richards (AO Institute, Davos, Switzerland) for advice on immunolabelling. I thank Prof. Adam Curtis for his interesting discussions (and for treating us all to ice cream on sunny days). Thank you to everyone in the Centre for Cell Engineering, the Sir Henry Wellcome Functional Genomics Facility, and Electronics and Electrical Engineering who have assisted me with this project, and made working towards a Ph.D. such an enjoyable experience.

I thank the Biotechnology and Biological Sciences Research Council (BBSRC) for providing the funding to support me during my studentship, and the Scottish International Education Trust (SIET) for awarding me a travel grant to attend an international conference.

Finally, thank you to all my friends within and outside the University (some of whom have also been mentioned above) for helping me, sharing a laugh and generally keeping me afloat! Love you all.

Author's Declaration

The work presented in this thesis is the candidate's own, and has not been submitted for a degree in another institution.

Laura Elizabeth McNamara, June 2010

List of Abbreviations and Symbols

-/- - Knockout (double knockout)

4E-BP1 – Eukaryotic translation initiation factor 4E binding protein 1

µCHIP – Micro chromatin immunoprecipitation

µCP – Micro-contact printing

µg - Microgram

µl - Microlitre

2D – Two-dimensional

3D – Three-dimensional

ACF7 – Actin cross-linking factor 7

ADAR1 – Adenosine deaminase acting on RNA

ADCYAP – Adenylate cyclase activating polypeptide 1

AKT – v-akt murine thymoma viral oncogene homolog

ANOVA – Analysis of variance

ANXA 5 – Annexin V/Annexin A5

APBB1 – Amyloid beta (A4) precursor protein binding, family B, member 1

ARHGDIA – Rho GDP dissociation inhibitor alpha

ARHGEF2 – Rho/Rac guanine nucleotide exchange factor 2

ARRB1 – Arrestin, beta 1

ARP 2/3 - Actin-regulating protein 2/3

ATF-1 – Activating transcription factor 1

B23 – Nucleophosmin

BAD – Bcl-xL/Bcl-2-associated death promoter

BAK – Bcl-2-antagonist/killer 1

BAR – Bin amphiphysin Rvs

Bcl-2 – B-cell lymphoma 2

BCL9 – B-cell chronic lymphocytic leukaemia/lymphoma 9

Bcl-XL – B-cell lymphoma-extra large

BHK – Baby hamster kidney

BIM – Bcl-2 interacting mediator of cell death

BLID – BH3-like motif containing, cell death inducer

BMP15 – Bone morphogenic protein 15

BOP1 – Block of proliferation 1

B-Raf – v-raf murine sarcoma viral oncogene homolog B1

BSA – Bovine serum albumin

C3G – Rap guanine nucleotide exchange factor 1

cAMP – 3’5’-cyclic adenosine monophosphate

CAPZA1 – Actin filment capping protein

CAS – Breast cancer anti-oestrogen resistance 1

CCD – Charge-coupled device

CDC25B – Cell division cycle 25 homolog B

Cdc42 – Cell division cycle 42

CDKN1 – Cyclin-dependent kinase inhibitor 1

CDKN1A – Cyclin-dependent kinase inhibitor 1A

CDKN1C – Cyclin-dependent kinase inhibitor 1C

cDNA – Complementary DNA

CELSR1 – Cadherin, EGF LAG seven-pass G-type receptor 1

c-Fos – FBJ murine osteosarcoma viral oncogene homolog

Ch - Chromosome

CHAPS - 3-[(3-Cholamidopropyl)dimethylammonio]-1-propanesulfonate

CHCA - α-cyano-4-hydroxycinnamic acid

CID – Collision induced dissociation

CLK2 – Cell division cycle-like kinase 2

CLSM – Confocal laser scanning microscopy

CK2 – Casein kinase 2

COL18A1 – Collagen, type XVIII

c-Raf – v-raf-1 murine leukaemia viral oncogene homolog

CRIP2 – Cysteine rich protein 2

cRNA – Complementary RNA

CSK – c-src tyrosine kinase

C-terminal – Carboxy-terminal

CYB5R3 – Cytochrome b5 reductase 3

Da - Dalton

DAG - Diacylglycerol

DAPI – 4’, 6’-diamidino-2-phenylindole

DDIT – DNA damage-inducible transcript 3

DHFR – Dihydrofolate reductase

DiGE – Fluorescence two-dimensional difference gel electrophoresis

DiGEmin – Minimal labelled two-dimensional fluorescence difference gel electrophoresis

DiGEsat - Saturation labelled two-dimensional fluorescence difference gel electrophoresis

DLL4 – Delta-like 4

DMEM – Dulbecco's Modified Eagles' Medium

DMF - Dimethylformamide

DMSO – Dimethylsulphoxide

DNA – Deoxyribonucleic acid

DNTTIP1 – Deoxynucleotidyl transferase, terminal, interacting protein 1

DTT – Dithiothreitol

DUSP1 – Dual specificity phosphatase 1

ECM – Extracellular matrix

EDTA – Ethylenediaminetetraacetic acid

EEF1δ - Eukaryotic translation elongation factor 1 delta

eEF1A - Eukaryotic translation elongation factor 1A

EEF1D - Eukaryotic translation elongation factor 1 delta

eIF4E – Eukaryotic translation initiation factor 4E

Elk-1 – ELK1, member of ETS oncogene family

EM – Electron microscopy

ER – Oestrogen receptor

ERK – Extracellular signal-regulated kinase

ERK 1/2 – Extracellular signal-regulated kinase 1/2

ESC – Embryonic stem cell

ESI – Electrospray ionisation

ESI-Q-TOF/TOF - Electospray Ionisation-Quadrupole-Time of Flight

F3 – Coagulation factor 3

FA – Focal adhesion

F-actin – Fibrillar actin

FAK – Focal adhesion kinase

FasL – Fas ligand

FBS – Foetal bovine serum

FGF1 – Fibroblast growth factor 1

Fig. - Figure

FISH – Fluorescence *In situ* Hybridisation

FITC – Fluorescein isothiocyanate

Fn – Fibronectin

FOS – FBJ murine osteosarcoma viral oncogene homolog

FOXA2 – Forkhead box A2

FOXO – Forkhead box O

FRAP – Fluorescence recovery after photobleaching

FSH – Follicle stimulating hormone

G1 – Gap phase 1

G-actin – Globular actin

GAP – Guanosine triphosphate acceptor protein

GDIA - Rho guanosine diphosphate association inhibitor alpha

GDP – Guanosine diphosphate

GEF - Guanine nucleotide exchange factor

GFP – Green fluorescent protein

GRASP55 – Golgi reassembly stacking protein of 55kDa

GRB2 – Growth factor receptor bound protein 2

GSK3 – Glycogen synthase kinase 3

GSTP1 – Glutathione S-transferase pi 1

GTP – Guanosine triphosphate

GTPase – Guanosine triphosphatase

GPCR – G-protein coupled receptor

h – Hour(s)

HA – Hydroxyapatite

HAX1 – Haematopoetic cell-specific lyn substrate 1 associated protein X-1

hCG – Human chorionic gonadotrophin

HEPES – 4-(2-hydroxyethyl)-1-piperazineethanesulfonic acid

HMGA1 – High mobility group AT-hook 1

HMGB1 – High mobility group box 1

HNF1A – Hepatocyte nuclear factor 1A

HSP-27 – Heat shock protein 27kDa

HSPA6 – Heat shock 70 kDa protein 6 (HSP70B')

HSPB8 – Heat shock 22kDa protein 8

hTERT – Human telomerase reverse transcriptase

Hz - Hertz

IAA – Iodoacetamide

ICAT - Isotope-Coded Affinity Tag

IDH – Isocitrate dehydrogenase

IDH3G – Isocitrate dehydrogenase 3 (NAD^+) gamma isoform a precursor

IEF – Isoelectric focussing

IL – Interleukin

IP3 – Inositol 1, 4, 5-triphosphate

IPA – Ingenuity Pathways Analysis

IPG – Immobilised pH gradient

IPTG - Isopropyl-β-D-1-thiogalactopyranoside

IRS p53 – Insulin receptor tyrosine kinase substrate p53

ISG20 – Interferon-stimulated exonuclease gene 20 kDa

ITGA3 – Integrin (alpha 3)

ITGB3 – Integrin (beta 3)

iTRAQ - Isobaric tags for relative and absolute quantification

Jnk – *Jun* N-terminal kinase

kDa – Kilodalton

KLF16 – *Kruppel*-like factor 16

KRT17 – Keratin 17

KSR – Kinase suppressor of Ras 1

LAP2 – Lamin-associated polypeptide 2

LBR – Lamin B receptor

LC – Liquid chromatography

LGALS1 – Galectin-1

LIMK – LIM domain kinase 1

LLG1 – Lethal giant larvae homolog

LPAL2 – Lipoprotein 2

LPS - Lipopolysaccharide

MALDI – Matrix-Assisted Laser Desorption/Ionization

MAR – Matrix attachment region

MAP27 – Mitogen-activated protein 27

MAP2K7 – Mitogen-activated protein kinase kinase 7

MAPKKK – Mitogen-Activated Protein Kinase Kinase Kinase

MAPKK – Mitogen-Activated Protein Kinase Kinase

MAPK – Mitogen-Activated Protein Kinase

MDCK – Madin Darby Canine Kidney

MEK – Mitogen-activated protein kinase/extracellular signal-regulated kinase kinase

MEK 1/2 – Mitogen-activated protein kinase kinase 1/2

MeOH - Methanol

MES – 2-(*N*-morpholino)ethanesulphonic acid

MGAT3 – Mannosyl (beta-1, 4)-glycoprotein beta-1,4-N-acetylglucosaminyltransferase

min - Minutes

miRNA – Micro ribonucleic acid

ml - Millilitre

MLC – Myosin light chain

MLCK – Myosin light chain kinase

MLCP – Myosin light chain phosphatase

MMP – Matrix metalloprotease

Mos – v-mos Moloney murine sarcoma viral oncogene homolog

MP1 – Mitogen-activated protein phosphatase 1

mRNA – Messenger ribonucleic acid

mRNP - Messenger ribonucleosome particle

MRTF – Myocardin-related transcription factor

MS – Mass spectrometry

MS/MS – Tandem mass spectrometry

MSC – Mesenchymal stem cell

MT1H – Metallothionein 1H

MYD88 – Myeloid differentiation primary response gene (88)

NAD^+ - Nicotinamide adenine dinucleotide

NPM1 – Nucleophosmin 1

NRG1 - Neuregulin 1

NF-κB – Nuclear factor kappa B

-NHS – *N*-hydroxy succinimide

NuMA – Nuclear mitotic apparatus

No. – Number

OCT1 – Octamer transcription factor-1

OD – Optical density

P38 MAPK – p38 Mitogen-activated protein kinase

P70 S6K – RPS6-p70-protein kinase

PAC1 – Dual specificity phosphatase 1

PAK – p21 activated protein kinase

PBS – Phosphate buffered saline

PBST – Phosphate buffered saline with TWEEN

PCL – Poly(caprolactone)

PCNA – Proliferating cell nuclear antigen

PDGF – Platelet-derived growth factor

PDK1 – Phosphoinositide-dependent kinase 1

PDMS – Poly(dimethylsiloxane)

PELP1 – Proline, glutamate and leucine rich protein 1

PER1 – Period homolog 1

PFA – Paraformaldehyde

PF4 – Platelet factor 4

PI3K – Phosphoinositol-3-kinase

PIP – Phosphatidyl inositol phosphate

PIP2 – Phosphatidylinositol 4, 5-bisphosphate

PIP3 – Phosphatidylinositol (3, 4, 5)-triphosphate

PIP5K – 1-phosphatidylinositol-4-phosphate 5-kinase

Pka – Protein kinase A

PKC – Protein kinase C

PLC – Phospholipase C

PMF – Peptide mass fingerprint

PMMA – Poly(methylmethacrylate)

POLD1 – Polymerase (DNA directed) delta 1, catalytic subunit, 125 kDa

pre-mRNA – Precursor mRNA

PPARγ – Peroxisome proliferator activated receptor gamma

PRAK – Mitogen-activated protein kinase activated protein kinase 5

pRb – Phosphorylated retinoblastoma protein

PSENEN – Presenilin enhancer protein 2

PTEN – Phosphatase and tensin homolog on chromosome 10

PTGS 2 – Prostaglandin-endoperoxide synthase 2

PTM – Post-translational modification

PYK2 – PTK2B protein kinase 2

qPCR – Quantitative polymerase chain reaction

RAC2 – Ras-related C3 botulinum toxin substrate 2

RIN – RNA integrity number

RNA – Ribonucleic acid

ROCK – Rho kinase

RPLS – Ribosomal protein L5

RPMI – Roswell Park Memorial Institute

rRNA – Ribosomal ribonucleic acid

scaRNA – Small Cajal-body specific ribonucleic acid

SDS – Sodium dodecyl sulphate

SDS-PAGE – Sodium dodecyl sulphate polyacrylamide gel electrophoresis

SEM – Scanning electron microscopy

SHC – Src homology 2 domain containing transforming protein 1

SILAC – Stable Isotopic Labelling by Amino Acids in Cell Culture

siRNA – Short interfering ribonucleic acid

SMC – Smooth muscle cell

snRNA – Small nuclear RNA

snoRNA – Small nucleolar ribonucleic acid

SNRPA1 – Small nuclear ribonucleoprotein polypeptide A'

SOS – Son of sevenless

Src – v-src sarcoma (Schmidt-Ruppin A2) viral oncogene homolog

SRF – Serum response factor

SSC – Saline sodium citrate

ssDNA – Single-stranded deoxyribonucleic acid

ST6GAL1 – ST6 β-galactosamide alpha-2, 6-sialyl transferase I

SUMO - Small ubiquitin-like modifier protein

SUN – Sad1-UNC-84 homology

STX3 – Syntaxin 3

T-75 – 75 cm^3 tissue culture flask

TCA - Tricarboxylic acid

TCEP – Tris(2-carboxyethyl)phosphine

TFA – Trifluoroacetic acid

TICAM – Toll-like receptor adapter molecule 1

TMEM – Transmembrane protein 158

TOF – Time of Flight

TPM1 – Tropomyosin 1

TPM3 – Tropomyosin III

TRAAK - Tandem of P domains in a weakly inward-rectifying potassium channel-related arachidonic acid stimulated potassium channel

TREK - Tandem of P domains in a weakly inward-rectifying potassium channel-related potassium channel

Tris – Tris(hydroxymethyl)aminomethane

TRPV – Transient receptor potential vanilloid

TWEEN – Polysorbate 20

TWIK - Tandem of P domains in a weakly inward-rectifying potassium channel

TX-100 – Triton X-100

UCHL1 – Ubiquitin C-terminal esterase/hydrolase L1

UV - Ultraviolet

v/v – Volume by volume

VEGF – Vascular endothelial growth factor

VEGF – Gene symbol for the gene encoding vascular endothelial growth factor

VEGFB – Vascular endothelial growth factor B

VEGFR2 – Gene symbol for the gene encoding the vascular endothelial growth factor receptor 2

w/v – Weight by volume

WASP – Wiskott-Aldrich syndrome protein

WAVE – WASP family Verprolin-homologous protein

WSB – WD repeat and SOCS-box containing 1

WT – Whole transcript

x (preceded by a number *e.g.* 20x) – Times (indicates a stock solution, and the concentration relative to the diluted working solution)

YY1 – Ying Yang 1

1 General Introduction

Note: Different extracts from this chapter have been published in a review article on proteomics for biomaterials applications (McNamara et al., 2010), and submitted as part of a review article on stem cell responses to nanotopography (McNamara et al., submitted) or as a book chapter on cell responses to nanotopography (McNamara et al., in press).

1.1 Biomaterials and the Cellular Response to Topography

Biomaterials are substrata compatible with living tissue, and include a variety of metals, ceramics, glasses and polymers, such as polycaprolactone (PCL), poly(methylmethacrylate) (PMMA) and poly(dimethylsiloxane) (PDMS). This class of materials have uses in laboratory, clinical and industrial settings, for example in the development and therapeutic application of orthopaedic implants. It is possible to pattern topographic features into many of these substrates, using techniques such as photolithography (described in (Madou, 2002)), electron-beam lithography (Vieu et al., 2000), colloidal lithography (Denis et al., 2002), phase separation of block copolymers (Ranade et al., 2005), and polymer demixing (Affrossman et al., 1996). In addition to possible clinical benefits, structured materials can be used to enhance our understanding of fundamental cell biology and cell-material interactions, as a non-invasive tool to investigate complex cell biological processes.

1.1.1 ***Fabrication: Photolithography, Dry-Etching and Replication***

Photolithography is useful for patterning compatible substrata with micron-scale topographical features. Fig. 1-1 illustrates the example of patterning quartz with microgrooves. Substrates are spin-coated with photoresist, and then exposed to ultraviolet (UV) light through a mask grating, leaving either a sensitised pattern in the resist where light has contacted it (in a negative resist), or initiating cross-linking in these regions (in a positive resist). Resist developer is added to complete the development of the pattern and is followed by a soft-baking step, where the structures are heated to remove acids generated during UV exposure. At this point, the resist can be hard-baked at high temperature and used as a master for replication into certain thermoplastic polymers, such as PMMA and PCL. Alternatively, the substrates can be etched, to generate topographical

features within the biomaterial itself. This can be performed using wet etching (using strong acids), or dry etching (where substrates are subject to reactive ion bombardment). Areas of the substrate which are not protected by a layer of resist are etched more rapidly than those covered by resist, generating the features within the substrate. The feature height can be controlled by the thickness of the layer of resist, and the length of the etching step. The remaining resist is then removed by lift-off, and the substrate is blanket etched to produce a uniform surface chemistry.

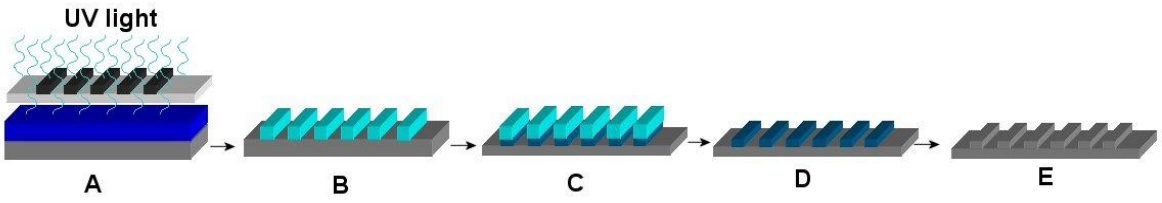

Figure 1-1: Summary of photolithographic and dry-etch development of a microgrooved pattern on a quartz substratum. *A = UV exposure of surface spin-coated with resist, through a chromium mask, to generate a microgrooved pattern in the resist, B = development of pattern, C = reactive ion etching, D = lift off of remaining resist, E = reactive ion etching, to generate a homogeneous surface chemistry. Adapted from illustration provided by M.O. Riehle.*

1.1.2 Fibroblasts as a Model System for Cell-Topography Interactions

Fibroblasts are one of the cell types responsible for laying down the extracellular matrix (ECM) *in vivo*, and can be derived from many tissue types. Immortalised fibroblasts have been widely used in biomaterials research. Such cells are particularly useful for cytotoxicity testing, technique development and proof of principle studies, due to their ease of culture, tractability, clonal origin and relatively rapid growth rate. These are considerable advantages over primary cells, which are typically slow growing, genetically variable, more difficult to culture and can only be passaged a limited number of times. The hTERT BJ-1 cell line was immortalised from BJ primary human foreskin fibroblasts by stable expression of an exogenous copy of the hTERT (human telomerase reverse transcriptase) gene, which prevents telomere shortening and the onset of cellular senescence. This cell line has been utilised in a number of investigations of cell response to topography (Dalby et al., 2004a; Dalby et al., 2007b; Dalby et al., 2003a; Dalby et al., 2007c; Dalby et al., 2004b; Dalby et al., 2007e; Dalby et al., 2004d; Dalby et al., 2004e; Dalby et al., 2004f; Dalby et al., 2004g; Dalby et al., 2005b; Dalby et al., 2003b), and its continued use enhances the comparability between studies. The use of human foreskin fibroblasts has the potential disadvantage that this cell type is unlikely to be particularly

mechanosensitive, compared with more specialised mechanosensory tissues, such as hair cells of the ear, or tissues constantly subjected to tensile strain, such as skeletal or cardiac muscle, or compressive force, such as cartilage, but present an appropriate 'generic' model cell type, particularly for epithelial tissues such as skin.

1.2 Cell Response to the Environmental Niche and Grooved Topography

Cells are responsive to chemical and topographic micro- and nanoscale cues *in vivo*, including protein, chemical and cell-cell signals, and the topology, homogeneity and mechanical properties of their local niche. Biomaterial surfaces with definable surface physicochemical characteristics are valuable tools for the study of processes such as mechanotransduction (downstream conversion of mechanical stimuli into gene- and protein-level effects), cell fate determination, tissue development, and cell-material interactions. Cells interact directly with the protein layer on these substrata, and the conformational state (Smith et al., 2007), density and arrangement of these adhesive proteins (Arnold et al., 2004; Chen et al., 1997; Lehnert et al., 2004), the stiffness of the underlying substrate (Engler et al., 2006a, Mammoto et al., 2009), and the topography underlying the presented adhesive stimulus are important for the precise cellular effects.

The size, shape and organisation of topographical features each affect the cellular responses. Topographical substrates can physically direct cells, for example, by alignment of the cell body (contact guidance) along micro- (Britland et al., 1996; Clark et al., 1987, 1990; Kurpinski et al., 2006; Lam et al., 2008; Oakley and Brunette, 1993; Park et al., 2006; Uttayarat et al., 2005; Walboomers et al., 1998; Wojciak-Stothard et al., 1995) and nanogrooves (Biggs et al., 2008; Gerecht et al., 2007; Kim et al., 2009; Loesberg et al., 2007; Uttayarat et al., 2005), cell trapping in micron-scale pits (Berry et al., 2004), nanopatterning by nanoscale substrates (Wood et al., 2008), distortion of the cell and nuclear membrane over micropillars (Davidson et al., 2009) and direction of filopodia (Dalby et al., 2004c; Dalby et al., 2004e).

Topographical substrates are valuable for the non-destructive modulation of cell morphology. Microtopographies, such as microgrooved substrata, are particularly useful in this respect, since the large features are capable of inducing considerable cellular reorganisation. Study of BHK (Baby Hamster Kidney) and MDCK (Madin-Darby Canine

Kidney) cells showed that increasing groove depth from 0.3 μm to 2 μm, and decreasing the groove pitch at intervals from 24 μm to 6 μm resulted in a corresponding increase in cell alignment to the pattern (Clark et al., 1990). In addition, the authors noted contact guidance of neurones on 2 μm deep grooves. Cells can also respond to much smaller grooved features, and from a study with multiple iterations in nanogroove dimensions it was calculated that fibroblasts were capable of aligning to features as shallow as 35 nm, if the pitch size was permissive (Loesberg et al., 2007). Although substrates can be patterned with adhesive proteins (*e.g.* Britland et al., 1996) or chemistry (Hironori and Toshizumi, 2009) to direct cell behaviour, deposited by processes such as micro-contact (von Philipsborn et al., 2006) or inkjet printing (Hironori and Toshizumi, 2009), topography has the advantage that it is less easily denuded from the surface.

Different dimensions of microgrooves and orthogonally positioned pro-adhesive protein stripes were used to investigate dominance in these aligning cues. BHK cells generally aligned to the protein cues, rather than the microgrooves, but the effect was less marked as the depth of topography was increased (to 5 μm), and the spacing decreased (to 6 μm) (Britland et al., 1996). This highlighted that the nature of the topographical stimulus is important in determining its ability to direct cells. Interestingly, Charest et al. later showed that osteoblasts aligned to 4 μm deep microgrooves with a 16 μm pitch (8 μm groove width), in preference to perpendicular protein cues of 10 μm width, spaced at intervals of 10, 20, 50 and 100 μm apart (Charest et al., 2006). The authors attributed the inter-study discrepancy to their use of broken chemical patterning, rather than the continuous adhesive lines in the Britland et al. study, and concluded that persistent migration may be important for alignment to protein cues. This probably also applies to microgrooved stimuli, although such features provide additional step cues, which can be perceived by cells if the grooves are sufficiently far apart, and increasing physical confinement with depth. Uttayarat et al. showed that the fibronectin density on fibronectin-coated PDMS was similar between planar and grooved surfaces, and that protein deposition on groove walls, ridges, or within the grooves was similar for surfaces of different depths (200 nm, 500 nm, 1 μm) (Uttayarat et al., 2005). In contrast, alignment was increased with depth on these surfaces, and the authors concluded that physical guidance was the predominant cue. This suggests that the topology of grooved surfaces is the principle mechanostimulus, rather than a perturbation in the arrangement of adhesive proteins due to the topographical features, although the results did not exclude the involvement of more subtle effects, such as protein conformation changes.

Interactions with grooved substrata can occur very rapidly following seeding, with alignment of fibroblasts to nanogrooves noted after 4h (Loesberg et al., 2007), to microgrooves after 1-4h (Walboomers et al., 1999), and endothelia to nanogrooves after 1-4h (Uttayarat et al., 2005). Interestingly, groove depth and width contributed to the speed of alignment in these studies, with the shallowest (Loesberg et al., 2007) or widest (Walboomers et al., 1999) substrata requiring the longest periods to induce contact guidance. It is probable that the cytoskeleton experiences less dramatic mechanical forces and architectural restrictions on the shallow and large pitch substrata. Clark et al. noted that neutrophils showed a diminished response to microgrooved cues relative to the other cell types studied (BHK and MDCK cells), and concluded this must be due to greater cytoskeletal deformability in neutrophils (Clark et al., 1987). Alternatively, this may have resulted from differences in the physiological status of the cells, since Wójciak-Stothard et al. (1995) showed that lipopolysaccharide-activated macrophages aligned better to microgrooves than unstimulated control cells (Wojciak-Stothard et al., 1995). This suggests that cells are able to modulate the threshold for mechanoinduction in a context-dependent manner. Lam et al. generated a 'switchable' topographic substrate that could be compressed to generate a microgroove-like pattern, and then relaxed back to a planar surface (Lam et al., 2008). Myoblasts were capable of aligning to the topography, and reverting back to a random orientation when the substrate was relaxed, for multiple cycles of compression. This illustrated that cells could reversibly adapt to topographical stimuli.

Using nanogrooves with consistent depth of 330 nm but variable groove-ridge pitch distances (10, 25 or 100 μm), Biggs et al. demonstrated that the pitch of the grooves was an important factor for cell adhesion and cytoskeletal alignment to the pattern in osteoblasts (Biggs et al., 2008). The study found that 10 μm spacing could induce contact guidance of the cells, and align adhesions and microtubules along the nanogrooves. On 25 μm pitch grooves, however, the adhesions were primarily localised to regions where the cells were bridging between adjacent grooves and ridges. On 100 μm-spaced grooves (step cues), the adhesions appeared similar in size, number and orientation to the planar control, and the cells had analogous cytoskeletal architecture. Kim et al. examined fibroblast responses on a gradient of grooves with different widths between 1 and 9.1 μm, each of 400 nm depth, with 1 μm wide ridges (Kim et al., 2009). Intermediate spacing (around 6.3 μm) permitted the greatest speed of fibroblast movement, and the authors suggested that this could have relevance to cell-ECM interactions during wound healing. It was concluded that this substrate promoted greater alignment of cell adhesions (the sites of cellular anchorage to

the substrate), since a greater number were in contact with the ridge edges, and adhesion growth would be more favourable along the direction of the grooves. Clark et al. had previously proposed that groove edges could prevent or guide the formation of cell adhesions and actin stress fibres (Clark et al., 1987). Microgrooved substrata have been shown to induce alignment of stress fibres (Walboomers et al., 1998) and microtubules (Oakley and Brunette, 1993). Such rearrangements of adhesions and cytoskeletal elements would be expected to have considerable downstream mechanotransductive effects. In addition, there is likely to be an association between elongation of the cell body noted on microgrooved substrata and the extension resulting from cell stretch. It seems probable, however, that mechanical stretching might more readily activate additional mechanotransductive pathways, such as stretch-sensitive ion channels (will be discussed in more detail in Section 1.3.2, and reviewed in (Martinac, 2004) and (Yin and Kuebler, 2010)), due to the exertion of large scale, often repetitive, extracellular forces. This seems particularly likely since certain ion channels appear to be antagonised by the cytoskeleton, and thus distension of the cytoskeletal elements might promote channel-mediated signalling (Maingret et al., 1999). The physiological extent of cell stretch is tissue-specific, with some tissues experiencing more extensive and repeated mechanical stresses as a result of their biological functions, such as cardiac and skeletal muscle (Brunello et al., 2007), which are contractile. Fibroblasts are likely to experience lower levels of physiological strain than muscle, but might conceivably experience greater tensile forces than normal during wound closure. Emerging evidence suggests that contractile forces are also important during early development, and mechanical stimuli have been shown to contribute to a number of key developmental processes including cell division and apposite cell localisation in the embryo (discussed in (Wozniak and Chen, 2009)).

To some extent, it is possible to summarise the apparent ‘laws’ of topography based on the literature to date. Nonspecific nano-scale roughening typically increases cell adhesion, on both polymeric (Shadpour and Allbritton, 2010) and metal surfaces (Deligianni et al., 2001). Chemical vapour deposition of diamond nanocrystals on titanium substrata indicated that the pro-adhesive and osteogenic effect of this were more effective in the range of 30-100 nm than at larger feature sizes approaching 1 μm (Yang et al., 2009). To date, 10 nm high nano-islands were the smallest topographical features shown to affect cell responses, and these structures induced filopodial guidance (Dalby et al., 2004e). The effects of topography can be masked by chemical effects, for example, if the surface chemistry of the substrate is poorly adhesive (*e.g.* hydrophobic, such as PDMS (Bodas and Khan-Malek, 2006), or passivated with poly(ethylene glycol) (Lussi et al.,

2006)), and then the cells will primarily respond to this cue. Subsequent functionalisation of the surface to render it more cell adhesive, however, should 'reveal' the topographical cues as the cells are able to adhere and spread efficiently (for example, using plasma treatment of PDMS (Bodas and Khan-Malek, 2006) or poly(caprolactone) (Formosa et al., 2010), or UV treatment of titanium (Ueno et al., 2010), to generate oxidised hydrophilic surface layers). In the nano range, there appears to be a continuum in the promotion of cell spreading and osteogenesis, with smaller features (such as nanocolumns of approximately 15 nm height) tending to stimulate these processes, while larger features (such as nanocolumns of approximately 100 nm height) tend to reduce spreading and osteogenesis, with intermediate sizes of features (such as 55 nm high nanocolumns) showing some character of both the smaller and larger substrata (McNamara et al., In preparation.; Sjostrom et al., 2009). Controlled disorder in the arrangement of nanopits, but not a totally random feature distribution, could also promote osteogenesis (Dalby et al., 2007d). As discussed by Dalby et al (2007), this is reminiscent of the organisation of nanocues in the bony matrix *in vivo*, and suggests that topographical biomimicry is likely to be beneficial for clinical applications. In the micron-scale range of feature sizes, the effects on the cell body can generally be increased to a plateau level (maximal effect) by increasing the depth of features, for example in enhancing cell trapping in deep micropits and cell elongation within deep microgrooves (in the range of 5-10 μm), as cells are 'forced' to conform to the features due to their inability to migrate out from deep structures that confine the entire cell body. Similarly, effective lateral confinement (with feature sizes closely matching the width of the elongated cell morphology for the particular cell type) would also enhance contact guidance.

The use of a microgrooved topography as a non-invasive mechanostimulus has a number of advantages. Firstly, it stimulates cell elongation to produce internal cytoskeletal tension that is likely to be physiologically relevant, as there is no requirement for the application of external force (such as uniaxial cell stretch applied with a cell stretching device). In addition, the same mechanostimulus can be reproducibly applied throughout all experiments and then compared with existing uses of the topography in the literature. The use of microgrooves is particularly interesting in the context of fibroblasts, which naturally align to each other at confluence (Elsdale, 1968), and thus the substrate might also mimic some of the mechanical effects of confluence in this cell type.

1.3 Mechanotransduction

Mechanotransduction is the process by which external mechanical stimuli are transmitted into the nucleus (discussed in (Wang et al., 2009)), resulting in adaptive gene- (Dahl et al., 2004; Dalby et al., 2007c; Dalby et al., 2005a; Dalby et al., 2002a; Kurpinski et al., 2006) and protein-level (Kantawong et al., 2008; Kantawong et al., 2009b) changes. Such mechanostimuli include cell stretch (Kurpinski et al., 2006; Ziegler et al., 2010), compression (Garcia and Knight, 2010), and interaction with surfaces such as defined topographies (Dalby et al., 2007c; Dalby et al., 2004g; Sjostrom et al., 2009), since alterations in surface topology or chemistry will alter cell spreading and morphology (Chen et al., 1997; Deligianni et al., 2001; Malmstrom et al., 2010; Yang et al., 2009), and thus affect the intracellular tension by modulating the cytoskeletal architecture. Signalling cascades can be induced at cell adhesions (Geiger et al., 2009), leading to indirect downstream effects on gene expression. Direct mechanotransduction, in contrast, involves physical modulation of the cytoskeleton and alterations in force experienced by the nucleus (Dahl et al., 2004; Maniotis et al., 1997). I hypothesise that it has the potential to modify gene transcription by imposing mechanical forces on nuclear components.

1.3.1 Cell Migration

Cell motility is mediated by a retrograde flow of actin, which moves rapidly from the leading lamella into the perpindicular cross-flow of a slower moving central region of perinuclear actin (discussed in (Geiger et al., 2009), in conjunction with the cyclical turnover of focal adhesions, the sites of cellular attachment to the substrate. It has been suggested that the flow of actin across focal contacts, which begin to establish the initial attachment to the ECM, might stimulate their growth, by mechanically "massaging" these sites (Geiger et al., 2009). The central components of focal contacts are integrins, which are heterodimeric proteins capable of bidirectional signalling (Wegener and Campbell, 2008) between the ECM, which can be comprised of proteins such as vitronectin, laminin and collagen (Thibault et al., 2007; Yarwood and Woodgett, 2001), and the cell interior. Integrins bind to their specific cognate amino acid sequences in the ECM, such as RGD (found in fibronectin, which acts as a recognition sequence for the $\alpha_5\beta_1$ integrin (Koivunen et al., 1993)) and IKVAV (found in laminin (Nomizu et al., 1995)). Different types of integrin heterodimer located on the same cell can influence the outcome of the other type of integrin binding to its recognition sequence. Ligation of the fibronectin-responsive $\alpha_v\beta_3$

integrin of endothelia, for example, is responsive to the status of the $\alpha_5\beta_1$ integrin, which is mediated by protein kinase A (Kim et al., 2000). Focal contacts are relatively weak initial interactions between the integrins and ECM, which form at the termination of F-actin stress fibres, and also incorporate adapter proteins such as paxillin, α-actinin and talin (DePasquale and Izzard, 1991). Such smaller, more transient focal contacts are located at the leading edge of the lamellipodium. As cells migrate, the contacts can mature into focal adhesions (approximately 2-5 μm in length), and super-mature adhesions (>5 μm long) (Bershadsky et al., 2006; Biggs et al., 2007; Goffin et al., 2006), with the accumulation and activation of signalling proteins such as zyxin, ROCK (Rho kinase), FAK (focal adhesion kinase), and tensin (discussed in (Geiger et al., 2009)). The lamellipodial extension is facilitated by Scar/WAVE (Wiskott-Aldrich syndrome protein-family verprolin homologous protein), which signals to the actin-related protein 2/3 (Arp 2/3) complex, inducing the formation of new actin filaments to drive the leading edge outwards (Hahne et al., 2001).

.

By correlating the traction patterns generated by migrating fibroblasts to the localisation of green fluorescent protein (GFP)-tagged zyxin, Beningo et al (2001) demonstrated that focal contacts at the leading edge generated a higher proportion of the locomotory force than the larger, more zyxin-enriched adhesions at other positions in the cell, or small adhesions at the trailing edge (Beningo et al., 2001). The authors concluded that downstream signalling changes were responsible for this disparity, suggesting that the initial interaction between the integrins and the ECM was critical in the generation of force to facilitate the cellular advancement. Towards the rear of the cell, the adhesions disagreggate, but some small adhesions are also formed at the trailing edge to enable the cells to remain adherent to the substrate and guide the direction of motility (Rid et al., 2005). The persistence of the directionality of cell migration has been shown to be moderated by the small G-protein Rho (discussed in (Petrie et al., 2009)).

1.3.2 Focal Adhesions and Indirect Mechanotransduction

Signalling cascades are initiated by exertion of mechanical forces at focal adhesions, leading to sequential post-translational modification events that transfer the message into the nucleus, and stimulate transcriptional effects. Focal adhesions are critical inducers of downstream signalling in response to topography. Physical pulling on adhesions can promote their growth in response to tyrosine phosphorylation of the GTPase

(guanosine triphosphatase) Rho (Riveline et al., 2001), which illustrates the mechanosensitivity of these sites. Integrins can become cross-linked in response to mechanical force (Friedland et al., 2009), and integrin signalling can stimulate cell survival, growth and differentiation by activating cascades such as the nuclear factor (NF)-κB and MAPK (Mitogen-Activated Protein Kinase) pathways (Reyes-Reyes et al., 2001). Integrins have also been implicated in nanoimprinting, where the cytoskeleton conforms to the underlying nanofeatures (Curtis et al., 2006; Wood et al., 2008). Variation in size of adhesive squares, and arrays of functionalised beads, revealed that a minimum spreading area was necessary for successful attachment of endothelia (Chen et al., 1997). Inter-ligand spacing is also critical for cell attachment (Arnold et al., 2004; Lehnert et al., 2004). Interestingly, when Chen et al. partitioned the same adhesive area into smaller attachment sites of 3 or 5 μm diameter, positioned at different intervals from each other, cell adhesion, survival and DNA replication were at the highest levels when the adhesive regions enabled the greatest cell spreading (Chen et al., 1997). The authors concluded that cellular shape was important for these effects, since the area of ECM attachment was kept constant (Chen et al., 1997).

The majority of adhesions are rich in vinculin, and possess kinases such as FAK (Li et al., 2002). The protein composition of adhesions has been shown to change in response to mechanical stretch, which was demonstrated using GFP-tagged protein localization studies and binding assays with extracted cytoskeletons (Sawada and Sheetz, 2002b). Tension can also induce conformational changes in adhesion proteins. It has been shown, for example, that tensile force could modify the shape of talin, allowing it to bind additional vinculin (del Rio et al., 2009), and affect the functionality of the adapter protein p130Cas in the promotion of integrin signalling (Sawada et al., 2006). Tensile strain has been shown to promote relocation of a transcriptional co-activator (myocardin-related transcription factor A) from the cytoplasm into the nucleus, via a Rho-dependent pathway (Zhao et al., 2007). Interestingly, a GTPase (guanosine triphosphatase) activating protein (GAP) for Rho (p190RhoGAP) was also recently shown to have a role in a mechanosensitive and vascular endothelial growth factor (VEGF)-responsive switch for transcription of *VEGFR2*, encoding the VEGF receptor, a key mediator of angiogenesis. The stiffness of the substrate and presence of VEGF both influenced transcription from this gene (Mammoto et al., 2009).

Cells also possess mechanosensitive ion channels that exhibit reversible gating to induce cellular ion fluxes in response to mechanical stresses, and it is likely that these

channels will contribute to the cellular response to topography. These channels include stretch-sensitive cation channels of the TRP (transient receptor potential) family (Nagata et al., 2005), including the TRP vanilloid receptor, and mechanosensitive potassium channels, such as TREK (tandem of P domains in a weakly inward-rectifying potassium channel (TWIK)-related potassium channel) and TRAAK (TWIK-related arachidonic acid stimulated potassium channel) (Maingret et al., 1999). TREK channels can be opened by a variety of stimuli, including heat, lipid-based signals, and mechanical stimuli, such as cell stretch (discussed in (Martinac, 2004). Interestingly, the cytoskeleton appears to have an antagonistic effect on the activation of TRAAK channels, since the depolymerisation of microtubules or actin can stimulate TRAAK (Maingret et al., 1999). As proposed by Martinac (2004), this suggests that opposing tension from the cytoskeleton could reduce the development of mechanical strain around the channel (Martinac, 2004). In addition, this might indicate that TRAAK ion channels have a greater contribution to mechanosignalling under conditions of reduced cytoskeletal tension. In the context of topography, this could occur when cells are cultured on relatively low adhesion nanotopographies, such as hexagonal arrays of nanopits (Dalby et al., 2007e). This might be more applicable to specialised cell types, however, since TRAAK channels are predominantly expressed in the central nervous system (Maingret et al., 1999). TRP channels, in contrast, are expressed in multiple tissue types (Kunert-Keil et al., 2006). In *C. elegans*, there is some evidence to suggest that the cytoskeleton interacts with a type of TRP channel, which might directly transfer force to the channel (Du et al., 1996), or alter the mechanical properties of the surrounding membrane (discussed in (Martinac, 2004)).

Perturbation of the resting membrane potential by ion fluxes induces the release of stored Ca^{2+} ions from the endoplasmic reticulum, and such spikes of Ca^{2+} induce biochemical signalling mediated by proteins such as the calcium binding protein calmodulin (Liedert et al., 2006). Most interestingly, Itano et al (2003) demonstrated that the perinuclear calcium release that occurred following activation of stretch sensitive channels at the cell periphery during cell spreading, also enabled calcium ions to enter the nucleus (Itano et al., 2003). The authors suggested that this might be a means of modulating gene expression. A model was proposed to explain the induction of signalling events following interaction with nanopits and nanopillars, in which BAR- (Bin, amphiphysin, Rvs) domain proteins that are sensitive to membrane conformation detect the distension of the membrane into nanopits, while its extension over nanopillars may be sensed by the force-induced opening of ion channels (Vogel and Sheetz, 2006).

It seems likely that a combination of mechanosensory mechanisms will be involved in the cellular response to topography. Kurpinski et al. used a microgrooved PDMS substrate (3 μm depth x 20 μm pitch) to apply uniaxial stretch to mesenchymal stem cells (MSCs), with 1 Hz strain applied for two days in parallel to the direction of cell alignment (Kurpinski et al., 2006). This led to the up-regulation of the contractile marker calponin-1 at the mRNA and protein levels. Interestingly, when strain was applied in a perpendicular direction, the cells remained contact guided, suggesting that topography was the dominant aligning stimulus, and most gene changes were unaffected by the directionality of the strain. The authors proposed that genes that had comparable expression levels, irrespective of the direction of applied strain, could be regulated by a subset of mechanosensory mechanisms that may be less sensitive to the orientation of applied force, potentially involving membrane dynamics, alterations in the volume of the cell or the extent of cellular spreading. Conversely, Kurpinski et al. suggested that genes appearing to show a degree of sensitivity to the direction of strain could be regulated by alternative mechanisms, such as cell adhesion and cytoskeletal force transmission, presumably by modulating the nuclear architecture to affect gene expression.

1.3.3 Direct Mechanotransduction – Signal Transmission into The Nucleus

1.3.3.1 The Lamina and the Nuclear Envelope

Direct mechanotransduction requires transmission of force into the nucleus in order to exert a physical change. A number of models have attempted to describe the mechanical properties of the cytoskeleton. In the viscoelastic solid model, for example, the cytoskeletal components contribute equally to the propagation of force (Karcher et al., 2003). Such ‘continuous’ models have been criticised for their failure to account for the loss of mechanical force with distance travelled (Wang et al., 2009). In tensegrity (‘tensional integrity’) theory, in contrast, the attainment of cytoskeletal rigidity with flexibility is attributed to the antagonistic relationship between tensile actin filaments and compressive microtubules, and the interaction with nucleoskeletal intermediate filaments (lamins). In this theory, these elements engender a ‘pre-stress’ upon the nucleus that dictates and alters nuclear morphology in response to mechanical stimuli (Ingber, 2003a, b; Mazumder and Shivashankar, 2010; Wang et al., 2001). Another interesting proposal is the isostatic model, which attempts to unite elements of tensegrity theory and its description of the discrete contributions from different cytoskeletal elements, with the

continuous models that view the cell as a more homogeneous mechanical unit (Blumenfeld, 2006).

The cytoskeleton is physically linked to the nucleoskeleton via bridging proteins including SUN (Sad1p, Unc-84) and the nesprins (Haque et al., 2006), which are components of the LINC (linker of nucleus and cytoskeleton) complex. On the nucleoplasmic side, DNA is physically associated with the lamina, at sites called matrix attachment regions (Fig. 1-2). Tension transmitted from the cytoskeleton can exert strain upon the nucleoskeleton. The physical properties of the lamina provide the nucleus with sufficient elasticity to respond by expansion, but the lamina also provides protection from compressive forces by enforcing a maximal threshold for compaction of the nucleus under physiological conditions (Dahl et al., 2004).

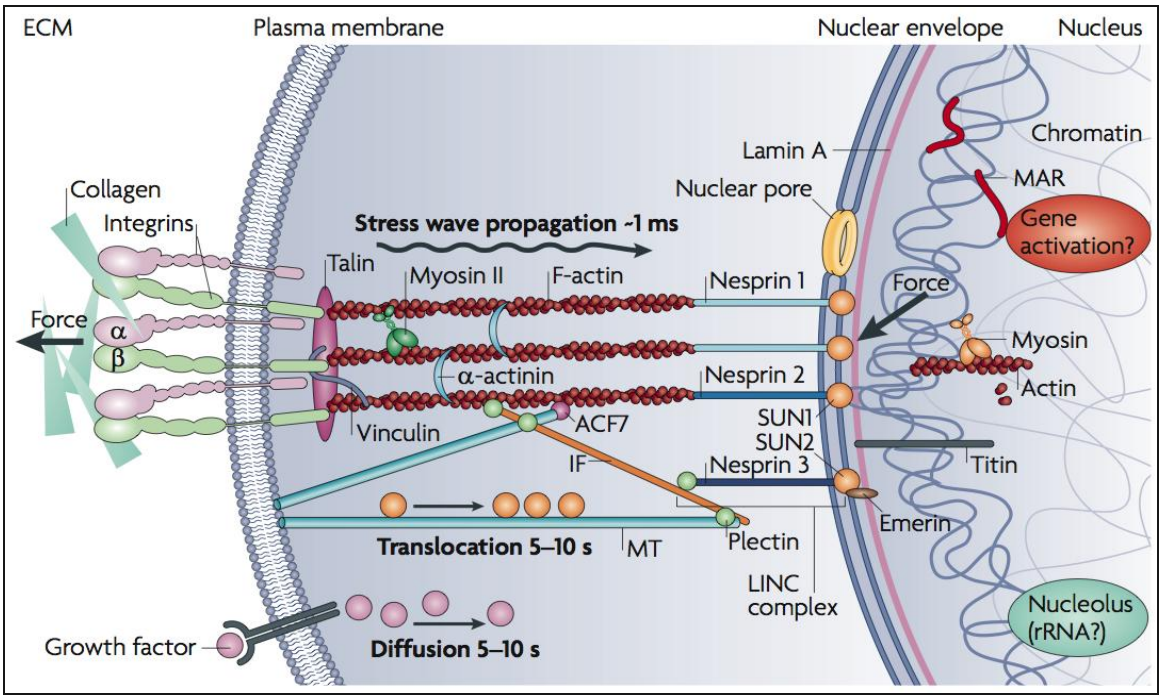

Figure 1-2: Transfer of mechanical stimuli into the nucleus. *Mechanical forces from the ECM (such as those induced by the constraints of topographical substrata) are sensed at focal adhesions by integrins, which are linked to the cytoskeleton via proteins such as talin, and transduced to the nucleus via signalling cascades and direct physical tugging of the cytoskeleton on the nucleus. F-actin and vimentin (IF) are linked to the nuclear lamina by SUN domain proteins and the nesprins. Microtubules (MT) are linked to F-actin by ACF7 (actin cross-linking factor 7), and to IFs via plectin. Within the nucleus, signalling events and mechanical shape changes could alter transcription, for example by changes in gene accessibility via local melting at matrix attachment regions (MARs). Nuclear actin, myosin and titin may also contribute to modulation within the nucleus. Note the rapidity of direct mechanotransduction via stress fibres (~1 ms), compared to the diffusion or translocation of signalling components in response to a growth factor (5-10 s). Reprinted by permission from MacMillan Publishers Ltd: [NAT REV MOL CELL BIOL] (Wang et al, 2009), copyright (2009).*

The lamins are an integral part of the nucleo-cytoskeletal link, and there are multiple forms of these type V intermediate filaments within the nucleoskeleton of most

mammalian cells. The lamins possess nuclear localisation sequences, and the precursor to lamin A can also be isoprenylated, a lipid modification which may assist in targeting to the nucleoskeleton (Hennekes and Nigg, 1994; Lin and Worman, 1993). Lamin A and lamin C are splice variants (Lin and Worman, 1993), whereas lamin B1 and B2 are expressed from separate genes. Nuclei from lamin B1 -/- (knockout) cells exhibited exaggerated rotation compared to control nuclei, as the bridge between the nucleus and cytoskeleton had been partially disrupted (Ji et al., 2007). This link was corroborated by a study showing increased nuclear rotation in vimentin null fibroblasts, which was mediated by microtubules and the motor protein dynein, and could be exaggerated by disruption of actin with Latrunculin B (Gerashchenko et al., 2009). The authors concluded that actin and vimentin were involved in maintaining nuclear positioning. Lamin A/C has a role in physically stabilising the nucleus (Lammerding et al., 2006), and interventional disruption of lamin A/C leads to altered size and distribution of chromosomal territories (Ondrej et al., 2008). Lamin B interacts with the DNA replication machinery (Moir et al., 1994; Moir et al., 2000a), components of the mRNA splicing machinery (Jagatheesan et al., 1999) and chromatin (Reddy et al., 2008). It can also bind epigenetic repressors of chromatin through the lamin B receptor (LBR) (Guarda et al., 2009), and siRNA-mediated depletion of lamin B has also been associated with alterations in interphase chromosome positioning (Malhas et al., 2007; Tang et al., 2008).

From electron microscopic (EM) observations, the lamina appeared as near-continuous staining at the nuclear periphery (Belmont et al., 1993), while fluorescence microscopy also revealed the presence of diffuse staining in the nucleoplasm (known as the 'veil') that can be punctuated with brighter speckle structures (Broers et al., 1999). Viewed in three dimensions (3D), these speckles can be roughly spherical in shape, or extend as partially or fully transnuclear processes (Fig. 1-3, (Broers et al., 1999)). Some lamin A/C speckles are associated with splicing factors and have a role in transcription from class II genes (Kumaran et al., 2002), while others contain lamin A precursors (Sasseville and Raymond, 1995). Lipophilic dyes were used to show that some lamin A/C tubular structures could be hollow (Bridger et al., 1993; Broers et al., 1999). As a result, Broers et al. (1999) proposed that they could have a role in transport, in addition to their likely function in structural support of the nucleus. It seems probable that these tubular structures may be involved in nucleo-cytoplasmic shuttling of nucleic acids and small molecules, and thus their organisation could be important for gene expression and protein production. Study of the dynamics of lamin A using GFP-tagged proteins and FRAP (fluorescence recovery after photobleaching) in interphase cells indicated that the

nucleoplasmic veil regained fluorescence following bleaching much more rapidly than the peripheral lamina and speckle features. This suggested that the latter structures had a longer turnover time, and were probably less freely diffusible than the nucleoplasmic proteins (Broers et al., 1999). Subsequently, Moir et al. performed a temporal FRAP study of GFP-tagged lamin A and B1 throughout the cell cycle, and found that the nucleoplasmic veils had a similar rate of turnover to the lamina, except in early G1 phase (Moir et al., 2000b). The authors concluded that the measurements in the Broers et al. study corresponded predominantly to early G1 cells, before the nucleoplasmic veil contained polymerised lamins, but conceded that the two populations of lamins may be architecturally distinct.

In addition to the lamins, other proteins such as emerin (Lammerding et al., 2005; Vaughan et al., 2001), and NuMA (nuclear mitotic apparatus) (Abad et al., 2007; Lelievre et al., 1998) also interact with the nucleoskeleton. Both of these proteins have been implicated in mechanotransduction. Emerin-deficient cells exhibited defective mechanotransduction (Lammerding et al., 2005), while disruption of NuMA organisation could induce dedifferentiation of mammary epithelial tissue (Lelievre et al., 1998), apparently due to its influence on chromatin architecture (Abad et al., 2007).

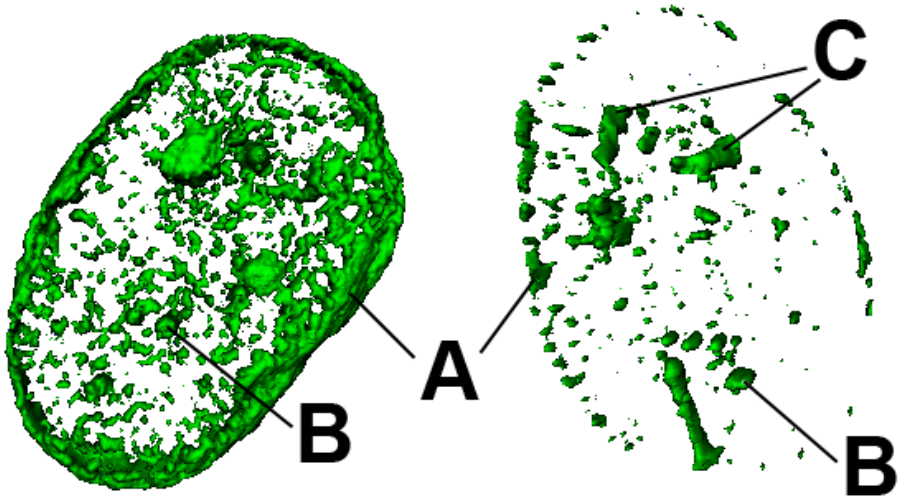

Figure 1-3. Partial cut-away views of 3D surface reconstructions of lamin B immunostained fibroblast nuclei. *The peripheral lamina (A), rounded speckles (B), and partially or fully transnuclear tubule-like structures (C) are indicated. McNamara et al. (unpublished data).*

1.3.3.2 Chromosomal Effects

Extraction experiments have supported a mechanical link between chromosomes and nucleoli (Maniotis et al., 1997). Nucleoli are the sites of ribosomal RNA (rRNA)

production in the nucleus. Viewed under EM, these non-membrane bound organelles are composed of fibrillar centres, surrounded by dense fibrillar components, where the rRNA is produced (Koberna et al., 2002), and both are located within granular clusters. These dynamic structures occupy interchromosomal spaces, and nucleolar morphology is altered in response to inhibitors of RNA polymerases I and II, as well as siRNAs directed against lamin B, but not lamin A/C (Martin et al., 2009). An interesting study was performed using micromanipulation of cells (Maniotis et al., 1997), where pulling exerted at the peripheral cytoplasm resulted in relocation of the nucleus and concurrent redistribution of nucleoli. It was concluded that the force had been transmitted between the cytoskeleton and nucleoskeleton. Similarly, Pajerowski et al. showed that direct aspiration of the nuclear lamina led to pulling of chromatin into the micropipette, which was followed by movement of nucleoli (Pajerowski et al., 2007). Using photobleaching as a means to quantify the distance travelled by each structure, the authors concluded that embryonic stem cell (ESC) nuclei were around 2.2-fold more pliable than embryonic fibroblasts, with adult stem cells showing an intermediate flexibility. This was attributed to the requirement for stem cells to force through developing tissues, which may necessitate greater deformability. Interestingly, the nuclei of two osteosarcoma cell lines were capable of large-scale distortion to adapt to the shape of a nanopillared substrate, whereas primary osteoprogenitor cells did not respond in this way (Davidson et al., 2009). The authors attributed this to altered cytoskeletal tension, but differential nuclear rigidity is also likely to have been a contributing factor.

The use of topography as a mechanoinducing signal has the additional advantage that it is a non-invasive stimulus, and thus cells are not damaged, unlike in traditional interventional approaches. In a microarray study of fibroblasts cultured on nanocolumns, chromosome 3 (Ch 3) was subject to cytological investigation using DNA FISH (Fluorescence *In situ* Hybridisation), a technique for visualisation of chromosome positioning in fixed nuclei. Nanocolumn substrates appeared to induce repositioning of Ch 3 (Dalby et al., 2007a; Dalby et al., 2007b) relative to controls. Compared with cells on the planar surfaces, cells cultured on nanotopography were less well spread, and had nuclei that appeared smaller with more closely apposed Ch 3 centromeres. These alterations were consistent with topography-induced direct mechanotransduction, as the authors proposed that the decrease in nuclear surface area and inter-chromosomal distances on the structured surfaces could be due to decreased cell spreading, resulting in less taut cytoskeletons, lowered tensile forces and reduced pulling on the nuclei. In nuclei of cells cultured on hexagonally arrayed nanopits, the inter-centromeric distance was reduced for both

chromosomes 3 and 11. The cells on nanopits were less spread than on nanocolumns, and markedly less spread than controls (Dalby et al., 2007a). Similarly to the nanocolumn substrates, the changes were consistent with the tensegrity model. Tension on the cytoskeleton and nucleus should have been reduced, which was likely to lessen the force exerted on chromosomes.

In general, the peripheral DNA at the edge of the nucleus, and bounding the nucleoli, is rarely transcribed - or transcriptionally silent - heterochromatin, while the more frequently expressed sequences are typically more centrally located (Felsenfeld and Groudine, 2003). This nuclear organisation is adopted by many mammalian cell types, including fibroblasts (Bolzer et al., 2005). There are exceptions to this organisation, however, such as the reversal of the typical eu- and heterochromatic organisation in the photoreceptor cells of nocturnal animals, to facilitate light capture (Solovei et al., 2009), and the preferential transcription of HIV proviral DNA at the edge of the nucleus (Chubb, 2009). Topography-induced redistribution of chromosomal territories (the space occupied by a given chromosome within the nucleus, discussed in (Cremer and Cremer, 2001), or intra-territory loci (the location of particular genes) could affect the cellular transcriptional profile. There are foci of transcriptional activity within the nucleoplasm, where active, transcription-competent RNA polymerase II and transcription factors are clustered. Genes can loop out from chromosome territories to move into these areas, and such repositioning can increase their likelihood of being transcribed ((Chambeyron et al., 2005; Osborne et al., 2004); discussed in (West and Fraser, 2005)). Alternatively, movement of genes or territories towards the heterochromatic periphery of the nucleus could promote down-regulated transcription.

Reddy et al. (2008) demonstrated an elegant method for enforced targeting of a chromosomally integrated reporter gene to the nuclear lamina. A series of LacI binding sites (*LacO*) were placed upstream of a thymidine kinase promoter fused to a hygromycin resistance gene (*Tk-hyg*). These reporter genes were transfected into cells stably expressing a GFP-tagged LacI protein (which binds the *LacO* site, but can be sequestered by isopropyl-β-D-1-thiogalactopyranoside (IPTG)) fused to the targeting sequence from a nuclear envelope protein. Removal of IPTG from the culture medium induced repositioning of the gene to the nuclear lamina. This reduced the amount of transcription from *Tk-hyg* and led to association of the gene with lamin B and inner nuclear membrane proteins LAP2 (lamin-associated polypeptide 2) and emerin. In addition, the gene became hypo-acetylated on histone H4 (representing the loss of an activating epigenetic

modification), but did not appear to be associated with nuclear pores. Most interestingly, this could also induce down-regulation of a flanking endogenous gene. The authors also investigated the ability of a transcription factor, OCT1, to access the *Igh* locus of immunoglobulin genes in pro-B cells (where the genes were being actively transcribed) and fibroblasts (where the genes were transcriptionally silent). In fibroblasts, lamin B and emerin were bound to this locus, unlike in pro-B cells, where *Igh* was not associated with these proteins, and remained accessible to OCT1. In addition, the interaction of *Igh* with the nuclear membrane proteins appeared to be specific to that genomic region, rather than solely as a result of propinquity to the nuclear matrix, as these proteins did not bind to another locus upstream. Wang et al. (2009) suggested a number of models by which tensile forces from FAs could modulate gene expression. It was proposed that the assembly or activity of transcription factor complexes could be affected directly or indirectly by tension-mediated alterations in the nucleoskeleton. In addition, local DNA melting at matrix attachment regions could affect its accessibility for transcription. Furthermore, the authors suggested that gene expression or mRNA transport could also be affected by tension-mediated changes in nuclear pores.

The mechanical changes exerted by topography will most likely have multiple, synergistic effects on the nucleus for the enforcement of gene-level changes. It is also probable that topography-invoked mechanotransduction will have various outputs, acting at both the mRNA and protein levels (Fig. 1-4): 1) transcriptional, with the physical accessibility of genes to transcription factors being altered, 2) post-transcriptional, with effects on mRNA splicing, editing or transport, 3) translational, by altering protein production, 4) post-translational, by rapidly altering the activity state of proteins, and 5) conformational, with changes in protein structure, composition of protein assemblies, and exposure of cryptic binding sites.

In this complex interplay, the complementary nature of direct and indirect (chemical signal-mediated) mechanotransduction can be seen. It would be anticipated that direct mechanotransduction would account for most of the physical changes in the cell, such as nuclear reshaping, delineation of chromosomal territories, force-induced changes in protein conformation, and mechanical alterations (*e.g.* in nuclear pore diameter) that might manipulate mRNA or protein transport. Conversely, chemical signals (such as integrin-linked signal cascades) would be expected to predominate in inducing the rapid-response modifications in protein activity state. Although one type of mechanotransduction may dominate for a particular functional response, it seems highly

likely that the two pathways ultimately act to reinforce each other to generate the complete and apposite cellular response to topography.

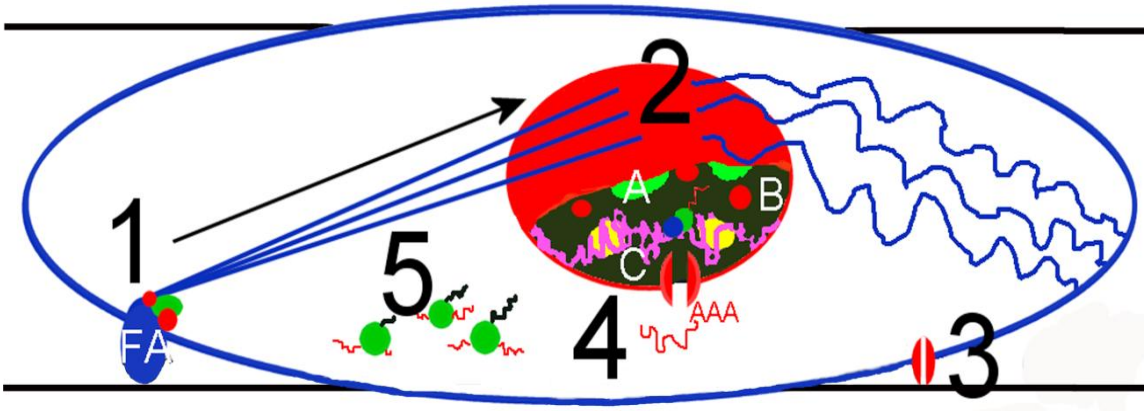

Figure 1-4. Summary of the potential mechanical effects of microgrooved topography on a generic cell of mesenchymal origin. *(1) Cell sensing of the microtopographical stimulus (black lines) is initiated at focal adhesions (FA). Protein recruitment, in addition to force-induced changes in protein conformation and binding, can occur at these sites, together with cytoskeletal remodelling and indirect chemical signalling to the nucleus (arrow). (2) Physical forces from the cytoskeleton, including tension from actin stress fibres (straight lines) and interactions between the intermediate filaments vimentin (wavy lines) and the lamins (red) induce direct mechanotransductive effects. Together with signalling inputs, these changes may include redistribution of chromosomes, nucleoli (A) and other nuclear components such as lamin speckles (B), epigenetic changes to DNA (pink) and histones (yellow), and accessibility of DNA to the transcriptional machinery (C). (3) Ion channels and certain membrane proteins may also be responsive to the microfeatures, leading to ion fluxes and additional signals. (4) The diameter of nuclear pores (red channel) may be manipulated by force from the cytoskeleton, potentially affecting mRNA transport. (5) Availability of mRNA, or other modulation of translation could alter protein production from ribosomes. Reproduced with modification from McNamara et al. (submitted).*

Appropriate mechanotransduction is crucial for tissue development and function. This principle was illustrated in studies of substrate rigidity (Engler et al., 2006a) and nanofeatures (Dalby et al., 2007d; Oh et al., 2009), with both types of mechanical stimuli implicated in the fate determination of MSCs. Furthermore, an increasing number of pathologies (Jaalouk and Lammerding, 2009) are being linked with defects in mechanotransduction. With the emergence of mechanical stimuli as critical modulators of cellular functionality, micro- and nanotopography should prove excellent tools for development of novel biomaterials capable of promoting desirable cellular behaviour, discouraging unwanted cell responses, and preventing or ameliorating pathological changes.

1.4 Transcriptomics and Proteomics in Biomaterials Research

1.4.1 Transcriptomics - Microarray

Study of the transcriptome, the mRNA profile of the cell, using microarray analysis has the major advantage that the transcript abundance of many thousands of genes can be studied simultaneously. This allows global study of gene expression in response to the conditions of interest. In addition, the mRNA can be amplified, permitting detection of even low abundance transcripts. These are both critical advantages for biomaterials research at academic level, where the source material is likely to be very scarce, and a wide-coverage study is advantageous in screening for novel molecular targets with potential relevance to topographical interactions and mechanotransduction.

Topographies present micro- and nanoscale features to cells that can lead to changes in number, size and arrangement of focal adhesions (Biggs et al., 2007), redistribution of cyto- and nucleoskeletal elements (Dalby et al., 2007b), and altered cell and nuclear morphologies (Dalby et al., 2007b). This combination of chemical signals and physical forces leads to the changes in transcript abundance that have been observed using microarray studies of various cell types on microgrooves (Dalby et al., 2003c), microgrooves with applied uniaxial strain (Kurpinski et al., 2006; Park et al., 2006), nanopits (Dalby et al., 2007c), nanopillars (Biggs et al., 2007), nanoislands (Dalby et al., 2002b), nanogrooves (Biggs et al., 2008) and partially disordered nanopatterns (Dalby et al., 2007d). The results of some of these studies are discussed in Chapter 3.

In microarray experiments, total RNA (mRNA, rRNA and small RNAs) is extracted from cells under the control and test conditions of interest. All other variables are kept constant, and the RNA is amplified in steps, firstly by synthesis of complementary DNA (cDNA, the reverse complement, or antisense, of the mRNA), which is then converted to double-stranded DNA for subsequent use as a template in transcription by RNA polymerase, to yield cRNA. The cRNA is then reverse transcribed to cDNA, fragmented, fluorescently labelled and hybridised to the target chip. In the case of Affymetrix® Human Gene 1.0 ST Arrays, the microarray chips contain immobilised target probes (antisense oligonucleotides corresponding to the known transcripts from each human gene), against which the samples are hybridised (Fig. 1-5). The Affymetrix®

platform utilises a design with one sample per chip, and inter-sample comparison is performed between chips. Once the microarrays have been scanned, the relative abundance of individual transcripts can be compared between the control and test chips. This requires statistical data processing to confirm the quality of the data, to normalise the data, and correct for batch variation, pairing effects and other unwanted variables.

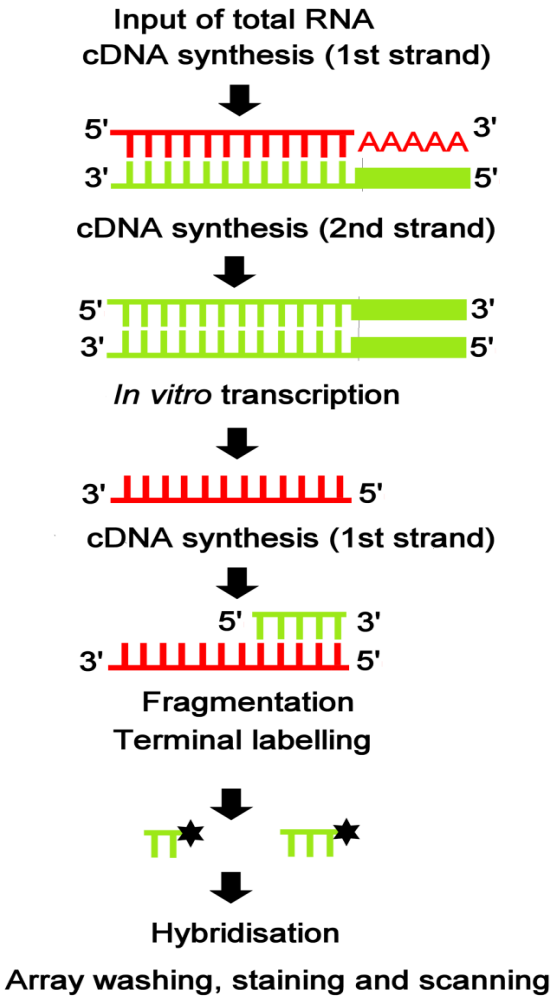

Figure 1-5: Overview of RNA processing for Human Gene Arrays (Affymetrix). *Total RNA extracts from control or test samples are used as the input for 1st and 2nd strand cDNA synthesis. The 2nd strand is used as a template for in vitro transcription of antisense RNA, which is then used to synthesise sense strand cDNA. This cDNA is fragmented and end-labelled with biotin, prior to hyridisation to the microarray, washing, staining and scanning of the chip. This process is conducted for each sample, with one sample per chip. Redrawn with modification from the Human Gene Array 1.0 ST manual (Affymetrix®).*

1.4.2 ***Proteomics – DiGE***

The cellular proteome is the total complement of proteins expressed by a cell under defined conditions. The composition and relative abundance of proteins in the proteome can change in response to a multitude of factors, which in a biomaterials context includes the interaction of cells with metals, polymers, and chemically or topographically micro- or

nanopatterned surfaces. In recent years, the development of DiGE (fluorescence two-dimensional difference gel electrophoresis) has offered additional scope for evaluation of cell-material interactions at the protein level, allowing relative changes in protein abundance and post-translational modifications (PTMs) to be mapped across the proteome between the control and test states. This is advantageous, since proteins are the functional effectors of cellular responses to biomaterials, and changes in protein expression or PTMs are likely to equate with changes in cellular state. This is not necessarily true of gene expression data, where the translational activity of each mRNA species in a microarray experiment is unknown, and transcript levels are subject to additional levels of control, including degradation (Wu et al., 2006) and sequestration (Liu et al., 2005b) of transcripts by the miRNA machinery, before the protein level is reached.

In biomaterials research, the use of DiGE affords the opportunity to investigate global changes in cellular protein profile in response to new materials, devices and implants, to identify responsive proteins of interest, and groups of proteins ('biomarkers') associated with the cell- and tissue responses to different materials or constructs. This has the potential to give valuable insight into cell-surface interfaces at the protein level, which should assist with the development of next-generation materials and implants with the capacity to tailor cellular responses to particular laboratory, industrial or therapeutic applications.

Samples for DiGE could be derived from *in vitro*, *in vivo* and clinical sources. In contrast to most other fields, in biomaterials research, many conventional biochemical techniques (such as binding assays and immunoprecipitation) are very difficult to perform, due to the typically small sample yield and often time-consuming and labour-intensive nature of sample generation from these sources. DiGE offers the capability for simultaneous screening of large numbers of proteins for changes in abundance between different conditions, combined with the ability to cope with very scarce samples. The analyses are readily multiplexable (up to three samples can be resolved on the same gel, due to the dye chemistry and fluorophore availability), allowing comparison between replicate samples, over time courses or between multiple conditions. These features have the potential to assist biomaterials researchers in maximising the data output of their experiments, while minimising the amount of sample required.

Prior to the advent of DiGE, evaluation of relative changes in protein abundance could be performed using traditional 2D-gel electrophoresis (2DE). In this technique,

individual samples are initially separated by native charge in the first dimension, using isoelectric focussing (IEF), and partitioned by molecular mass in the second dimension using SDS-PAGE (Carrette et al., 2006). In the biomaterials field, this approach has been applied to investigate the response of monocyte-derived macrophages to polycarbonate-urethane (Dinnes et al., 2007), and dermal fibroblasts to titanium surfaces (Derhami et al., 2001). The technique suffers from gel-to-gel variation and poor reproducibility, however, as one sample is resolved per gel in the absence of an internal standard, and therefore a large number of gels are required to perform a robust pairwise comparison. In addition, relatively large quantities of protein are required for this approach (at least 50 µg for silver staining, the most sensitive non-fluorescent post-stain, and up to ~500 µg protein with colloidal Coomassie Blue staining, equivalent to two or three 75cm^3 tissue-culture flasks of confluent adherent cells). Sufficient protein was generated in the aforementioned investigations by using relatively high cell densities (Derhami et al., 2001; Dinnes et al., 2007) and small format gels (less protein required, but with lower resolution - fewer distinct spots - than large format gels) (Derhami et al., 2001). These approaches are not always practicable depending on the biomaterial system, since protein samples can be very scarce, and high resolution is desirable.

Current alternatives to DiGE for quantitative comparative proteomics are all gel-free approaches that involve chromatographic separation of peptides followed by mass spectrometry (MS; reviewed in (Aebersold and Mann, 2003)). The principle techniques include stable isotopic labelling by amino acids in cell culture (SILAC), an approach for metabolic isotopic labelling of proteins in cultured cells (Amanchy et al., 2005; Ong et al., 2002), ICAT (isotope-coded affinity tag) technology, dimethyl labelling, which involves stable isotopic labelling of protein extracts (Hsu et al., 2003) or cell cultures (Boersema et al., 2009), and the iTRAQ (isobaric tags for relative and absolute quantification) approach (Wiese et al., 2007; Wu et al., 2005). The latter approach was used to compare the response of osteoblasts to hydroxyapatite and hydroxyapatite reinforced with carbon nanotubes (Xu et al., 2008). There are also label-free quantitation methods, which involve enumeration of the spectral peaks corresponding to individual peptides (Zhu et al., 2010). Gel-free comparative approaches can be easier to perform than DiGE, but are generally difficult to multiplex, can be less quantitative, and may not be well suited to the study of PTMs. In addition, iTRAQ can suffer from difficulties in isolating suitable ions for fragmentation (Wu et al., 2005). These methods are better suited to the investigation of certain groups of proteins, such as hydrophobic proteins, that are difficult to evaluate using

2D gels. The above techniques are discussed more fully elsewhere (Mirza and Olivier, 2008; Wu et al., 2005), and can be complementary to DiGE studies.

In DiGE, protein is extracted from control and test samples, fluorescently labelled using Cy3 or Cy5 CyDyes™, and separated in the first dimension by native charge using isoelectric focussing and in the second dimension by mass using SDS-PAGE. There are two main labelling strategies for DiGE. The minimal labelling approach (DiGEmin) utilises –NHS (*N*-hydroxysuccinimidyl) ester dyes to label ~3-5% lysine residues in proteins, and has Cy3 and Cy5 dyes for labelling the control and test samples, and the option of using Cy2 to label a pooled internal standard for inter-gel matching. Saturation labelling DiGE (DiGEsat) uses maleimide dyes to label all cysteine residues within a protein, and is a higher sensitivity approach than miminal labelling. This enables detection of additional features, and allows the study of very scarce protein samples of 5 μg (compared with the 50 μg protein required for minimal labelling). Considerably less material has been studied in some applications, such as specimens obtained by laser capture microdissection (Kondo and Hirohashi, 2007; Kondo et al., 2003). The workflow for DiGEsat is shown in Fig. 1-6.

Although saturation labelling of cysteines limits detection to proteins containing this less common residue, about 96.3% of proteins (Sitek et al., 2005) contain at least one cysteine residue, and this potential disadvantage is overcome by the increased sensitivity of the technique. The success for mass spectrometric identification of proteins is similar for minimal and saturation labelling approaches (Greengauz-Roberts et al., 2005). In both labelling strategies, it is advisable to use a high-load preparative gel (containing ~250-500 μg protein) for protein identification. For minimal labelling, this gel would be post-stained with a fluorescent total protein stain such as the Sypro™ dyes, and matched to the analytical gels prior to spot picking. This prevents any false or failed protein identification that may result from aberrant spot picking due to the mass shifting (between labelled and unlabelled species) that results from labelling only a small proportion of the proteins in the analytical gels. In saturation labelling experiments, the preparative gel is also labelled with Cy3 dye. Saturation labelling leads to a protein-specific increase in mass, depending on the number of cysteine residues contained in each protein species, and thus an altered spot pattern relative to unlabelled proteins. The use of Cy3 dye to label both analytical and preparative gels improves the accuracy of inter-gel matching for protein identification.

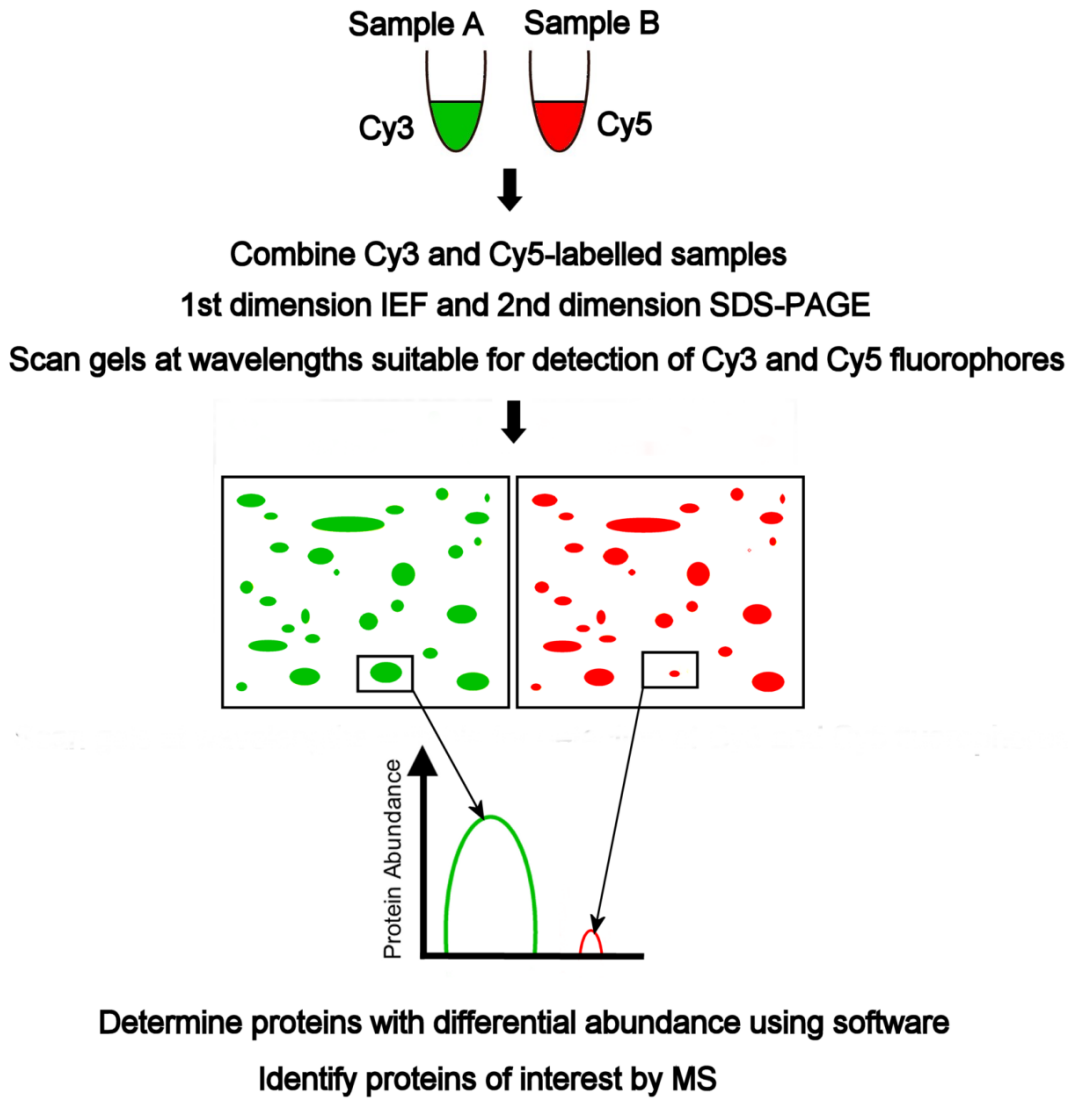

Figure 1-6: The DiGEsat workflow. *Samples labelled with Cy3 (e.g. control) and Cy5 (e.g. test) saturation dyes are combined, and resolved by 2DE. The fluorescent dyes are detected by scanning the gels at suitable wavelengths, and differential abundance is assessed using software (e.g. DeCyder or SameSpots). Subsequently, proteins of interest are usually picked for MS analysis.*

Mass spectrometry (MS) is utilised to identify proteins of interest from gel spots. Such spots are excised manually or using a robotic spot picker, enzymatically digested to peptide fragments, usually using trypsin, and analysed by a solid or liquid-phase mass spectrometric technique. In the first round of MS, a 'survey' scan is conducted to generate peptide masses (peptide mass fingerprints, or PMFs), which can be utilised for peptide mass fingerprinting in databases such as Mascot. These masses can be compared against a database of theoretical trypsin-derived peptides for identification. In tandem MS (MS/MS), additional rounds of fragmentation are induced. The strong mass peaks detected during the survey scan are further fragmented to generate peptide sequence data. This is often by collision-induced dissociation (CID), where the peptide ions are collided with an inert gas to give smaller fragments or daughter ions. In TOF (time of flight) MS instruments, the ionised peptides are passed in a vacuum along a TOF tube to a detector,

and each detected fragment is assigned a PMF based on its mass over charge (m/z) ratio. TOF-TOF instruments have a collision cell which permits further fragmentation to individual amino acids. MS/MS can also be achieved using quadrupole instruments, which have several electrically gated chambers, including a collision chamber responsible for inducing CID in selected peptides, and ion trap mass spectrometers, which arrest the ions to allow selection for MS/MS. The structure of a number of different types of mass spectrometer are summarised in Fig. 1-7. MS/MS data can often give more robust identifications in protein databases than PMFs alone, but it can be helpful to use both approaches to allow a combined search (MS and MS/MS) to be performed, and utilise both datasets.

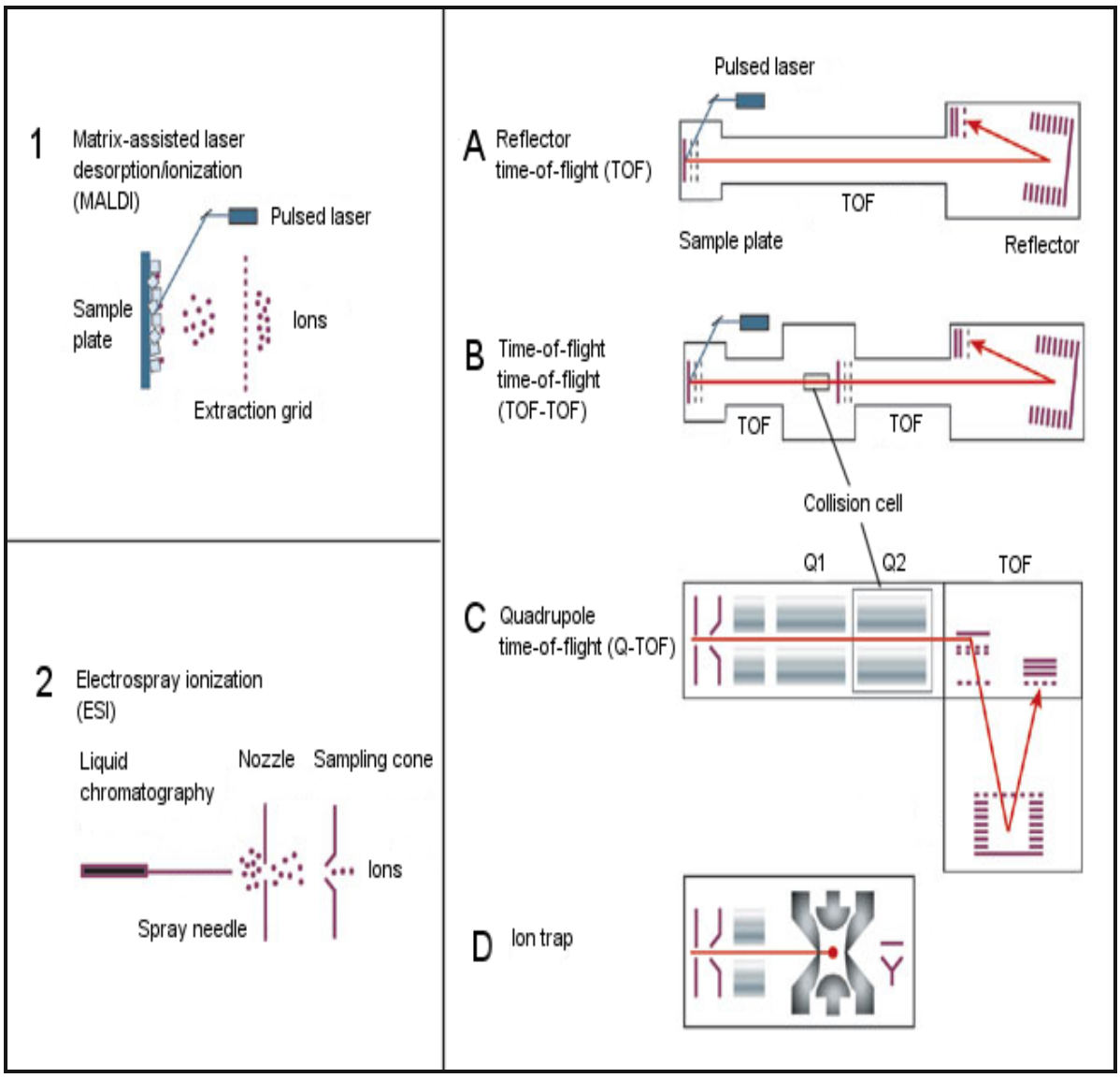

Figure 1-7: Illustration of the major ionisation strategies for MS, and the principle approaches for MS. *Samples soft-ionised from the solid phase using MALDI (1) are compatible with TOF (A) and TOF-TOF (B) systems. Samples are sprayed through a narrow aperture in ESI, and ionised by a high-power electric current. ESI is frequently coupled with Q-TOF (C) and ion trap (D) mass spectrometers. B, C and D are capable of MS/MS analysis. Adapted by permission from Macmllan Publishers Ltd: [NATURE] Aebersold and Mann (2003), copyright (2003).*

It is useful to combine two forms of mass spectrometry to increase the likelihood of generating successful protein identifications. A high-throughput solid-phase approach, such as matrix-assisted laser desorption/ionization-time of flight (MALDI-TOF/TOF) MS/MS, where peptides are soft-ionised by the surrounding matrix, is useful for maximising the number of protein identities, for example when attempting to identify as many spots from a gel as possible to create a comprehensive spot map. When particular spots are of interest, however, such as differentially regulated spots highlighted in a DiGE experiment, a lower throughput, higher sensitivity approach, such as electospray ionisation-quadrupole-time of flight (ESI-Q-TOF) is advisable. In the investigation of cellular response to topographical substrata, DiGE has been used to investigate osteoprogenitor response to microgrooves (Kantawong et al., 2009a) and nanodisordered surfaces (Kantawong et al., 2008; Kantawong et al., 2009b). The results of these studies are discussed in greater detail in Chapter 5.

1.5 Project Rationale

The potential for use of topography as a non-invasive means to influence signalling, cytoskeletal arrangement, nuclear shape, subnuclear architecture and gene expression makes it an attractive tool for fundamental cell biology and translational research. Microgrooves are particularly useful for the study of mechanotransduction, since these structures are capable of inducing contact guidance and large-scale cytoskeletal reorganisation. Prior to this thesis, the effects of microgrooves on chromosomal territories and the nuclear lamina had not been investigated, and thus the impact of these structures on subnuclear events and architecture merited further study. The 3D organisation of the nucleoskeleton and cytoskeleton had not been examined on these substrata, to assess whether this could offer additional insight into topography-induced mechanotransduction. In addition, the proteomic response to a microgrooved substrate had been documented in only a single cell type (human osteoprogenitor cells) in previous research, and no studies had examined both the transcriptomic and proteomic effects of this topographical stimulus in the same cell type under comparable conditions, or attempted to unite these data. The use of complementary transcriptomic and proteomic techniques allows the inclusive, global nature of transcriptomics to be combined with an evaluation of changing protein abundance at the level of the functional effectors.

A multi-layered approach was adopted in this study, to begin to characterise 2D and 3D architectural changes in the cyto- and nucleoskeleton, study the impact of the topography on chromosome territories, and identify alterations at both the mRNA and protein levels. The aim of this multifaceted approach was to begin to provide a more integrated view of the changes induced by a topographical mechanostimulus. Increased knowledge of the physical and molecular changes resulting from cell-material interactions should provide valuable insights for the development of future topographical surfaces.

2 Two- and Three-Dimensional Investigation of Cellular Architecture

2.1 Introduction

2.1.1 2- and 3D Confocal Microscopy

Optical microscopy, including epifluorescence and confocal microscopy, is well suited to the study of micron scale topographies. The structural features are visible within the limits of resolution, and samples can be observed under atmospheric pressure following a less harsh specimen preparation regime than for electron microscopy. The presence of confocal apertures in confocal microscopes reduces blurring from out-of-focus light, which enables visualisation of multiple focal planes as separate 'slices'. Such optical sections can be obtained from different heights in the same cell, allowing the generation of *z*-stacks that can be reconstructed into 3D projections.

In relation to cell-topography interactions, the major disadvantage of 2D microscopy is that cells and surfaces are generally imaged at a single plane of focus, such that additional structural details at other planes may be overlooked, and the directionality of the topographic surface (for example, the distinction between grooves and ridges in a microgrooved topography) is not always apparent. A 3D approach, by contrast, should provide more subcellular information, with data on 3D morphology, and clarify the positions of cells relative to the substrate. This approach is very time-consuming, however, and photobleaching can be a major problem due to the length of time required to generate enough high-resolution optical slices to produce a *z*-stack. The fluorescent dyes utilised in high-resolution reconstructions must be selected for photostability, and conditions for microscopy should be optimised for each sample to reach an appropriate compromise between maximising the speed of optical sectioning, to increase data yield and minimise photobleaching, while retaining resolution.

In this study, 2D epifluorescence and confocal microscopy was used to evaluate the cellular architecture of relatively large numbers of cells at a limited number of focal planes. This was combined with *z*-stack optical sectioning, to produce high-resolution 3D reconstructions of a small number of cells. Use of an optically transparent substrate, quartz, facilitated the production of 3D phase contrast images of the topography. It was

also possible to generate 3D phase contrast images of the topography of a less optically transparent surface, PDMS, by modifying the substrate attachment and mounting procedure to ensure the substrates were appropriately flattened.

2.2 Method Development

2.2.1 Nucleoskeletal Staining

It was necessary to develop suitable staining conditions for the optimal detection of lamin A/C and lamin B on the structured substrates. A previous study of lamins on biomaterials had used formaldehyde as a fixative (Dalby et al., 2007b), but this did not yield satisfactory results in the present study, giving generalised staining in both the cytoplasm and nucleus, suggestive of improper fixation of the structures, non-specific antibody interactions, or both. Trinkle-Mulcahy et al. used methanol, and methanol/2-(*N*-morpholino)ethanesulfonic acid (MES) as fixatives for subnuclear structures termed speckles and paraspeckles (Trinkle-Mulcahy et al., 1999). These fixatives, and 3.8% (v/v) formaldehyde in PBS (with 2% (w/v) sucrose), were utilised to elucidate the optimal conditions for the staining of the nucleoskeletal structures (Table 2-I). To reduce the amount of non-specific staining, the protocol was further modified to include a longer initial blocking step with a higher concentration of BSA (3% (w/v)), an additional short blocking step with 3% (w/v) BSA between the primary and secondary antibodies, and longer washes with 0.1% (v/v) Tween-20 in PBS (three washes per step, with the length of each final wash increased to 10-15 minutes). Formaldehyde fixation was not sufficient to yield convincing lamin staining (Fig. 2-1A), but fixation with methanol (Fig. 2-1B) or methanol/MES gave excellent staining of lamin A/C with little or no background staining. Interestingly, methanol/MES fixation with immunostaining gave particularly bright staining of the punctate foci of lamin A/C, suggesting that the addition of the MES buffer could either enhance staining or aid retention of these structures. As the two methods of fixation gave otherwise comparable results, however, methanol was selected as the fixative as it was more straightforward to prepare and comparable with a greater number of studies in the literature.

Table 1. Details of fixatives, fixation conditions and wash buffers utilised during the optimisation of lamin A/C staining.

Fixative	Fixation conditions	Wash buffer	Success of lamin A/C Staining	Additional details
3.8% (v/v) PFA	15 min, 37°C	0.05% (v/v) Tween-20 in PBS	-	High background and cytoplasmic staining
3.8% (v/v) PFA	15 min, 37°C	0.075% (v/v) Tween-20 in PBS	-	High background and cytoplasmic staining
3.8% (v/v) PFA	15 min, 37°C	0.1% (v/v) Tween-20 in PBS	-	High background and cytoplasmic staining
100% methanol	**2 min, buffer prechilled to –20°C**	**0.1% (v/v) Tween-20 in PBS**	**Successful**	**Specific staining in appropriate pattern, minimal background**
90% (v/v) methanol/10% (v/v) MES (100 mM MES, pH 6.9, 1mM EGTA, 1 mM $MgCl_2$)	**2 min, buffer prechilled to –20°C**	**0.1% (v/v) Tween-20 in PBS**	**Successful**	**Specific staining in appropriate pattern, minimal background**

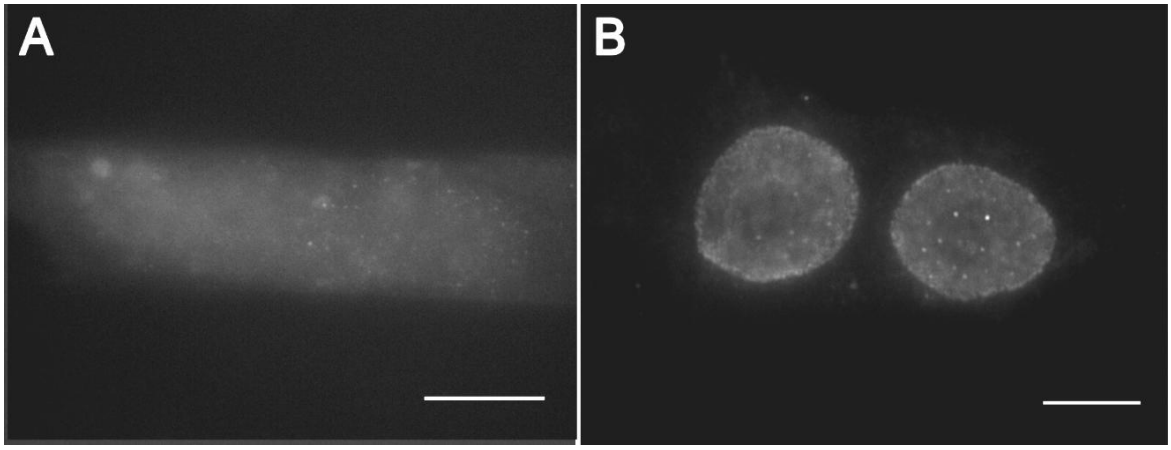

Figure 2-1: Examples of unsuccessful (A) and successful (B) protocols for lamin A/C staining. *Note the faint, nonspecific staining in A (3.8% (v/v) PFA fixation for 15 min at 37°C, washes in 0.05% (v/v) Tween-20 in PBS), and the appropriate pattern of nuclear staining of lamin A/C in B (2 min fixation in -20°C chilled methanol, washes in 0.1% (v/v) Tween-20 in PBS). Bars: 10 μm.*

The anti-lamin A/C antibody gave a consistently weaker signal than the anti-lamin B antibody. Technical difficulties were encountered in generating high-resolution 3D confocal images from lamin A/C-stained samples, due to photobleaching during optical sectioning, and as such the resulting images were not particularly informative (results not shown).

To investigate the interaction between the nucleoskeleton and the cytoskeleton, the double staining of lamin B and vimentin was also optimised (the method is detailed in Section 2.3.4.3). Initially, a polyclonal goat anti-vimentin antibody was used with a monoclonal lamin B antibody, with detection using Texas red-conjugated horse anti-mouse antibody, and biotinylated sheep anti-goat antibody followed by a layer of fluorescein-labelled streptavidin. Only non-specific staining was visible in the TRITC (vimentin) channel, which probably resulted from cross-reaction between the anti-goat secondary antibody and BSA, the blocking agent. This could probably have been circumvented using secondary antibodies raised in the same species, with serum from this species as the blocking agent. As these resources were unavailable, however, an alternative method was developed using monoclonal antibodies directed against lamin B and vimentin. Initially, these antibodies were incubated simultaneously with the samples, and detected with a biotinylated horse anti-mouse antibody and fluorescein-labelled streptavidin. This amplification step was required for the detection of the lamin B signal, as the Texas red-conjugated secondary antibody was not bright enough to permit detection of the lamin B signal in single-labelled sections. The triple-layer stain resulted in successful, strong signals for both vimentin and lamin B in the FITC channel.

The protocol was further modified to allow the structures to be immunostained with different colours of fluorophores. Firstly, the samples were stained for lamin B using a monoclonal primary antibody and the triple-layer approach detailed in Section 2.3.4.2, followed by blocking in 3% (v/v) BSA, and staining against vimentin using a monoclonal primary antibody and a Texas red-conjugated horse anti-mouse secondary antibody. Both structures were stained appropriately by this method, with no evidence of crosstalk between the channels by epifluorescence microscopy. Using confocal microscopy, it was possible to generate a 3D reconstruction of a double-stained cell on the grooved topography (Fig. 2-2), but the resolution was sub optimal due to photobleaching of the samples. This difficulty was intensified by the requirement for increased laser power to retain sustainable detection of the lamin B signal throughout the *z*-stack. This resulted in bleed-through into the vimentin channel, which was circumvented by use of multi-track detection of the fluorophores. This doubled the time required to generate a *z*-stack, however, and exacerbated the photobleaching problem, typically resulting in relatively rapid loss of the weaker vimentin signal. These issues may have been alleviated by use of an unconjugated anti-mouse blocking antibody between the two antibody stains, permitting a triple-layer fluorescein stain for lamin B, followed by a triple-layer Texas red stain for vimentin to raise the signal intensity of the vimentin staining. The additional blocking step

with 3% (v/v) BSA between the sequential antibody stains offers an affordable alternative, however, if such strong signal intensity (as demanded by confocal optical sectioning) is not a prerequisite.

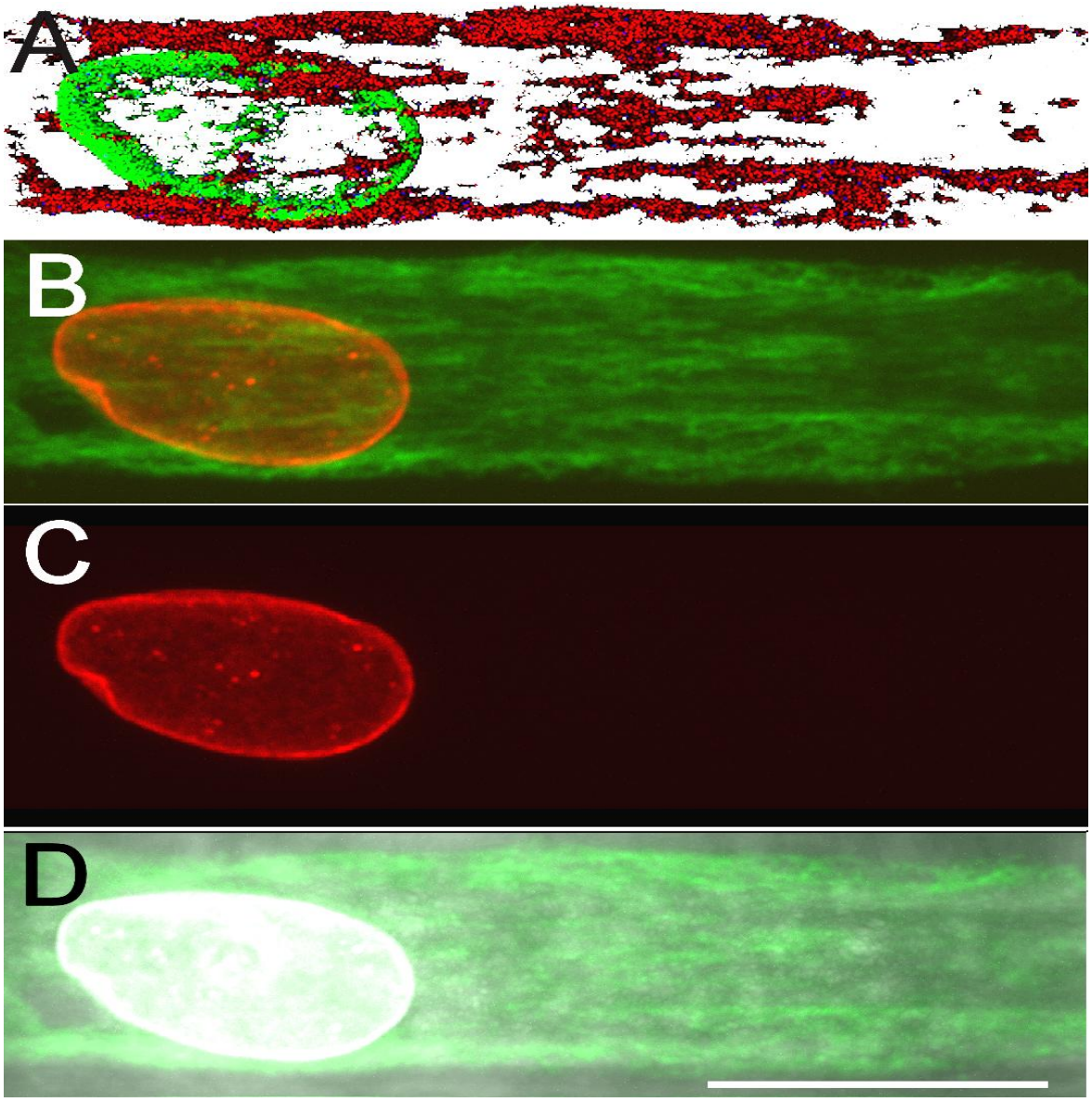

Figure 2-2. 3D reconstructions of a fibroblast successfully double immunostained for lamin B and vimentin. *A – 3D surface reconstruction of lamin B (green) and vimentin (red), B – 3D projection of lamin B (red) and vimentin (green), C – 3D projection of lamin B (red), D – 3D projection of lamin B (white), vimentin (green) and microgrooved topography (transmitted light; grey). Note that additional intranuclear detail is visible in A compared with C, due to the angle of orientation of the projection, and that there is no visible bleed-through between the vimentin and lamin B signals, due to the use of multi-track image acquisition. Bar: 20 μm.*

2.3 Materials and Methods

2.3.1 Preparation of Biomaterials

2.3.1.1 Fabrication of Quartz Master Substrates

Microstructured quartz substrates were fabricated by Ms. Sara McFarlane at the James Watt Nanofabrication Centre (University of Glasgow) using the following protocol: quartz slides were acid cleaned (7:1 H_2SO_4:H_2O_2) for 5 min, and spin-coated with AZ primer (4000 rpm, 30s). A layer of Shipley S1818 photoresist (Shipley) was spun onto to the spin-coated slides, and then soft-baked for 30 min at 90^{o}C. The samples were exposed to UV light on a MA6 mask aligner with exposure energy of ca. 7.1 mJ/cm^2 for each second in hard contact, through an electron-beam fabricated chrome mask with 12.5 μm wide lines. The resist was developed (1:1 AZ developer [Microchemicals]:water) for 65s and the slides were rinsed and dried prior to etching. Substrates were etched in a trichloromethane environment at a rate of 25 nm min^{-1} in a reactive ion etching unit (RIE80, Plasma Technology) using the polymer pattern as an etch resist to generate 2 μm deep grooves. The remaining resist was removed with acetone, and the slide was blanket etched for an additional 1 min to produce a homogenous surface chemistry. Planar slides were blanket etched to ensure that the chemistry was comparable with the structured substrates.

2.3.1.2 Cleaning of Quartz Substrates

Quartz substrates were cleaned in Caro's acid solution (2:1 H_2SO_4:H_2O_2) for 20 minutes, rinsed six times with double-distilled water and air-dried under a Class I or II sterile flow hood.

2.3.1.3 Sterilisation of Substrates

Acid-cleaned quartz substrates and coverslips were sterilised in ethanol for 20 minutes, then transferred through three dip-rinses in HEPES saline, and two rinses in complete medium (~30s/rinse).

2.3.2 Tissue Culture

2.3.2.1 Maintenance of Cells

Infinity™ telomerase-immortalised hTERT BJ-1 fibroblasts (Clonetech Laboratories, Palo Alto, USA) were maintained in 71% (v/v) DMEM (Sigma), supplemented with 17.7% (v/v) medium 199, 9% (v/v) FBS, 1% (v/v) 200 mM L-glutamine (Gibco), 0.9% (v/v) 100 mM sodium pyruvate and antibiotics (6.74 U/ml Penicillin-Streptomycin, 0.2 μg/ml Fungizone) at 37^{O}C in a 5% CO_2 environment. Cells were passaged at 70-80% confluence, and the medium was replaced regularly.

2.3.2.2 Cryopreservation of Cell Stocks

Cells were frozen at regular intervals in 1 ml of cryopreservative (70% (v/v) FBS, 20% (v/v) complete medium, 10% (v/v) DMSO) at -70^{0}C overnight, and moved to liquid N_2 the following day for long-term storage, or retained at -70^{0}C for shorter storage periods.

2.3.2.3 Revival of Cryopreserved Stocks

Cells were rapidly thawed at 37^{o}C, gently mixed with 0.5-1 ml warm complete medium and placed into a T-75 tissue culture flask. Warm complete medium (15 ml) was added slowly to the flask, and replaced the following day.

2.3.2.4 Growth of Cells on Biomaterials

Cells were counted using a haemocytometer (Mod Fuchs-Rosenthal, Gallenkamp, UK), and seeded at a density of ~ 150 cells/mm^2 material on quartz substrates, with a 24h culture period. The 25 x 75 mm quartz substrates were used for all microscopy, with the exception of the 7 day nucleolar study, which utilised 25 x 25 mm quartz substrata. Note that the *n* numbers in this chapter refer to the number of substrates used in each experiment (with the exception of the graphs relating to lamin B and lamin A/C quantification, where *n* is also used to refer to the numbers of nuclei counted in each case). In each experiment, the substrates were seeded at the same time, with the exception of the samples for the short-term nucleolar analysis, which were seeded in two temporally distinct batches and then cultured for 24h.

2.3.3 Cell Staining

2.3.4 Immunofluorescent staining

2.3.4.1 Cytoskeletal Staining

Cells were fixed for 15 minutes at 37°C in 3.8% (v/v) formaldehyde in PBS (74mM Na_2HPO_4, 15mM KH_2PO_4, 1.36M NaCl, 27mM KCl, pH 7.4) with 2% (w/v) sucrose, permeabilised for 5 minutes using chilled (4°C) permeabilising buffer (50mM NaCl, 3mM $MgCl_2.6H_2O$, 20mM HEPES, 0.1% (w/v) sucrose, 0.5% (v/v) TX-100 in PBS, pH 7.2), then blocked at 37°C with 1% (w/v) BSA in PBS, for 10 minutes. The blocking solution was replaced with primary antibody (1:50 for anti-tubulin (Sigma), anti-vimentin (Sigma), or 1:200 for anti-vinculin (clone hVin-1, Sigma) in 1% (w/v) BSA/PBS) and incubated at 37°C for 1-1.5 hours, then washed three times (5 minutes/wash) in wash buffer (0.5% (v/v) Tween 20 in PBS). Biotinylated secondary anti-mouse antibody (Vector Laboratories Inc., Burlingame, CA, USA) and Rhodamine- or Alexa 488-labelled phalloidin (Molecular Probes, Invitrogen, Glasgow, UK) were both added at 1:50 in 1% (w/v) BSA/PBS, and incubated for 1 hour at 37°C. The samples were washed three times in wash buffer, and then incubated with FITC-conjugated streptavidin (1:50, Vector Laboratories) for 30 minutes at 4°C, washed three times in wash buffer, and mounted using Vectashield (Vector Laboratories) mountant with DAPI or propidium iodide nuclear stains. Two 25 x 75 mm replicate slides were used for each experiment (*n*=2 grooved, *n*=2 planar).

2.3.4.2 Nucleoskeletal Staining (Optimised Protocol)

Cells were fixed in cold (-20°C) methanol for 2 minutes. The fixative was removed, and cells were washed three times in PBS, and then blocked for 1h in 3% (w/v) BSA/PBS at 37°C. The blocking solution was replaced with mouse anti-lamin A/C (1:50 in 1% (w/v) BSA/PBS; clone JOL3, Insight Biotechnology, Wembley, UK) or anti-lamin B1 (1:50 in 1% (w/v) BSA/PBS; clone 101-B7, Calbiochem, Nottingham, UK), and incubated at 37°C for 1.5h. After the primary antibody was removed, samples were washed three times in 0.1% (v/v) Tween 20 in PBS (5 min/wash, last wash 10 min), and placed in blocking solution for 10 minutes at 37°C. Samples were treated with secondary antibody, FITC-conjugated streptavidin and mounted as in Section 2.3.4.1, with the exception that washes were conducted with 0.1% (v/v) Tween 20 in PBS. Two 25 x 75 mm replicate slides were used in each experiment (*n*=2 grooved, *n*=2 planar).

2.3.4.3 Lamin B/Vimentin Double Staining (Optimised Protocol)

Cells were fixed, blocked and incubated in primary mouse anti-lamin B antibody and secondary antibody as above (Section 2.3.4.2). After washing, samples were incubated in FITC-conjugated streptavidin for 45 minutes at 4^{o}C. This was replaced with 3% (w/v) BSA/PBS and incubated overnight at 4^{o}C. Monoclonal anti-vimentin antibody (1:50, Sigma) was added and incubated at 37^{o}C for 1.5h. Samples were washed three times in 0.1% (v/v) Tween 20 in PBS, and then incubated with Texas Red conjugated anti-mouse secondary antibody for 1.5h at 37^{o}C. Samples were washed three times in 0.1% (v/v) Tween 20 in PBS and mounted in Vectashield mountant with DAPI stain. Two 25 x 75 mm replicate slides were used in the experiment (*n*=2 grooved, *n*=2 planar).

2.3.4.4 Nucleolar Staining – Propidium iodide

Cells were fixed in 3.8% (v/v) formaldehyde in PBS with 2% (w/v) sucrose for 10 minutes at 37^{o}C, permeabilised as described above in Section 2.3.4.1, and mounted in Vectashield mountant with propidium iodide. Four 25 x 75 mm replicate slides (*n*=4 grooved, *n*=4 planar) were used for the 3D reconstructions, and three 25 x 25 mm replicates (*n*=3 grooved, *n*=3 planar) were used for 2D microscopy.

2.3.4.5 Nucleolar Staining – RNASelect Stain

Cells were rinsed twice in warm PBS, fixed for 2 minutes in pre-chilled methanol (-20^{o}C), and rinsed twice with PBS. Cells were labelled with fresh SYTO® RNASelect stain (500 nM in PBS; prepared by a dilution series according to the manufacturer's instructions; Invitrogen) for 20 minutes, and washed three times in PBS.

2.3.5 Microscopy

2.3.5.1 Epifluorescence Microscopy and Generation of Image Overlays (Composites) from Immunofluorescence Images

Immunostained cells were imaged using an Axiovert 200 inverted fluorescence microscope (Carl Zeiss, Jena, Germany), and images were captured using a side-port CCD camera. Coloured composites were generated from monochrome immunofluorescence

images by adjustment of overall image brightness and contrast, followed by the creation of coloured overlays in Adobe Photoshop CS (Adobe Systems Inc., Ireland).

2.3.5.2 Confocal Microscopy, 3D Rendering and Image Analysis

Cells were imaged using an LSM 510 META confocal laser scanning microscope (Carl Zeiss, Jena, Germany). Cells were optically sectioned at 0.41 µm intervals with 1024x1024 resolution or greater, and projected into 3D at 64 angles of rotation (difference angle 6^{o}) with maximum transparency, using the LSM 510 software (Carl Zeiss). For surface reconstructions, the 3D module of the LSM 5 LIVE software (Carl Zeiss) was used to surface render stacks of optical slices, which were projected into 3D at 64 angles of rotation (difference angle 6^{o}). Brightness and contrast were adjusted to maximize visibility of structures using LSM 510, LSM 5 LIVE or Image J software (version 1.34s; Rasband, W.S., ImageJ, U.S. National Institutes of Health, Maryland, USA, http://rsb.info.nih.gov/ij/, 1997-2009). Screenshots of 3D images were captured at particular orientations of interest. Orthogonal sections were prepared using the 'Ortho' function in the LSM 510 software. Image J software, equipped with the LSM toolbox plugin, was used to measure the angles of orientation of nucleoli in 3D reconstructions.

2.3.5.3 Nucleolar Quantification

3D reconstructions of cells stained for nucleoli and actin were used to enumerate the length and orientation of nucleoli within the nucleus, relative to a horizontal axis (0^{o}, which corresponded to perfect alignment to the grooved pattern on the microgrooved substrate), using Image J software (version 1.34s; Rasband, W.S., ImageJ, U.S. National Institutes of Health, Maryland, USA, http://rsb.info.nih.gov/ij/, 1997-2009).

2.3.5.4 Lamin Scoring and Statistical Analysis

Images of nuclei immunostained for lamins A/C or B (40x magnification) were scored for the presence (score: 1) or absence (score: 0) of tubule-like structures or involutions. These scores were divided by the total number of nuclei examined in the group (*e.g.* all nuclei scored from the planar substrate), and these values were converted to a percentage. The binomial probability was calculated from the percentage data by converting the data to a fraction of 100, and thus examining the probability of success in

100 trials. The binomial probability was calculated using Microsoft Excel 2007 (Microsoft Corporation) according to the following equation:

$$b(x;n,p) = \binom{n}{x} p^x (1-p)^{n-x}$$

b (x; n, p): Binomial probability (the likelihood – statistical probability – that the number of 'successes' (frequency of nuclei with tubule-like structures, expressed as a decimal fraction of 100) will equal *x*).

p: The probability of 'success' in each trial (frequency of nuclei on the planar substrate containing one or more tubules, expressed as a decimal fraction of 100).

1 – *p*: The probability of 'failure' in each trial (probability that any given nucleus would not contain at least one tubular structure, expressed as a decimal fraction of 100; the remainder when the probability of 'success' has been subtracted from 1).

$\binom{n}{x}$: The number of combinations of *n* factors (100, due to the conversion of the frequency of tubule-like structures to percentages), with *x* items in each combination (percentage of tubule-like structures, expressed as a whole number).

These analyses tested the null hypotheses that there was no difference in the frequency of nuclei containing lamin (B or A/C) tubule-like structures or involutions between cells cultured on the planar and microgrooved substrates.

2.4 Results - Part 1: Cytoskeleton

2.4.1 *Actin*

On the planar quartz substrate, the 3D reconstructed cells were well spread, often with a polarised fibroblastic morphology, and the actin stress fibres extended into the periphery of the lamellipodium (Fig. 2-3A). In contrast, on the microgrooved quartz surface, the stress fibres were generally aligned to the topography, forming parallel struts traversing the full length of the cells (Fig. 2-3B, and also Fig. 2-6B); this was observed with both 2D epifluorescence and confocal microscopy. Using a 3D confocal approach, it was noted that on both substrates, these fibres appeared to predominate on the peripheral upper surface and 'sides' of the cells, with fewer fibres on the undersides or in the main volume of the cytoplasm. The stress fibres formed a cage-like structure over the cells,

presumably forming a structural support to the cells, and contributing to repositioning of the cytoplasmic contents. On the planar quartz substrate, one reconstructed cell showed evidence of indentation in the vimentin network, even across the nucleus, in response to overlying tension from actin stress fibres extending into a particularly lengthy membrane protrusion (Fig. 2-4).

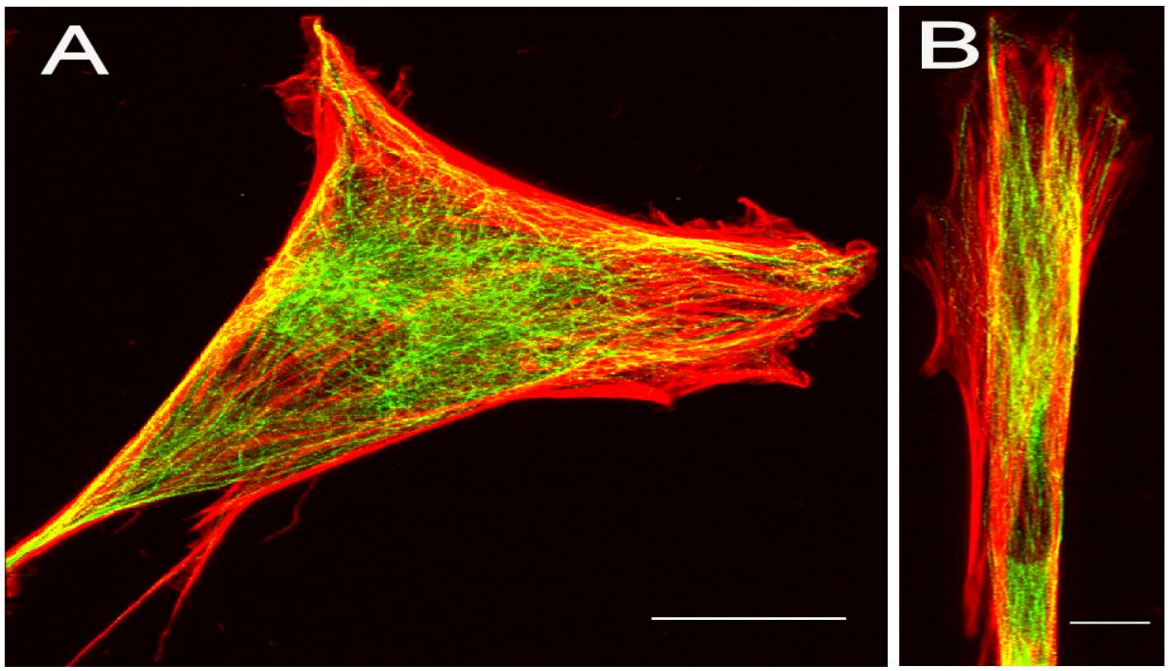

Figure 2-3. 3D reconstructions of fibroblasts cultured on planar (A) or 2 µm deep, 25 µm pitch (B) quartz substrates, co-stained for actin (red) and tubulin (green). *Note the expansive tubulin network in A, and the more compressed tubulin network in B, aligned to the topography, particularly across the nucleus. Bars: A - 20 µm, B – 10 µm. (n=2 planar, n=2 microgrooved 25x75 mm quartz substrata - multiple fields of view (>10) were examined on each surface for consistency with epifluorescence data, and then 2 representative cells were selected for reconstruction on each substrate).*

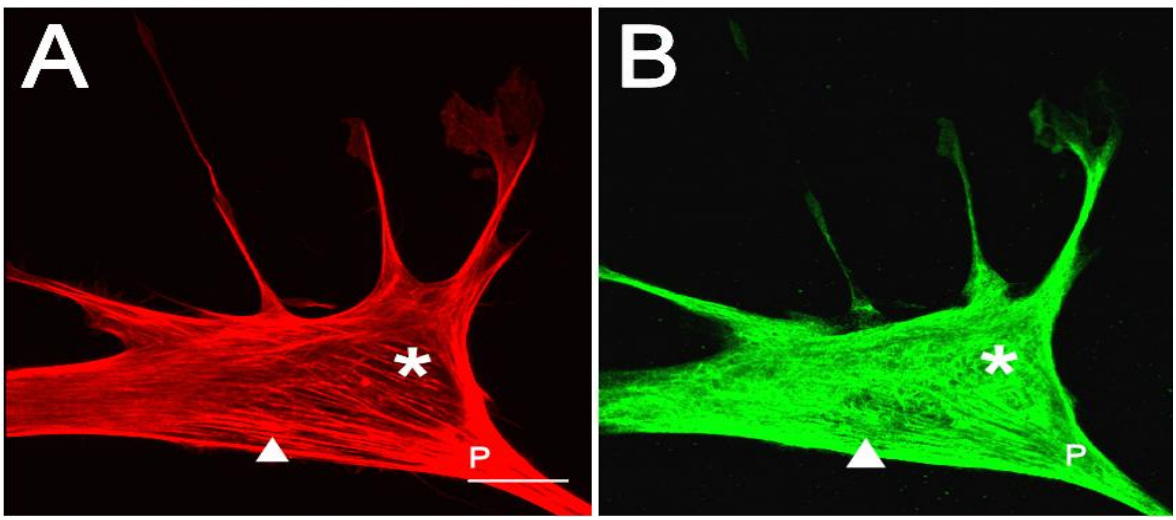

Figure 2-4. A 3D reconstruction of a z-stack series of optical sections at 0.41 µm intervals through a fibroblast cultured on a planar quartz substrate, co-stained for actin (A) and vimentin (B). *Note the group of tensile stress fibres in A (marked with an arrowhead), extending from a particularly long cell projection (marked 'P' in A and B) corresponding to an indented region in the underlying vimentin network in B (marked with an arrowhead), and the adjacent region where the vimentin filaments appear to be bulging upwards (marked * in B), corresponding to a gap in the actin filaments (* in A). Bar: 20 µm. (n=2 planar 25x75 mm quartz substrata - multiple fields of view (>10) were examined on the surfaces).*

2.4.2 Tubulin

Using 2D epifluorescence microscopy, it was noted that microtubules formed an expansive network on the planar quartz substrate, which was compressed by the lengthened cell morphology on the microgrooved quartz (Fig. 2-5). The tubulin network appeared quite aligned along the long axis of topographically elongated cells, particularly across the nucleus, presumably due to lateral confinement. Similarly, this could also be observed in cells on the planar substrate that adopted a more extended morphology (Fig. 2-5B).

Two reconstructed cells were examined in 3D for both the planar and grooved quartz surfaces. Consistent with the 2D observations, on the control, cells had well-organised tubulin networks (Fig. 2-3A), which appeared constrained on the microgrooved topography, where the cells had a tighter meshwork of tubulin filaments (Fig. 2-3B). This confinement appeared to result in the assembly of a 'cage' of aligned tubulin over the nucleus.

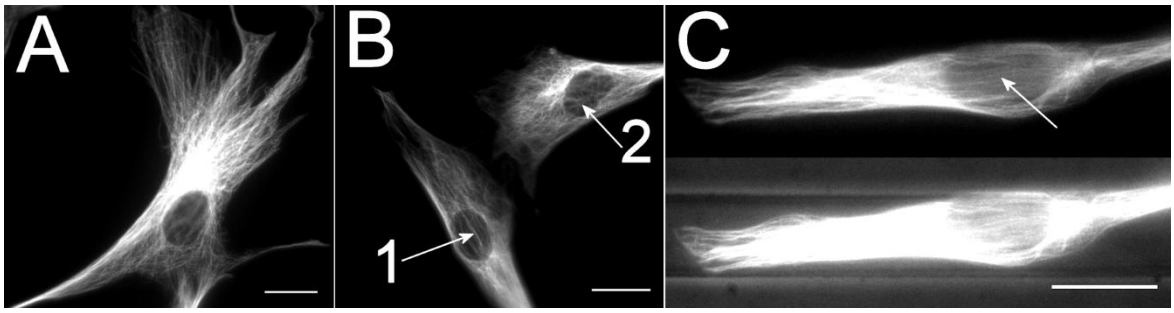

Figure 2-5. Epifluorescence microscopy of fibroblasts immunostained for tubulin. *A and B show cells on the control substrate, and C shows a cell on the microgrooved topography. Note the expansive microtubule network in A, and in the cell at the top right of image B. The microtubular network was more restricted in cells from the microgrooved topography (C), with evidence of the alignment of microtubules, particularly across the nucleus (arrow). Note that the cell with 'intermediate' morphology from the lower left of image B has character of cells from both the planar and microgrooved substrates (relatively expansive network but partially elongate morphology, with alignment of microtubules across the nucleus). Bars: 20 µm. (n=2 planar, n=2 microgrooved 25x75 mm quartz substrata - multiple fields of view (>20) were examined for consistency on each surface with both low- and high-power magnification, and representative cells were imaged on each substrate).*

2.4.3 Vimentin

On the grooved quartz surface, the vimentin network was evaluated in 3D for two cells, and appeared to show similar compaction to that observed for tubulin, with alignment of vimentin fibres across the nuclei (orientated in the direction of the long axis of the cells, along the grooves) (Fig. 2-6A). Fine detail of this alignment was observed

under high magnification with 2D epifluorescence microscopy (Fig. 2-6C). On the planar quartz surface, the 3D reconstructed cells showed expansive vimentin networks (Figs. 2-4B, 2-6B), with minimal evidence of the alignment of vimentin fibres across the nucleus, consistent with observations from 2D epifluorescence microscopy (Fig. 2-6D *cf.* Fig. 2-6C). On this substrate, the extent of such alignment of vimentin fibres across the nucleus varied with cell morphology: fewest aligned fibres were noted in highly spread cells, whereas more elongated cells tended to possess some aligned fibres. Speculative potential sites of attachment of vimentin to the nucleoskeleton suggested by visual observation are shown in Figs. 2-6C (grooved substrate) and D (planar substrate).

Interestingly, the cell that exhibited tension-induced indentation in the vimentin network in response to the overlying actin (Fig. 2-4) also exhibited a compensatory bulge (visible in the *z*-direction) in the vimentin network adjacent to the indented region.

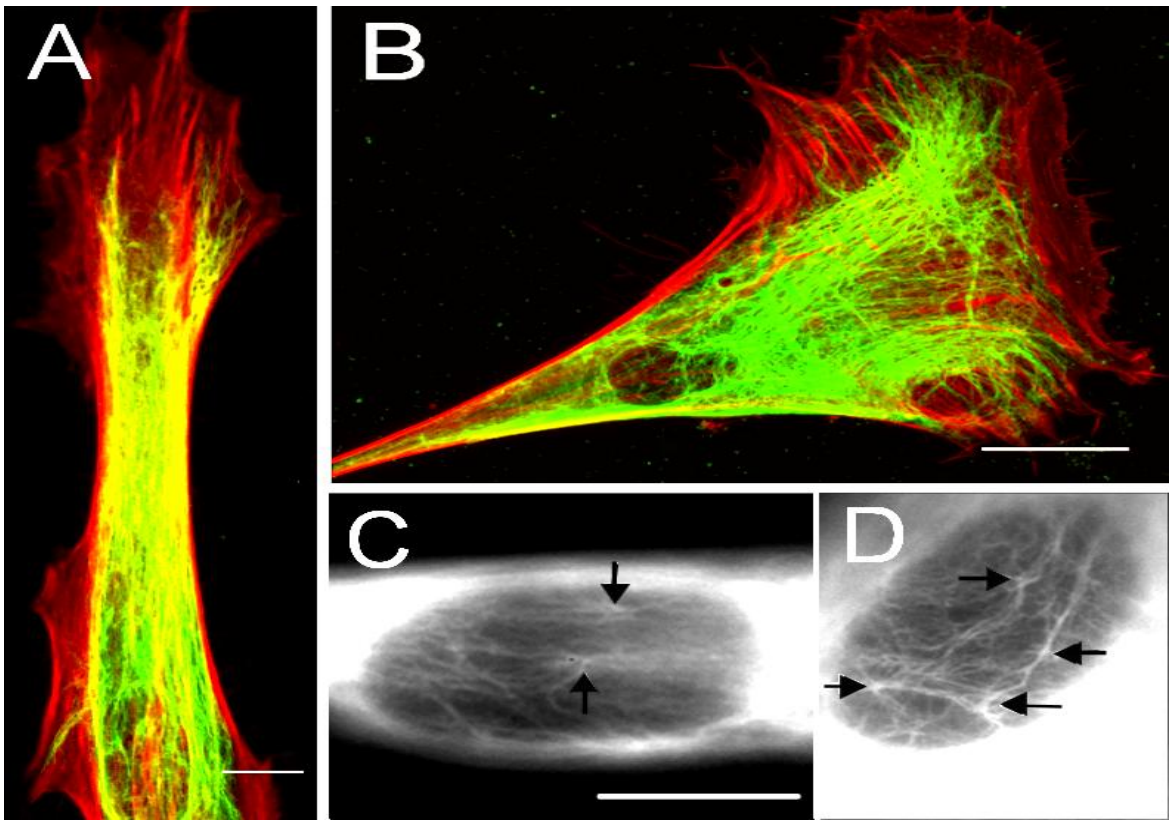

Figure 2-6. Alignment of vimentin by microgrooved topography. *A, B. 3D reconstructions of z-stack series (0.41 μm slice intervals) through fibroblasts cultured on 2 μm deep, 12.5 μm wide microgrooved quartz (A) or planar (B) substrates, co-stained for actin (green) and vimentin (red). C, D. 2D epifluorescence images of cells stained for vimentin, cultured on 2 μm deep, 12.5 μm wide microgrooved (C) or planar (D) quartz substrata. Note the possible sites of attachment of vimentin to the nuclear lamina in C and D (marked with arrows). Note the alignment of the vimentin fibres in A and C. Bars: A, C, D - 10 μm; B – 20 μm. (A, B: n=2 planar, n=2 microgrooved 25x75mm quartz substrata - multiple fields of view (>10) were examined on each surface for consistency with epifluorescence data, and then 2 representative cells were selected for reconstruction on each substrate. C, D: multiple fields of view (>20) were examined for consistency on each surface with both low- and high-power magnification, and representative cells illustrating features of interest were imaged on each substrate).*

2.4.4 Vinculin

Relative to those on the microgrooved substrate, cells on the planar quartz substrates had more focal adhesions (as judged by vinculin staining in 2D and 3D), which also tended to be larger than those in cells cultured on the grooved surface (Fig. 2-7A). On the topography, the reconstructed cells showed fewer, smaller adhesions that were generally aligned in the direction of the grooves. One reconstructed cell had a lamellapodial extension bridging from the groove (where the main cell body was located) on to an adjacent ridge, which, from qualitative observations appeared to contain a greater number of adhesions, which appeared to be orientated in a greater variety of directions (Fig. 2-7B).

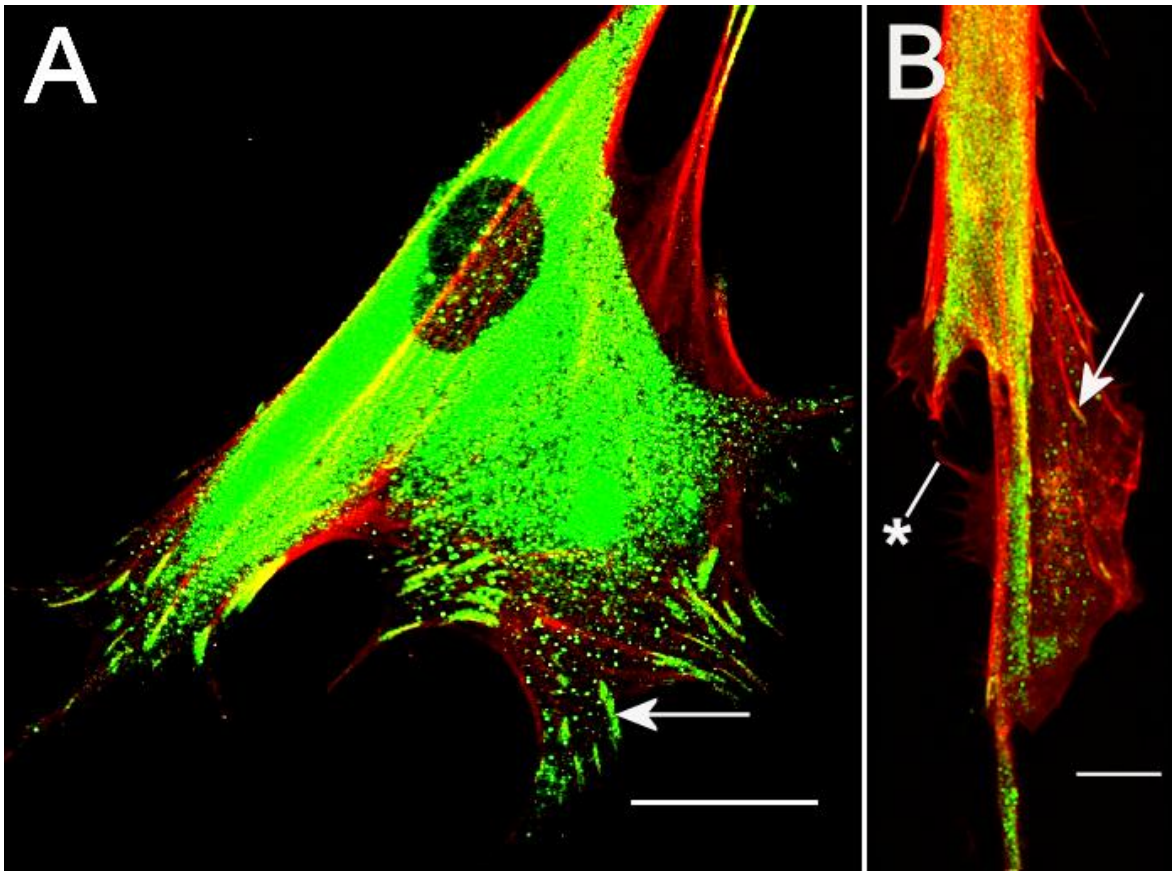

Figure 2-7. Vinculin reconstructions. *3D confocal reconstructions of fibroblasts immunostained for vinculin (green) and actin (red), cultured on planar (A) or 2 μm deep, 12.5 μm wide (B) microgrooved quartz substrata. Note the larger adhesions in A (an example is marked with an arrow), the smaller, less numerous adhesions in B (arrow), and the cellular projection exploring the substrate (marked *) in B. Bars: A – 20 μm, B – 10 μm. (n=2 planar, n=2 microgrooved 25x75mm quartz substrata - multiple fields of view (>10) were examined on each surface for consistency with epifluorescence data, and then 2 representative cells were selected for reconstruction on each substrate.)*

2.5 Results - Part 2: Nucleus, Nucleoskeleton and Nucleoli

2.5.1 Nuclei and Nucleoli

On the quartz microtopography, aligned cells tended to have more elongate nuclei than those on the planar substrate. The extension of the cell body to adapt to the confining substrate appeared to exert a mechanical pull on the nucleus, resulting in its reshaping. To examine the effect of this mechanostimulus on subnuclear structures, nucleolar positioning and morphology were studied. Nucleoli were selected since these structures are relatively large, occupy inter-chromosomal spaces, and as sites of ribosomal RNA (rRNA) production, their modulation could impact upon protein production. To examine nucleoli, the nucleic acid stain propidium iodide was used, which preferentially detects RNA over DNA. In general, this staining gave a strong nucleolar signal, due to rRNA, with a faint nucleoplasmic signal corresponding to DNA, and a relatively strong cytoplasmic signal, related to mRNA. RNASelect®, an RNA-specific dye, was used to confirm that the staining pattern was equivalent, and this dye also showed staining in the nucleoli and cytoplasm. PI was retained for the main study, however, as the RNASelect® staining was faint, and therefore unsuitable for confocal analysis (results not shown). From visual observations, on the control quartz surface, nucleoli generally appeared more rounded and flattened than on the topographical substrate, and were present both centrally and peripherally within the nucleoplasm. Fig. 2-8A shows orthogonal sections through a nucleus with three nucleoli, one of which is centrally located, rounded and flattened in the *z*-direction, and another, present at the edge of the nucleus that appears squashed by the nuclear boundary. This also seems to have promoted its extension in the *z*-direction, and suggests that it is the confines of the nucleus and the mechanical constraints imposed upon it that directs nucleolar positioning. Consistent with this, in cells aligned by the topography, the nucleoli tended to be found in the central nucleoplasm and align along the long axis of the nucleus. Fig. 2-9 illustrates that most nucleoli were aligned by the topography (73.3% of nucleoli had angles of orientation of 0-20^{o}) whereas there was a greater spread of nucleolar angles of orientation on the planar surface (only 21.8% of nucleoli were orientated within 0-20^{o} of the horizontal axis).

Where nuclear elongation was marked, and the nucleoli were well aligned, the nucleoli generally also extended in the *z*-direction, probably in response to the lateral

restrictions imposed by the topography. In addition, when nuclei were bridging between adjacent groove-ridge boundaries, with the main volume of the nucleus located within the groove, the overhanging regions of nuclei were generally compressed in the *z*-direction on the ridges, and typically devoid of nucleoli. It is likely that this nuclear compaction would present a mechanical obstruction to the nucleoli, and probably other subnuclear structures such as chromosome territories. The orthogonal sections shown in Figs. 2-8B1 and 2-8C1 illustrate this topography-induced nucleolar alignment and extension. Fig. 2-8C is also an example of nucleolar restriction within the groove, where a cell had been bridging between a groove and a ridge. The nucleolus appears to have been strongly aligned and restricted to a position within the groove by nuclear deformation at the groove edge boundary. Fig. 2-8D shows an optical section of a cell where the nucleolus has been confined to the ridge. Interestingly, this appears to be the result of a zig-zag arrangement of actin within the groove, which is likely to have prevented the nucleoli from entering the rest of the nucleus in the groove, resulting in relatively strong alignment of the nucleoli at the groove-ridge boundary.

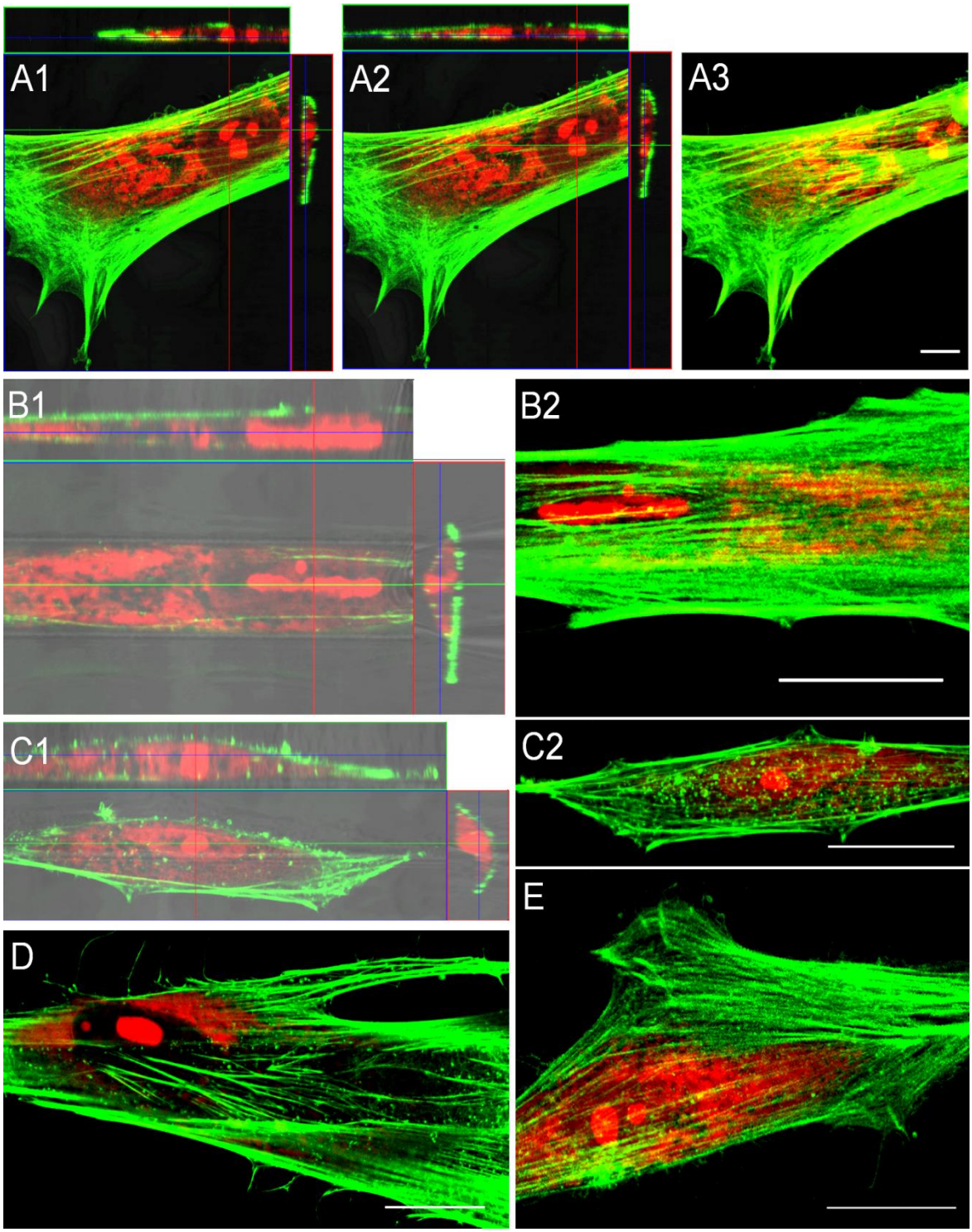

Figure 2-8. Nucleolar confinement by the cytoskeleton and microgrooved topography. *Orthogonal sections of fibroblasts on planar quartz (A1, A2) and microgrooved (2 µm depth x 25 µm pitch) topography (B1, C1). 3D reconstructions of the same cells are shown in A3, B2 and C2. A 2D optical section of a cell on the microgrooved topography is shown in D, and a 3D reconstruction of a cell with an 'intermediate' nucleolar morphology (rounded, flattened nucleoli that are located along the central axis of the nucleus) on the planar substrate is shown in E. Note the nucleolar alignment (B), elongation in x (horizontal) and z- (vertical) directions (B) and confinement by groove-ridge boundaries (C, D) on the micrgrooved substrate, versus the more flattened, rounded nuclei on the planar substrate (A, E). Red – RNA/DNA, Green – Actin. Bars: A3 – 10 µm; B2, C2, D, E – 20 µm. (Multiple fields of view (>10) were examined for consistency with epifluorescence data on each surface, and representative cells illustrating features of interest were imaged on each substrate).*

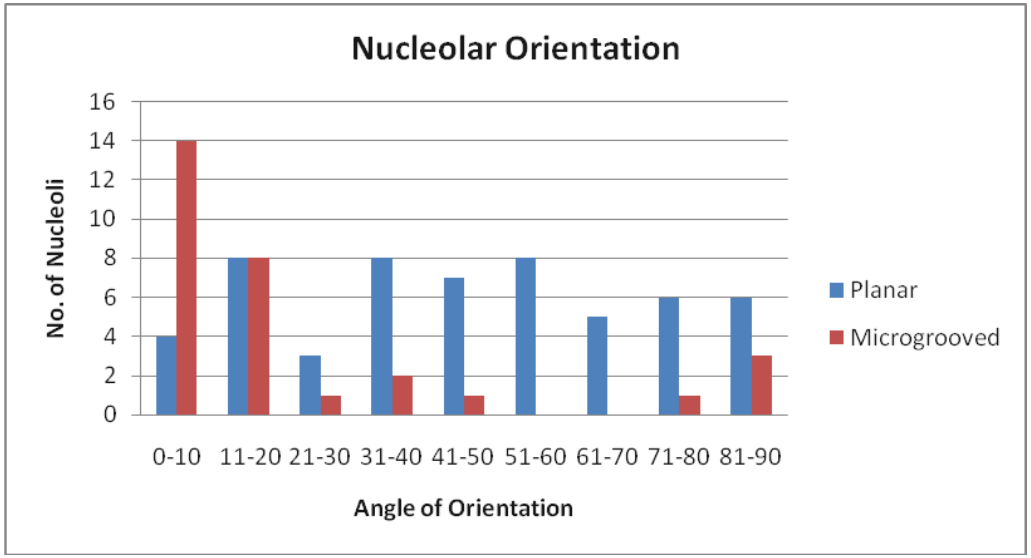

Figure 2-9 (left). Orientation of nucleoli in the nuclei of cells cultured on quartz microgrooved (25 µm pitch x 2 µm depth) and planar surfaces (n=30 nucleoli on microgrooved substrate, n=55 nucleoli on planar surface). *On both surfaces, $0^{o}C$ is the horizontal axis, which represents complete alignment along the grooves in cells on the microgrooved topography. Measurements were obtained from confocal 3D reconstructions of cells on both substrates. The difference in nucleolar orientation between the substrata was considered significant at $p<0.01$ using a Mann-Whitney Rank Sum Test.*

Figure 2-10 (below). Fibroblasts cultured for 7 days on microgrooved (25 µm pitch x 2 µm depth) (A) and planar (B, C) quartz substrates. *Note the predominance of centrally located, aligned nucleoli within the elongate nuclei in A and C (areas of higher cell density), versus the variety of nucleolar orientations in B (at an area of the substrate with a lower cell density). Arrows indicate regions on the topography where nucleoli were confined to ridges. Key: A, C – RNA/DNA, B - blue – actin, red – RNA/DNA. Bars: 50 µm. (n=3 planar, n=3 microgrooved substrata; multiple fields of view (>20) were examined for consistency on each surface, and representative cells illustrating features of interest were imaged on each substrate).*

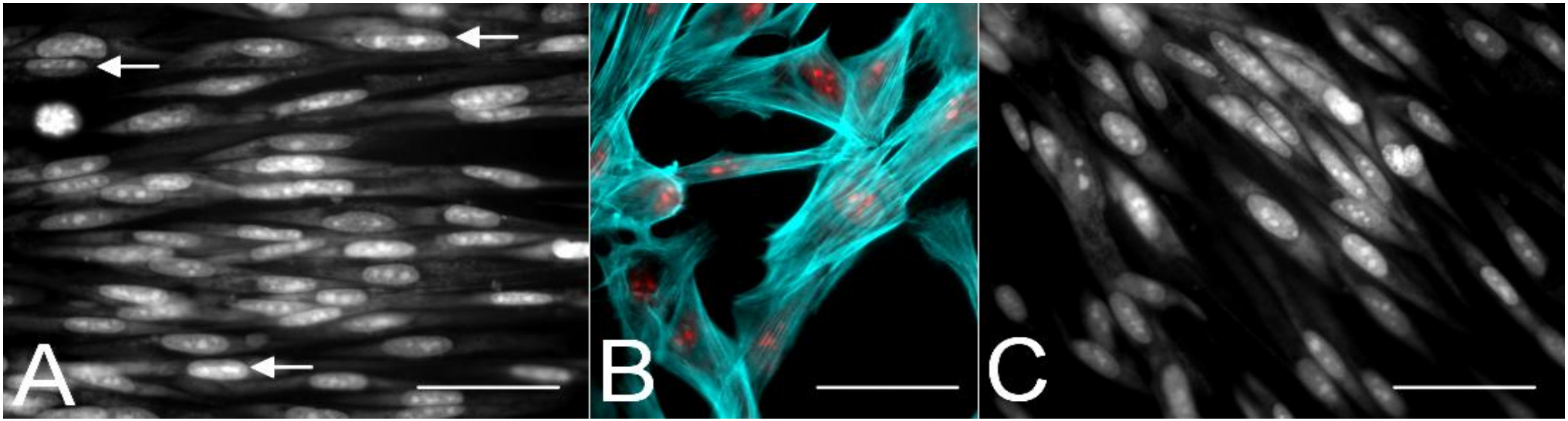

The nucleolar alignment effect appeared to follow a continuum based on cell morphology. The most laterally and longitudinally spread cells on the planar substrate typically showed the most rounded nuclei and nucleoli, with topographically aligned cells containing elongate nuclei and nucleoli at the opposite end of the spectrum. Cells of 'intermediate' morphology were also observed on the planar substrate. The cell in Fig. 2-8E, for example, had a fairly lengthened cell body and nucleus, with centrally located nucleoli, but the nucleoli were still relatively rounded and flattened, as assessed qualitatively. It seems likely that at low cell density, these effects are related to cell motility, with highly spread cells likely to have more focal adhesions and a more flattened cytoskeletal arrangement than those exhibiting bipolar or near-bipolar morphologies.

Preliminary data suggests that this effect can become more marked with increasing groove depth (5 µm depth x 25 µm pitch PDMS grooves were also examined). Cells were strongly aligned by the deeper topography and exhibited exaggerated nucleolar elongation. In addition, it was noted that a defect in the pattern that formed a narrow ridge (approximately 1-2 µm in width) on the quartz microgrooves could induce very neat nucleolar confinement (Fig. 2-11).

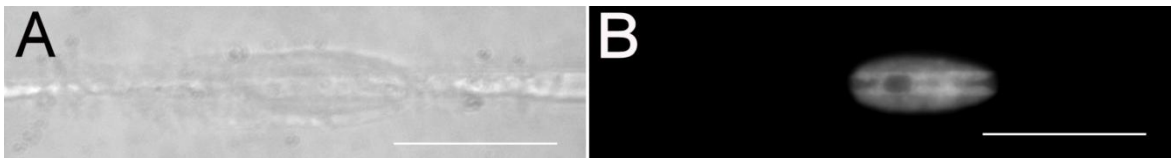

Figure 2-11. Tight nucleolar confinement by a pattern defect in the microgrooved substrate. *The narrow ridge, a pattern defect present in a small area of one of the microgrooved structures (visible in the phase contrast image, A) tightly confined the nucleolus (darker ellipse visible within the nucleus in B) in this cell. The nucleus was also indented by the underlying ridge-like topography (darker line along centre of nucleus). A – phase contrast image, B – stained for DNA. Bars: 20 µm.*

Together, these data suggest that nucleolar morphology can be modulated by contact guidance, apparently on a continuum with the extent of the elongation.

2.5.2 Relevance of Nucleolar Observations to Cells in Tissue Culture

Preliminary data showed that after 7 days of culture on the quartz substrates, the cells had formed a near-confluent monolayer on the majority of the surface of both the planar and microgrooved substrates. The fibroblasts were aligned to each other by intercellular contact, and on both substrates the nuclear and nucleolar morphology approximated that of aligned cells on the microgrooved topography at the earlier time-point (Fig. 2-10 A, C). In areas of higher cell density, nuclei and nucleoli were highly

elongate, suggesting that this morphology may more closely represent the situation in tissue culture, and perhaps also *in vivo*, where fibroblasts are a naturally aligning cell type. This was also noted in cells in tissue culture flasks, where lengthened cells had aligned nucleoli, and those with well-spread cell bodies had rounded nuclei and unaligned nucleoli. In confluent cultures, the nucleoli were aligned and centrally located within the nucleus. This suggests that single cells on the topography share a greater morphological similarity with cells from confluent monolayers on planar surfaces than with monodisperse cultures on the planar quartz substrate.

2.5.3 Nucleoskeleton: lamin B

The nucleoskeletal protein lamin B was also examined on the quartz substrates. The staining was localised to the nuclear periphery, and present in foci within the nucleoplasm. On both the planar and grooved substrata, speckles of lamin B were generally found to be associated with nucleoli, often forming ring-shaped clusters around these structures that could be observed with epifluorescence microscopy (Fig. 2-12). Interestingly, these speckles appeared to be redistributed by the grooved topography, and could often be noted in the central nucleoplasm, presumably as a consequence of the constraints on the nucleus resulting in redistribution of these structures.

When high-resolution 3D confocal reconstructions were generated from three nuclei from the planar substrate, and four nuclei from the grooved substrate, it was noted that some of the punctate staining of lamin B corresponded to partially or fully transnuclear tubule-like structures (Fig. 2-13A). From the 3D reconstructions (n=3 nuclei reconstructed per substrate), the lamin B tubular structures appeared to be more prevalent on the planar structure than the grooved surface, where speckles appeared to predominate (Fig. 2-13B).

This result suggested that the frequency of tubule-like structures might be different between the grooved and planar substrates. Following the reconstruction of an additional lamin B-stained nucleus on the grooved substrate, however, it was revealed that a number of transnuclear laminal structures were present, and arranged in a fence-like pattern along the central plane of the nucleus, presumably due to topographic confinement (Fig. 2-14). This nucleus was also bridging between an adjacent groove and ridge, and showed evidence of an involuted region with an enrichment of shorter lamin B tubular structures, perhaps acting as a structural reinforcement to prevent additional compaction at this site.

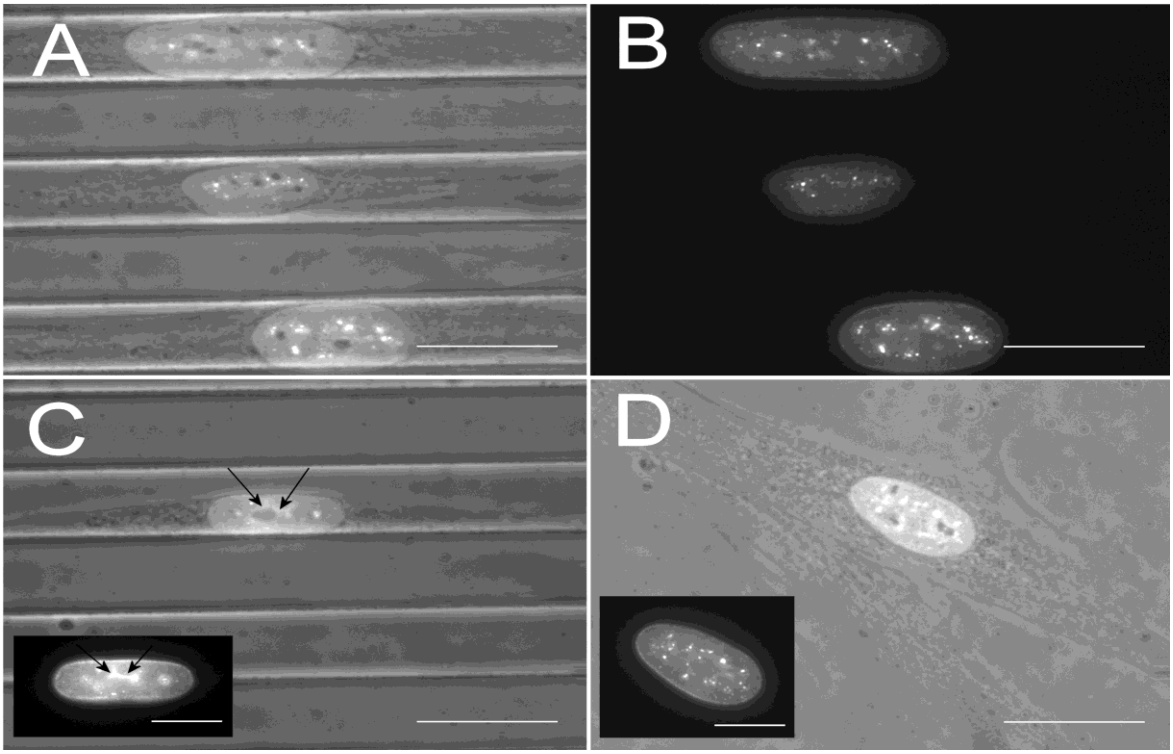

Figure 2-12. Lamin B speckles cluster with nucleoli on control and microgrooved substrata. *Lamin speckles were generally clustered close to nucleoli, particularly on microgrooved substrates. Such clusters often encircled nucleoli (particularly evident in A and D). A, C and D show phase contrast images of cells on microgrooved (A, C) or planar (D) substrates where the fluorescent label has been simultaneously excited to allow visualisation of cell morphology and lamin B. B, and inset images in C and D, show only the signal from lamin B, corresponding to the phase contrast images shown in A, C and D, respectively. Note that a tubule-like structure appears to tightly confine the shape and positioning of the nucleolus in C (arrows). Bars: A-D: 20 μm, insets in C and D: 10 μm. (n=2 planar, n=2 microgrooved substrata; multiple fields of view (>20) were examined for consistency on each surface).*

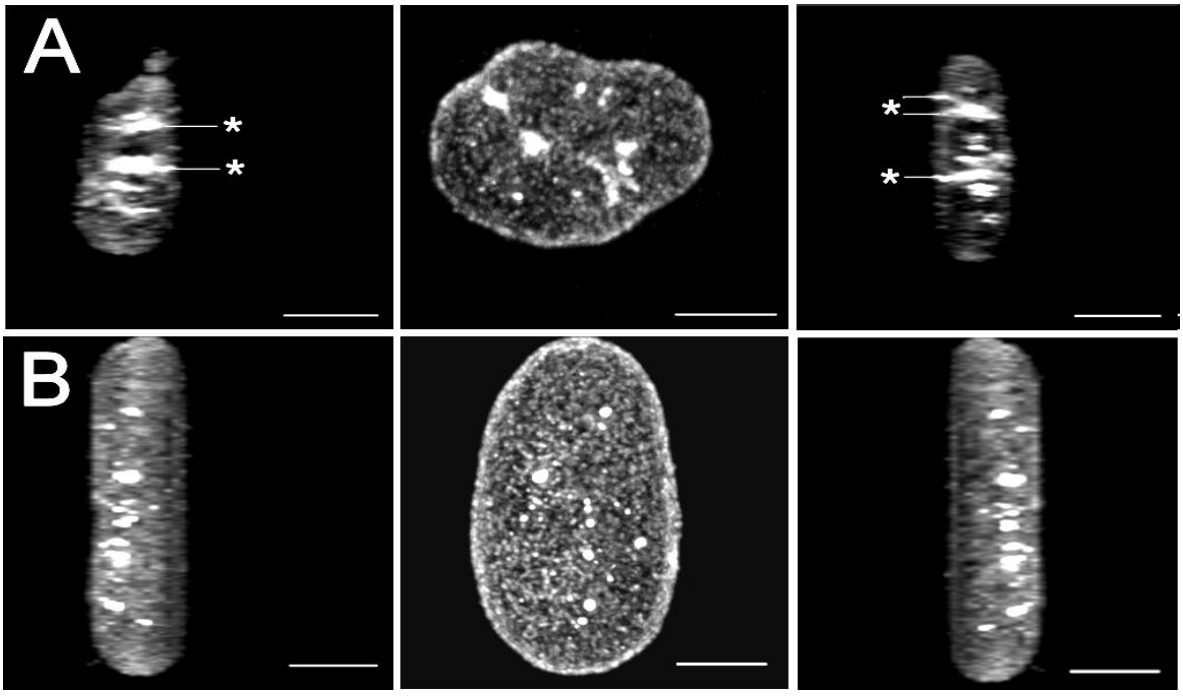

Figure 2-13. 3D projections of confocal z-stacks of lamin B immunostained nuclei from cells cultured on planar (A) and quartz microgrooved (2 μm depth, 25 μm pitch) (B) substrates. *From left-right, images show left (z-direction), top (x-y direction), and right (z-direction) views of the reconstructed nuclei. Note the transnuclear tubule-like structures (*) in A, and speckles in B. Bars: 5 μm. (n=2 planar, n=2 microgrooved substrata; multiple fields of view (>10) were examined for consistency with epifluorescence data on each surface, and representative cells were imaged on each substrate).*

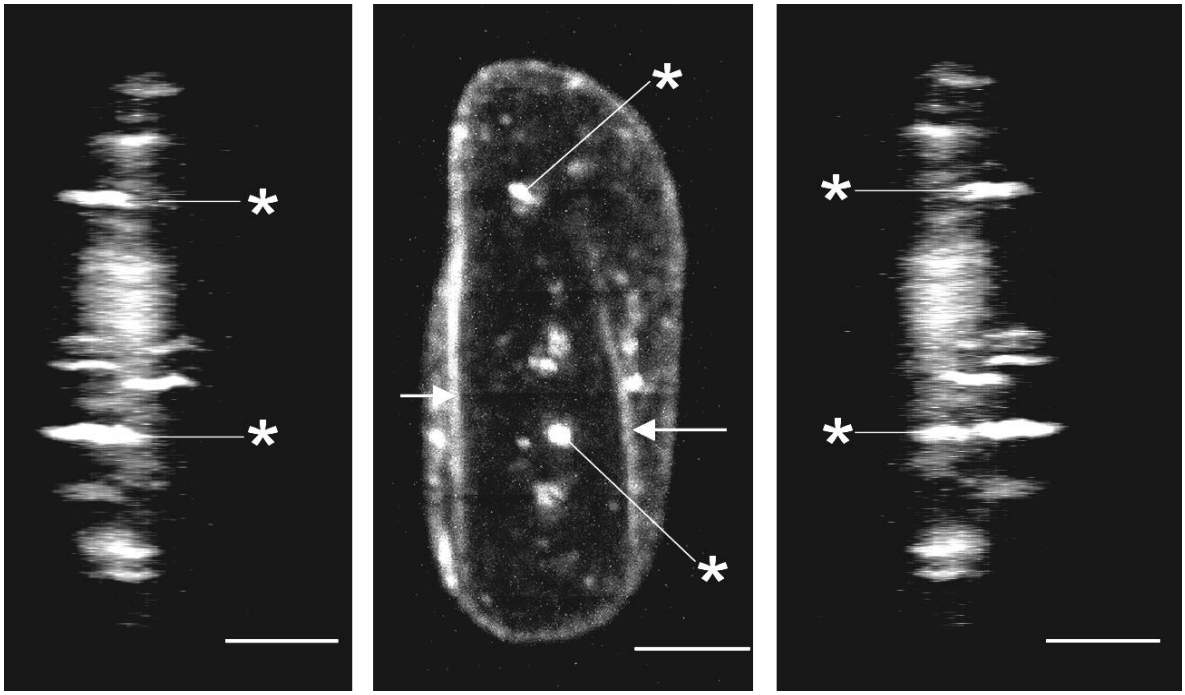

Figure 2-14. 3D projection of confocal optical sections (0.41 µm intervals) through a lamin B immunostained nucleus from a fibroblast cultured on the quartz microgrooved (2 µm depth, 25 µm pitch) topography. *From left-right, images show left (z-direction), top (x-y direction), and right (z-direction) views of the reconstructed nucleus. Note the presence of two large nuclear involutions (arrows) and a number of aligned tubule-like structures within the central nucleoplasm; some of the larger tubular structures are marked with an asterisk (*). Bars: 5 µm. (n=2 planar, n=2 microgrooved substrata; multiple fields of view (>10) were examined for consistency on each surface, and representative cells were imaged on each substrate).*

To assess the prevalence of tubular structures in cells on the planar and grooved substrates in a larger number of cells, an epifluorescence microscopy strategy was adopted. Although it was acknowledged that this would not enable visualisation of completely vertical structures, it allowed larger numbers of nuclei to be examined, since the technical difficulty and time required to generate large numbers of sufficiently high-resolution reconstructed nuclei made this unfeasible in the context of this multi-level study. To attempt to account for this, cells were scored only for the apparent presence or absence (rather than number) of tubular structure(s) and nuclear involutions, on the assumption that the visible oblique structures would account for only a proportion of the possible structures, as was suggested by the reconstructions. Fig. 2-15 shows that on the planar substrate, approximately 45% of nuclei examined (n=144) possessed at least one tubular structure. On the grooved substrate, in contrast, only 21% of nuclei (n=147) had detectable tubule-like structure(s). Using a binomial probability test, this corresponded to a highly significant p-value of $p = 1.22 \times 10^{-7}$. Nuclei were also scored for the presence or absence of involutions (nuclear infolding, visible in the lamina) (Fig. 2-15). On the planar substrate, approximately 24% of cells had such structures, whereas only 17% of cells on

the grooved substrate possessed such features. This was significant at $p<0.05$ using a binomial test ($p = 0.025$).

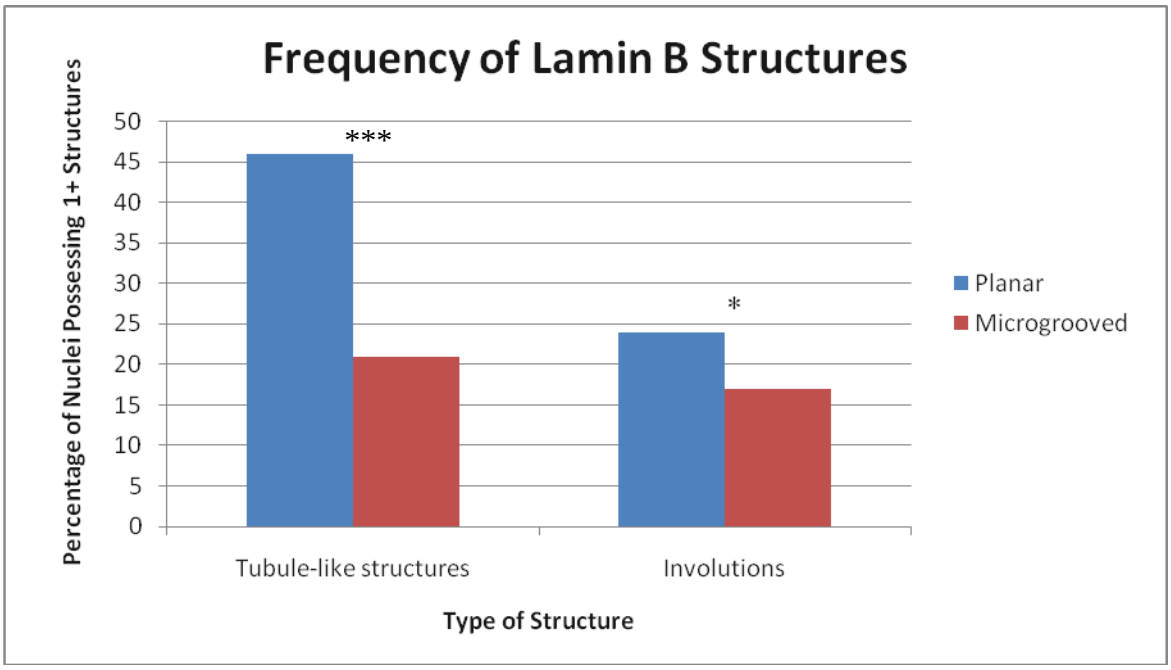

Figure 2-15. Graph of frequency of lamin B tubule-like structures and involutions in fibroblasts cultured on planar and microgrooved (2 µm depth x 25 µm pitch) quartz substrates. **** Denotes significance at $p < 1 \times 10^{-6}$ and * denotes significance at $p < 0.05$, using a binomial test. n = 144 nuclei (from n=2 planar substrata), n = 147 nuclei (from n=2 microgrooved substrata).*

2.5.4 Nucleoskeleton: lamin A/C

On the planar quartz substrate, lamin A/C was present at the periphery of the nucleus, and in discrete intra-nuclear speckles. In aligned cells on the microgrooved quartz, the lamina appeared to elongate in accordance with the stretched nuclei. Speckles were also noted in nuclei on the microgrooved substrate. The speckles sometimes clustered together, but did not generally appear to be associated with nucleoli. The frequency of lamin A/C with one or more tubule-like structures was reduced from 32% of nuclei (n=190) on the planar substrate, to 18% of nuclei (n=182) on the microgrooved substrate, which was considered highly significant in a binomial probability test ($p<0.001$) (Fig. 2-16). Relatively few cells had lamin A/C involutions, but the frequency of involutions appeared to be increased on the microgrooved substrate ($p<0.05$) (Fig. 2-16).

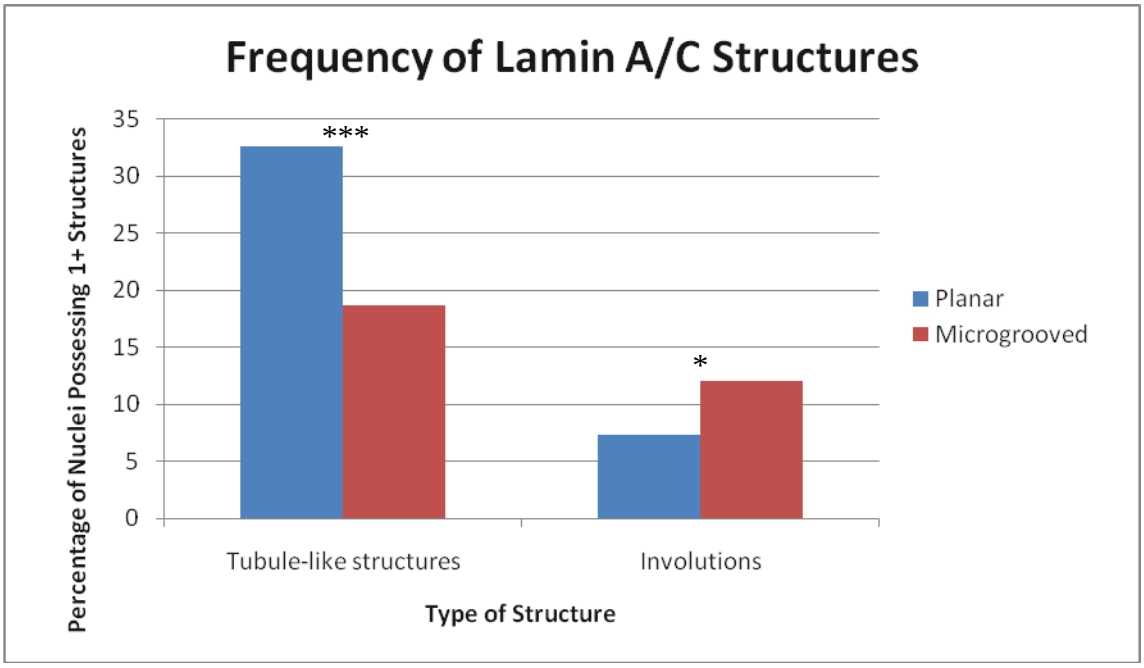

Figure 2-16. Graph of frequency of lamin A/C tubule-like structures and involutions in fibroblasts cultured on planar and microgrooved (2 µm depth x 25 µm pitch) quartz substrates. **** Denotes significance at $p < 0.001$ and * denotes significance at $p < 0.05$, using a binomial test. n = 190 nuclei (from n =2 planar substrata), n = 182 nuclei (from n=2 microgrooved substrata).*

2.6 Discussion

Compared with cells cultured on the planar controls, fibroblasts on the microgrooved topography had fewer, smaller adhesions. This suggests that the confinement of the substrate limits adhesion formation, and would be expected to have downstream effects on chemical signalling. A previous study showed that reduced levels of the scaffolding protein RACK1 could promote contact guidance on a grooved substrate with micron-scale width (12.5 µm) and nano-depth (350 nm) (Dalby et al., 2008). Given that the accessibility of binding sites for signalling proteins can be affected by cell stretch (Sawada and Sheetz, 2002a), and that over-expression of RACK1 impaired contact guidance on nanogrooves (Dalby et al., 2008), it seems likely that the microgrooved topography would have affected the assembly of signalling complexes at focal adhesions, since these mediators are becoming implicated in cell alignment to microgrooves.

In both the 2D and 3D cytoskeletal studies, there was evidence of alignment of vimentin, tubulin and actin along the long axis of the cells on the grooved topography, particularly across the nucleus. On the planar substrate, cells generally had well-organised, expansive cytoskeletons. This is consistent with other research (Kurpinski et al., 2006; Oakley and Brunette, 1993; Walboomers et al., 1998), which has been extended in the current study by the use of quartz substrates, and particularly by the evidence of alignment

in 3D, and across the nucleus, on the grooved substrata. Consistent with the tensegrity model, the actin stress fibres appeared to form the tensile element of the cytoskeleton, and had the potential to contribute to nuclear reshaping and downstream redistribution of subnuclear components. This is supported by research indicating that nuclear shrinkage occurs upon the chemical depolymerisation or targeted ablation of actin filaments (Mazumder and Shivashankar, 2010). Extreme tension of the actin filaments could lead to indentation of the underlying vimentin network, as noted in a cell on the planar substrate (Fig. 2-4). This is consistent with the existence of a pre-stress component within the tensegrity model. The interaction between these cytoskeletal elements is likely to affect the induction of mechanical effects in the nucleus, since both of these filaments are linked to the lamina, via nesprins and SUN domain proteins. This suggests that the tensile force from the sites of cell adhesion resulted in redistribution of the underlying intermediate filaments in this cell (Fig. 2-4). It appeared to have caused constriction of the vimentin network at the site where a long cellular projection met the cell body, and forced the intermediate filaments into the surrounding cytoplasm, resulting in the localised 'ballooning' effect a short distance away. There was a concurrent gap in the actin filaments at this region, suggesting that the swollen bulge of intermediate filaments underlying this area may have disrupted the arrangement of stress fibres. Alternatively, a pre-existing absence of stress fibres at this site may have allowed the vimentin fibres to bulge upwards. It is likely that this 'bulging' response compensated for the tensile squashing of the underlying cytoskeleton and cytoplasm, and contributed to mechanical redistribution of subcellular components via physical attachment (*e.g.* cytoskeletal tugging on the nucleoskeleton causing nuclear reshaping) and indirect 'squeezing' of the cytoplasmic contents. Such a balance of responsiveness between the intermediate filaments and the actin cytoskeleton is also supportive of the concept of pre-stress, as described in the tensegrity model.

In the tensegrity model, microtubules act to bear compression, and oppose the tensile forces from overlying tensile actin filaments. Microtubules were relatively aligned in cells on the grooved topography, particularly across the nucleus. It is likely that the lateral confinement of the grooved topography contributed to compaction of the microtubular network, perhaps to increase compressive force on the nucleus in the *z*-direction, and balance out the tensile strain acting along the long axis of the cell. Consistent with this, depolymerisation of microtubules with nocodozole led to nuclear expansion in murine fibroblasts, suggesting that the nucleus is typically subject to compression from the microtubular network (Mazumder and Shivashankar, 2010).

Within the nucleus, there was evidence of reorganisation of the laminar nucleoskeleton by the topography, including a modest change in nuclear involutions. It seems likely that the redistribution of the lamin proteins would impact upon the structural properties of the nucleus, or on the nucleo-cytoplasmic transport of small molecules and RNA. If these changes, or the alterations in nucleolar morphology, impacted upon the production or transport of rRNA or mRNA, it is probable that there would be downstream effects on protein production. The nucleolar morphology in cells cultured on the grooved topography most closely approximated that of cells in confluent monolayers cultured on tissue culture plastic (or the quartz substrates). It is possible that the topographical mechanostimulus promoted the cells to exhibit some of the character of cells within a confluent monolayer or tissue, if the analogous nucleolar morphology or chromosomal positioning resulted in a related cellular transcript and protein profile. This would require additional research, but is unlikely to be completely identical between the topography and the tissue context, in the absence of intercellular cues that would be present in the confluent cell layers. The dynamic reorganisation of the nucleoli and lamina should serve as a useful indirect marker of changing chromosomal positioning on the topography. In addition, the association between these structures is likely to contribute to the spacing and redistribution of chromosomal territories, since both occupy inter-chromosomal regions. Furthermore, it seems that rather than the topography having a direct effect on nucleolar positioning, with the possible exception of the narrow feature of the structural defect, it is the nuclear shape and orientation imposed by the microgrooved substrate that is the important feature in relocating the nucleoli. Consistent with this, Chou et al. showed that cells on a microgrooved topography (3 μm depth x 6-9 μm pitch) were 'taller' in height (*z*-direction) than those on a planar substrate, presumably due to lateral confinement, which is consistent with the apparent extension of nucleoli in the *z*-direction in this study (Chou et al., 1995). Nuclear reorganisation and repositioning of subnuclear components is also consistent with the tensegrity model, since the model predicts the existence of multiple inter-connected tensegrity units within the cell, from the outer cytoskeletal unit, to the inner nucleoskeletal tensegrity unit within the nucleus.

Epifluorescence observations suggested that lamin B speckles were often closely associated with nucleoli. This is consistent with the work of Fricker et al., who showed that a proportion of intranuclear tubular structures extending from the nuclear periphery into the nucleus, detected with lipophilic dyes, were associated with nucleoli (Fricker et al., 1997). The authors also noted that these structures could be co-stained for lamin A/C and

concavalin A, suggesting that the tubular structures contained both laminar and membrane components. These are likely to be the same type of structures as were documented in this study, and by Broers et al., for lamin A/C (Broers et al., 1999), and related to those noted for lamin B in 2- and 3D in this thesis. From the 3D reconstructions, it appeared that the grooved topography could induce the reorganisation and even alignment of the transnuclear lamin B 'tubules'. The formation of a fence-like arrangement of these structures in one reconstruction from a cell on the 2 μm deep microgrooved topography was strikingly suggestive that these structures could have the ability to partition the nucleus and confine the positioning of subnuclear components. This was supported by 2D microscopy showing that such tubular structures could confine nucleoli. Lamin B speckles have also been shown to co-localise with components of the DNA replication machinery, such as proliferating cell nuclear antigen (PCNA) (Moir et al., 1994; Moir et al., 2000a). The marked decrease in the number of nuclei with visible tubule-like structures on the grooved topography is strongly suggestive that the topography was affecting their assembly or arrangement, which is consistent with the results from the 3D reconstructions.

Disruption of the lamin B nucleoskeleton can interfere with DNA replication, which was demonstrated using dominant negative lamin B constructs (Moir et al., 2000a) and transcription, using siRNA directed against the protein (Tang et al., 2008). Topography-induced modulations in the number or assembly of lamin B tubules seem likely to affect nucleo-cytoplasmic transport, transcription or DNA replication, although this would require additional investigation. Interestingly, Thakar et al. showed that the 3D volume of SMC nuclei was affected by altering the adhesive surface area available to cells, via μCP protein patterning (Thakar et al., 2009). In contrast, the nuclear volume appeared to be unaffected in cells cultured on microgrooves, although the nuclei were more elongate. This correlated with a reduction in DNA replication and a decreased proliferative index in cells on the microgrooves. It is possible that modulation of the nucleoskeletal organisation contributed to changes in DNA synthesis, via the interaction with proteins such as PCNA, or altered distribution of other factors.

2.7 Conclusion

The microgrooved topography promoted cell alignment, an elongate cell morphology, and cytoskeletal reorganization, and the changes were consistent with the tensegrity model. Within the nucleus, the nucleoskeleton was rearranged, and both lamin

A/C and lamin B tubule-like structures were reduced in frequency, which might contribute to alterations in processes such as DNA replication and nucleocytoplasmic transport. Alignment of lamin B tubule-like structures on the microgrooved topography also had the potential to partition the nucleus. Lamin B tubule-like structures could also confine nucleoli. In conjunction with nuclear elongation, such architectural rearrangements of the lamina are highly likely to have contributed to the repositioning and remodeling of nucleoli. This could potentially alter rRNA production or transport, and was suggestive of effects of chromosomal territories. Together, the data from this chapter support the involvement of cytoskeletal and nuclear reorganisation in direct mechanotransduction induced by a topographical mechanostimulus.

3 Transcriptomic Analysis

3.1 Introduction

In view of the considerable cytoskeletal remodelling and nuclear alterations induced by the topographical mechanostimulus (Chapter 2), it was logical to attempt to characterise the downstream effects on gene expression. A microarray study was used to investigate this, as the technique allows the comparison of the relative abundance levels of a large number of cellular transcripts between control and one or more test conditions (in this case, cells cultured on planar and microgrooved quartz substrates). The aim of the microarray study was to produce an overview of the functional classes of topography-responsive genes and highlight specific differentially abundant transcripts with potential relevance to topographic mechanotransduction.

There have been a number of previous microarray studies of the cellular response to topography. Culture of mesenchymal stem cells on 330 nm deep nanogrooves stimulated differential expression of genes involved in MAPK signalling, which is a key pathway involved in the modulation of cell growth and differentiation (Biggs et al., 2009). On nanogrooves with a 10 μm pitch, human osteoprogenitor cells typically had smaller focal adhesions compared with cells cultured on 100 μm pitch grooves of the same depth, which correlated with mRNA-level differences in the capacity of the substrates to promote osteogenic differentiation. In addition, transcripts involved in integrin and PDGF signalling were down-regulated in cells cultured on the 10 μm pitch nanogrooves, whereas transcripts corresponding to these pathways were up-regulated in cells cultured on nanogrooves with a pitch of 100 μm (Biggs et al., 2008). On two low adhesion nanotopographical substrates (square and hexagonal arrays of nanopits), mesenchymal stem cells showed down-regulation of multiple transcripts associated with MAPK signalling, and effects on the Wnt/β-catenin pathway, which regulates intercellular cohesion (Biggs et al., 2009). Fibroblasts cultured on a low adhesion hexagonal array of nanopits showed downregulation of integrin and fibroblast growth factor signalling. On this surface, and another low adhesion substrate (10 nm nanocolumns), fibroblasts also down-regulated mRNAs encoding ECM proteins (Dalby et al., 2007c). In contrast, transcripts for various signalling proteins were up-regulated in fibroblasts cultured on polymer-demixed nanoislands (Dalby et al., 2002b). These observations illustrate that different topographies can induce a distinct transcriptional response as a result of the

specific character of the mechanostimulus, which makes these substrates attractive as versatile tools for the study of cell biology.

A study of human fibroblasts cultured on 2 μm depth, 12.5 μm pitch microgrooves showed up-regulation of transcripts with roles in cell signalling, transcription, translation, the cytoskeleton and the ECM after 24h culture using a 1718 gene microarray (Dalby et al., 2003c). The use of microarrays with substantially greater coverage of the human genome (examining 28869 genes) has the potential to generate a more in-depth picture of the transcriptomic effects of the microgrooved topography. The Dalby et al. (2003) study was also conducted without the use of Ingenuity Pathways Analysis (IPA) software. Additional information could have been gained by the use of this program, which permits improved analysis of transcript functions and gene product interactions. In this study, HuGene 1.0ST (Affymetrix, High Wycombe, UK) microarrays were used to examine differential transcript abundance between cells cultured on the microgrooved (2 μm depth, 25 μm pitch) and planar quartz substrates, with data analysis using IPA software.

3.2 Methods

3.2.1 Cell Culture

3.2.1.1 Growth of Cells on Biomaterials

Fibroblasts (hTERT BJ-1) were counted using a haemocytometer (Mod Fuchs-Rosenthal, Gallenkamp, UK), and seeded at a density of ~ 150 cells/mm^2 material on quartz substrates, with a 24h culture period. The 25 x 75 mm quartz substrates were used for RNA extraction experiments, and cells were cultured for 24h in the supplemented culture medium described in section 2.3.2.1, at 37^{o}C in a humidified atmosphere with 5% CO_2. For RNA extraction, three biological replicates were generated from cells extracted after three temporally distinct culture periods of 24h, and each was pooled from two replicate structures (grooved or planar). Throughout this Chapter, all Figures refer to these replicates (denoted as n=3).

3.2.2 Microarrays

3.2.2.1 RNA Extraction, Quantification and Assessment of Quality (Optimised Protocol)

Cells were lysed for 4 minutes in lysis buffer (100 µl/sample) from the Absolutely RNA Nanoprep Kit (Stratagene, Cheshire, UK), and then mechanically disrupted using cell scrapers (Greiner Bio-One, Stonehouse, UK). The lysates from two equivalent surfaces (control or grooved) were combined, and total RNA was prepared from the resulting pooled samples using the Absolutely RNA Nanoprep Kit essentially according to the manufacturer's instructions, with two elutions at the final step to maximise RNA yield, and an extended column drying time following the low-salt wash (5 minutes), and for elution of RNA (5 minutes/elution). RNA extraction was repeated three times (following temporally distinct cell culture periods) to generate three pairs of control and test samples (n=3, described as 'n=3 pairs of biological replicates' in the Figure legends).

RNA concentration was quantified using a NanoDrop (Agilent Technologies, West Lothian, UK), which was blanked using distilled RNase-free water. The A260/A280 and A280/320 ratios were used to estimate the purity of the samples. RNA quality was assessed using a NanoChip and BioAnalyser 2100 (Agilent Technologies) according to the manufacturer's instructions. The resulting electropherograms and RNA Integrity Numbers (RIN) were used to confirm that the RNA samples were high quality and non-degraded before proceeding.

3.2.3 cRNA and cDNA Synthesis (Optimised Protocol)

Synthesis of cDNA and cRNA was performed according to the GeneChip Whole Transcript (WT) Sense Target Labelling Assay Manual Version 4 (Affymetrix, High Wycombe, UK) by Dr. Jing Wang (Sir Henry Wellcome Functional Genomics Facility, University of Glasgow). To generate cRNA, the 100 ng Total RNA Labelling Protocol was followed, but with a starting input of 300 ng total RNA. The GeneChip WT cDNA Synthesis Kit, the GeneChip WT cDNA Amplification Kit and the GeneChip Sample Cleanup Module (Affymetrix) were used according to the manufacturer's instructions to prepare and amplify first and second-strand cDNA, with the exception that 8 µg first-strand cDNA was used as the input for second-strand synthesis. The resulting double-stranded cDNA was used as a template for cRNA synthesis, using the GeneChip IVT

Labelling Kit (Affymetrix), and the cRNA concentration was measured using a NanoDrop. The GeneChip WT cDNA Synthesis Kit and the GeneChip Sample Cleanup Module (Affymetrix) were used to generate cDNA and digest the cRNA template. The cDNA concentration was measured using a NanoDrop. Single-stranded DNA (5 µg) was subsequently fragmented using the GeneChip WT Terminal Labelling Kit (Affymetrix), according to the manufacturer's recommendations. Fragmentation was confirmed by electrophoretic separation of the samples in an RNA NanoChip (Agilent Technologies), which was visualised using the Bioanalyzer 2100 (Agilent Technologies).

3.2.3.1 ssDNA Labelling and Hybridisation to Microarray

Single-stranded DNA was labelled using the GeneChip WT Terminal Labelling Kit, according to the manufacturer's instructions. The hybridisation cocktail was made according to the volumes described for the 169 Format Array, supplemented with herring sperm DNA (10 mg/ml) and acetylated BSA (50 mg/ml), and used as described in the GeneChip Hybridization, Wash and Stain Kit (Affymetrix) to achieve probe hybridisation. Microarrays (Human Gene (HuGene) 1.0 ST Array, Affymetrix) were incubated in a hybridization oven at 45^{o}C for 16-16.5h.

3.2.3.2 Array Washing, Staining and Scanning

Arrays were washed and stained using the GeneChip Fluidics Station 420/250 and Fluidics Script Protocol FS450_0007 (for 169 Format Arrays), according to the instructions in the GeneChip WT Sense Target Labelling Assay Manual (Affymetrix). Stained arrays were scanned using a GeneChip Scanner 3000 7G.

3.2.4 Statistical Analysis and Bioinformatics

The quality of the data from the gene array was checked using the quality control metrics in the Affymetrix Expression Console software (Affymetrix), including quality controls for inter-sample consistency, hybridisation and labelling (discussed in the Quality Assessment of Exon and Gene Arrays Whitepaper, Affymetrix). The data was subsequently normalised and processed to remove batch and pairing effects using Partek Genomics Suite (Partek, Missouri, USA), and analysed using a 2-way ANOVA (Analysis of Variance) test by Dr. Pawel Herzyk (Sir Henry Wellcome Functional Genomics Facility, University of Glasgow). The samples were extracted in paired batches of one grooved

sample and one planar control sample (each pooled from two slides). This necessitated the removal of pairing effects to enable a 2-way ANOVA to be conducted (Schelle, 1959), which evaluated multiple comparative analyses between the surfaces in order to to generate *p*-values (probabilities that the null hypotheses – that there was no difference in transcript abundance between RNA extracts from cells cultured on planar and grooved surfaces, for each gene examined – were true) and F-statistics (based on the ratio between the observed and expected variation for the two surfaces). The resulting gene list was submitted for Ingenuity Pathways Analysis (Ingenuity Systems, http://www.ingenuity.com/), with an applied significance threshold of $p<0.05$, and fold change thresholds of 1.2, 1.3 or 1.4. These thresholds were chosen based on the ANOVA data and the number of molecules that were eligible for IPA analysis. Applying increasingly higher (more stringent) fold change thresholds reduced the number of molecules that were eligible for IPA analysis.

To generate lists of functional and canonical pathways, the software computed two values for the data. IPA calculated the ratio between the number of molecules from the dataset that matched to a given pathway, and the total number of molecules that matched to the pathway (the sum of the differentially expressed genes from the dataset, and the 'invited' genes that completed the network), and the *p*-values, using a right-tailed Fisher's exact test (testing the null hypothesis that the association between the genes from the dataset and a given canonical or functional pathway occurred only by chance). This non-parametric test utilises contingency tables to generate exact *p*-values, and is suitable for the analysis of small sample numbers. For network analysis, the *p*-values were generated by IPA using a right-tailed Fisher's exact test, and the scores (-log *p*-values from the Fisher's exact test data) were assigned with consideration given to the number of differentially expressed molecules in a given network, in relation to the total number of molecules in the network, and within the entire database. The score gives an indication of the match between the molecules from the dataset and the network, by providing a probability for the observed network arising by chance, but this does not necessarily reflect greater biological relevance.

For the small RNA and ribosomal transcript 'population' analysis, the difference between the percentages of each type of transcript (small RNA or ribosomal; differentially expressed at the levels of 1.2- and 1.4-fold change and thresholded at $p<0.05$) was determined using a binomial probability test (binomial probability tests were described in greater detail in Chapter 2, Section 2.3.5.4). This test was applicable because the continuous data was converted to a discontinuous categorical variable, wherein it could be

included in (a 'success') or excluded from (a 'failure') each of the thresholded fold-change datasets. Conversion of the data to percentages facilitated the comparison of unequal sample sizes. The probability was calculated based on 100 trials, due to the use of percentage data, and *p*-values less than $p=1 \times 10^{-4}$ were considered highly significant. The ribosomal genes examined were the following: **RPL**3, -3L, -4, -5, -6, -7, -7A, -8, -9, -10, -10A, -10L, -11, -12, -13, -13A, -14, -15, -17, -18, -18A, -19, -21, -22, -22L1, -23, -23A, -23AP13, -24, -26, -26L1, -27, -27A, -28, -29, -30, -31, -32, -32P3, -34, -35, -35A, -36, -36A, -36AL, -37, -37A, -38, -39, -39L, -41; **RPLP**0, -1, -2; **RPN**1, -2; **RPP**14, -21, -25, -30, -38, -40, -H1, -M, -ML; **RPS**2, -3, -3A, -4X, -4Y1, -4Y2, -5, -6, -6KA1, -6KA2, -6KA3, -KA4, -KA5, -KA6, -KB1, -KB2, -KC1, -KL1, -7, -8, -9, -10, -11, -12, -13, -14, -15A, -16, -17, -18, -19, -19BP1, -20, -21, -23, -24, -25, -26, -26L, -26L1, -27A, -27L, -28, -29.

3.2.4.1 Method Development: Microarray for RNA Extracts from Biomaterial Sources

Compared with protein studies, examination of RNA has the advantage that nucleic acids can be amplified if the yield is low. For applicability to microarray studies, this has the caveat that the RNA must also be intact (undegraded) and high quality (with low DNA and protein contamination, and minimal buffer carryover to reduce the amount of interfering substances). In this study, to maximise the amount of RNA yielded by the substrates, RNA from two grooved or planar substrates was pooled to generate each sample. The Absolutely RNA Nanoprep Kit (Stratagene) was used for these samples, as it gave better RNA yields than the Absolutely RNA Miniprep Kit (Stratagene), presumably because the Nanoprep columns had a smaller dead volume. The time for lysis was increased from 2 to 4 minutes to ensure lysis had proceeded effectively prior to cell scraping. RNA harvest was challenging on these substrates, due to the relatively small volume of lysis buffer that had to be spread over a large surface area, and low cell density used. A small volume had to be used to prevent overdilution of the RNA samples. Due to the relatively low RNA yields from the monodisperse cell populations, therefore, it was necessary to amplify the RNA samples. Frequent difficulties were encountered during amplification using the 100 ng protocol recommended by the manufacturer, but the success rate of the first stage amplification was improved by using 300 ng of input RNA.

3.3 Results

3.3.1 Microarray Reproducibility: Quality Control

To confirm the reproducibility of the arrays, a number of quality control metrics were assessed using Expression Console Software (Affymetrix). Firstly, the positive and negative control probe spots were compared in a ratiometric manner (Figure 3-1). The positive controls were directed against 'housekeeping' genes such as beta actin, which are typically constitutively expressed. The negative controls are probes directed against the intons of the housekeeping genes, but it should be noted that these are not 'true' negative controls, as there can be some signal from these probes if the introns remain unspliced in the transcripts (described in the Quality Assessment of Exon and Gene Arrays Whitepaper, Affymetrix). A score above 0.8 is considered a 'pass', and theoretically, 1.0 would be considered a perfect array. As shown in Figure 3-1, all the arrays had values between 0.88 and 0.91, passing this level of quality control and suggesting that there were unlikely to be problems with hybridisation of the probes to the arrays.

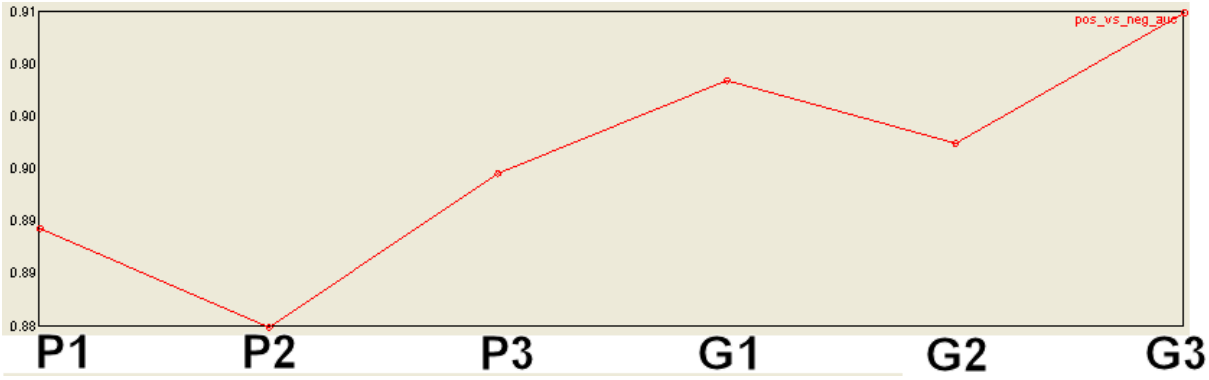

Figure 3-1: Comparison of the 'area under the curve' (auc) values for the positive and negative control probes on each microarray, a metric that enables examination of the relative signal contribution from the negative and positive control probesets to determine array quality. *P1-3 denote biological replicate arrays for extracts from fibroblasts cultured on the planar substrata, and G1-3 indicate replicate arrays from fibroblasts cultured on the microgrooved substrates. Values below 0.8 are considered likely to be poor quality arrays, and scores of 1.0 would denote theoretically 'perfect' arrays.*

To confirm that the brightness was similar for all the arrays, the mean signal intensity was plotted for each of the microarrays across all the probesets (Quality Assessment of Exon and Gene Arrays Whitepaper, Affymetrix). Biological replicates were expected to show the most congruence, and as shown in Figure 3-2, the values were

very consistent between the biological replicates of the same type, and even between the two groups (P and G).

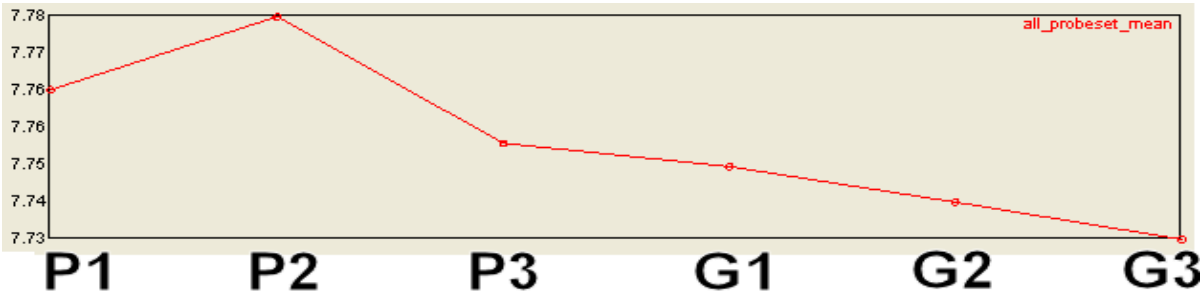

Figure 3-2: Comparison of the reproducibility of brightness across each microarray, by examining the mean signal for the whole probeset. *P1-3 denote biological replicate arrays for extracts from fibroblasts cultured on the planar substrata, and G1-3 indicate replicate arrays from fibroblasts cultured on the microgrooved surfaces. Note the consistency between arrays, particularly between replicate arrays of the same sample type.*

Figure 3-3 illustrates that the mean absolute expression values were similar between all arrays (Fig. 3-3A), and the inter-quartile ranges were also closely matched, with no evidence of outlier arrays (Fig. 3-3B). Following data normalisation, the median values were approximately zero (Fig. 3-3B), which suggests that normalisation had been successful (discussed in the Quality Assessment of Exon and Gene Arrays Whitepaper, Affymetrix).

Polyadenylated control transcripts for *Thr*, *Lys*, *Phe* and *Dap* were spiked into the RNA sample at the start of the protocol in stoichiometric ratios, before the amplification and labelling steps had been performed, and were detected in the expected order: *Lys* < *Phe* < *Thr* < *Dap*, as shown in Figure 3-4. This illustrated that the amplification and labelling steps had proceeded effectively across all the arrays, as described in the Quality Assessment of Exon and Gene Arrays Whitepaper (Affymetrix).

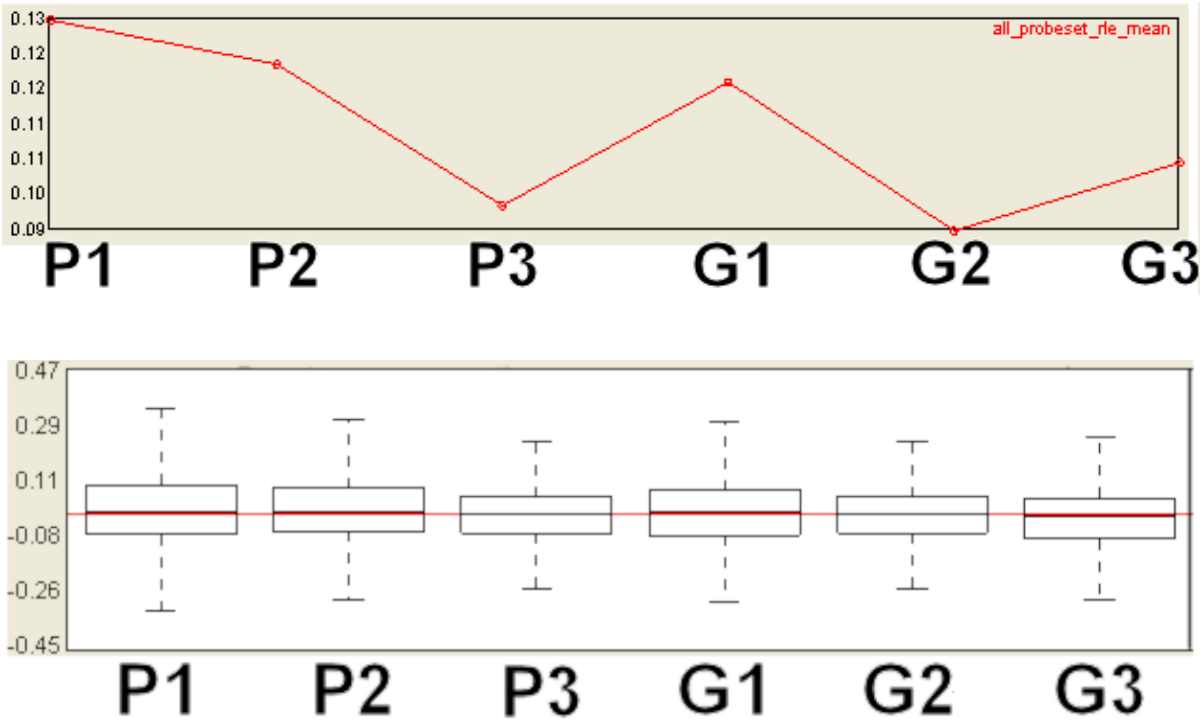

Figure 3-3. Assessment of array consistency: mean absolute relative log expression values for all the arrays, represented as a line graph (upper image), and the relative log expression values, shown as a box plot (lower image). *These metrics compare the signal from all the probes in each probeset against the median signal for that probset, and calculate the mean values for this ratio across all of the probesets. Large, deviant values are suggestive of arrays that are behaving as outliers (not observed in this dataset). P1-3 denote biological replicate arrays for extracts from fibroblasts cultured on the planar substrata, and G1-3 indicate replicate arrays from fibroblasts cultured on the microgrooved surfaces. Note the highly consistent median values and mean value (red line) between arrays, as indicated in the boxplot.*

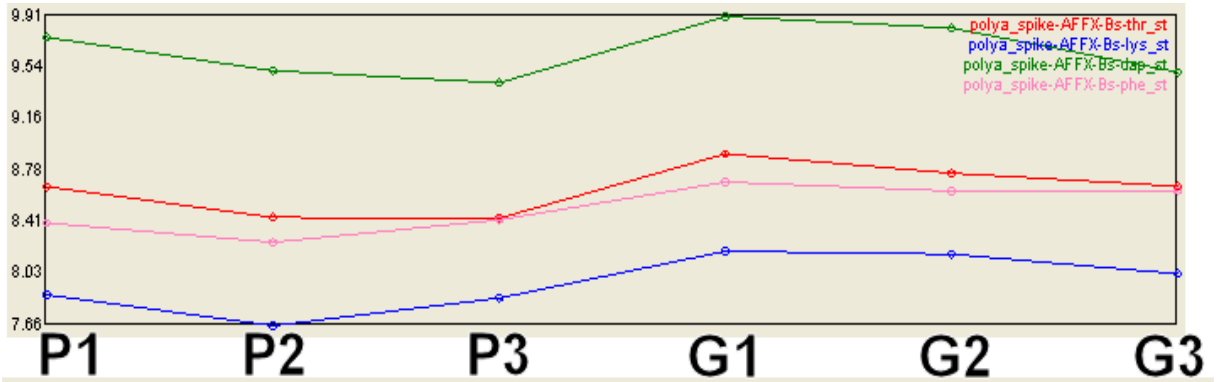

Figure 3-4. Assessment of the success of amplification and labelling, by the relative intensity of the poly-A controls. *P1-3 denote biological replicate arrays for extracts from fibroblasts cultured on the planar substrata, and G1-3 indicate replicate arrays from fibroblasts cultured on the microgrooved substrates. Blue line: Lys, pink line: Phe, red line: Thr, green line: Dap. Note that the order of the transcripts (Lys < Phe < Thr < Dap) is as expected from the relative concentrations of each control transcript, illustrating that amplification and labelling had proceeded effectively.*

Prior to hybridisation, the samples were spiked with the bacterially-derived RNAs *BioB*, *BioC*, *BioD* and *Cre*. The ratio of these RNAs was such that the *BioD* transcript should theoretically have been detected 70% of the time, and the order of the transcripts (in

order of signal intensity) should have been *BioB* < *BioC* < *BioD* < *Cre* (Quality Assessment of Exon and Gene Arrays Whitepaper, Affymetrix). This was the order observed in the experiment (Figure 3-5), illustrating that the hybridisation had been successful.

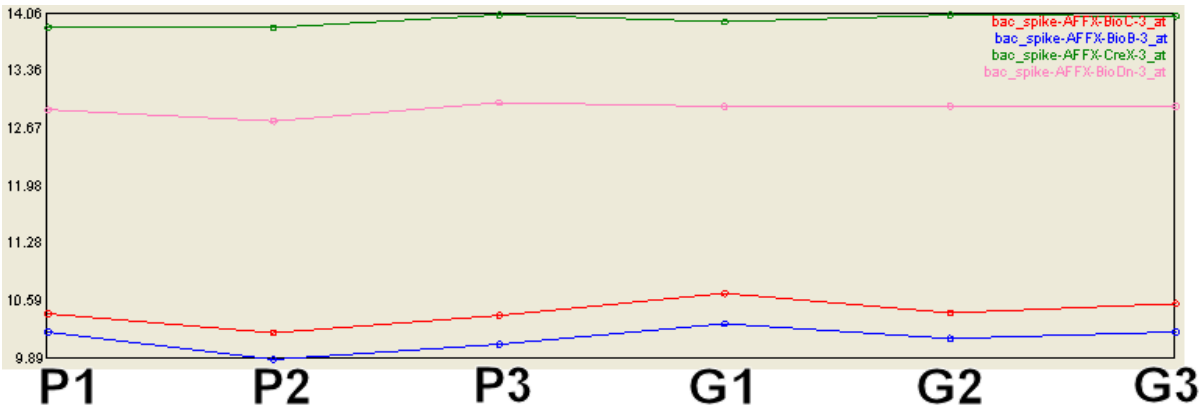

Figure 3-5. Assessment of the quality of probe hybridisation across all arrays. *P1-3 denote biological replicate arrays for extracts from fibroblasts cultured on the planar substrata, and G1-3 indicate replicate arrays from fibroblasts cultured on the microgrooved substrates. Blue line: BioB, red line: BioC, pink line: BioD, green line: Cre. Note that the order of the transcripts (BioB < BioC < BioD < Cre) is as expected from the relative concentrations of each transcript, indicating that hybridisation was successful on all arrays.*

To assess the relatedness of the arrays, based on signal intensity, the software calculated the Spearman Rank Correlation to generate a heatmap of array similarity. Typically, replicates of samples of the same type (*e.g.* extracts from fibroblasts cultured on planar substrates) are more related to each other than to other sample types (*e.g.* extracts from fibroblasts cultured on microgrooved substrata). Figure 3-6 illustrates that the arrays were consistent with each other, potentially suggesting that the arrays had broadly similar expression profiles, with relatively few gene expression changes. This perhaps reflects the non-invasive nature of the mechanostimulus and early time-point examined. Replicates G2 and G3 appeared to be more related to each other than to G1. F1 and F2 were most related to each other, but F3 was a slightly anomalous replicate, as it was very similar to F2, but more similar to G2 and G3 than to F1. Given the narrow range (compressed scale) of the heatmap, however, and thus the general similarity between all of the arrays, it is unlikely that this minor discontinuity had any effect on the interpretation of the results.

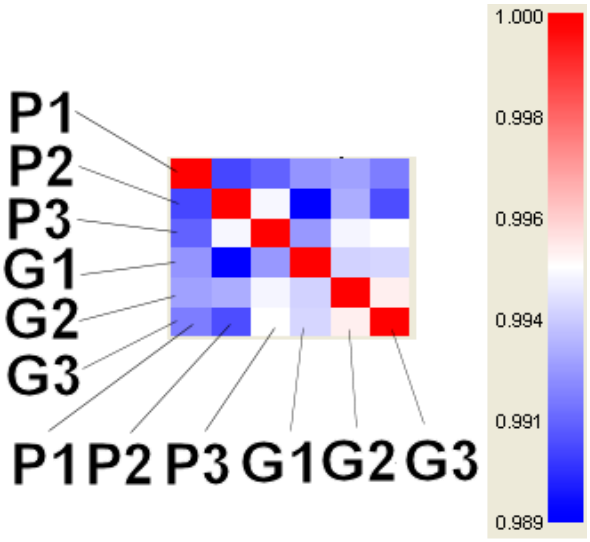

Figure 3-6. Heatmap representation of Spearman Rank Correlation between individual arrays. *P1-3 denote biological replicate arrays examining samples derived from fibroblasts cultured on planar quartz substrates, and G1-3 denote the corresponding arrays from fibroblasts cultured on 2 µm deep, 25 µm pitch quartz microgrooves. The coloured bar indicates the correlative score for each pair of arrays. Note that the heatmap examines pairs of arrays, for example the top left square examines P1 against P1 (itself), and thus has a perfect correlation of 1.0.*

Principle Component Analysis was performed to confirm that the arrays were predominantly clustered by sample type, rather than another variable (such as a pairing effect). The results were visualised in a 3D space by decreasing the number of principle components down to the three main factors that resulted in the largest contribution towards the description of the total variation within the model (thus reducing the multidimensionality of the dataset). Figure 3-7 A and B show that there was a clear contribution from a pairing effect, prior to data processing to remove it, as the pairs of samples (P1 and G1, P2 and G2, P3 and G3) were located at distinct, non-intersecting regions of the 3D space (Figure 3-7A), although the samples were still assorted by type (P or G; Figure 3-7B). Following removal of the pairing (batch) effect, however, the sample pairs were successfully transposed within the grid, such that the central point bisecting each pair of samples was common to all pairs of samples. This common intersection (known as a centroid) illustrated that the pairing bias had been successfully removed, as the sample pairs were no longer segregated to specific regions of the 3D space.

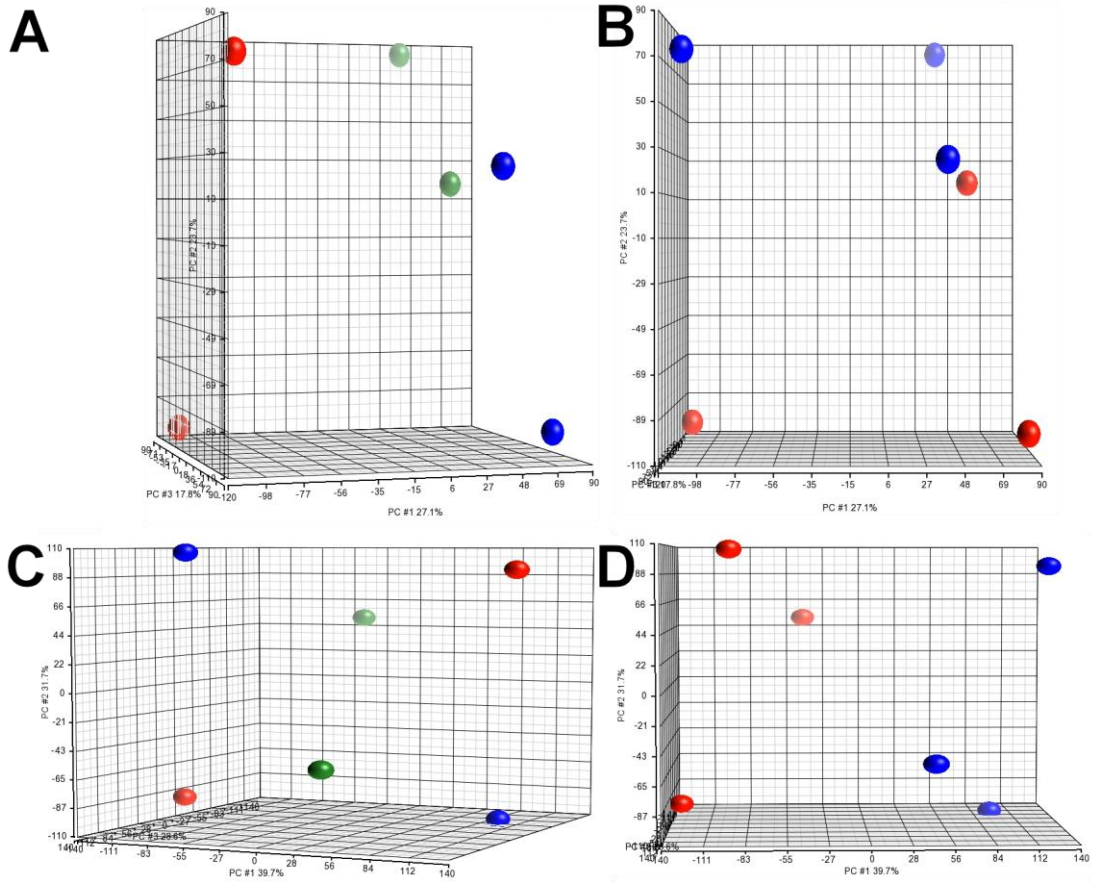

Figure 3-7. Principle Component Analysis of the clustering of the replicates before (A, B) and after (C, D) the exclusion of pairing effects due to the sequential temporal extraction of the three pairs of samples.
A, C) Green: sample pair 1 (P1, G1), Red: sample pair 2 (P2, G2), Blue: sample pair 3 (P3, G3). B, D) Red: samples from grooved substrates, Blue: samples from planar substrates. Note that the pairs of samples appear segregated to different regions of the 3D space prior to removal of the pairing effects (A, B), but are arranged with a centroided transposition (C) and cluster according to sample type (D) following the removal of the pairing effects.

3.3.2 Microarray Analysis and Ingenuity Pathways Analysis

3.3.2.1 Interaction Analysis and Transcripts with a High Magnitude of Change in Abundance

IPA was used to identify functional classes of differentially expressed genes, and to find potential interactions between differentially regulated molecules by generating pathways of functional interactions between gene products. At a stringent 1.5-fold change threshold, the highest scoring network (score: 40) is shown in Fig. 3-8, with the genes involved potentially contributing to a number of important roles including cell proliferation, cytoskeletal functions, cell signalling and chromatin remodelling/transcription. It was particularly interesting that FOXA2 and HNF1A were down-regulated in cells on the microgrooved topography, as the former is a transcriptional

activator (van der Sluisa et al., 2008), and the latter can function as a chromatin-remodelling machine (Pontoglio et al., 2001). This suggests that there are likely to be subtle, specific effects on gene expression and accessibility in addition to direct mechanical effects on the nucleus. SNRPA1 (small nuclear ribonucleoprotein polypeptide A'), which is involved in mRNA splicing (Sillekens et al., 1989), was also down-regulated in cells on the topography, suggesting effects at the level of transcript processing.

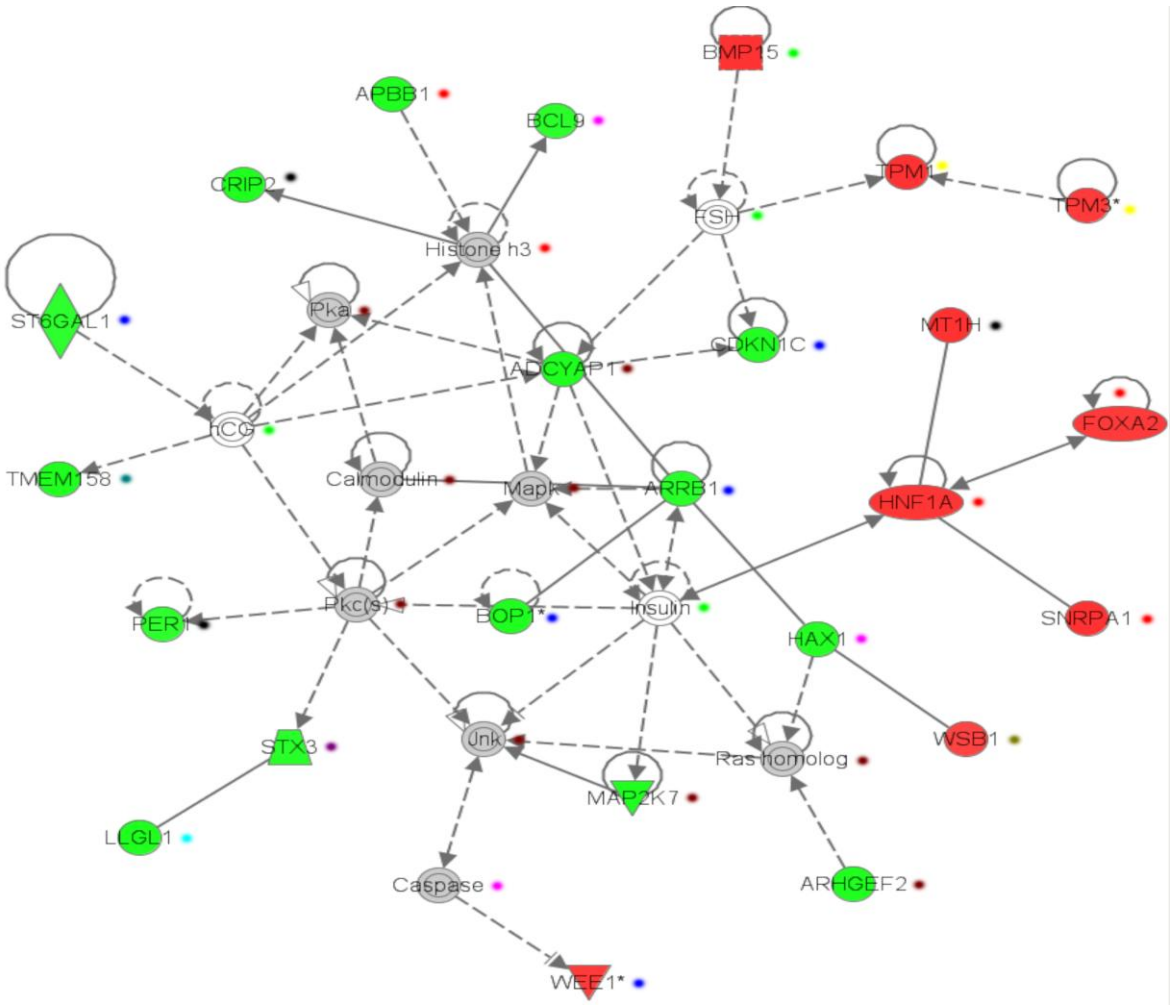

***Figure 3-8*. Ingenuity Interaction Pathway 1 (score: 40, fold-change threshold: 1.4, $p<0.05$; n=3 pairs of biological replicate arrays).** *Up-regulated transcripts in cells on microgrooves – Green, Down-regulated transcripts in cells on microgrooves – Red, Transcripts with unchanged abundance relative to controls – Grey, Transcripts not examined by microarray - White. Unbroken lines indicate direct interactions (involving physical contact of the molecules), and broken lines indicate indirect interactions (e.g. via the induction of a signalling cascade). Arrowheads indicate the direction of influence. Lines with no arrow indicate binding only, open arrowheads indicate 'translocates to' and closed arrows with a small perpendicular line behind the arrowhead indicate that the molecule at the base of the arrow 'inhibits and acts on' the molecule at the arrowhead. The key to the abbreviations and potential functional classifications (denoted by coloured dots) is shown on the following page. Functional classifications were based on information from the Ingenuity Knowledge Base in the IPA software.*

Key to Figure 3-8:

Cell division: ***ARRB1*** *– arrestin, beta 1,* ***BOP1*** *– block of proliferation,* ***CDKN1C*** *– cyclin-dependent kinase inhibitor 1C,* ***ST6GAL1*** *– ST6 β-galctosamide alpha-2,6-sialyl transferase I,* ***WEE1*** *– WEE1 homolog*
Apoptosis: ***BCL9*** *- B-cell chronic lymphocytic leukaemia/lymphoma 9,* ***Caspase****,* ***HAX1*** *– haematopoetic cell-specific lyn substrate 1 associated protein X-1*
Transcription factors/chromatin remodelling machinery/maintenance of nuclear architecture: ***APBB1*** *– amyloid beta (A4) precursor protein binding, family B, member 1 (Fe65),* ***FOXA2*** *– forkhead box A2,* ***Histone h3****,* ***HNF1A*** *– hepatocyte nuclear factor 1A,* ***SNRPA1*** *– small nuclear ribonucleoprotein polypeptide A'*
Signalling proteins: ***ADCYAP1*** *– adenylate cyclase associated protein 1,* ***ARHGEF2*** *– Rho/Rac guanine nucleotide exchange factor 2,* ***Calmodulin****,* ***Jnk*** *– Jun N-terminal kinase,* ***Mapk*** *– mitogen-associated protein kinase,* ***MAP27*** *– mitogen-activated protein 27,* ***MAP2K7*** *– mitogen activated protein kinase kinase 7,* ***Pka*** *– protein kinase A,* ***Pkc(s)*** *– protein kinase C,* ***Ras homolog***
Growth factors/hormones: ***BMP15*** *– bone morphogenic protein 15,* ***FSH*** *– follicle stimulating hormone,* ***hCG*** *– human chorionic gonadotrophin,* ***Insulin***
Vesicular trafficking: ***STX3*** *– syntaxin 3*
Molecular transport: ***TMEM*** *– transmembrane protein 158*
Protein ubiquitination: ***WSB1*** *– WD repeat and SOCS-box containing 1*
Cytoskeleton-related/contractility: ***TPM1*** *– tropomyosin I,* ***TPM3*** *– tropomyosin 3,*
Cytoskeleton-related/cell polarity: ***LLGL1*** *– lethal giant larvae homolog*
Other: ***CRIP2*** *– cysteine rich protein 2,* ***MT1H*** *– metallothionein 1H (binding of heavy metals),* ***PER1*** *– period homolog 1 (circadian control)*

Relaxing the fold-change stringency to 1.2-fold change, to examine more modest up- and down-regulation, revealed another interaction network (Fig. 3-9). The ECM remodelling factor MMP-7 (matrix metalloprotease 7) was up-regulated in cells on microgrooves. From the microarray data, mRNAs for three other MMPs (MMP-12, -14 and -17) were up-regulated at 1.3-fold change or greater in cells on the grooved topography ($p<0.05$), which suggests that ECM remodelling was being promoted on this surface. Cell adhesion and the cytoskeleton were also highlighted in this pathway, with up-regulation of mRNAs for alpha and beta integrins in cells on the topography, and the actin-regulatory factors cdc42 (involved in actin bundling (Disanza et al., 2006) and polymerisation (Reid et al., 1999)), ARHGDIA (a GTPase activating protein for Rac and Rho), the kinase Akt (Vandermoere et al., 2007) and the G-protein Rho (Chellaiah et al., 2000). Several signalling factors were also present in the network, with extracellular signal-regulated kinase (ERK) appearing to act as a pivotal hub for inter-molecular interactions, without directly being differentially expressed.

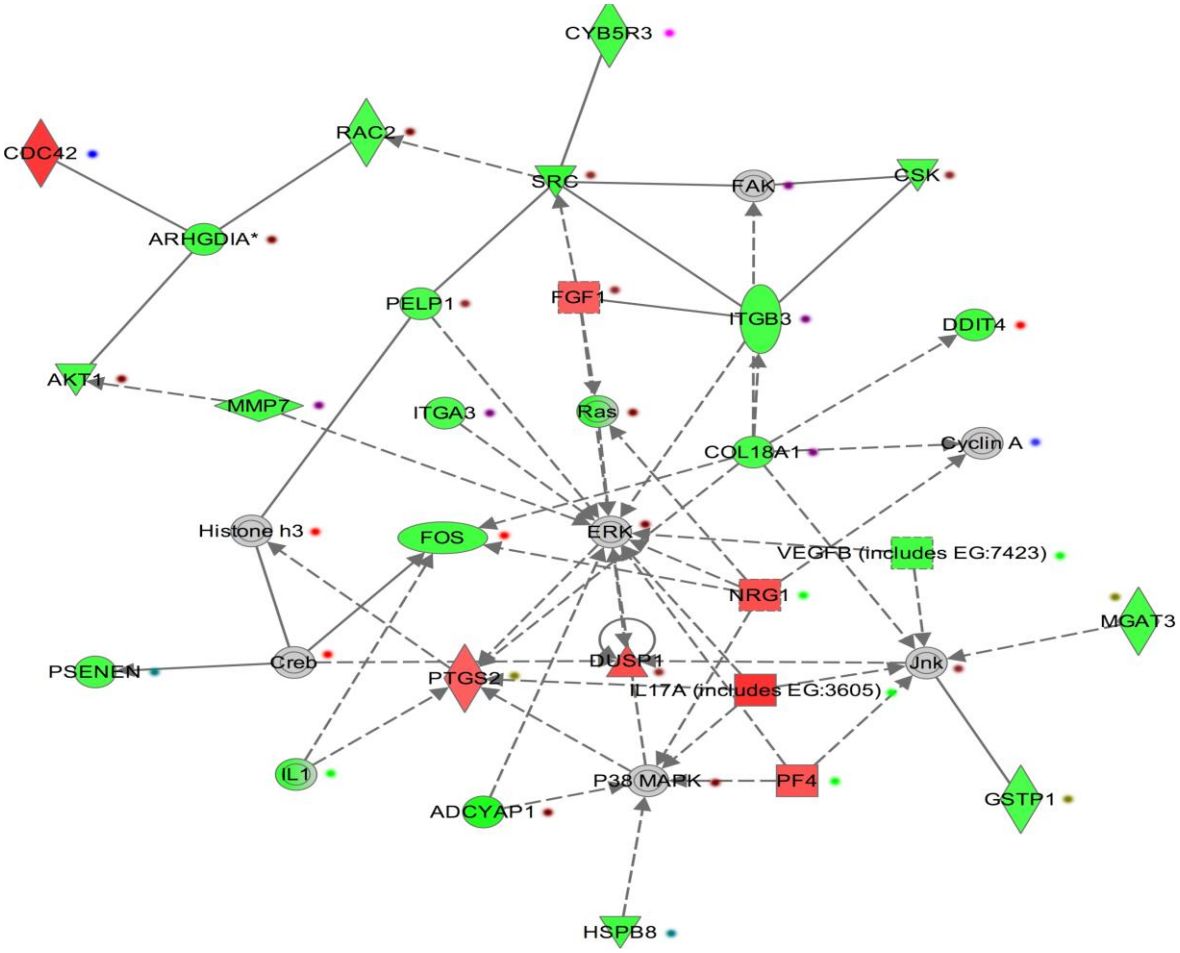

Figure 3-9. Ingenuity Interaction Pathway 2 (score: 19, fold-change threshold: 1.2, p<0.05; n=3 pairs of biological replicate arrays). *Up-regulated transcripts in cells on micrgrooves - Green, Down-regulated transcripts in cells on microgrooves – Red, Transcripts with unchanged abundance relative to controls – Grey. Unbroken lines indicate direct interactions (involving physical contact of the molecules), and broken lines indicate indirect interactions (e.g. via the induction of a signalling cascade). Arrowheads indicate the direction of influence. Lines without arrowheads indicate binding only. The key to the abbreviations and potential functional classifications (denoted by coloured dots) is shown below. Functional information was primarily derived from the Ingenuity Knowledge Base in the IPA software.*

Key to Fig. 3-9:

*Cell division: **CDC42** – cell division cycle 42, **Cyclin A***
*Energy production: **CYB5R3** – cytochrome b5 reductase 3*
Transcription factors/maintenance of DNA architecture/DNA repair:
Creb**, **DDIT** – DNA damage-inducible transcript 3, **FOS** – FBJ murine osteosarcoma viral oncogene homolog, **Histone h3
*Signalling proteins: **ADCYAP1** – adenylate cyclase activating polypeptide 1, **AKT** – v-akt murine thymoma viral oncogene homolog, **ARHGDIA** – Rho GDP dissociation inhibitor alpha, **CSK** – c-src tyrosine kinase, **DUSP1** – dual specificity phosphatase 1, **ERK** – extracellular signal-regulated kinase, **FGF1** – fibroblast growth factor 1, **Jnk** – Jun N-terminal kinase, **P38 MAPK** – P38 mitogen-activated protein kinase, **PELP1** – proline, glutamate and leucine rich protein 1, **RAC2** – Ras-related C3 botulinum toxin substrate 2, **Ras**, **SRC** - Src*
*Growth factors/cytokines: **IL-1** – interleukin 1, **IL-17A** – interleukin 17A, **PF4** – platelet factor 4, **NRG1** – neuregulin 1, **VEGFB** – vascular endothelial growth factor B*
*ECM production/remodelling or cell adhesion: **COL18A1** – collagen, type XVIII, **FAK** – focal adhesion kinase, **ITGA3** – integrin alpha 3, **ITGB3** – integrin beta 3, **MMP7** – matrix metalloprotease 7*
*Protein processing: **HSPB8** – heat shock 22kDa protein 8 (chaperone, protein folding), **PSENEN** – presenilin enhancer protein 2 (cleavage of certain transmembrane proteins e.g. Notch)*
*Enzymes involved in biosynthesis/detoxification: **GSTP1** – glutathione S-transferase pi 1 (detoxification), **MGAT3** – mannosyl (beta-1,4-)-glycoprotein beta-1,4-N-acetylglucosaminyltransferase (synthesis of glycoprotein oligosaccharides), **PTGS 2** – prostaglandin-endoperoxide synthase 2 (prostanoid synthesis).*

3.3.2.2 Transcripts with the Highest Magnitude of Differential Expression Change

The transcripts with the largest magnitude of differential expression change between cells cultured on the planar and microgrooved substrata, which could also be matched to the Ingenuity database, are shown in Table 3-I.

Table 3-I. Transcripts with the greatest magnitude of differential abundance between cells cultured on the microgrooved and planar substrates (which could be successfully matched to the Ingenuity database). *All values were significant at $p<0.05$ in a paired two-way ANOVA test (n=3 pairs of biological replicate arrays). Functional information was primarily derived from the literature-based Ingenuity Knowledge Base in the IPA software.*

Gene Name	Protein Name	Fold Change (G:P)	Function
BLID	BH3-like motif containing, cell death inducer	-2.081	Pro-apoptotic protein (Broustas et al., 2004).
DHFR	Dihydrofolate reductase	-2.070	Reduces dihydrofolate to tetrahydrofolate (Wright et al., 2003). Required for synthesis of purines and some amino acids.
RPLS	Ribosomal protein L5	-2.049	Component of 60S ribosomal subunit (Robledo et al., 2008; Yu et al., 2006a). Required for transport of 5S rRNA into nucleolus.
LPAL2	Lipoprotein 2	-1.990	Lipid transport.
HSPA6	Heat shock 70kDa protein 6 (HSP70B')	-1.877	Induced by unfolded proteins.
SNRPA1	Small nuclear ribonucleoprotein polypeptide A' (U2-A')	-1.872	mRNA splicing (Sillekens et al., 1989).
MIR21	MicroRNA 21	-1.865	Targets specific mRNAs for cleavage or repression (Gabriely et al., 2008; Zhu et al., 2007b).
EID3	EP300 Interacting Inhibitor of Differentiation 3	-1.861	Transcriptional regulator. Can interact with the co-activator CREBBP (cAMP responsive element binding protein binding protein) (Båvner et al., 2005).
TXNDC9	Thioredoxin domain containing 9	-1.729	Function undefined, role in cell differentiation.
NPPB	Natriuretic peptide precursor B	-1.667	Diuretic hormone.
RAB7A	Rab7A	+1.844	Regulates vesicular traffic in late endosomes and from late endosomes to lysosomes (Jopling et al., 2009; Papini et al., 1997).

TMLHE	Trimethylysine hydroxylase epsilon	+1.795	Carnitine biosynthesis. Redox reactions.
ANGPTL4	Angiopoietin-like 4	+1.756	In some cancers, may reduce metastasis by blocking vascular activity and inhibiting cell movement (Ito et al., 2003).
GAA	Glucosidase alpha	+1.752	Degradation of glycogen to glucose in lysosomes (Kamphoven et al., 2004).
PSME2	Proteasome activator subunit 2 (PA28 beta)	+1.732	Regulates Pa28/20S proteasome (involved in MHC class I peptide presentation) (Wojcik, 2002).
MYL12A	Myosin light chain 12A	+1.719	Regulates actin and myosin (Murthy et al., 2003).
ADAM11	A disintegrin and a metalloprotease metallopeptidase domain 11	+1.669	Involved in cell motility (Cichy and Pure, 2003). Candidate tumour suppressor gene.
ABCB8	ATP-binding cassette, subfamily B (MDR/TAP) member 8	+1.666	Transmembrane transporter. May transport phospholipids into membranes, and peptides from mitochondra to nucleus.
SNAI1	Snail homolog 1	+1.659	Transcriptional repressor (Sato et al., 2010).
PPP1R10	Protein phosphatase I, regulatory (inhibitor) subunit 10	+1.653	Inhibitory effect on protein phosphatase 1. Associates with chromatin during mitosis.

The large magnitude of down-regulation of a transcript corresponding to a pro-apoptotic protein suggests that the cells on the grooved substrate were not being stimulated to undergo apoptosis. Down-regulation of DHFR mRNA suggests that cells may be beginning to reduce their synthesis of purines or certain amino acids, or use alternative synthetic pathways. Up-regulation of trimethylysine hydroxylase ε transcripts could reflect an increased metabolic demand of cells on the topography, as it is required for synthesis of carnitine, an essential metabolite involved in transport of fatty acids in mitochondrial energy generation. There is also evidence that transcription appears to have been affected, with differentially abundant transcripts encoding the transcriptional regulators Snail homolog 1 (Sato et al., 2010) and EP300 (Båvner et al., 2005) in cells on the topography. This is consistent with the array data highlighting differential expression in many genes. In addition, an inhibitor of protein phosphatase I, which interacts with chromatin during cell division (Keller and Krude, 2000), was up-regulated by 1.65-fold in cells on microgrooves. Molecular transport was also highlighted, with up-regulation of mRNA corresponding to a transmembrane transporter (MDR/TAP member 8) and Rab7A, which is involved in vesicular trafficking (Jopling et al., 2009; Papini et al., 1997), in cells on the

topography. This suggests that the movement of proteins and lipids may be altered, and interestingly, the transcript encoding lipoprotein 2 was also down-regulated.

Transcripts encoding protein synthesis processing functions appeared to be down-regulated, including the chaperone HSP 70kDa, the splicing factor snRP A' (Sillekens et al., 1989), and the ribosomal protein L5, a structural component of the 60S subunit of the ribosome (Robledo et al., 2008; Yu et al., 2006a). Interestingly, PA28 beta subunit mRNA was more abundant in cells on the topography, suggesting that antigen presentation may be being promoted (Wojcik, 2002). Myosin light chain mRNA was up-regulated in cells cultured on microgrooves, suggesting that there are likely to be alterations in actin-mediated contractility (Murthy et al., 2003), and motility may also be affected by the up-regulated expression of ADAM11. The differential abundance of some other mRNAs between the substrata are more difficult to explain, for example angiopoietin-like 4, natriuretic peptide B and glucosidase alpha, which are likely to be tissue-specific factors. These transcript abundance changes do not necessarily correlate with functional protein changes. Interestingly, natriuretic peptide B has been shown to be up-regulated at the transcript and protein level in cardiac myocytes in response to mechanical strain, in the form of cyclic biaxial cell stretch. This required an intact actin cytoskeleton, and also appeared to involve MAPK or Jnk (*Jun* N-terminal kinase) (Liang et al., 1997).

3.3.3 Small RNA Analysis

Interestingly, with a more stringent threshold of 1.5-fold change ($p<0.05$) applied, twenty-one small RNAs emerged as differentially abundant, twenty of which were down-regulated in cells on the grooved topography relative to those on the planar control (Table 3-II). At this threshold, only a total of 212 transcripts appeared to be differentially abundant, such that small RNAs accounted for 9.9% of these changes. One miRNA (*miR-21*) was down-regulated in cells on the grooved topography, and it has been shown to function as an oncogene in cancer progression, by targeting tumour suppressors involved in tumour cell migration, such as TPM1 (tropomyosin I), for translational repression (Zhu et al., 2007a; Zhu et al., 2008).

Table 3-II. Small RNAs differentially regulated between cells on the quartz microgrooved (G) and planar (P) substrates. *Thresholds of +/-1.5 fold change and significance of $p<0.05$ (from a paired two-way ANOVA test) were applied to the microarray dataset (n=3 pairs of biological replicate arrays).*

Name of small RNA gene	**Name of small RNA**	**Fold change (G:P)**	***p*-value**
SNORA23	Small nucleolar RNA, H/ACA box 23	-2.91254	3.53×10^{-3}
SNORD114-2	Small nucleolar RNA, C/D box 114-2	-2.37042	1.62×10^{-2}
SNORD21	Small nucleolar RNA, C/D box 21	-2.00104	4.48×10^{-6}
MIRN21	microRNA 21 (*mir-21*)	-1.86472	4.98×10^{-3}
SNORA1	Small nucleolar RNA, H/ACA box 1	-1.7772	1.84×10^{-3}
SNORD6	Small nucleolar RNA, C/D box 6	-1.77607	7.93×10^{-4}
SNORA50	Small nucleolar RNA, H/ACA box 50	-1.75582	3.24×10^{-2}
SNORA36A	Small nucleolar RNA, H/ACA box 36A	-1.75578	1.99×10^{-3}
SNORD45B	Small nucleolar RNA, C/D box 45B	-1.73348	2.49×10^{-3}
SNORD30	Small nucleolar RNA, C/D box 30	-1.66573	1.18×10^{-3}
SNORD4B	Small nucleolar RNA, C/D box 4	-1.65442	1.29×10^{-2}
SNORD26	Small nucleolar RNA, C/D box 26	-1.65205	2.78×10^{-2}
SNORD8	Small nucleolar RNA, C/D box 8	-1.60119	3.77×10^{-3}
SNORD61	Small nucleolar RNA, C/D box 61	-1.59667	3.47×10^{-3}
SCARNA12	Small Cajal-body specific RNA 12	-1.59667	3.47×10^{-3}
SCARNA7	Small Cajal-body specific RNA 7	-1.58548	4.68×10^{-4}
SNORD113-4	Small nucleolar RNA, C/D box 113-4	-1.55447	1.69×10^{-2}
SNORD5	Small nucleolar RNA, C/D box 5	-1.53109	3.95×10^{-2}
SNORA14B	Small nucleolar RNA, H/ACA box 14B	-1.52654	7.23×10^{-3}
SNORD50B	Small nucleolar RNA, C/D box 50B	-1.51147	9.63×10^{-3}
SNORA22	Small nucleolar RNA, H/ACA box 22	+1.50143	3.23×10^{-3}

Two Cajal-body specific RNAs (scaRNAs) were also down-regulated. The Cajal body is a subnuclear structure that may function in the modification and recycling of small nuclear RNAs (snRNAs) and small nucleolar RNAs (snoRNAs) (Darzacq et al., 2002; Verheggen et al., 2002). The scaRNAs are thought to function in promoting pseudouridylation of some spliceosomal snRNAs. Pseudouridylation is a form of RNA editing, involving the isomerisation of uridine residues. The majority of the differentially regulated small RNAs were C/D or H/ACA box snoRNAs. A number of H/ACA box snoRNAs appear to function in the pseudouridylation of rRNA (Kiss et al., 2004), while the C/D box family are involved in the 2'-*O*-ribose methyation of RNA (Darzacq et al., 2002; Filipowicz and Pogacic, 2002; Verheggen et al., 2001). In addition, the transcripts for a small RNA activating complex (19kD, polypeptide 5) (*SNAPC5*) and a small nuclear RNA pseudogene (*RNU13P2*) were also down-regulated at the 1.5-fold change threshold.

To further investigate the global pattern of abundance of small RNAs, the relative levels of scaRNAs and snoRNAs examined in the microarray study that were reproducibly differentially abundant ($p<0.05$) at ratios of 1.2- and 1.4-fold change were plotted in Fig.

3-3, and compared to the equivalent graphs for ribosomal transcripts. It should be noted that some transcripts had multiple values, as some genes had multiple gene array probes (≤ 7) assigned to them, and the data was plotted according to the result for each Affymetrix probe. At each of the fold-change thresholds examined, the number of differentially expressed transcripts and the magnitude of differential expression was higher amongst the group of small RNAs than the group of ribosomal RNAs (Fig. 3-10). Indeed, 67% of the small RNAs were differentially expressed at a level of 1.2-fold or greater, compared with only 46.5% of transcripts encoding ribosomal proteins (Fig. 3-11). This differential was considered to be highly statistically significant in a binomial probability test (p=1.75 x 10^{-5}). At a threshold of 1.4-fold change, 34% of the small RNAs were differentially abundant (30/88), compared with only 12% of ribosomal protein transcripts examined (7/58, thresholded at p<0.05). This was considered highly significant using a binomial probability test (p=6.19 x 10^{-9}).

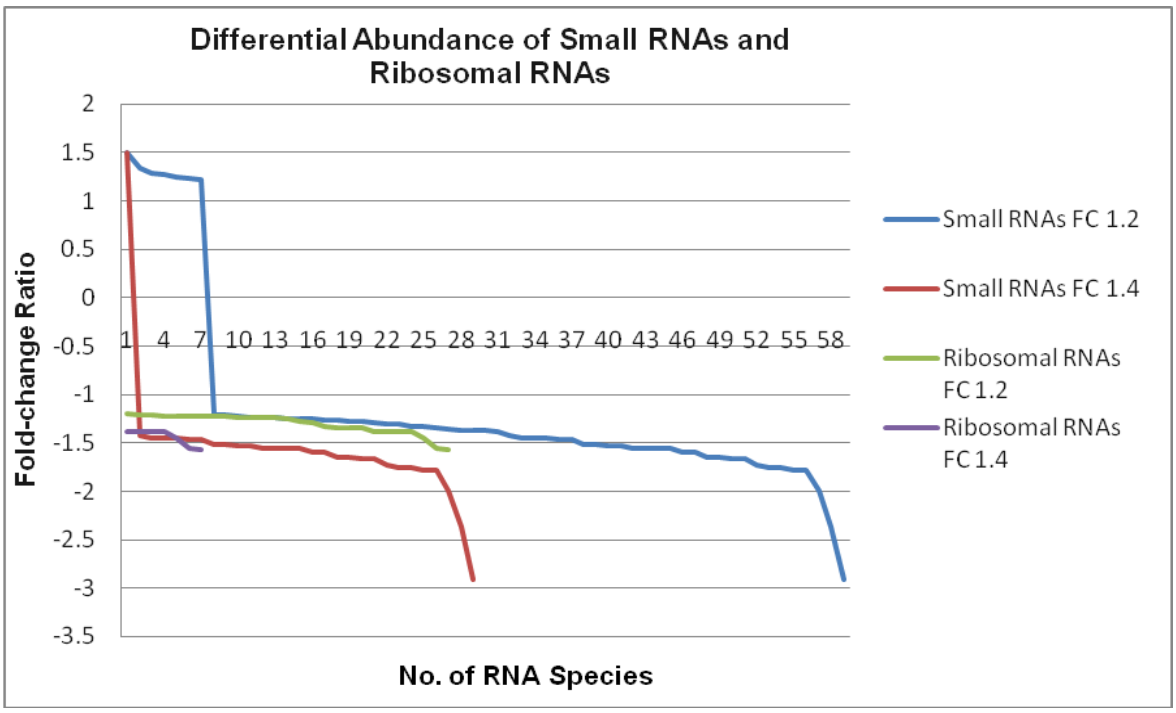

Figure 3-10. Transcript abundance of small RNAs (SNORDs, SCARNAs) and ribosomal transcripts examined by microarray, and the transcript abundance for statistically significant results (p<0.05). *The distribution of small RNAs is shown with respect to fold-change in abundance (FC). The directionality of the differential expression is indicated for the grooved substrate relative to the planar substrate. Note the larger numbers and higher magnitude of fold-change of small RNAs (relative to ribosomal RNAs) at thresholds of both 1.2- and 1.4-fold change (n=3 pairs of biological replicate arrays).*

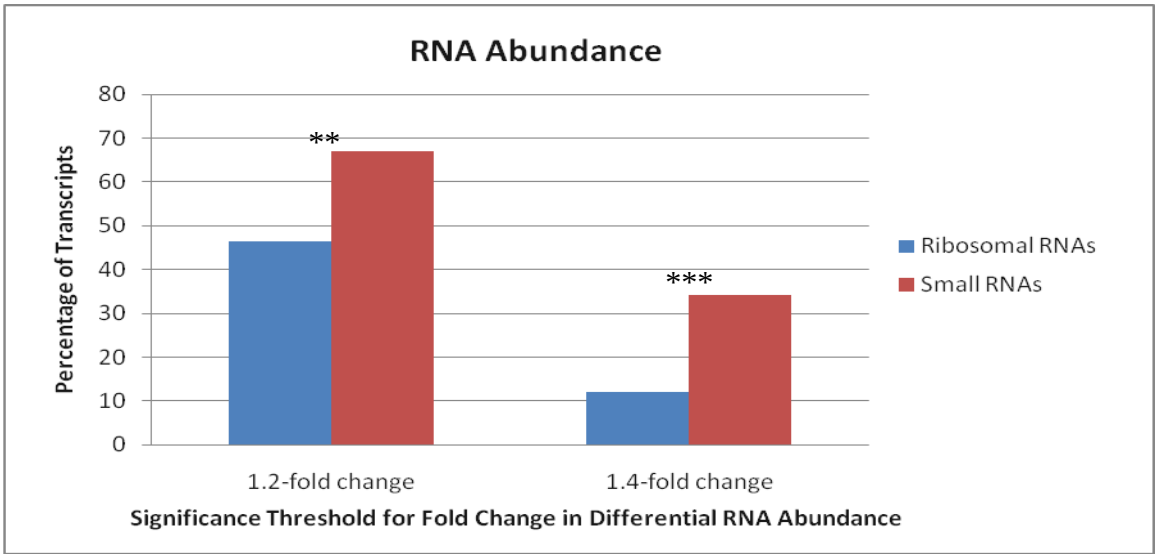

Figure 3-11. Percentage of small RNA and ribosomal protein transcripts that were differentially abundant at 1.2 and 1.4 fold-change thresholds (significant at p<0.05 in a 2-way ANOVA). *Data was derived from the number of such transcripts, divided by the total number of small RNAs or ribosomal transcripts that were significant at p<0.05 in a 2-way ANOVA. ** Indicates highly significant at p< 1 x 10^{-4}, *** indicates highly significant at p< 1 x 10^{-9} using a binomial probability test (n=3 pairs of biological replicate arrays).*

3.3.3.1 IPA Analysis: Biological and Canonical Functions

At a threshold of 1.4-fold change, a number of logical biological functions were highlighted following IPA analysis. These included cellular morphology and organisation, signalling, DNA replication, RNA trafficking, molecular transport and gene expression (Fig. 3-12A). Figure 3-12B illustrates that some classes of transcripts did not appear to be regulated in response to the microgrooved substrate, including genes corresponding to immunological functions, auditory and nutritional pathologies, and organismal survival. Interestingly, transcripts relating to hair and skin development and function did not appear to be substantially regulated in response to the topography, suggesting that the microgrooved substrate was unlikely to be modulating the basic epithelial functionality of the fibroblasts.

A

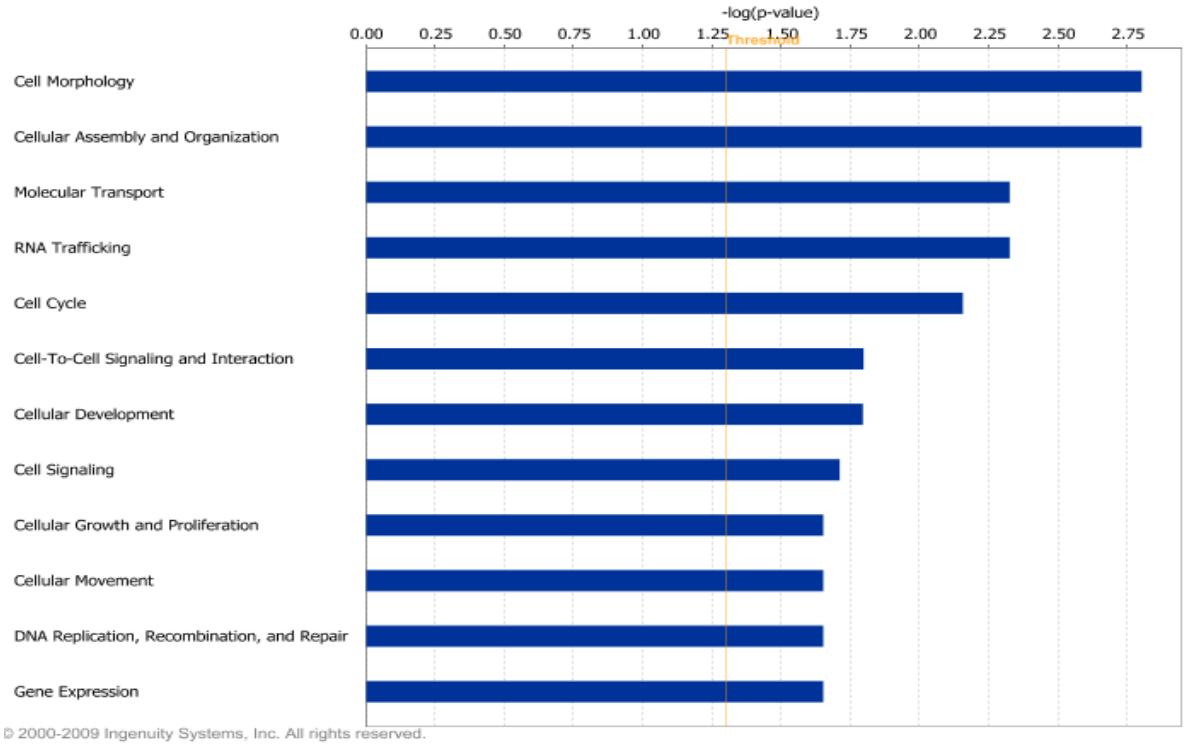

B

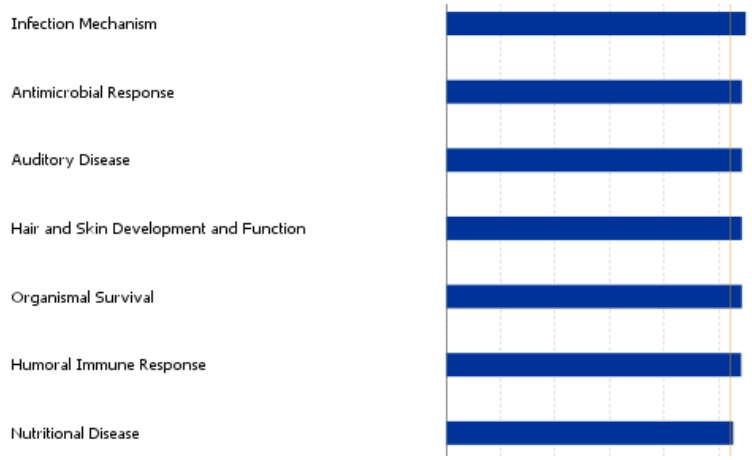

Figure 3-12. Illustration of some functional classes of transcripts that were A) differentially abundant or B) not apparently subject to differential regulation between cells cultured on the microgrooved and planar substrata. *Applied thresholds were 1.4-fold change and $p<0.05$ ($n=3$ pairs of biological replicate arrays). Note that the same scale applies to A and B, and the threshold line (orange line) has been aligned between images to facilitate.comparison of A and B.*

At a threshold of 1.2-fold change (retaining the $p<0.05$ threshold for significance), some canonical signalling pathways became significant, notably insulin receptor signalling, Wnt/β-catenin signalling, PTEN signalling and the PI3K/AKT cascade. The urea cycle was also noted at the significance threshold. These pathways were not

significant at the more stringent 1.5 fold-change threshold, however, which suggests that the subtle modifications in gene expression could be sufficient to effect the necessary changes in levels of signalling proteins, or that the differential expression was only beginning to reach prominence at the time-point examined. Alternatively, additional noise may have been introduced by reducing the fold-change threshold. It is important to note, however, that only 458 genes appeared to be differentially expressed at this threshold, with 279 of these also present at the 1.4-fold change threshold. Both of these numbers were considerably less than 800 genes, the quantity recommended by the developers of IPA as an upper limit for inclusion in an analysis to avoid noise. In addition, even if a canonical pathway is not highlighted as statistically significant by the software (*i.e.* containing more differentially expressed molecules than would be expected by chance), the results can still have biological significance. Thus, the regulation of the actin cytoskeleton (Fig. 3-13) and ERK/MAPK (Fig. 3-15) signalling were also of interest, particularly in light of the substantial reorganisation of F-actin noted on the grooved topography in Chapter 2.

In the actin signalling pathway, three upstream regulators were differentially expressed (threshold: 1.2-fold change), with potential effects on various actin-related functions (Fig. 3-13). It was particularly interesting that transcripts encoding Rac and Rho were both up-regulated in cells on the grooved topography. Rac has been shown to act as a switch for persistent migration (Pankov et al., 2005). It seems plausible that the lateral confinement by the topography (which predominantly forces cell migration within the grooves) could be stimulating up-regulation of Rac mRNA, to compensate for the restricted directionality of movement likely to be induced by alignment to the topography. Insulin receptor tyrosine kinase substrate p53 (IRSp53) is involved in lamellipodium and filopodial formation (Nakagawa et al., 2003) and was up-regulated in cells on grooves, as were PAK (p21 activated protein kinase) and LIMK (LIM domain kinase). PAK stimlulates LIMK, and LIMK prevents cofilin-mediated scission of actin filaments by phosphorylating cofilin (Ding et al., 2008; Edwards et al., 1999). Rho guanosine diphosphate dissociation inhibitor alpha (GDIA), and WASP (Wiskott-Aldrich syndrome protein), which activates the Arp2/3 complex to initiate assembly of new actin filaments (Dayel and Mullins, 2004), were also up-regulated.

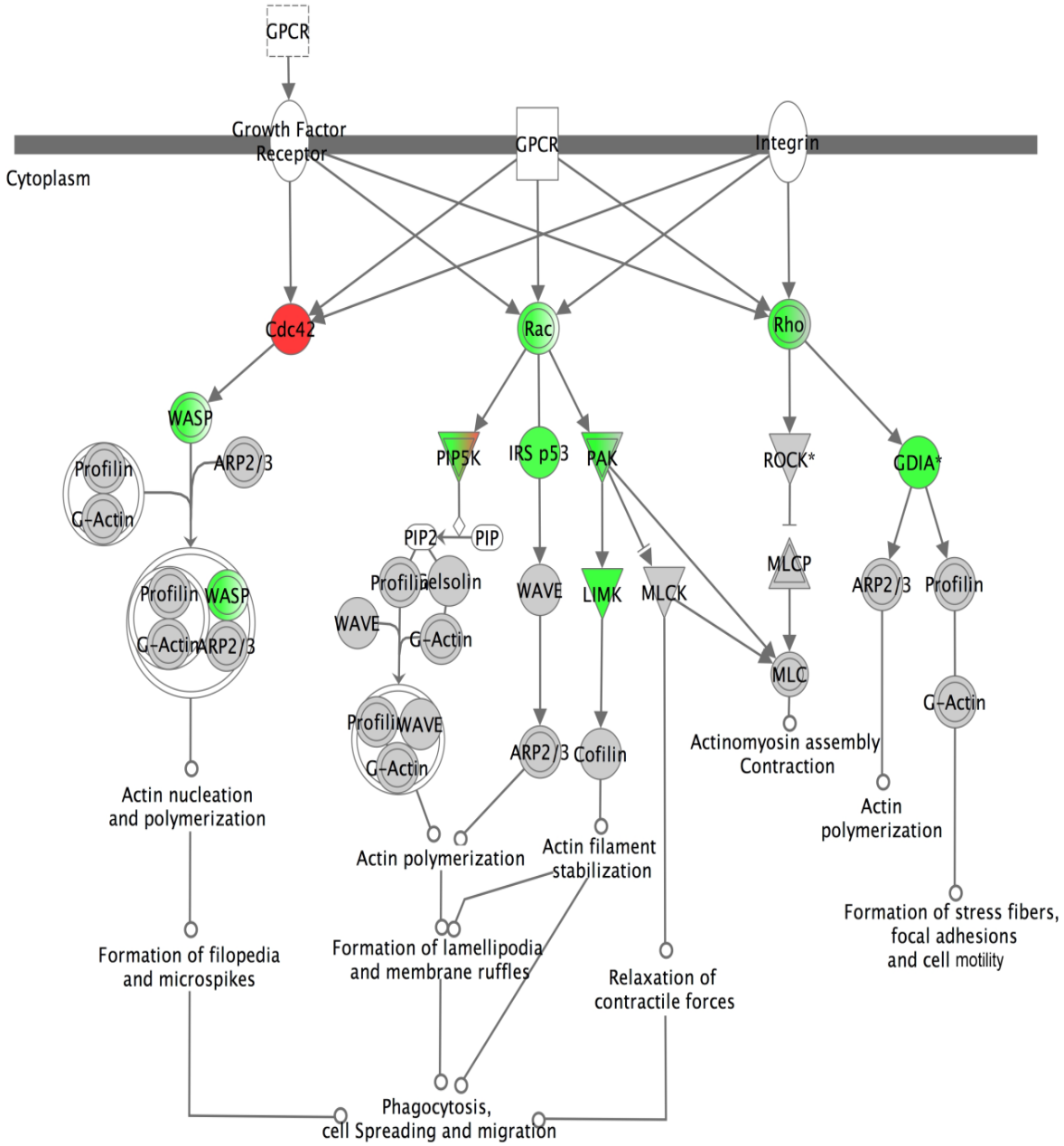

Figure 3-13. Actin signalling (fold-change threshold: 1.2; n=3 pairs of biological replicate arrays). *Up-regulated transcripts in cells on the microgrooved topography – Green, Down-regulated transcripts in cells on the microgrooved topography – Red; Transcripts with unchanged abundance relative to control – Grey, Not measured – White. Key:* ***ARP2/3*** *– actin-regulating protein 2/3,* ***Cdc42*** *– cell division cycle 42,* ***GDIA*** *– Rho guanosine diphosphate association inhibitor alpha,* ***GPCR*** *– G-protein coupled receptor,* ***IRS p53*** *– insulin receptor tyrosine kinase substrate p53,* ***LIMK*** *– LIM domain kinase 1,* ***MLC*** *– myosin light chain,* ***MLCK*** *– myosin light chain kinase, MLCP – myosin light chain phosphatase,* ***PAK*** *– p21 activated protein kinase,* ***PIP*** *– phosphatidyl inositol phosphate,* ***PIP2*** *– phosphatidylinositol 4, 5-bisphosphate,* ***PIP5K*** *– 1-phosphatidylinositol-4-phosphate 5-kinase,* ***ROCK*** *– Rho kinase,* ***WASP*** *– Wiskott-Aldrich syndrome protein,* ***WAVE*** *– WASP family Verprolin-homologous protein.*

In the PTEN (phosphatase and tensin homolog) signalling pathway (Fig. 3-14), transcripts for the small G-protein Ras and MEK1/2 - components of the Ras/Raf/MEK/ERK signalling pathway - were up-regulated in cells cultured on microgrooves. This could have been promoting a reduction in focal contacts and increased cell migration (Fig. 3-14). Closer examination of the MAPK signalling pathways showed

that Src mRNA was also up-regulated in cells on the topography, which can stimulate Ras (Fig. 3-15). There appeared to be a fine balance between inhibitory and stimulatory factors in the MAPK pathway, with evidence that both types were up-regulated at the transcript level in cells on the grooved topography. A-Raf, which has a stimulatory effect on MEK 1/2, was up-regulated. Two upstream phosphatases of MEK 1/2 and ERK 1/2 were also up-regulated, however, which inhibit MAPK activity. A similar situation was observed with the up-regulation of MNK 1/2 and eIF4E. The kinase MNK 1/2 is a downstream target of ERK signalling, and stimulates translation by phosphorylation of eIF4E (Ueda et al., 2004). Perhaps to counterbalance this, 4E-BP1 was also increased, which acts to reduce mRNA translation. Certain transcription factors modulated by p90RSK or ERK 1/2 were differentially regulated, including c-Fos and Ets, both of which were up-regulated in cells on microgrooves. These factors act as terminal effectors of MAPK signalling by binding to serum-response elements (Ets) or AP-1 elements (c-Fos) in target genes, which include genes associated with cell growth, proliferation, differentiation and those for matrix metalloproteases (Crowe and Brown, 1999). .

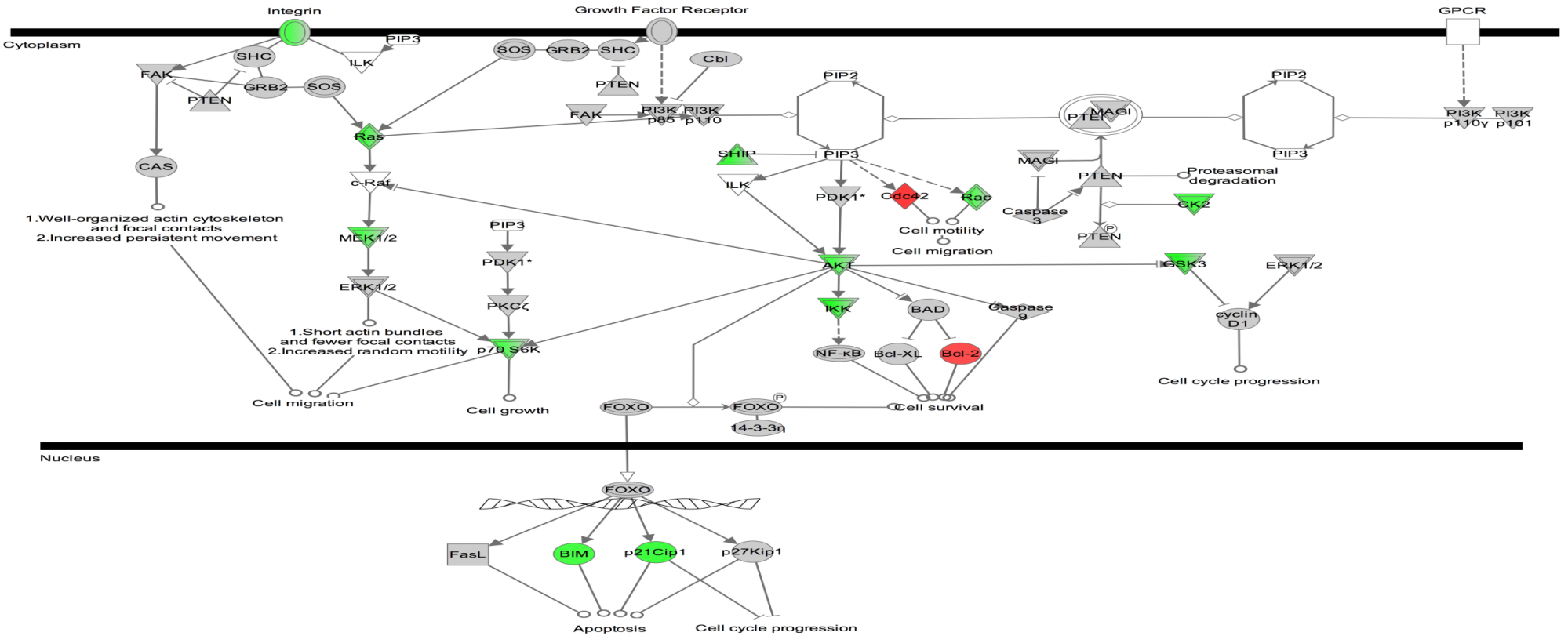

Figure 3-14. PTEN signalling (1.2-fold-change, p<0.05; n=3 pairs of biological replicate arrays). *Up-regulated transcripts in cells on the microgrooved substrate – Green, Down-regulated transcripts in cells on the microgrooved substrate – Red, Transcripts with unchanged abundance relative to control – Grey, Not measured – White.* ***Key: 14-3-3η*** *- 14-3-3 eta,* ***AKT*** *– protein kinase B,* ***BAD*** *– Bcl-xL/Bcl-2-associated death promoter,* ***Bcl-2*** *– B-cell lymphoma 2,* ***Bcl-XL*** *– B-cell lymphoma-extra large,* ***BIM*** *– Bcl-2 interacting mediator of cell death,* ***Caspase 3***, ***Caspase 9***, ***Cbl***, ***CK2*** *– casein kinase 2, cyclin D1, c-Raf,* ***ILK*** *– integrin-linked kinase,* ***IKK*** *– IkB kinase,* ***Integrin***, ***ERK1/2*** *- extracellular signal-regulated kinase 1/2,* ***FAK*** *– focal adhesion kinase,* ***FasL*** *– Fas ligand,* ***FOXO*** *– Forkhead box O,* ***GRB2*** *– growth factor receptor bound protein,* ***GSK3*** *– glycogen synthase kinase 3,* ***MAG***, ***MEK1/2*** *– mitogen-activated protein kinase kinase 1/2,* ***NF-kB*** *– nuclear factor kappa B,* ***p21Cip1***, ***p27Kip1***, ***p70 S6K*** *– RPS6-p70-protein kinase,* ***PDK1*** *– phosphoinositide-dependent kinase 1,* ***P13K p110*** *– phosphoinositide kinase-3 p110 subunit,* ***PI3K p185/110/110γ/101*** *- phosphoinositide kinase-3 p185/110/110γ/101 subunits,* ***PIP2*** *– phosphatidylinositol 4, 5-bisphosphate,* ***PIP3*** *- phosphatidylinositol (3, 4, 5)-triphosphate,* ***PKCζ*** *- protein kinase C zeta,* ***PTEN*** *– phosphatase and tensin homolog deleted on chromosome 10,* ***Ras***, ***SHC –*** *Src homology domain containing transforming protein 1,* ***SOS*** *- son of sevenless.*

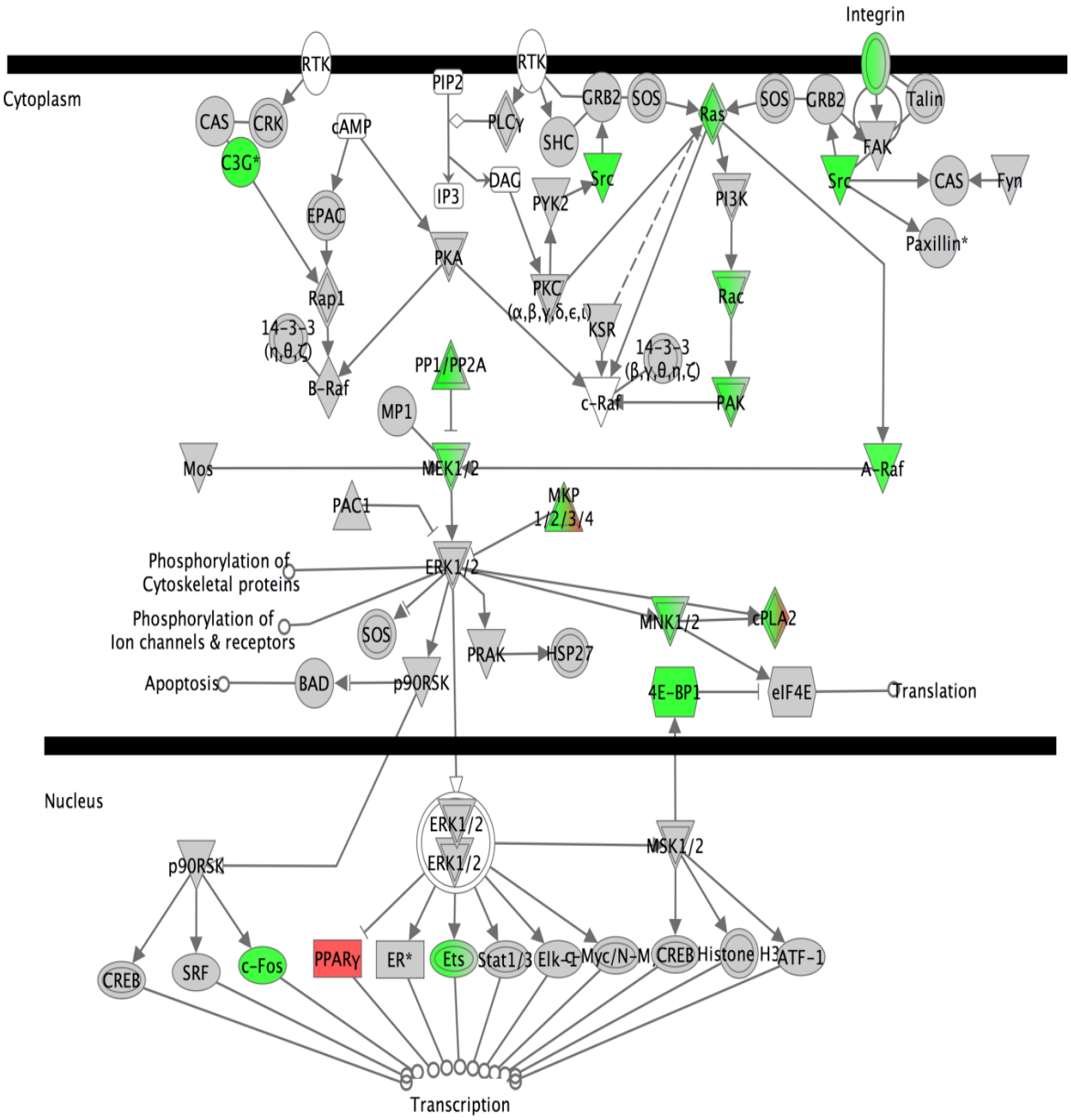

Figure 3-15. ERK/MAPK signalling (fold-change threshold: 1.2, n=3 pairs of biological replicate arrays). *Up-regulated transcripts in cells on the microgrooved substrate – Green, Down-regulated transcripts in cells on the microgrooved substrate – Red, Transcripts with unchanged abundance relative to the control – Grey, Not measured – White.* ***Key: 4E-BP1*** *– eukaryotic translation initiation factor 4E binding protein 1,* ***14-3-3 β, γ, θ, η, ξ*** *– 14-3-3 beta, gamma, theta, eta, zeta, 14-3-3 η, θ, ζ – 14-3-3 eta, theta, zeta,* ***A-Raf*** *– c-raf murine sarcoma 3611 viral oncogene homolog,* ***ATF-1*** *– activating transcription factor 1,* ***BAD*** *– Bcl-xL/Bcl-2-associated death promoter,* ***B-Raf*** *– v-raf murine sarcoma viral oncogene homolog B1,* ***C3G*** *– Rap guanine nucleotide exchange factor 1,* ***cAMP*** *– 3'5'-cyclic adenosine monophosphate,* ***CAS*** *– breast cancer anti-oestrogen resistance 1,* ***c-Fos*** *- FBJ murine osteosarcoma viral oncogene homolog,* ***c-Raf*** *- v-raf-1 murine leukaemia viral oncogene homolog,* ***DAG*** *– diacylglycerol,* ***eIF4E*** *– eukaryotic translation initiation factor 4E,* ***Elk-1*** *– ELK1, member of ETS oncogene family,* ***ER*** *– oestrogen receptor,* ***ERK1/2*** *– extracellular signal-regulated kinase 1/2,* ***HSP-27*** *– heat shock protein 27kDa,* ***FAK*** *– focal adhesion kinase,* ***Fyn*** *– FYN oncogene related to SRC, FGR, YES,* ***GRB2*** *– growth factor receptor bound receptor 2,* ***IP3*** *– inositol 1,4,5-triphosphate,* ***KSR*** *– kinase suppressor of Ras 1,* ***MEK1/2*** *– mitogen-activated protein kinase kinase 1/2,* ***MKP 1/2/3/4***, ***Mos*** *– v-mos Moloney murine sarcoma viral oncogene homolog,* ***MP1*** *– mitogen-activated protein kinase scaffold protein 1,* ***p90RSK*** *– ribosomal protein S6 kinase,* ***PAC1*** *– dual specificity phosphatase 1,* ***PAK*** *– p21 activated protein kinase,* ***Paxillin***, ***PI3K*** *– phospatidyl inositol 3 kinase,* ***PKC α, β, γ, δ, ε, ι*** *– protein kinase C (alpha, beta, gamma, delta, epsilon, iota),* ***PIP2*** *– phosphatidylinositol 4, 5-bisphosphate,* ***PLCγ*** *– phospholipase C gamma,* ***PPARγ*** *– peroxisome proliferator activated receptor γ,* ***PRAK*** *– mitogen-actiated protein kinase activated protein kinase 5,* ***PYK2*** *– protein tyrosine kinase 2 beta,* ***Rap1***, ***SHC*** *– Src homology 2 domain containing transforming protein 1,* ***SOS*** *– son of sevenless,* ***Src*** *– v-src sarcoma (Schmidt-Ruppin A2) viral oncogene homolog,* ***SRF*** *– serum response factor,* ***Talin***

3.4 Discussion

Microarray analysis enabled a global assessment of differential transcript abundance between cells cultured on the microgrooved and planar substrata. A number of very logical functional classes of transcripts appeared to be differentially regulated. It is particularly interesting that molecular transport, RNA trafficking and DNA replication were among these, given their relevance to the mechanical effects on the nucleoli and nuclear lamina discussed in Chapter 2. The cells could be attempting to exaggerate or compensate for the effects of topography by altering the expression of genes involved in these processes. It is likely that reorganisation of the nuclear lamina would affect the nucleo-cytoplasmic transport of RNA and small molecules, and potentially alter DNA replication by the association of lamin B with proliferating cell nuclear antigen (PCNA).

An interesting consequence of the mechanical reorganisation induced by the topography appeared to be the differential expression (predominantly down-regulation) of 21 small RNAs at the stringent 1.5-fold change threshold. Differential abundance of the small RNAs remained striking at the 'population' level in comparison with transcripts for ribosomal proteins. The ribosomal proteins were selected as a relatively large group of related transcripts that were not expected to show a large difference between the two substrates. Ribosomal protein L5 was markedly down-regulated on the grooved topography, however. If this was suggestive that this group of transcripts could be exhibiting more differential expression than would be expected from a set of 'housekeeping' genes, this would still be tolerated, as it should only lead to an underestimation of the magnitude of difference between the baseline group (ribosomal protein transcripts) and the greatly differentially expressed group (small RNAs). It is likely that the differential abundance of the small RNA transcripts between the two substrata serves as a rapid-response mechanism for modulation of mRNA translation or degradation by the RNAi machinery (in the case of *miR-21*), or transcript editing (in the case of snoRNAs and scaRNAs). It is tempting to speculate that the morphological changes in the nucleoli (elongation and alignment within the microgrooves, Chapter 2) may be regulating the production of small RNAs, particularly the snoRNAs, which function at this site.

Differential regulation of transcripts for key signalling proteins (such as Rac, Rho) involved in cell motility and actin dynamics could be important for cytoskeletal

reorganisation on the topography (as noted by microscopy in Chapter 2), and potentially directed cell movement. The involvement of components of MAPK/ERK signalling could signify alterations in cell growth, and may have become more significant at a later time-point. Although ERK itself did not appear to be differentially expressed at the mRNA level between cells on the two substrates, the differential expression of its interacting partners may have been sufficient to effect downstream changes in this pathway. MAPK/ERK signalling was previously highlighted in other transcriptomic (Biggs et al., 2009) and proteomic (Kantawong et al., 2009b) studies of cellular response to topography. Using interaction analysis, other transcripts of interest were highlighted, including those involved in cell adhesion and motility. This is consistent with the typical change in cell morphology from more expansively spread (planar) to bipolar (microgrooves) (Chapter 2), with probable consequences for cell motility. There was also a potential involvement of ECM remodelling, with up-regulation of the transcripts for a number of MMPs. Consistent with this, fibroblastic MMP activity appears to be affected by culture on nano- and microgrooved polycaprolactone substrates, as assessed by zymography (A.S. Brydone, M.J. Dalby, R.M.D. Meek and L.E. McNamara, manuscript in preparation), and MMP abundance can be increased by cell stretch in response to MAPK activation (Ziegler et al., 2010). Changes in the transcription and chromatin remodelling machinery would be consistent with the apparent alterations in gene expression.

In comparison with the previous microarray study of cells on the same dimensions of microgrooves (Dalby et al., 2003c), similar categories of differentially regulated genes were highlighted in this larger coverage study, including those related to the cytoskeleton, cell morphology, cell signalling, proliferation, DNA replication and gene expression. The authors selected 25 specific differentially regulated genes of interest, 18 of which could be identified in data from the current microarray study. Of these, three genes appeared to be somewhat similarly expressed ($p<0.05$) (Table 3-III).

Table 3-III. Transcripts with similar abundance between a previous study of cells cultured on the 2 μm depth and 25 μm pitch microgrooved or planar quartz (Dalby et al., 2003b) and the present study.

Name of Gene Product (from Dalby et al. 2003)	Fold change (from Dalby et al. 2003)	**Name of Comparable Gene Product (Affymetrix arrays)**	**Fold-change (G:P)**	***p*-value**
DNA-directed RNA polymerase II	+1.25	Polymerase (RNA) II (DNA directed) polypeptide E, 25 kDa	+1.1806	2.7×10^{-3}
Developmentally regulated GTP-binding protein DRG	+1.59	Developmentally regulated GTP binding protein 1	+1.239	4.2×10^{-3}
Eukaryotic translation initation factor 3 beta subunit	+1.45	Eukaryotic translation initiation factor 3, subunit 2 beta	+1.21763	1.0×10^{-2}

Although the magnitude of response appeared to be slightly reduced for these genes in the present study (lower fold-change), their recurrent up-regulation on this topography in two studies suggests that the key functions afforded by these molecules (transcription, translation, and potentially cytoskeletal control mediated by translational factors) are likely to be of reproducible importance. With respect to the other genes, this suggests that although the functional categories of differentially regulated genes are likely to be maintained between studies of cells on comparable topographical substrata, the specific transcripts involved can differ, perhaps due to slight differences in cellular status, or functional redundancy among the gene products.

In general, the magnitude of differential expression was not particularly high between the two substrates for genes that were statistically significant, which probably resulted from a combination of the early time-point examined, and the relatively low number of replicates used. With fewer replicates, some higher magnitude changes may have been overlooked, as the higher standard deviation between replicates could have resulted in an increased incidence of type II statistical errors (an artefactual failure to reject the null hypothesis). After the short culture period, it seems plausible that the magnitude of differential expression change in certain genes could be more moderate due to the gradual induction of gene expression in a slower, but sustained, response to the topographical stimulus. This seems particularly likely given that there was a fairly rapid response at the levels of the direct effectors, such as small RNAs, and proteins, as will be discussed further in Chapter 5. Importantly, however, because changes in the abundance of transcripts do not necessarily represent alterations at the effector level, the sizes of the

gene expression changes do not necessarily reflect the scale of the biological effect. This is particularly apt, since a small increase in transcript abundance has the potential to become 'amplified' by other functional levels of control, including translation. It is probable that the modulation of transcript abundance did not result exclusively from mechanotransductive effects, since the global nature of microarray experiments is such that many transcript species can be investigated simultaneously and with high sensitivity, but the causative stimulus for observed differential expression changes cannot be definitively determined from the resulting dataset. It is possible that there may be some contribution from 'noise' effects due to the analysis of a large dataset, although this should have been minimised during data processing, or some other cryptic biological processes, but the mechanostimulus should still remain the predominant, overarching variable mediating changes between the two substrata.

For validation of specific transcripts of interest, it would be useful to to perform quantitative PCR, including analysis of small RNAs with specific TaqMan small RNA probes, which are designed with stem-loop structures to enable greater discrimination and permit association with only one species of mature small RNA per probe (Chen et al., 2005). It would also be important to examine these transcripts at the level of the functional effectors, which could be performed using Western blotting or targeted antibody arrays (Huang et al., 2010), and may also be partially covered by non-targeted proteomic studies.

3.5 Conclusion

Compared with controls, cells cultured on the microgrooved substrate showed altered expression of transcripts involved in key cell processes relating to cell morphology, RNA trafficking, DNA replication, gene expression, and signalling. Many small RNAs, including snoRNAs, scaRNAs and a microRNA, were down-regulated in cells on the topography. This seems likely to be a relatively rapid response mechanism to facilitate protein-level alterations as an adaptation to the topological mechanostimulus. The data from this chapter support the induction of a transcript-level mechanoresponse, via modulation of small RNA effectors and mRNAs involved in important cellular functions.

4 Chromosomal Analysis

4.1 Introduction

Chromosome territories are dynamic, and can be relatively rapidly repositioned within the nucleus. Following serum starvation of human fibroblasts, for example, chromosome (Ch) 1 relocated from a more central location in the nucleus to a more peripheral location at the nuclear edge (Mehta et al., 2010). This would be anticipated to correlate with gene silencing, perhaps reflecting a general down-regulation of gene expression in response to the removal of serum, and associated growth factors. Bolzer et al showed the positioning of all the chromosomes in human fibroblasts from a male donor in G_0 phase, using a modification of FISH that permits staining of all chromosomes within the same nucleus (Fig. 4-1) (Bolzer et al., 2005). The precise arrangement of chromosomes within the nucleus appears to be cell-type dependent, which probably reflects functional specialisation. In general, however, the chromosomes appear to be arranged according to gene richness, with gene-poor chromosomes typically located nearer the edge of the nucleus (Boyle et al., 2001), or size, with smaller chromosomes towards the centre of the nucleus (Bolzer et al., 2005).

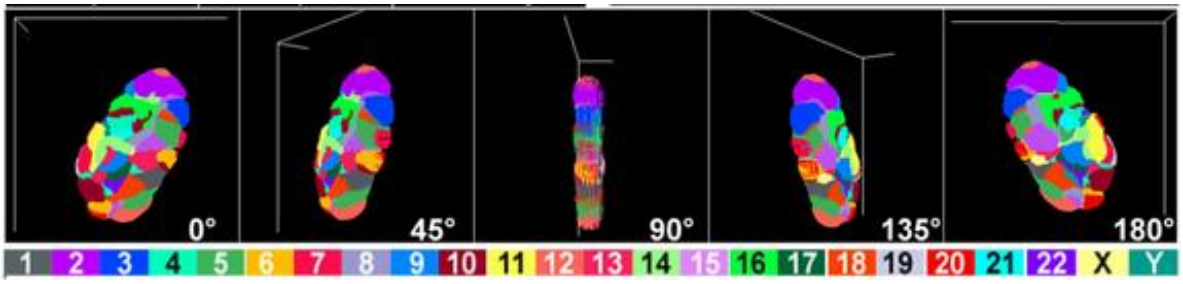

Figure 4-1. Chromosome territory positioning in G_0 phase fibroblasts. *3D confocal reconstruction of chromosomal territories in male human fibroblasts stained using goldFISH, a modification of FISH that permits visualisation of all chromosome territories within the same nucleus. Reproduced with modification from (Bolzer et al., 2005).*

Heterochromatin also contributes to the maintenance of nuclear architecture. It appears to bear cytoskeletal forces (Mazumder and Shivashankar, 2007) and is involved in linking the cytoskeleton with the nucleus. Laser ablation of the nuclear heterochromatin led to a reduction in nuclear size, consistent with the role of heterochromatin in maintaining nuclear structure (Mazumder and Shivashankar, 2010). Epigenetic modifications, including methylation (Shilatifard, 2006; Zhang and Reinberg, 2001), acetylation (Ramsey et al., 2010), phosphorylation (Lo et al., 2005), ubiquitinylation (Shilatifard, 2006) and SUMOylation (Shiio and Eisenman, 2003) of histones, can induce

reversible modulation of the chromosomal organisation and accessibility by affecting the extent of packing of the chromosomal components. Chromosomal organisation was affected in the cells of patients suffering from a condition that leads to aberrant histone methylation (Matarazzo et al., 2007). This affected both relocalisation of particular gene loci to the exterior of chromosome territories, and the organisation of territories within the nucleus. Chromosome 19, a gene-rich chromosome, was shown to be enriched in trimethylated H3K4 (addition of three methyl groups to lysine 4 of histone 3), an 'activating' mark for transcription, compared with the relatively gene-poor chromosome 18 (Zinner et al., 2007). The process of epigenetic gene silencing was studied by Mutskov et al. using the stable integration of a transgene into the genome. The speed of transgene silencing was correlated with the site of insertion, with heavily chromatinised regions of endogenous flanking DNA promoting faster silencing. The mechanism of silencing involved multiple epigenetic modifications, including hypoacetylation of histones H3 and H4, dimethylation of H3 K9, and DNA methylation (Mutskov, 2004). Using an inducible expression system, Oyer et al. showed that a transient reduction in gene expression can result in inappropriate silencing (Oyer et al., 2009), which can occur in pathologies such as cancer, when oncoprotective genes are aberrantly silenced. Chromatin remodelling machines can affect gene accessibility by directly altering chromatin packaging, or the distribution of epigenetic marks, which can be recognised by secondary remodellers. Small RNAs (miRNAs) can also contribute to gene silencing, by interacting with the promoter region of genes, apparently via interactions between the miRNA and cognate short intra-promoter transcripts, to induce the establishment of a repressive chromatin architecture following epigenetic modulation and chromatin remodelling (discussed in (Moazed, 2009).

In view of the large number of differentially expressed genes (including transcription factors and chromatin remodelling machines) noted in Chapter 3, it was important to determine whether particular chromosomes were 'hotspots' for this observed differential expression, and whether mechanical redistribution of chromosomes within the nucleus could contribute to such an effect.

4.2 Data Mining of Microarray Data and Development of Rationale for FISH Analysis

4.2.1 Analysis of Microarray Data

To identify chromosomal 'hotspots' for differential gene expression, the microarray data (see Chapter 3) was used to identify chromosomes for FISH analysis. Differentially regulated transcripts (thresholds of +/- 1.5-fold change, $p<0.05$) were grouped by chromosome, subcategorised by the directionality of the differential expression (Fig. 4-2), and analysed for the sub-chromosomal band positioning of differentially regulated genes (Fig. 4-3). Ch 1 had the largest number of genes that were differentially expressed in response to culture on the microgrooved substrate. Ch 1 also had the largest number of genes that were down-regulated in response to the topography. The chromosome with the most up-regulated genes was Ch 19, while Ch 18 had the fewest gene-level changes.

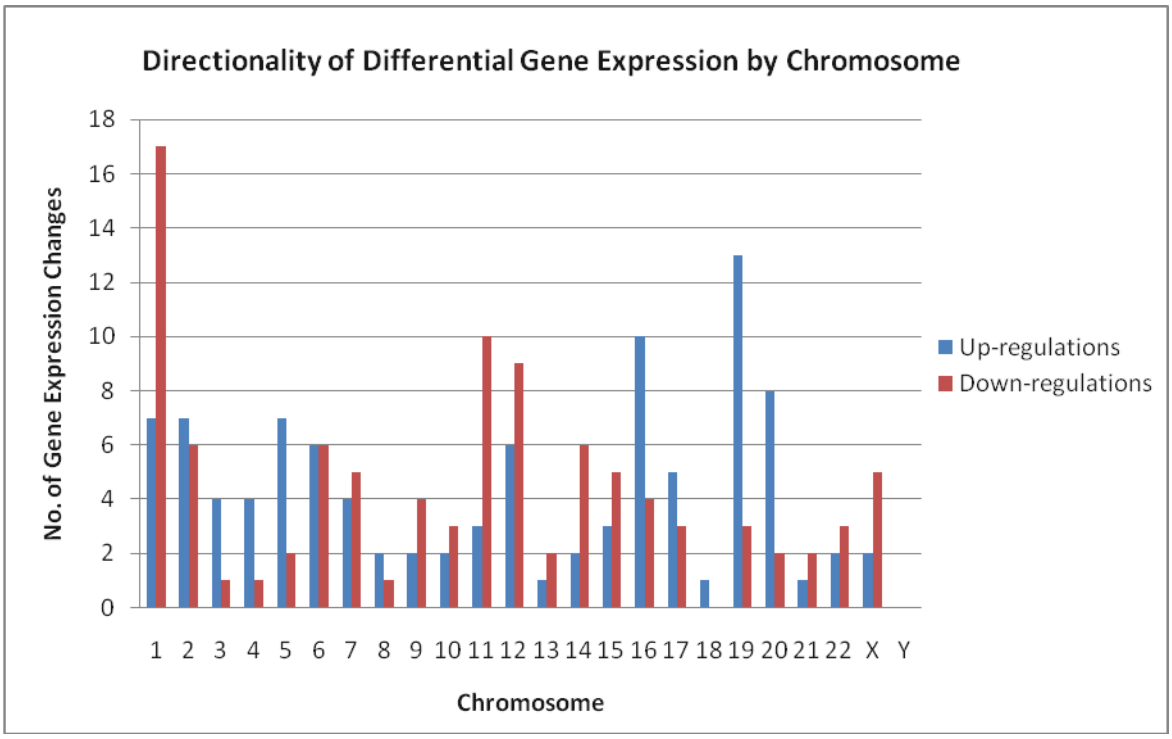

Figure 4-2. Chromosomal locations of genes differentially expressed in response to the microgrooved topography. *The directionality of differential gene expression is shown, based on the microarray data, for Chs 1-22, X and Y (thresholds 1.5-fold change, p<0.05). Up-regulations/down-regulations refer to the transcript abundance in cells cultured on the microgrooved quartz surface (25 μm pitch, 2 μm depth) relative to the planar substrate. (Data was derived from n=3 microarrays from fibroblasts cultured on planar substrata, and n=3 microarrays from fibroblasts on microgrooved substrata).*

Combining the band positioning results from all the chromosomes illustrated the general trend for sub-chromosomal sites of differential expression (Fig. 4-3). There

appeared to be a peak of differential expression around bands 11-13, with a broader region around bands 21-26, and few or no detectable differentially expressed genes around bands 1-10, 16-20, 27-30 and 38-41. Most differentially expressed genes were located within chromosome band 13 for both the p- and q-arms.

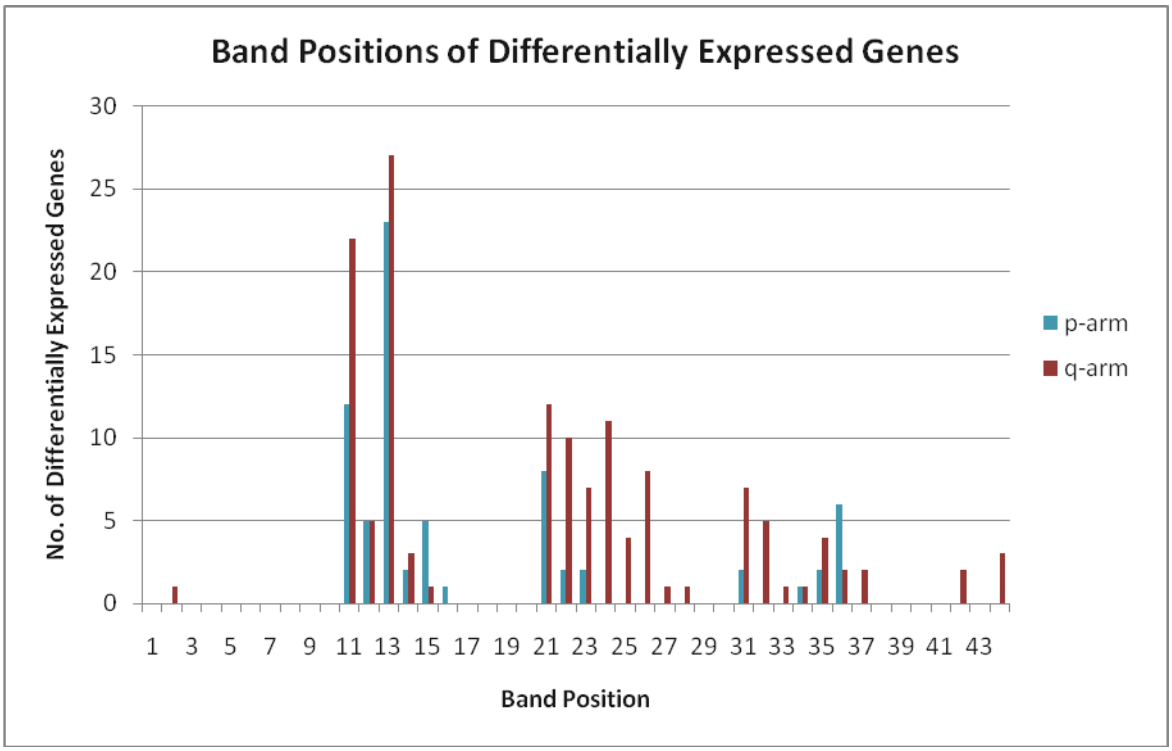

Figure 4-3. Sub-chromosomal band positions of genes exhibiting differential expression on the microgrooved topography. *Band positions are shown for all chromosomes with genes exhibiting differential expression at a threshold of 1.5-fold change ($p<0.05$); p-arm and q-arm refer to the short (p-), and long (q-) arm of each chromosome. (Data was derived from n=3 microarrays from fibroblasts cultured on planar substrata, and n=3 microarrays from fibroblasts cultured on microgrooved substrata).*

Interestingly, on Ch 19, the differentially expressed genes were predominantly localised to band 13 on both the p- and q-arms (Fig. 4-4). On Ch 1, by contrast, there was a greater spread in localisation of the differentially expressed genes, with peaks around bands p31-36 and q21-24 (Fig. 4-4). The differentially expressed gene on Ch 18 was located at band 11 on the p-arm.

To examine whether direct mechanotransduction could be contributing to the transcriptomic changes via repositioning of chromosome territories, whole-chromosome Fluorescence *In situ* Hybridisation (FISH) was employed.

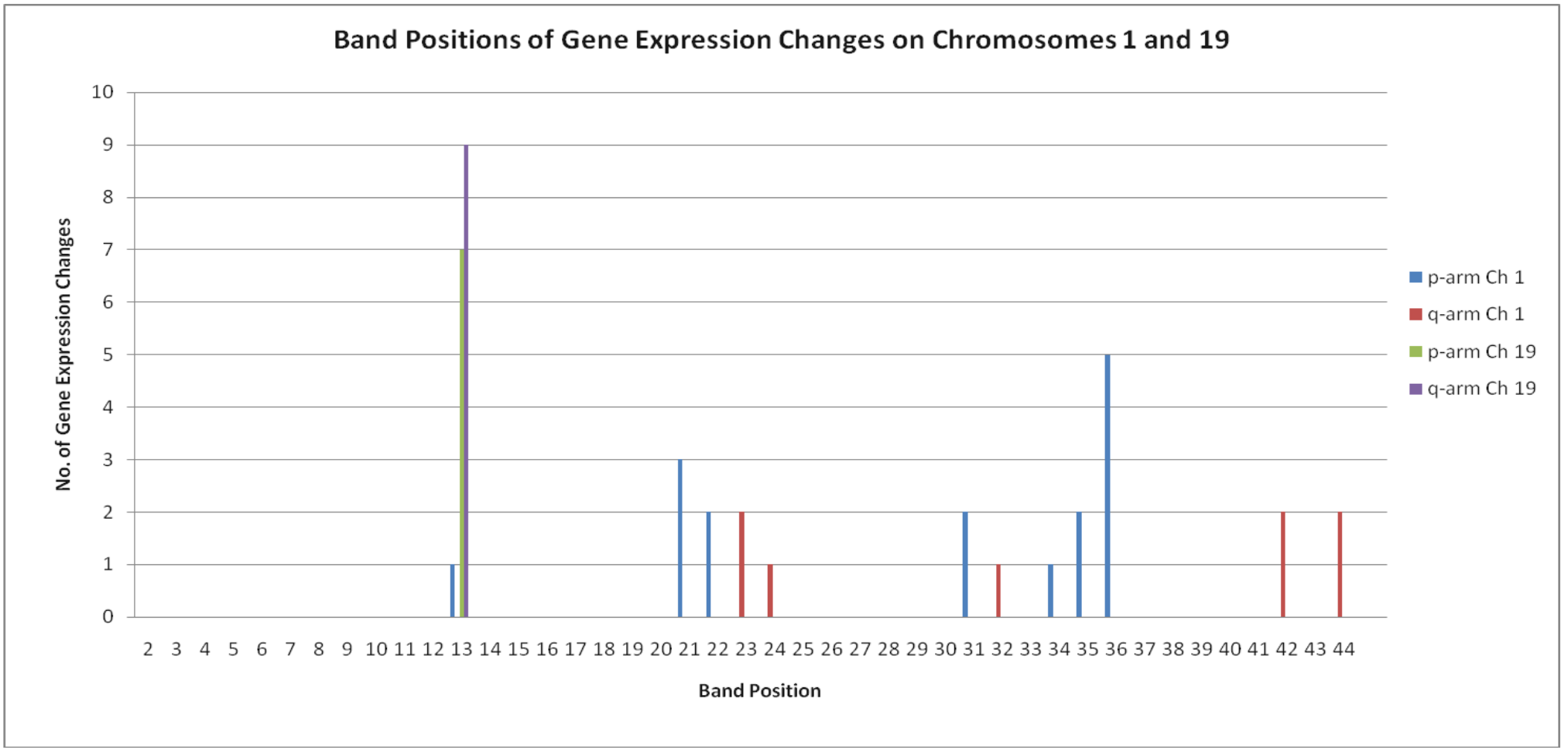

Figure 4-4. Band positions of genes differentially expressed on Ch 1 and 19 between cells on the microgrooved and planar substrates. *The thresholds chosen for differential gene expression were 1.5-fold change and $p<0.05$. The longer chromosomal arm (q-arm) is distinguished from the shorter arm (p-arm) in this diagram. Note that differentially expressed genes were located at bands19p13 and 19q13 on Ch 19, but more widely distributed across Ch 1. (Data was derived from n=3 microarrays from fibroblasts cultured on planar substrata, n=3 microarrays from fibroblasts cultured on microgrooved substrata).*

4.3 Materials and Methods

4.3.1.1 Growth of Cells on Biomaterials

Fibroblasts (hTERT BJ-1) were seeded at a density of ~ 150 cells/mm^2 material, with a 24h culture period. The 25 x 25 mm quartz substrates were used for all FISH experiments, with the exception of the lamin A/C siRNA knockdown study. Due to the limited number of quartz substrates, in the knockdown experiments, a 25 x 75 mm substrate was used for the transfection controls (untransfected or negative control siRNA-transfected cells). This permitted examination of the same surface area of material corresponding to the two sets of three 25 x 25 mm 'test' substrates (three planar and three grooved substrata) incubated with siRNA directed against lamin A/C, allowing a direct comparison by enabling cells to be seeded at the same time as on the test substrata. Note that the *n* numbers in the text refer to the number of substrates used in each experiment.

4.3.2 FISH (Fluorescence In situ Hybridisation)

4.3.2.1 Territory Staining

Cells were fixed in 3:1 methanol:acetic acid for 30 minutes at room temperature, and rinsed in 2x SSC (Saline Sodium Citrate; diluted from 20X stock of 3M NaCl, 0.3M *tri*-sodium citrate, pH 7.4) for 3h at 37^{o}C. Towards the end of this incubation step, the appropriate chromosome probe (ready-to-use biotinylated human chromosome 1, 3, 18 or 19 paint; Cambio, Cambridge, UK) was brought to 37^{o}C, vortexed, and pelleted by centrifugation for ~3 seconds at 11000x*g*. The required volume of probe was removed into a sterile Eppendorf tube, and denatured at 65^{o}C for 10 minutes, followed by a 30-60 minute incubation at 37^{o}C. The slides were rinsed in double-distilled water for 30s, and then transferred through a dehydrating ethanol series, with a 2-minute incubation at each step (70% (v/v), 90% (v/v), 90% (v/v)), followed by a 5-minute dehydration step in 100% ethanol. The samples were air dried for 1 minute, then incubated in denaturation solution (7:1 formamide:2x SSC buffer) at 65^{o}C for 2 minutes. The samples were quenched using an ice-cold version of the dehydration series described above (70% (v/v), 90% (v/v), 90% (v/v), 100% ethanol steps), and air-dried for 1 minute.

Denatured probe (8-15µl) was added to each sample; the samples were covered with coverslips, and incubated for 44h at 37^{o}C in a humidified chamber. Following this hybridisation step, the slides were rinsed in 45^{o}C pre-warmed 1x SSC buffer for 5 minutes. The slides were washed twice in stringency wash solution (1:1 formamide:1x SSC) for 5 minutes per wash. The probe was detected using the Biotin Painting Kit (Cambio), according to the manufacturer's instructions. Three replicate 25 x 25 mm structures (*n*=3 microgrooved, *n*=3 planar) were used in each experiment.

4.3.2.2 siRNA-FISH (Optimised Protocol)

To disrupt higher aggregates of siRNA, siRNA stock solutions (20nM) were heated to 90^{o}C for 1 minute, then incubated at 37^{o}C for 1h, and frozen at -20^{o}C for storage. Cells (0.5 x 10^{6} per transfection) were suspended in Nucleofector® solution according to the manufacturer's instructions, and mixed with 100 pmol of Lamin A/C or 100 pmol AllStars® Negative Control siRNA, fluorescently labelled with rhodamine (QIAGEN, Crawley, UK). Additional control cells were cultured under the same conditions without electroporation ('untransfected'). Electroporation was performed using a Nucleofector® device (Amaxa) set to program T-16, and cells were allowed to recover for at least 10 minutes in 500 µl pre-warmed complete RPMI medium in 1.5 ml tubes, and remained in a hot block at 37^{o}C until all samples had been electroporated. The concentration of siRNA, electroporation program, culture period and use of RPMI medium had been optimised in initial siRNA titration experiments. Cells were transferred to sterile coverslips that had been pre-incubated in DMEM at 37^{o}C, and were cultured for 48 (FISH) in 2 ml complete DMEM/199 medium at 37^{o}C. The medium was replenished after approximately 24h, and the cells were trypsinised after 48h and seeded at a density of 150 cells/mm^{2} on the planar and microgrooved substrata, as described in Section 4.3.1.1, cultured for 24h at 37^{o}C and prepared for FISH as described in Section 4.3.2.1, and analysed as detailed in Section 4.3.2.3.

4.3.2.3 Territory Analysis: Inter-Territory Distances and Edge of Nucleus-Centre of Territory Distances

Nuclei accepted for analysis had minimal background staining with defined territories. The brightness and contrast of the images were adjusted using Image-Pro Plus version 6.0 (Media Cybernetics, Inc., MD, USA) to maximise the visibility of the

territories, and dual coloured overlays (DAPI/FITC channels) were generated using this software. Brightness and contrast were further enhanced for presentation using Paint Shop Pro V7 (Corel, USA) and Corel Paint Shop Pro Photo X2 (Corel). The distances between the centres of chromosomal territories, and from the nearest edge of the nucleus to the centre of the chromosomal territory were measured in the dual coloured images using Image J (version 1.34s; Rasband, W.S., ImageJ, U.S. National Institutes of Health, Maryland, USA, http://rsb.info.nih.gov/ij/, 1997-2009). Statistics were generated using Microsoft Excel 2003 (Microsoft Corporation) and SigmaStat (Cosmol, Östringen, Germany), testing the null hypotheses that there was no statistically significant difference in the spacing of territories from the edge of the nucleus into the centre of the territories, or between pairs of territories within the same nucleus, using a two-tailed *t*-test for unequal variance. This parametric test was chosen to permit comparison between the mean distances between territories or from the nuclear edge-centre of territory, as it performs equally well whether the variance (or sample size) is equal or unequal between populations, but the Student's *t*-test is impaired when variance (or sample size) is unequal (Ruxton, 2006), as in the chromosomal distance datasets. The threshold for significance was set at $p<0.05$. The data was sorted into categorical bins of suitable sizes (*e.g.* covering a range of 0.5 μm per category) for graphical representation as histograms, and the modal category (most frequently observed range of distances) was noted for Ch 1 and 19. If the data was not normally distributed, violating an assumption of the *t*-test, a non-parametric Mann Whitney Rank Sum Test was performed using SigmaStat software (Cosmol)**.** In this test, each data point was ranked relative to the others in the group, and the ranks were assessed for random assortment between the two groups (planar and microgrooved), to examine whether the order of ranks could be described by the same distribution (and were therefore not significantly different).

4.4 Results

4.4.1 Analysis of FISH Data

Sample FISH-stained nuclei for Chs 1, 18 and 19 are shown in Fig. 4-4. One or two chromosome territories could be detected per cell in nuclei that were successfully stained. Interestingly, on the microgrooved substrate, it was occasionally observed that chromosomes appeared to be subject to locally confinement by the topography. Fig. 4-5D and E show nuclei where the stained chromosomes (1 and 19) seemed to be confined to the ridges, apparently resulting from the nuclei bridging between adjacent grooves and ridges.

Fig. 4-5D and E are included as a point of interest, but it should be stressed that such features were not commonly observed, unlike Fig. 4-5A-C, which reflect the common effects on the cell culture as a whole.

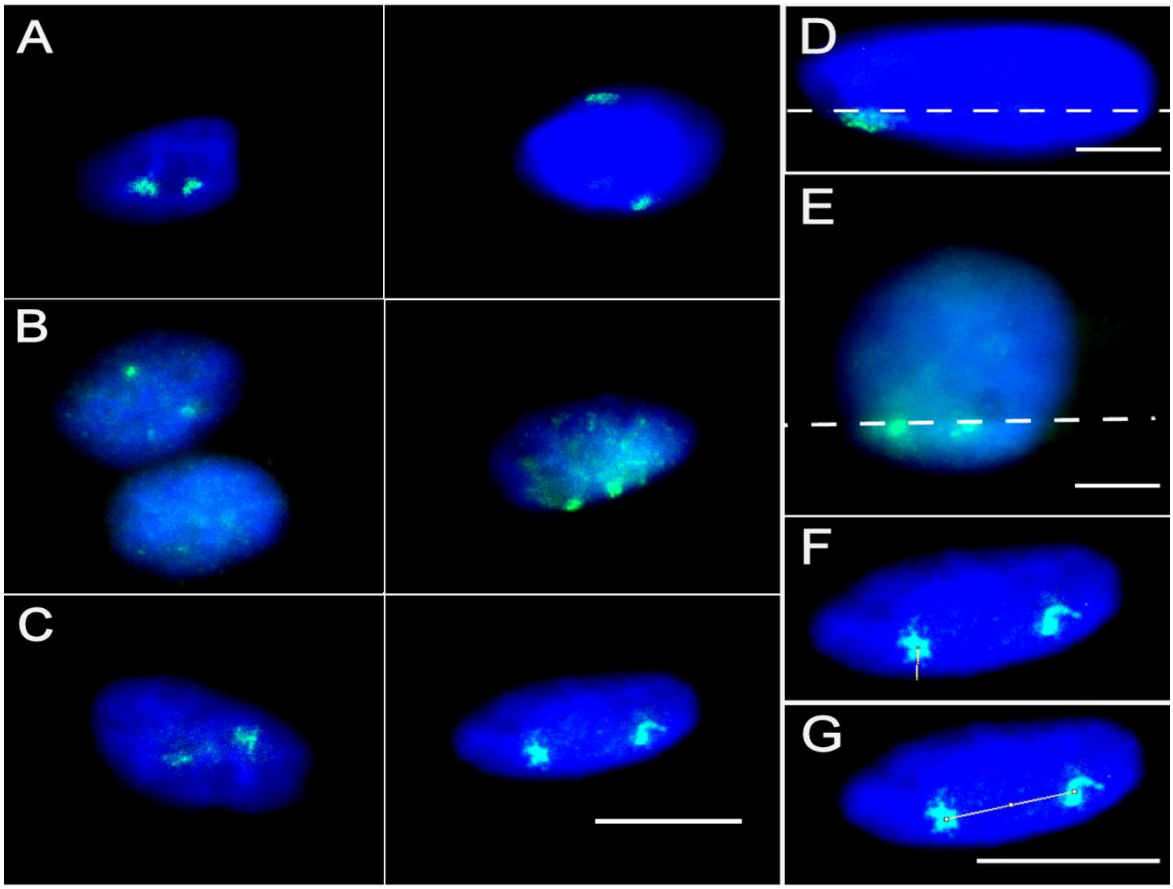

Figure 4-5: FISH staining for chromosomal territory positioning. *Examples of FISH staining of Ch 1 (A), 18 (B) and 19 (C) in nuclei of fibroblasts on planar (left column) and microgrooved (right column) quartz substrates. Occasionally, nuclei appeared to show evidence of chromosomal confinement by the topography (D and E; dotted lines indicate the location of the groove-ridge boundary nearest the labelled territories). Note that the cell in B had orientated perpendicular to the grooved topography (relatively rarely observed). Distances from the nearest edge of the nucleus to centre of the chromosomal territory were measured as shown in F, and inter-territory distances were measured between chromosomal territories as shown in G. Key: Blue – DNA; Green: Ch 1/18/19 territories. Bars: A-C, F, G - 10 μm, D, E - 5 μm. A-C, F and G are representative images from n=3 planar and n=3 microgrooved 25 x 25 mm substrates.*

4.4.2 Chromosome 1

The distance between the nearest edge of the nucleus and the centre of the Ch 1 territories was altered between nuclei on the planar and microgrooved substrates (Figure 4-6) (p=0.011, considered significant at p<0.05). The distribution of data was shifted to the left on the microgrooved substrate, relative to the planar substrate. The modal categories for the distance from nearest edge of the nucleus to the centre of the territory were distinct: 1.01-1.5 μm on the microgrooved substrate, and 2.01-2.5 μm on the planar substrate. On the microgrooved topography, the territories were generally localised nearer the periphery

of the nucleus than those on the planar substrate. For Ch 1, the positions of the chromosome territories were also mapped relative to each other in cells with two visible chromosomal territories. There did not appear to be a difference in the trend for chromosomal positioning between cells on the planar and microgrooved quartz substrates (Fig. 4-7), suggesting that the inter-territory distance was not affected by the topography (p=0.52). It should be noted, however, that there were relatively few cells on the planar substrate where two territories were visible, and it is possible that an effect may have become manifest in a larger sample size.

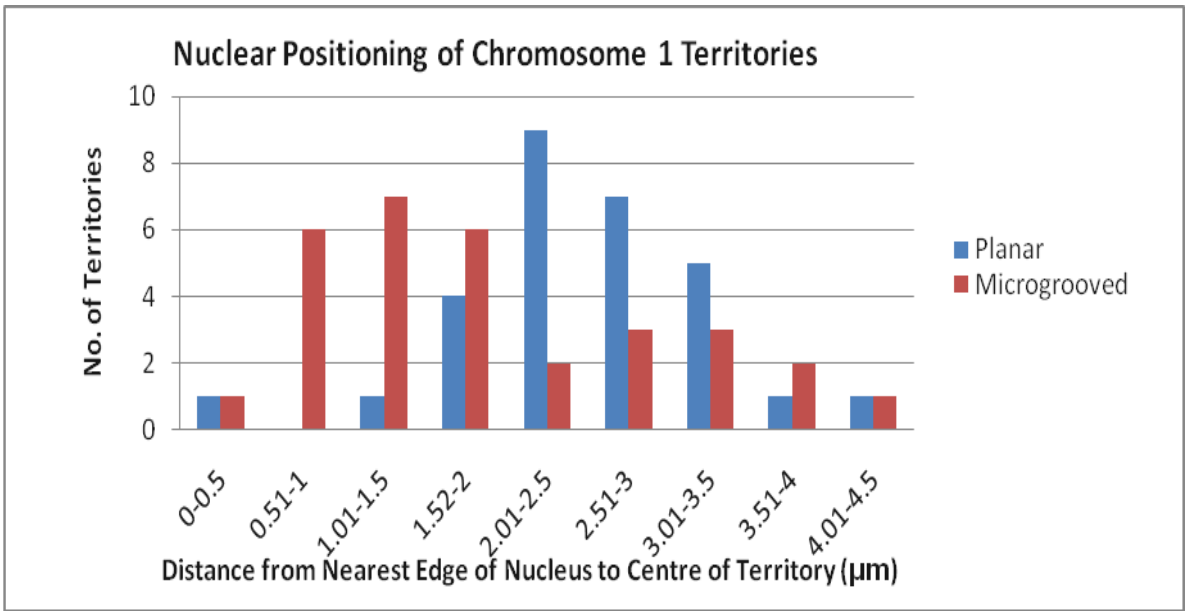

Figure 4-6. Ch 1 territory positioning within the nucleus. *Quantification of the positioning of Ch 1 relative to the nuclear periphery in cells cultured on the microgrooved (25 µm pitch, 2 µm depth) and planar quartz substrates. The difference in average Ch 1 positioning between the grooved and planar substrate was considered significant at $p<0.05$ ($p=0.011$, two-tailed t-test for unequal variance). n=31 territories from the microgrooved substrates (3 replicate 25x25 mm structures) and n=29 territories from the planar substrates (3 replicate 25x25 mm structures).*

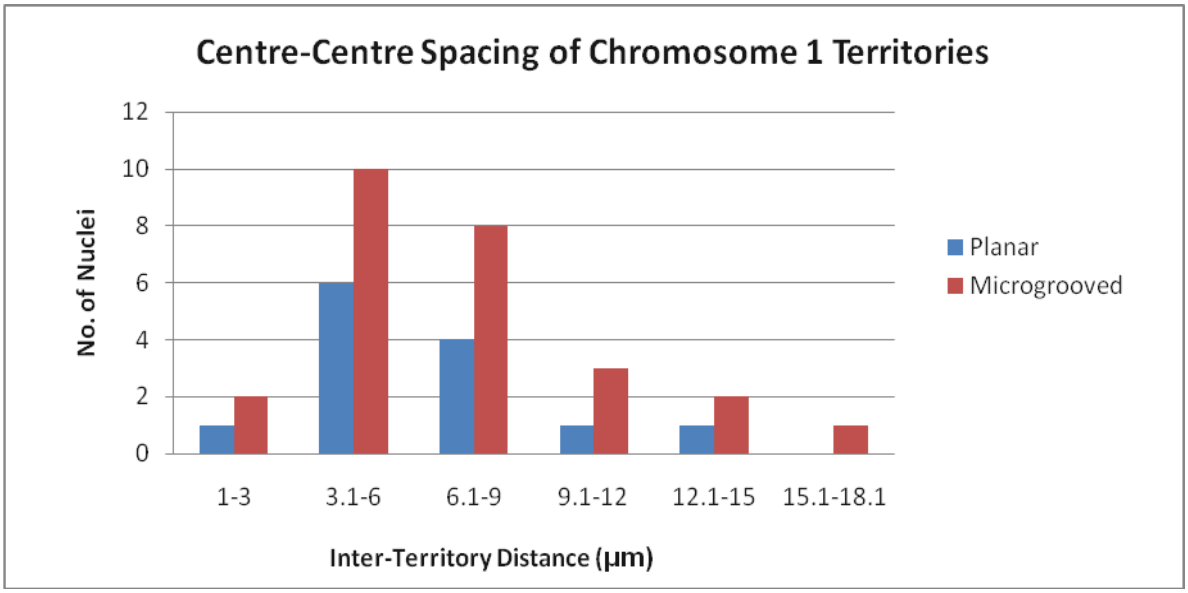

Figure 4-7. Quantification of inter-territory distances between Ch 1 territories. *Measurements of the spacing between pairs of Ch 1 territories in cells cultured on the microgrooved (25 µm pitch, 2 µm depth) and planar quartz substrates. The difference in average spacing of chromosome territories was not considered significant (p=0.35, Mann-Whitney Rank Sum Test). n=13 pairs of territories from the planar substrates (3 replicate 25x25 mm structures) and n=26 pairs of territories from the microgrooved substrates (3 replicate 25x25 mm structures).*

4.4.3 *Short Interfering RNA (siRNA)-Mediated Depletion of Lamin A/C*

To investigate a possible mechanistic basis for the repositioning of Ch 1 between cells on the planar and microgrooved substrata, siRNA directed against lamin A/C was used with the aim of partially disrupting the nuclear lamina, since chromatin is anchored to the lamina (Luderus et al., 1992), and it acts as a mechanosensitive bridge between the nucleus and cytoskeleton (Ji et al., 2007). On transfection of fibroblasts with siRNA directed against lamin A/C, the spread of chromosome distribution appeared to be more similar between cells on the planar and microgrooved substrata (Fig 4-8), which suggests that the presence of an intact nuclear lamina is likely to be important for the differential localisation of the territories between the two substrata.

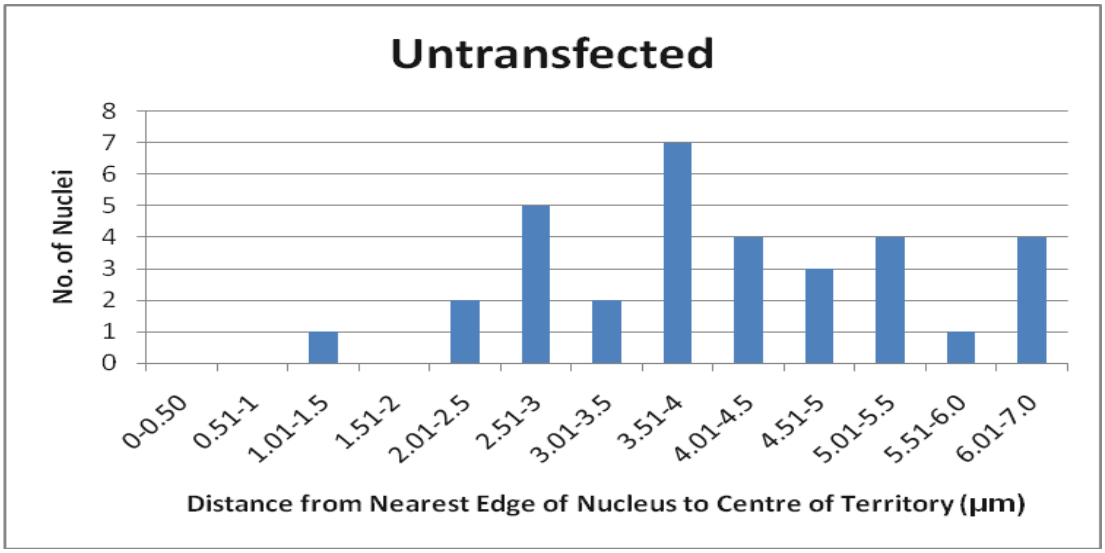
Untransfected
No. of Nuclei
0
1
2
3
4
5
6
7
8
0-0.50
0.51-1
1.01-1.5
1.51-2
2.01-2.5
2.51-3
3.01-3.5
3.51-4
4.01-4.5
4.51-5
5.01-5.5
5.51-6.0
6.01-7.0
Distance from Nearest Edge of Nucleus to Centre of Territory (µm)

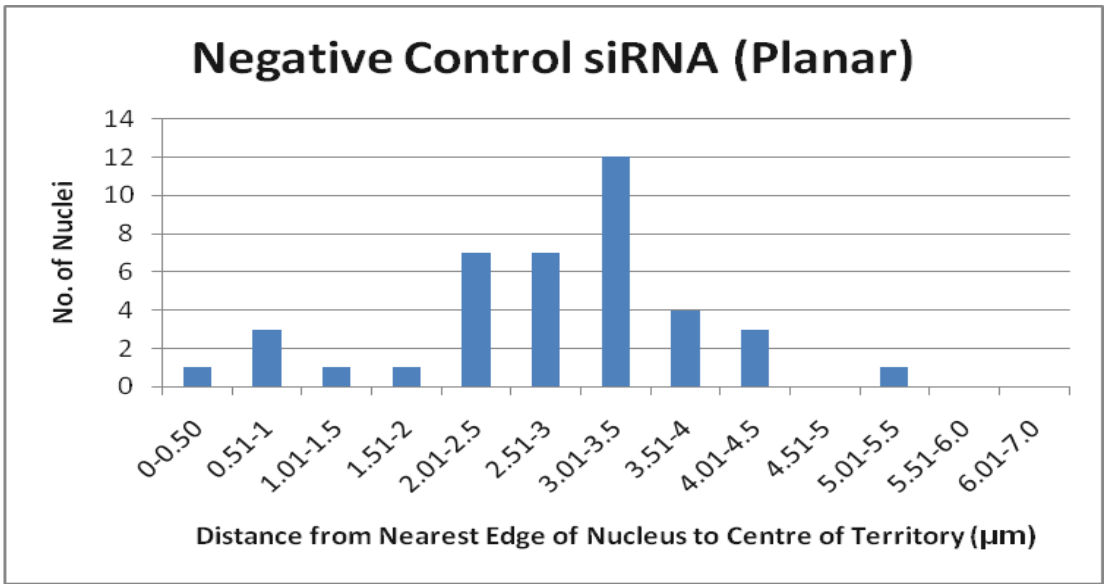
Negative Control siRNA (Planar)
No. of Nuclei
0
2
4
6
8
10
12
14
0-0.50
0.51-1
1.01-1.5
1.51-2
2.01-2.5
2.51-3
3.01-3.5
3.51-4
4.01-4.5
4.51-5
5.01-5.5
5.51-6.0
6.01-7.0
Distance from Nearest Edge of Nucleus to Centre of Territory (µm)

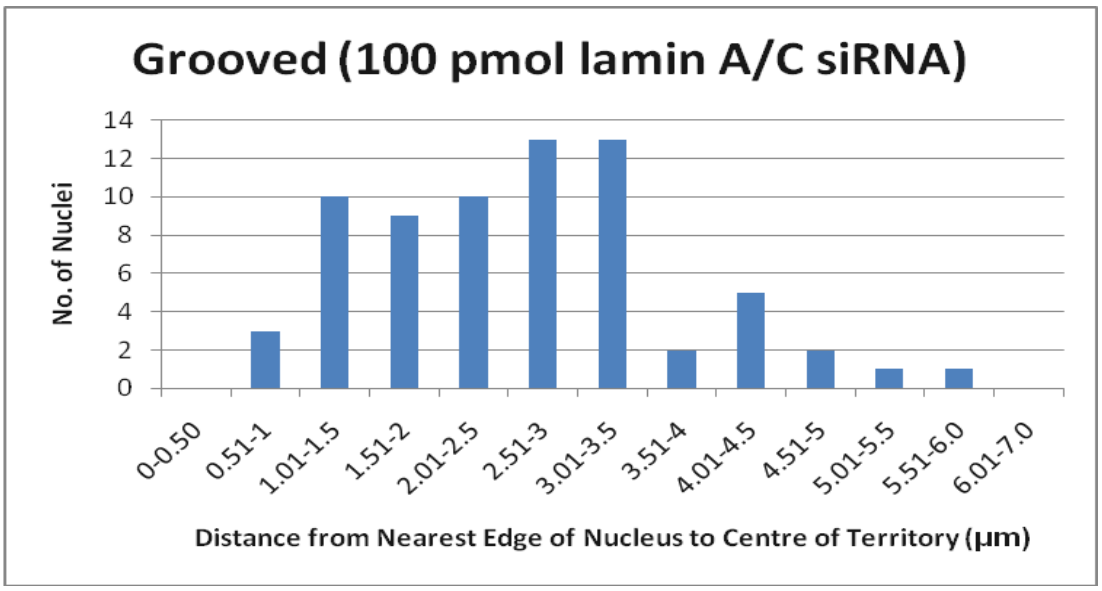
Grooved (100 pmol lamin A/C siRNA)
No. of Nuclei
0
2
4
6
8
10
12
14
0-0.50
0.51-1
1.01-1.5
1.51-2
2.01-2.5
2.51-3
3.01-3.5
3.51-4
4.01-4.5
4.51-5
5.01-5.5
5.51-6.0
6.01-7.0
Distance from Nearest Edge of Nucleus to Centre of Territory (µm)

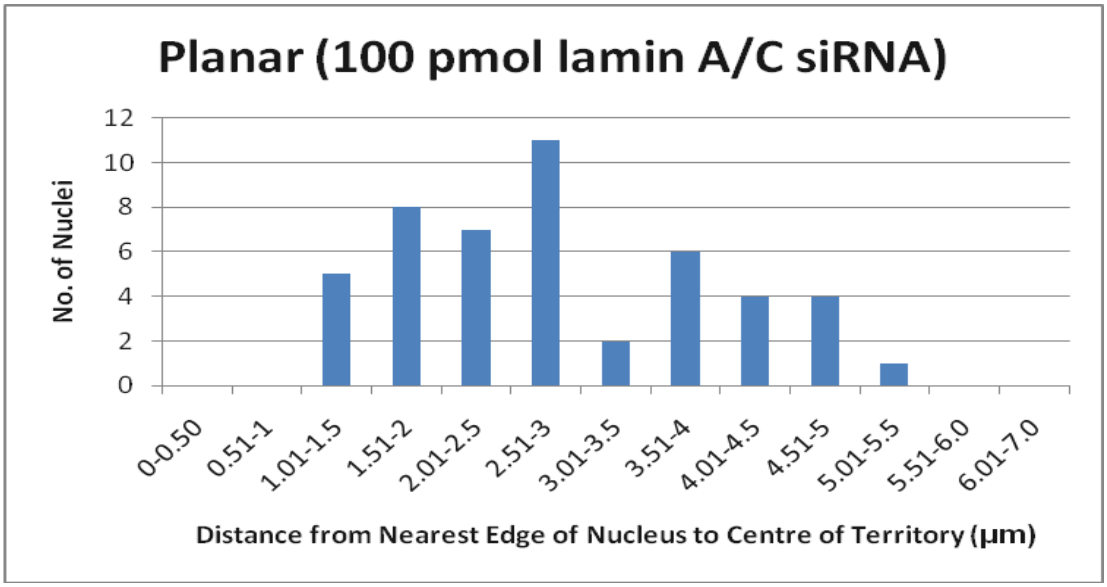

Figure 4-8. Ch 1 territory positioning within the nucleus following depletion of lamin A/C using siRNA. *Quantification of the positioning of Ch 1 relative to the nuclear periphery in cells cultured on the microgrooved (25 µm pitch, 2 µm depth) and planar quartz substrates (thresholds: 1.5-fold change, $p<0.05$) in the presence of 100 pmol siRNA directed against lamin A/C, or untransfected cells cultured on the planar substrate. Results for each siRNA lamin A/C histogram were pooled from three grooved and three planar substrates (25x25 mm), and histograms for untransfected and negative control siRNA-transfected cells were generated from cells cultured on one large planar substrate of equivalent size (25x75 mm) per condition. The differences between all groups were not considered significant at $p<0.05$ using a Mann-Whitney rank sum test. n=33 territories (untransfected), n=40 (negative control siRNA), n=71 (microgrooved with lamin A/C siRNA), n=48 (planar with lamin A/C siRNA).*

4.4.4 Chromosome 18

The range of distances observed between the nearest edge of the nucleus and the Ch 18 territories appeared to follow a very similar pattern for nuclei from the grooved and planar substrates (Fig. 4-9). This suggests that the territories were unlikely to have been repositioned, at least in a homogeneous manner, and is consistent with the microarray data indicating that there were very few transcripts originating from Ch 18 that were differentially expressed between the grooved and planar substrata.

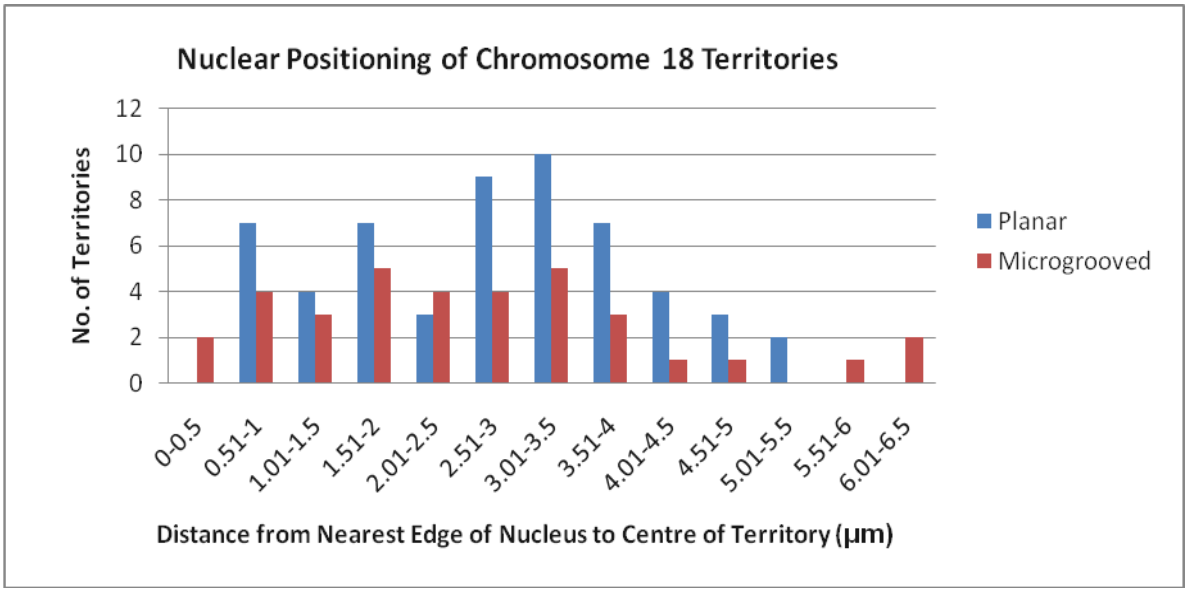

Figure 4-9. Ch 18 territory positioning within the nucleus. *Quantification of the positioning of Ch 18 relative to the nuclear periphery in cells cultured on the microgrooved quartz (25 µm pitch, 2 µm depth) and planar substrates. The difference in average Ch 18 positioning between the grooved and planar substrate was not considered significant (p=0.52, two-tailed t-test for unequal variance). n=35 territories (microgrooved) from n=3 25x25 mm microgrooved substrata, n=56 territories (planar) from n=3 25x25 mm planar substrates.*

4.4.5 Chromosome 19

Ch 19 had the most up-regulated transcripts in cells cultured on the microgrooved topography. Interestingly, however, there appeared to be little difference ($p>0.05$) in the distribution of nearest edge localisation for the Ch 19 territories from the two substrates at distances <4.0 µm from the nuclear edge (Fig. 4-10). Over this range, the distribution histograms were a similar shape and not shifted between nuclei on the planar and microgrooved substrates. In addition, the modal categories for each of these distributions were the same (2.51-3.0 µm from the nearest nuclear edge), suggesting that this was a common location for Ch 19 on both substrates. On the planar substrate, however, there were also two categories of distances in excess of 4 µm (4.01-4.5 µm and 5.01-5.5 µm), which did not make a consistent trend (category 4.51-5.0 µm contained only one member), but contained sufficient members to skew the distribution and make the overall difference between the substrates significant at $p<0.01$ ($p=0.001$). This suggests that Ch 19 may be more exaggeratedly centrally located in some nuclei on the planar substrate, but that the broad distribution is similar for the two substrates. The inter-territory distances between cells on the microgrooved and planar substrates were similar ($p>0.05$) (Fig. 4-11), with the possible exception that there were more nuclei with inter-territory distances of 8-14 µm on the planar substrate than the microgrooved substrate.

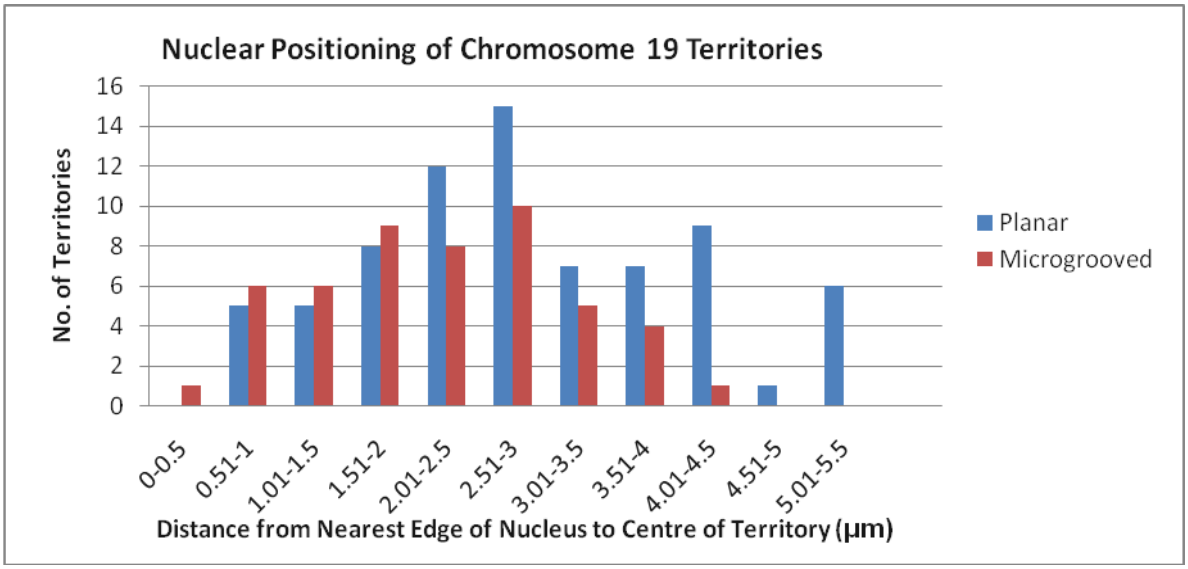

Figure 4-10. Ch 19 territory positioning within the nucleus. *Quantification of the positioning of Ch 19 relative to the nuclear periphery in cells cultured on the microgrooved (25 µm pitch, 2 µm depth) and planar quartz substrates (thresholds: 1.5-fold change, $p<0.05$). The difference in average Ch 19 positioning between the grooved and planar substrate was not considered significant at $p<0.05$ for distances less than 4 µm from the nuclear edge ($p=0.182$, two-tailed t-test for unequal variance), but the difference between the two whole datasets was considered significant at $p<0.01$ ($p=0.001$, two-tailed t-test for unequal variance). Distances >4 µm were predominantly observed in territories on the planar substrate. n=75 territories (planar) from n=3 25x25 mm planar substrata, n=50 territories (microgrooved) from n=3 25x25 mm planar substrates*

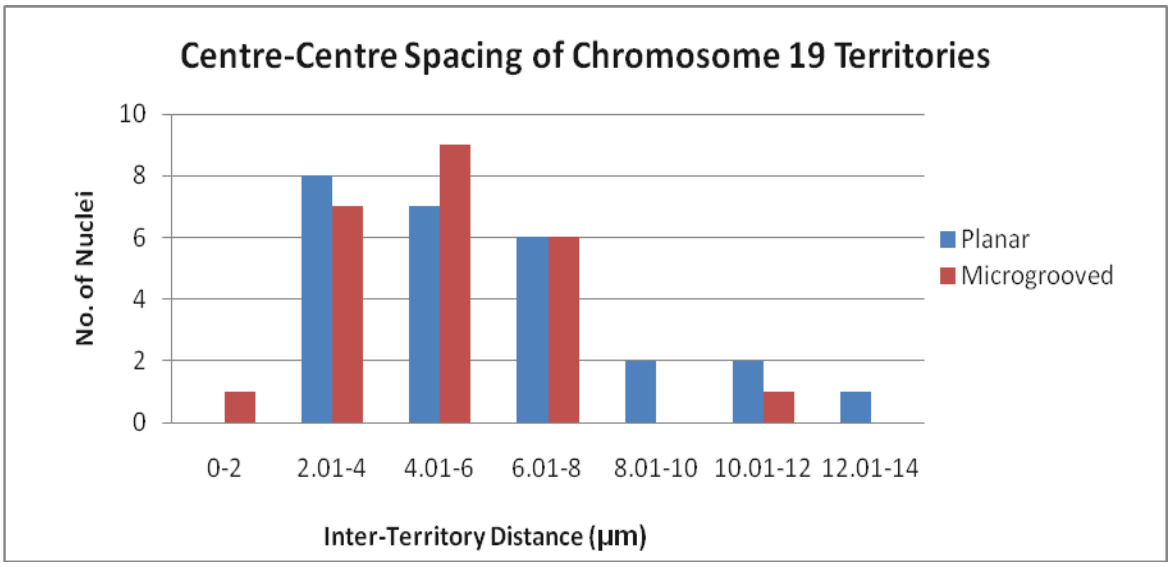

Figure 4-11. Quantification of inter-territory distances between Ch 19 territories. *Measurements of the spacing between pairs of FISH stained chromosomes in cells cultured on the microgrooved (25 µm pitch, 2 µm depth) and planar quartz substrates for Ch 19. The difference in average spacing of chromosome territories was not considered significant for Ch 19 ($p=0.157$, t-test for unequal variance). n=23 pairs of territories (microgrooved) from n=3 25x25 mm microgrooved substrata, n=26 pairs of territories (planar) from n=3 25x25 mm planar substrates*

4.5 Discussion

Consistent with the observations of nucleolar confinement noted in Chapter 2, the microgrooved topography could also restrain chromosomal territories, and potentially affect their accessibility for transcription. Although most nuclei did not show such tight confinement of chromosomes to ridges as the nuclei shown in Fig. 4-5D and E, nuclear reshaping resulting from topography-mediated cell elongation was expected to induce repositioning of certain chromosomal territories within the nucleus.

From the chromosome measurements, Ch 1 appeared to become repositioned from a central to a more peripheral location in the nucleus on the grooved topography ($p<0.05$), seemingly without a change in relative positioning of the sister chromosomes ($p>0.05$). This is consistent with the microarray data showing that this chromosome had the most down-regulated genes, since this would be anticipated to correspond to a move from a more euchromatic to a more heterochromatic region of the nucleus (Felsenfeld and Groudine, 2003). This is strongly suggestive of a direct mechanotransductive effect of the microgrooved topography on the territories. Ch 18, which had the fewest differential expression changes, was not expected to exhibit positional effects between the topography and the control, and the measurements supported this hypothesis.

It was anticipated that Ch 19 may be repositioned from a heterochromatic to a relatively euchromatic position in the nucleus on the topography, as it had the most up-regulated genes on this substrate. Unexpectedly, at distances less than 4.0 μm from the edge of the nucleus, the distribution of chromosome territories was similar ($p=0.182$) in the nuclei of both substrata. On the planar substrate, two categorical bins of territories were present further from the edge of the nucleus (>4 μm) than the majority of territories on the microgrooved substrate, which skewed the dataset at this tail and resulted in a difference between the two datasets that was considered significant at $p<0.01$. This suggests that Ch 19 was more centrally located in nuclei on the planar substrate in some cases (for approximately 21% of territories in the dataset), but that its positioning was probably broadly similar to the microgrooved topography, given the similar distributions between the substrates at distances <4 μm ($p=0.182$). Given that most Ch 19 territories were located at similar positions in the nuclei of cells on each substrate, and that some Ch 19 territories appeared more centrally located in nuclei from the planar substrate than those from the microgrooved substrate (Fig. 4-10; predominantly the site of euchromatic DNA),

the data seems weighted against repositioning as a mechanism for the up-regulated gene expression on Ch 19 that was inferred from the microarray data. It is possible that most Ch 19 territories were located in regions that were already sufficiently conducive to gene expression, such that any positional differences at distances in excess of 4 μm from the nuclear edge may have had less of an impact on the expression of genes on this chromosome. One explanation for the relative up-regulation of gene expression on Ch 19 in cells on the microgrooved substrate could be the induction of facultative (reversible) heterochromatin assembly on Ch 19 at positions in excess of 4 μm from the nuclear edge on the planar substrate, but this is unlikely to be a major contributor to the altered gene expression, due to the lack of a consistent difference in territory positioning across the whole data distribution (Fig. 4-10).

In comparison to Ch 1, where there was a disparity in localisation in nuclei between the two kinds of substrata, with a shift in the overall distribution of data between the two surfaces and different modal values, the distribution of data for Ch 19 was not shifted, excepting the skewed right tail at distances >4 μm, and the mode was the same for the two substrates. This suggests that there was a distinction between Ch 1 and 19, and that mechanotransductive repositioning of Ch 19 was unlikely to be responsible for the changes at the transcript level. There are at least two possible explanations for this. There may be a size dependency for the direct mechanotransductive effects, with the greatest magnitude of effects on the larger chromosomes, such as Ch 1, and lesser effects on smaller chromosomes such as Ch 19. This would be consistent with the work of (Dalby et al., 2007a), who utilised FISH (with centromeric probes) to show the greatest magnitude of repositioning on Ch 3, with some effect on Ch 11, and minimal effects on Ch 16, in response to two nanotopographies with differing effects on the cytoskeleton. In addition, sub-chromosomal events, such as looping out of particular loci towards transcription factories, are likely to have contributed to the effects at the transcript level. Consistent with this, the majority of the changes on Ch 19 were located at band 13 on the p- and q-arms. This suggests that these could be hotspots for looping out in response to the topography.

There is currently some contention in the literature about the ‘bystander’ effect, concerning the effects on expression of genes adjacent to a gene whose expression is affected by the looping event. There is evidence that bystander silencing can be induced by artificially repositioning of loci to nuclear pores (Reddy et al., 2008), but bystander

activation did not appear to occur when territories were relocated near to transcription factories (Morey et al., 2009).

Interestingly, in a study of Ch 19 positioning in lamin B1-depleted cells, Ch 19 became repositioned from a central nuclear location to a more peripheral site (Tang et al., 2008). Knockdown of lamin B1 would be expected to result in a large-scale reduction in lamin B1 and major nucleoskeletal alteration. The effects of topography on the nucleoskeleton (Chapter 2) probably primarily involve reorganisation, rather than depletion, of the protein. Lamin B1 did not appear to be differentially regulated in response to the topography at the transcript level (Chapter 3). Thus, the topography-induced effects on the lamina are likely to be more subtle than siRNA-mediated knockdown. Indeed, the mechanisms of chromosomal repositioning may be distinct. Following siRNA knockdown, chromatin loops became opened up, and cells eventually became apoptotic following the reduction in RNA polymerase II and I transcription. In addition, lamin A/C did not appear to complement the deficiency in lamin B. This showed that lamin B1 was necessary for maintenance of territory positioning. The alteration in mechanical forces would be non-physiological, with the possible exception of embryonic stem cells, which lack lamin A/C. Thus, the changes in chromosome positioning could have resulted from decreased attachment to matrix attachment regions, leaving chromosomes less tightly condensed, or perhaps responding to the earliest stages of apoptosis.

On the topography, in contrast, it seems more likely that mechanical tugging on the nucleoskeleton, in response to cytoskeletal forces and nuclear elongation, would lead to physical repositioning of the chromosomal territories. Consistent with this, the siRNA-mediated knockdown of lamin A/C appeared to greatly diminish, or even abrogate, the effect of topography on Ch 1 localisation (Chapter 4), suggesting that the lamina is likely to perform an important role in coupling the transfer of topographical mechanocues from the exterior of the cell into the chromosomes. As fibroblasts naturally align to each other, it seems highly likely that the aligning effect of the microgrooved topography is within the normal spectrum of cellular morphologies that would occur *in vivo*. In view of this, topography provides a model for the study of direct mechanotransduction that would probably more effectively mimic the physiological limits of direct mechanical processes than RNAi directed against mechanosensitive proteins, or invasive physical approaches.

Despite the differences between Ch 1 and 19 in their apparent sensitivity to mechanotransductive repositioning induced by a microgrooved topography, it was interesting to note that the inter-territory distances remained similar, with most pairs of chromosomes located within 2-9 μm distance of each other. Topography did not appear to markedly affect the distance of inter-chromosomal spacing, although the Ch 19 territories may have been somewhat closer together on the structured surface (visible as a possible effect in Fig. 4-11, with a greater number of nuclei showing inter-territory distances of 8-14 μm on the planar surface than the topography). Topography-induced nuclear elongation and reshaping could be responsible for this modest repositioning. This may have contributed to the up-regulated gene expression on Ch 19, if the territories were moved closer to transcription factories, or became more accessible to the transcriptional machinery (*e.g.* through greater exposure of the DNA at 19p13 and 19q13, where the differential gene expression was focussed). Alternatively, repositioning of other nuclear components (*e.g.* lamins, transcriptional elements) or alterations in nuclear pores during nuclear reshaping may have been sufficient to promote altered transcription. Additional research would be required to investigate these hypotheses further.

The use of 2D-FISH has the inherent limitation that the nuclei were being examined in two dimensions, which overlooks information relating to territory volume and position in 3D space. Although territory area could have been quantified, which has previously been performed for 2D-FISH (Ondrej et al., 2008), this was not examined in this thesis, as the approach is limited by the fact that variations in exposure time, brightness and contrast settings could have affected the apparent size of the territories, which would have greatly complicated the inter-sample comparison and most likely have led to some inaccuracy in the results. In this study, a number of options were considered in order to obtain quantitative data relating to territory positioning. Subdivision of the nucleus into smaller squares, larger segments or orbital ellipses by overlaying grids was considered too challenging due to inconsistencies in nuclear shape that would have over-complicated inter-nuclear comparison. Some studies elected to subdivide the nucleus into five zones to categorise the localisation of chromosome territories to assess repositioning (Malhas et al., 2007; Mehta et al., 2010). Blinded nuclear scoring for apparent territory position (with categories such as peripheral and central) was also considered as a potential means of evaluating the territory positioning, but had the disadvantage that the data would not have been quantitative, and potentially more subjective. In view of these issues, the territory positioning was evaluated by using the centre of the chromosome territories as a marker point, which should not have been affected by any discrepancies in brightness and

contrast. Images of territories overlaid on nuclei stained for DNA were used to map the locations of territories within the nucleus to improve the delineation of the nuclear periphery. Mehta et al (2010) applied this quantification in one part of the study, but predominantly used the subdivision approach described above to generate nuclear 'shells' that could be used to more rapidly, but qualitatively, assess the territory localisation under different conditions (Mehta et al., 2010). It would be interesting to extend this study by examining the changing chromosomal positioning in 3D using 3D-FISH, and with multiple probes. In this study, because the FISH signals were relatively faint, it was not feasible to attempt the optical sectioning required to generate confocal z-stacks of sufficient resolution to visualise the territory positioning in 3D, but this would be a valuable experiment to gain additional spatial data and confirm that the positional results were not affected by visualisation of a single plane in 2D-FISH. Vital imaging of chromosomes in living cells would also be useful for visualising the dynamics of repositioning in response to topographical stimuli. Muller et al (2010) recently described an exciting technical development that enables tracking of GFP-tagged histones on specific chromosomes by targeted photoactivation (Muller et al., 2010), a technique that should prove valuable for the real-time study of chromosome dynamics, and preclude any possible issues relating to disruption of the nuclear architecture during fixation or sample preparation for FISH.

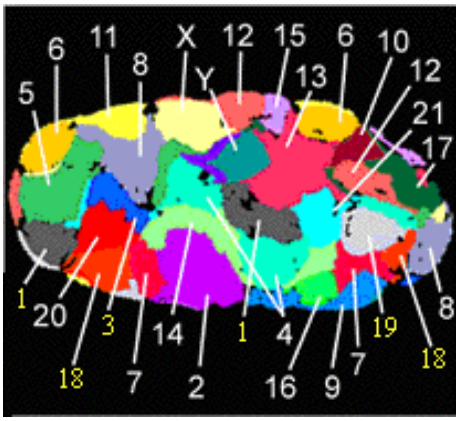

Figure 4-12. Territory positioning in human male fibroblasts in G_0. *Chromosomes were visualised using goldFISH with 3D confocal reconstruction. The positioning of Chs 1, 3, 18 and 19 has been highlighted in yellow. Ch 1, 18 and 19 were examined in this thesis, and Ch 3 was previously shown to respond to nanotopography (Dalby et al. 2007). Reproduced with modification from (Bolzer et al., 2005).*

The positions of Chs 1, 3, 18 and 19 are highlighted in Fig. 4-12 (modified from (Bolzer et al., 2005)) for fibroblasts on a planar substrate from a male donor in G_0. This nucleus had a relatively elongate morphology, which could correspond to a more 'motile' cell shape. This could be extrapolated to correlate with the more elongate nuclei observed on the planar quartz surface, and the less dramatically elongated nuclei on the topography,

such as those shown in Fig. 4-5. In this nucleus, both copies of Ch 18 were located near the nuclear periphery (associated with heterochromatic silencing). One copy of Ch 19 appeared to be more centrally located, with the other copy nearer the nuclear edge. Ch 1 had a similar location, with one copy near the periphery, and the other occupying a central location in the nucleus, a site likely to be enriched in transcription factories. Interestingly, Ch 3 was previously shown to be repositioned in response to nanotopographical substrates. In common with Ch 1, it is one of the largest chromosomes, and occupied a similar position in the G_o nucleus, with one territory more centrally located, and the other at the periphery. It seems plausible that the 'resting' position and size of chromosomes may be some of the characteristics determining their likelihood to be repositioned in response to a topographical stimulus. Disruption of heterochromatin led to inhomogeneous nuclear shrinkage in murine embryonic fibroblasts with ovoid nuclei, with collapse focussed on the shorter nuclear axis (Mazumder and Shivashankar, 2010). The authors noted that this was consistent with an unequal distribution of attachment sites at the nuclear periphery. Given this disparity, it seems likely that certain portions of the nucleus, most likely at the periphery, will be more sensitive to mechanical effects. Computer modelling should provide a useful means of modelling such features, to assist in describing and predicting the topography-mediated redistribution of chromosomes.

4.6 Conclusion

Data mining of the microarray results highlighted Ch 1 and 19 as potential 'hotspots' for differential expression, and Ch 18 was identified as having the fewest expression changes between cells on the microgrooved and planar substrates. Chromosomal territories could be repositioned within the nuclei of human fibroblasts in response to the topographical mechanostimulus, the magnitude of which seemed likely to vary on a continuum according to chromosome size. Ch 1 appeared to be repositioned towards the nuclear periphery on the microgrooved substrate. It is difficult to dissect out the contribution of biochemical and mechanical mediators to the differential gene expression, but it seems probable that the size of chromosomes and their positions within the nucleus will affect their susceptibility to tensile forces, and subsequent likelihood for transcription.

5 Proteomic (DiGE) Analysis

5.1 Introduction and Method Development

Fluorescence two-dimensional difference gel electrophoresis (DiGE) has great potential to offer insight into the process of mechanotransduction and cell-material interactions, and has very recently begun to be applied to the study of cell response to topographical substrata. On a surface with a partially disordered arrangement of nanopits, this technique revealed that the cytoskeletal proteins actin and vimentin were increased in abundance relative to the control after five weeks of culture (Kantawong et al., 2008). This may have facilitated cytoskeletal reorganisation and altered the cellular capacity for direct mechanotransduction. This was supported by down-regulation of the FA-associated protein zyxin. In addition, GRASP55 (Golgi reassembly stacking protein of 55 kDa), which is involved in MAPK signalling and implicated in promoting cell growth and division (discussed in Kantawong et al., 2008), was down-regulated in cells cultured on the nanopits. In combination with other proteomic data and histological results, the authors concluded that this was consistent with the tendency towards differentiation, rather than proliferation, in cells cultured on the nanosurface.

DiGE was also used to examine the temporal response of ostetoprogenitors to disordered nanotopography over six weeks of culture (Kantawong et al., 2009b). Osteoid nodule formation was noted on the nanotopographical substrate two weeks before nodules appeared on the control surface, and the authors concluded that the topography had enhanced maturation of these cells. Unlike the DiGE studies discussed above, which only examined cellular proteins, in this investigation an extraction regime was used that permitted harvest of both intracellular and ECM proteins. Compared with controls, vimentin and osteonectin (an ECM protein specific to bone lineage cells) were up-regulated in cells on the topography following three weeks of culture. These proteins are markers of differentiation in this cell type, and interestingly, the abundance of both proteins was not distinguishable from levels in the control cells at later time-points. The authors noted differential regulation of a number of proteins involved in MAPK-ERK signalling, further implicating this pathway as an important regulator of the cellular response to nanotopography. Most of the differential protein regulation occurred before the sixth week (prior to osteoid mineralisation), which the authors corroborated with a

liquid chromatographic (LC) technique, dimethyl labelling, at the week six timepoint. This showed minimal changes between the control and nano-surfaces.

In a third DiGE study of osteoprogenitor cells on a microgrooved (2 μm depth x 25 μm) polycaprolactone substrate, galectin-1, actin, a transmembrane transporter (similar to chloride intracellular channel 1 (p64)), Ran-specific GTPase activating protein and a SUMO (small ubiquitin-like modifier protein) precursor (responsible for post-translational protein modification) were up-regulated after four weeks of culture. In addition, zyxin, thioredoxin, osteonectin, heat shock protein 27, ribonuclease inhibitor and GRASP55 were down-regulated at this time-point (Kantawong et al., 2009a). The authors concluded that the FAK and MAPK signalling pathways were likely to be key to the induction of these proteomic changes.

The research discussed above examined bone lineage cells over prolonged culture periods on polymeric substrates. The proteomic effects in other cell types, and following short-term cell culture periods, had not been investigated using this approach, and the previous DiGE studies of cells on topographical substrates had not been conducted in parallel with microarray work. To address this, hTERT BJ-1 fibroblasts were selected for short-term 24h culture on microgrooved quartz topographies for evaluation by saturation labelling DiGE. As discussed in Chapter 1, DiGEsat is useful for biomaterials applications, in permitting the study of very low abundance protein samples, and enabling the global analysis of differential protein regulation.

Prior to the advent of the three-dye minimal labelling multiplex system, a two-dye experimental design was commonplace (Unlu et al., 1997; Zhou et al., 2002). The ability to include an internal standard, composed of an equal fraction of all the samples in an experiment, improved inter-gel comparison. It has been noted that this design can lead to statistical bias, however, through the matching of both control and test samples to the internal standard (Karp et al., 2007). The authors of this study proposed that an alternative design of one sample per gel (control or test), together with a pooled standard, should be utilised. The disadvantages of this design are that twice as many gels are required to conduct a pairwise analysis, and inter-gel matching is needed to compare between control and test samples. This increases the cost of the experiment, and would be expected to lower the robustness of comparison between samples (due to gel-to-gel variation). In addition, prohibitive quantities of protein would need to be harvested from biomaterial substrates to construct the pooled standard, unless protein from a related source was

utilised, but this would be suboptimal. The extraction of sufficient protein for a pooled standard becomes even less feasible when examining near-monodisperse cell populations, which were required in this study to minimise cell-cell interactions that might have confounded analysis of mechanotransductive responses to the topography. The three possible DiGEsat experimental designs considered for application in this project are illustrated in Fig. 5-1.

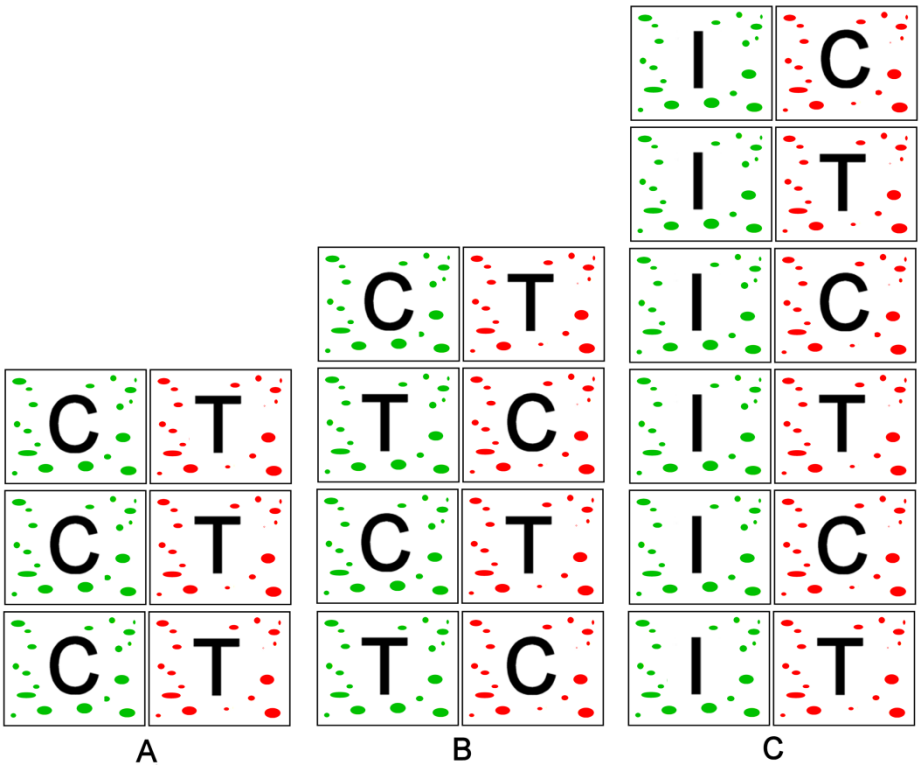

Figure 5-1. Illustration of three possible DiGEsat experimental designs considered for this study (subsequent to dye titration and identification of potentially dye-biased spots). *A) 3 gel approach, B) 4 gel approach with paired dye flips, C) 6 gel approach (3 sample pairs) with pooled internal standard. Key: Green – Cy3 dye, Red – Cy5 dye; C – gel with control sample, T – gel with test sample, I – gel with pooled internal standard.*

In view of the issues discussed above for application of the one sample per gel approach (Fig. 5-1C), an alternative design was adopted. One control sample, labelled with Cy3, was compared against a partner (paired) test sample, prepared under the same conditions and labelled with Cy5. This was performed for three biological replicates (Fig. 5-1A). To prevent bias in dye swapping, dye flips were not utilised, due to the odd number of replicates (an example of a 'balanced' dye-flip design with an even number of replicates is shown in Fig. 5-1B). To address possible issues of dye bias (preferential binding of Cy3 or Cy5 to particular proteins, giving rise to potential errors in assessment of differential regulation), the dye titration (same/same) gels were analysed for spots that consistently

appeared to be subject to differential regulation in more than two gels. The experimental design utilised in this study has also been applied to other DiGEsat studies of cells on biomaterial substrata (Kantawong et al., 2008; Kantawong et al., 2009a; Kantawong et al., 2009b), although these studies did not attempt to identify potentially dye-biased spots.

5.1.1 Method Development I: Optimisation of 2D-GE

The use of additional SDS (4% (w/v), increased from 2% (w/v)) and DTT (1% (w/v), increased from 0.5% (w/v)) in the equilibration buffer resulted in improved resolution in the 2D gel. Longer incubation with colloidal Coomassie dye (increased to 7 days) improved the sensitivity for spot detection in the 2D gels using post-staining. The use of a slow step (0.5W for 30 mins) at the start of the second dimension electrophoretic program was also useful in increasing resolution, presumably by improving the transfer of proteins from the first to the second dimension gels. Narrower pH range IPG strips (pH 4-7) greatly improved the resolution of the gels, compared to broad range strips (pH 3-10). The use of high-grade reagents (particularly PlusOne (GE Healthcare) agarose and CHAPS, for the overlay solutions and lysis buffers) also appeared to improve the quality of the 2D gels (reducing streaking artefacts and contributing to improved resolution).

5.1.2 Method Development II: Optimisation of CyDye Labelling by Dye Titration

To optimise the conditions for saturation labelling, three gels were used, with different concentrations of TCEP (reducing agent: 1, 2, and 3 nmol) and dye (2, 4, and 6 nmol), with 5 μg protein labelled per dye (Cy3 and Cy5). The 2 nmol gel had the most horizontal streaks, probably due to insufficient labelling (Fig. 5-1A). By contrast, the 4 nmol gel appeared properly labelled, with a large number of well-defined spots (Fig. 5-1B). The 6 nmol gel was also well-resolved and labelled, but marginally less so than the 4 nmol gel. As the use of this additional CyDye was deemed unnecessary, 2 nmol TCEP:4 nmol dye was selected for further work.

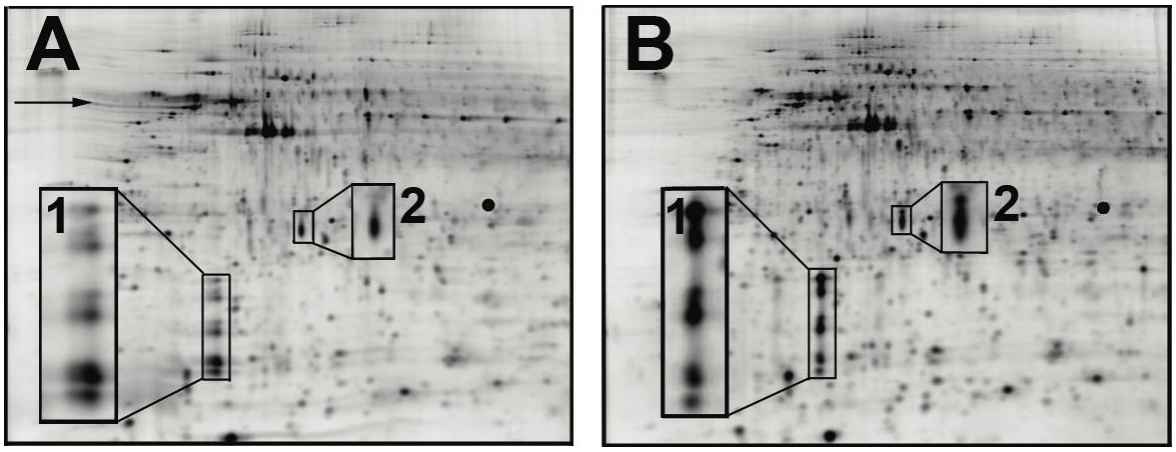

Figure 5-2. Part of a saturation labelling dye titration experiment using the same protein extract (extracted from hTERT BJ-1 fibroblasts grown to approx. 70% confluence on tissue-culture grade polystyrene) labelled with two different reducing agents and dye concentrations. *A – 1 nmol TCEP, 2 nmol dye; B – 2 nmol TCEP, 4 nmol dye. Underlabelling issues are visible in A: (horizontal streaking (arrow), spot doubling (inset 1), mass shifting in certain proteins (insets 1 and 2)), cf. optimal labelling stoichiometry in B (no visible artefacts). Reproduced from McNamara et al. (2010).*

5.2 Materials and Methods

5.2.1 2D Gel Electrophoresis

5.2.1.1 Preparation of Cell Lysate and Precipitation of Protein

Confluent monolayers of fibroblasts (hTERT BJ-1) were washed twice in 10 ml HEPES saline (5.4 mM KCl, 0.14M NaCl, 5.5 mM d-Glucose, 10 mM HEPES, 0.01% (v/v) phenol red, pH 7.5), then detached using 3 ml trypsin-Versine (3.4% (v/v) 10x trypsin (Sigma) in EDTA), with a five-minute incubation at 37^{o}C. The cells were pelleted by centrifugation (1400 rpm, Sigma S-16, rotor 11180) in 15 ml Falcon tubes, and resuspended in 3 ml of sterile ice-cold PBS. The cells were pelleted by centrifugation, and then washed again in 3 ml cold PBS. The PBS was removed and replaced with 500 µl DiGE lysis buffer (7M urea, 2M thiourea, 4% (w/v) CHAPS, 30 mM Tris base) supplemented with 10 µl/ml 10x General Protease Inhibitor Mix (Sigma). The tubes were incubated on ice for 30 minutes, then 2 ml acetone was added to each, and the samples were left to precipitate for 3h or overnight (~18h) at -20^{o}C. The samples were allowed to thaw, and then the protein and contaminating salts were pelleted by centrifugation (10 minutes, 13000x*g*). The acetone was removed, replaced with 500 µl ice-cold 80% (v/v) acetone, and the pellets were disrupted manually using pipette tips. The protein was pelleted by centrifugation (10 minutes, 13000x*g*), then the acetone was removed and the pellet left to air-dry to near-dryness for five minutes. The pellets were then resuspended in

a known small volume (<50 μl) of 2x rehydration buffer stock (7M urea, 2M thiourea, 4% (w/v) CHAPS), and frozen at -20^{o}C for storage.

For the preparative saturation labelled gel, cells were extracted as above, with the exception that the protein was re-precipitated at -20^{O}C for 1h following the first wash in 80% (v/v) acetone, pelleted by centrifugation (10 minutes, 13000x*g*) and resuspended in 500 μl ice-cold 80% (v/v) acetone prior to air-drying of the protein pellet. The pellets were resuspended in known small volumes (<50 μl) of DiGE saturation lysis buffer and stored at -20^{o}C.

Fibroblasts were seeded on 25 x 75 mm quartz substrates at a density of ~ 150 cells/mm^{2} material, and cultured for 24h in the culture medium described in section 2.3.2.1, at 37^{o}C in a humidified atmosphere with 5% CO_2. For protein extraction, three biological replicates were generated from cells extracted after three temporally distinct culture periods of 24h (denoted as *n*=3 in the text), and each biological replicate was pooled from cells cultured on four replicate substrates per structure (planar or microgrooved). Cells were washed twice in 6 ml HEPES saline, detached and pelleted as above, except that 3 ml of trypsin-Versine was used per structure. Cells were pooled from four equivalent structures, and 1 ml PBS was used per pooled sample for each wash. Cells were lysed in 250 μl DiGE lysis buffer for saturation labelling (7M urea, 2M thiourea, 4% (w/v) CHAPS, 30 mM Tris base, pH 8.0) with protease inhibitors. Protein was precipitated as above, with the addition of another step: following resuspension of the pellet in 80% (v/v) acetone, the protein was re-precipitated at -20^{o}C for 1h, pelleted by centrifugation (conditions as above), and resuspended a second time in 80% (v/v) acetone. At the final step, protein pellets were resuspended in known small volumes (<20 μl) of DiGE saturation lysis buffer and stored at -20^{o}C.

5.2.1.2 Determination of Protein Concentration

The protein concentration of samples was determined using the Bradford method Protein Assay Kit (Bio-Rad), with minor modifications to the manufacturer's instructions. The Bradford reagent was diluted 1:4 in double-distilled water to a working concentration, and the standards (generated from 2 mg/ml bovine serum albumin) were created in a dilution series (1:2, 1:30, 1:60, 1:90, 1:120, 1:240, 1:360, 1:540, 1:720) with the first dilution (1:2) using DiGE lysis buffer as the diluent, and subsequent dilutions in double-distilled water. Samples were serially diluted (1:20, 1:40, 1:80, 1:160, 1:320, 1:640) with

double-distilled water. The optical density (OD) values for the standards and samples were taken at 595 nm using a MR7000 spectrophotometer. The protein concentrations of the samples were determined by comparison with the linear region of the standard curve, by substituting the OD values into the best-fit trendline with equation y = mx + c (where y = y-axis intercept value, x = x-axis intercept, m = gradient of line, c = a constant).

5.2.1.3 Protein Labelling with Saturation Dyes

For analytical gels, 5 µg protein was reduced with 1, 2 or 3 nmol TCEP (Fluka Analytical, Buchs, Switzerland), mixed well, with brief centrifugation in a benchtop microfuge (Eppendorf, Cambridge, UK) and incubated at 37^{o}C for 1h in the dark. Saturation dye (Cy3/Cy5; 2, 4 or 6 nmol; from 2 mM stocks (GE Healthcare) in dimethylformamide (DMF) (USB Corporation, Cleveland, USA)) was added to the samples, which were mixed well, pelleted as above and incubated at 37^{o}C for 30 min in the dark. To stop the reaction, an equal volume of Stop Solution 1 (2% (v/v) IPG buffer pH4-7, 130 mM DTT, 7M urea, 2M thiourea, 4% (w/v) CHAPS) or 200 µl Stop Solution 2 (2% (v/v) IPG buffer pH4-7, 13 mM DTT, 7M urea, 2M thiourea, 4% (w/v) CHAPS) was added, mixed well and briefly pelleted by centrifugation. The pairs of Cy3 and Cy5 samples were combined. Rehydration Buffer 1 (7M urea, 2M thiourea, 4% (w/v) CHAPS, 0.5% (v/v) IPG buffer, 0.2% (w/v) DTT, trace bromophenol blue) was added to samples treated with Stop Solution 1 to make the volume up to 470 µl. The samples were incubated at room temperature for 1 hour, before being briefly pelleted by centrifugation (pulse setting on an Eppendorf benchtop centrifuge, to remove particulates that may interfere with IEF) and loaded into the IEF strip holder. Rehydration Buffer 2 was added to samples treated with Stop Solution 2 to make the volume up to 450 µl, and then the samples were loaded into the IEF strip holder. For the preparative gel, 500 µg protein was labelled under the conditions above, but with 10 µl 20 mM TCEP and 10 µl Cy3 dye (20 mM stock in DMF), and 430 µl Stop Solution 2, before loading the sample into the IEF strip holder. For same/same analysis (dye titration), pseudoreplicates from the same cell extract were labelled with Cy3 and Cy5; for differential analysis (control/test), control samples were labelled with Cy3 and grooved samples with Cy5.

5.2.1.4 First Dimension Isoelectric Focussing (IEF)

For 2D gels (non-DiGE gels), 500 µg of protein was resuspended in working rehydration buffer (7M urea, 2M thiourea, 4% (w/v) CHAPS, 0.5% (v/v) IPG buffer, 0.2%

(w/v) DTT, trace bromophenol blue) to a total volume of 470 µl, then left at room temperature for 30 min-1.5h. Particulates were pelleted by brief centrifugation (pulse setting on an Eppendorf benchtop centrifuge), and 450 µl of solution was loaded into a clean Strip Holder (GE Healthcare). For both DiGE and 2D gels, a 24 cm IEF strip was inverted into the solution (pH 3-10 or pH 4-7), and covered with 1 ml of mineral oil. The Strip Holder was placed on the electrodes of the Multiphor IPGPhor II IEF machine and IEF was performed according to one of the following programs:

Program 1 (22h): ~75000 Volt hours (Vhr) to step 5 (program was stopped after ~80000 Vhr during step 6)

Step No.	Voltage (V)	Length of step (h)
Step 1 – Step-n-hold	30	10
Step 2 – Step-n-hold	300	2
Step 3 – Gradient	300-1000	1
Step 4 – Gradient	1000-8000	1
Step 5 – Step-n-hold	8000	8
Step 6 - Step-n-hold	1000	24

Program 2 (28h): ~87000 Vhr (program was stopped after ~80-85000 Vhr)

Step 1 – Step-n-hold	30	12
Step 2 – Step-n-hold	300	2
Step 3 – Gradient	1000	2
Step 4 – Gradient	8000	5
Step 5 – Step-n-hold	8000	8

Program 3 (26.5h): ~81000 Vhr

Step 1 – Step-n-hold	30	12
Step 2 – Step-n-hold	300	1
Step 3 – Gradient	600	1
Step 4 – Gradient	1000	1
Step 5 – Gradient	8000	3
Step 6 - Step-n-hold	8000	8.5

5.2.1.5 Second Dimension Sodium Dodecyl Sulphate Polyacrylamide Gel Electrophoresis (SDS-PAGE)

IEF strips were equilibrated for 15-20 minutes in 10 ml Equilibration Buffer 1 (100 mM Tris pH8, 6M urea, 30% (v/v) glycerol, 2% (w/v) SDS, 0.5% (w/v) DTT), or Equilibration Buffer 2 (50 mM Tris pH8.8, 6M urea, 30% (v/v) glycerol, 4% (w/v) SDS, 1% (w/v) DTT). For non-DiGE 2D gels, this was followed by a second equilibration step

of equivalent length in Equilibration Buffer 1 or 2, supplemented with 4.5% w/v iodoacetamide. The IEF strips were rinsed briefly in running buffer and sealed onto the second dimension 12% (w/v) acrylamide gel using molten sealing solution (0.5% (w/v) agarose in running buffer, ~0.002% (w/v) bromophenol blue). Electrophoresis was performed, with or without an initial low power start up period (0.5W for 30 min), at 1-2W/gel (overnight) or 30-50W/gel (3-4h), with 1x running buffer (25 mM Tris, 192 mM glycine, 0.1% (w/v) SDS) in the lower, and 2x buffer in the upper electrophoresis tank chambers, and was stopped when the dye front reached the bottom of the gels.

5.2.1.6 Colloidal Coomassie Staining

Gels were fixed for 1-2h in 40% (v/v) ethanol/10% (v/v) acetic acid, then stained for 4-7 days in Colloidal Coomassie stain (4 parts dye stock (0.1% (w/v) Coomassie Brilliant Blue G, 10% (w/v) $(NH_4)_2SO_4$, 1% (v/v) H_3PO_4): 1 part methanol), destained in several changes of distilled water, and scanned using an ImageScanner (Amersham Biosciences, Little Chalfont, UK) with LabScan (Amersham Biosciences) or Photoshop (Adobe) software.

5.2.1.7 DiGE Gel Fixation, Analysis and Statistical Analysis

DiGE gels were scanned at 100 μm resolution using a Typhoon 4800 laser scanner (GE Healthcare) at 488 nm (Cy3) and 633 nm (Cy5). Gel spot intensities were assessed using ImageQuant software (Amersham Biosciences) and the laser intensities chosen to ensure maximum intensity values between the Cy3 and Cy5 images were within 15% of each other and that images were not saturated. Following gel scanning, the preparative gel was fixed in 7% (v/v) acetic acid/10% (v/v) methanol. The Differential In-gel Analysis and Biological Variation Analysis modules of DeCyder V5.0 (GE Healthcare) software were used to normalise the post-scan spot intensities and detect proteins that were differentially regulated under the control and test conditions. Microsoft Excel (Microsoft Corporation) was used for statistical analysis, including calculation of the mean fold-change and standard deviation. The data was $\log_{10}$ transformed to homogenise the variation between sample pairs, and satisfy the assumptions of normality for parametric tests. A paired, two-tailed Student's *t*-test was used to generate *p*-values for the assessment of differential expression, with $p<0.05$ used as the threshold for significance.

5.2.2 Mass Spectrometry

5.2.2.1 Automated Spot Picking and Peptide Generation

Gel spots of interest were selected using DeCyder V5.0 software (GE Healthcare), and added to a pick-list, which was exported to the Ettan Spot Handling Workstation (Amersham Biosciences) for automated spot picking and digestion. The pick-list defined the picking references (*x* and *y* co-ordinates) for the selected gel plugs, which were excised and placed into a 96-well plate. Using the robotic system, the gel plugs were washed three times in 100 μl 50 mM ammonium bicarbonate, shrunk with two washes of 100 μl 75% (v/v) acetonitrile and dried. Sequencing grade modified porcine trypsin (Promega, Hampshire, UK) was added (0.2 μg/μl in 25 mM ammonium bicarbonate, 10 μl/well) and incubated at 37^{o}C for 4h. Following the incubation, the gel plugs were washed twice in 100 μl 50% (v/v) acetonitrile/0.1% (v/v) trifluoroacetic acid to extract tryptic peptides. The tryptic peptides were collected in 96-well plates and dried for storage at -20^{o}C, or mixed with a saturated solution of α-cyano-4-hydroxycinnamic acid matrix in 0.3% (v/v) trifluoroacetic acid, 50% (v/v) acetonitrile and spotted onto stainless steel MALDI targets (ABI-192 format; Applied Biosystems, Warrington, UK) for mass spectrometry.

5.2.2.2 MALDI-MS/MS and Protein Identification

Samples spotted onto MALDI targets were submitted for MALDI analysis in a MALDI TOF/TOF 4700 Proteomics Analyser (Applied Biosystems). Spectra were collected in the mass range 800-4000 Da, and CID was initiated for up to ten of the strongest peaks to collect MS/MS data. MS and MS/MS data were submitted to MASCOT (http://www.matrixscience.com) using Global Proteome Server Explorer Software (Applied Biosystems), with the following parameters: *Homo sapiens* NCBInr database, examining monoisotopic 2^{+} and 3^{+} product ions, with a peptide tolerance of +/- 1.2 Da and MS/MS tolerance of +/- 0.6 Da, trypsin as the enzyme, cysteine carbamidomethylation as a fixed modification, and methionine oxidation as a variable modification.

5.2.2.3 Sample Preparation for Liquid Chromatography Tandem Mass Spectrometry (LC-MS/MS) and Protein Identification

For each peptide sample from the Cy3-labelled preparative gel, 5 μl was dried in a vacuum centrifuge and submitted for LC-MS/MS in a Q-STAR Pulsar i^{TM} (Applied

Biosystems) ESI Q-TOF hybrid mass spectrometer by Dr. Richard Burchmore. The samples were resuspended in 2% (v/v) acetonitrile/0.5% (v/v) formic acid, and peptides were separated using a Pepmap C18 reversed-phase nano-LC column (LC Packings, Netherlands) with a 20-minute 5-40% (v/v) gradient of acetonitrile, at a flow rate of 0.2 μl/min. LC eluate was analysed by online ESI-Q-TOF, with a duty cycle consisting of a survey scan (MS only, 3s), followed by fragmentation of the four strongest peaks (MS/MS, 3s per peak). MS data was submitted to MASCOT using a script within Analyst QS V 1.1.5 (Mascot.dll, Applied Biosystems). The parameters were chosen as follows: *Homo sapiens* NCBInr database, examining monoisotopic 2^+ or 3^+ product ions, with a peptide tolerance of +/- 1.2 Da and MS/MS tolerance of +/- 0.6 Da, trypsin as the enzyme, cysteine carbamidomethylation as a fixed modification, and methionine oxidation as a variable modification.

5.2.2.4 Ingenuity Pathways Analysis – Integration of Proteomic and Transcriptomic Data

Proteins that were found to be consistently differentially abundant across the replicate gels were submitted for IPA (Ingenuity Systems, http://www.ingenuity.com). The protein data was integrated into the transcriptomic data by obtaining the probeset IDs corresponding to each protein in the HuGene 1.0 ST 192 microarray chip format (Affymetrix) from the microarray data list. The abundance data for the transcripts corresponding to these proteins was replaced with a significance value of p=0.04 and fold-change of 1.5, to ensure the proteins would be present in the subsequent analysis, when the IPA thresholds were set at p<0.05 and 1.3 fold-change. Proteins that could be successfully mapped to the IPA database were eligible for analysis.

5.3 Results

5.3.1 Evaluation of Dye Bias

To address possible issues of dye bias (preferential binding of Cy3 or Cy5 to particular proteins, giving rise to potential errors in assessment of differential regulation), the dye titration (same/same) gels were analysed for spots that consistently appeared to be subject to “differential regulation” in more than two gels. A small number of such spots were identified, and excluded from the control/test comparison. One protein that was

apparently subject to dye bias between Cy3 and Cy5, and subsequently identified, was vinculin. This protein is a key mechanosensor, and this observation suggests that this experimental design was not adequate to analyse its abundance between the conditions studied. An alternative technique, such as Western blotting, may be more appropriate. The exception to the exclusion of potentially dye-biased spots was galectin-1, which appeared to exhibit a dye bias in the opposite direction to the observed differential regulation. This spot was still included in the main experimental analysis, as it was deemed that the effect of the bias would only underestimate, rather than exaggerate, the magnitude of the differential regulation.

5.3.2 Comparative Proteomic Analysis of Extracts from Cells Cultured on Planar and Microgrooved Structures

Following DiGE/MS analysis of protein extracts from cells cultured on planar and microgrooved (2 μm depth x 25 μm pitch) quartz substrates (*n*=3 analytical gels), around forty proteins were noted as potentially subject to differential regulation. An example of a protein spot apparently subject to differential regulation is shown as it appeared in the gel analysis software (DeCyder v5.0, GE Healthcare) in Fig. 5-3. Several of these proteins were successfully identified using a combination of MALDI-TOF MS/MS and ESI-Q-TOF MS/MS, and their potential functional classifications are noted in Table 5-I.

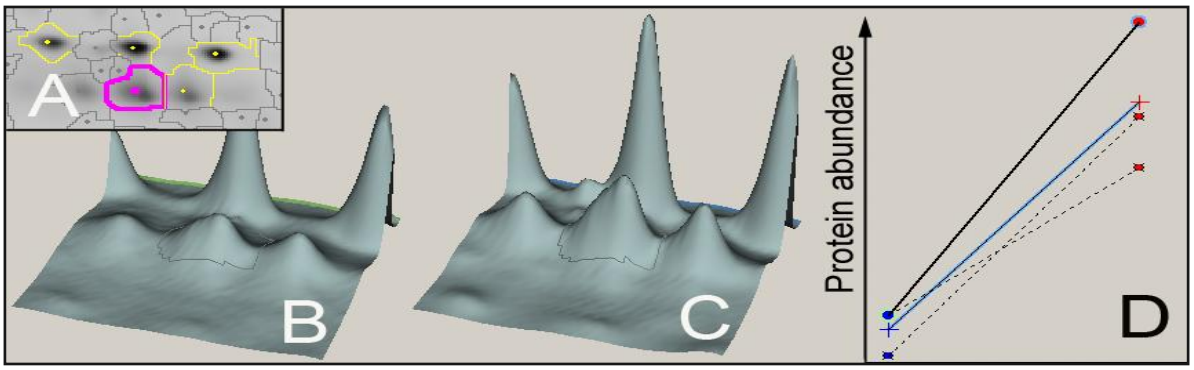

Figure 5-3. Example of a protein spot (circled in pink on the 2D gel in A) that was more abundant in cells on the microgrooved (C) than the planar (B) substrate. *This is represented graphically in D (n=3 gels: blue dots represent extracts from cells on the planar substrate, red dots represent extracts from cells on the microgrooved surfaces). The blue line indicates the mean of the three replicate spots, and the unbroken and broken black lines represent each of the individual replicates. The protein was subsequently identified as nucleophosmin (spot 1925).*

Table 5-I. Functional classifications of proteins up-regulated in cells cultured on the quartz microgrooved topography. *Key to symbols: A- Adhesion, C- Cytoskeleton, D- DNA Replication, Ch- Protein Chaperone, M- Metabolism, Mi- Cell Migration, P- Proliferation, S– Protein Synthesis, Co- Collagen Synthesis, Sh– Protein Shuttling, T– Protein Turnover, U– Unknown (putative Ca^{2+} transporter). Data in italics in the Protein Name column is ESI-Q-TOF data (note: confidence interval data was not available for protein IDs derived from ESI-Q-TOF), and non-italic indicates MALDI-TOF/TOF data (includes confidence intervals). Data on rate of turnover reproduced from a SILAC study of protein turnover rates in HeLa cells by (Doherty et al., 2008), included for information (- indicates data unavailable for this protein). p-values are shown from a paired T-test, values in bold are considered significant at the p<0.05 level. *Galectin-1 spots were consistently up-regulated on the grooved topography (n=3), but due to peak intensity saturation, accurate quantification of the magnitude of up-regulation was not possible (although it was >2-fold in each spot).*

Protein Name (Protein MOWSE score/no. of matched peptides/protein score confidence interval)	Functional Classification	Mean Fold Change (G/F)/ Percentage Change (%; G:F)	Standard Deviation	*p*-value	Rate of Protein Turnover (K_{deg}, h^{-1}) in *HeLa* cells (from (Doherty et al., 2008)
B23 Nucleophosmin (*107/3*)	Ch, P, Sh	+ 1.45 / 145	+/- 0.14	**0.022**	0.00852
B23 Nucleophosmin (108/5/100%)	Ch, P, Sh	+ 1.57 / 157	+/- 0.17	**0.020**	0.00852
Isocitrate Dehydrogenase 3 (NAD^+) gamma isoform a precursor (*48/2*)	M	+ 1.81 / 181	+/- 0.28	**0.022**	0.0609
Enolase I Variant (192/8/100%)	M	- 1.23 / 81	+/- 0.20	0.294	-
Enolase I (*260/8*)/ Calreticulin precursor (*173/6*)	M	- 1.39 / 71	+/- 0.22	0.219	-
Laminin-binding protein (*219/7*) (315/10/100%)	A	+ 1.28 / 128	+/- 0.11	**0.039**	0.01717 (Laminin receptor-like protein LAMRL5)
Prolyl-4-hydroxylase beta precursor (*753/22*)	Co	- 1.55 / 64	+/- 0.1	**0.043**	-
Proliferating Cell Nuclear Antigen (PCNA) (*165/5*)	D, P	+ 1.57 / 157	+/- 0.35	0.076	-
Actin Filament Capping Protein (86/6/99.949%)	C	+ 1.68 / 168	+/- 0.63	0.172	Subunits: α_1 – 0.02665 α_2 – 0.06288 β - 0.00772

Actin Filament Capping Protein (95/5/99.993%)	C	+ 1.49 / 149	+/- 0.60	0.124	Subunits: α_1 – 0.02665 α_2 – 0.06288 β - 0.00772
Galectin-1 (*83/4*)	Mi	+ 2.02 / 202 (Slight peak saturation)*	+/- 0.43	**0.048**	-
Galectin-1 (*91/3*)	Mi	> + 2 (Saturated peak)*	-	-	-
Eukaryotic translation elongation factor delta (134/9/100%)	S, C	+ 1.39 / 139	+/- 0.04	**0.002**	0.01536
Ubiquitin C-terminal esterase/hydrolase L1 (*102/3*)	T	+ 2.23 / 223	+/- 0.36	**0.020**	0.00599
Annexin V (*243/7*) (447/10/100%)	U	+ 1.67 / 167	+/- 0.73	0.099	0.03902

5.3.3 Functional Implications of Up-Regulation of Identified Proteins

5.3.3.1 Nuclear and Nucleolar Functions

B23 nucleophosmin is a nucleolar phosphoprotein with chaperone activities. It can shuttle between the nucleus and cytoplasm and has multiple functions. It is intimately linked with ribosome biogenesis, supporting nuclear export of rRNA and ribosomal subunits, and as result, protein translation and cell proliferation (Maggi et al., 2008). In addition, it has been shown to regulate the SUMO (small ubiquitin-like modifier protein) pathway (Yun et al., 2008), and is required for export of the 40S and 60S ribosomal subunits and rRNA from the nucleus (Maggi et al., 2008). It also participates in the maintenance of nucleolar morphology and plasticity (Martin et al., 2009). It was up-regulated in cells on the grooved topography in two independent gel spots ($p<0.05$) (Fig. 5-4).

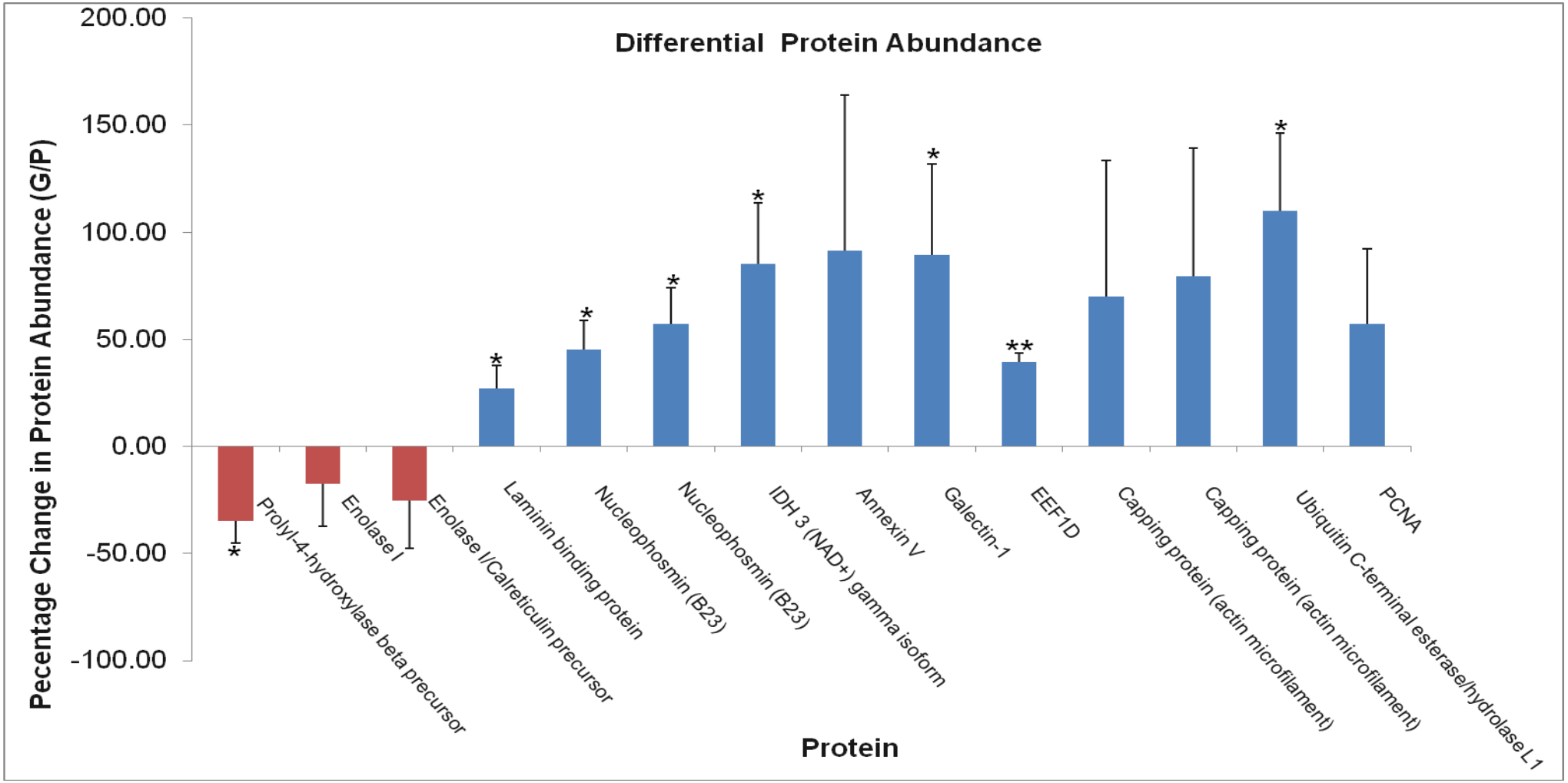

Figure 5-4. Percentage change in abundance in some protein spots potentially subject to differential expression in cells cultured on planar and microgrooved (2 µm depth, 25 µm pitch) quartz substrata, for proteins detected by DiGEsat and identified by MS (n=3 replicate gels). *Key: EEF1D – Eukaryotic elongation factor delta isoform, IDH3 – Isocitrate dehydrogenase 3, PCNA – Proliferating cell nuclear antigen. Bars indicate SD, a single asterisk (*) indicates significance at $p<0.05$, and a double asterisk (**) indicates significance at $p<0.01$, using a Student's T-test of log_{10}-transformed data. n=3 biological replicates (3 protein samples) per surface; each sample was prepared by pooling cells from 4 replicate structures.*

Proliferating Cell Nuclear Antigen (PCNA) is involved with the elongation phase of DNA replication and associates with foci of lamin B (Moir et al., 1994; Moir et al., 2000a), which represent areas of active replication. It was consistently up-regulated in cells on the grooved topography, but the up-regulation was just outside the significance threshold (n=3, p=0.076), due to differences in the magnitude of up-regulation between samples (Fig. 5-4). It seems probable that this result could become significant if more replicates were to be performed.

5.3.3.2 Metabolism

Isocitrate dehydrogenase 3 is a tricarboxylic acid cycle enzyme, and the up-regulation of its precursor in cells on the grooved topography may reflect an increased metabolic demand of cells on this surface as they investigate their new environment. It should be noted that this enzyme was identified with less confidence than the other proteins in the study, since its peptide score of 48 is relatively close to the MOWSE threshold for significance (score: 42), and it had only 2 spectra detected. In contrast, the other proteins in Table 5-I were identified with high confidence, since each had at least a score of 86 with 3 spectra matched. Annexin V is a Ca^{2+}-binding membrane protein, which translocates from the inner to the outer membrane leaflet in apoptotic cells. Its physiological role in non-apoptotic cells is undefined, although it may function as a Ca^{2+} channel (Kubista et al., 1999). Its up-regulation was not statistically significant with the number of replicates employed, due to the relatively large standard deviation between samples (Fig. 5-4).

5.3.3.3 ECM, Adhesion, Cytoskeleton and Cell Motility

Prolyl-4-hydroxylase is a key enzyme in collagen synthesis (reviewed in (Kivirikko et al., 1989)), and its precursor was down-regulated on the grooved topography (p<0.05) (Table 5-I, Fig. 5-4). Laminin-binding protein is a pro-adhesive protein responsible for interacting with laminin and other proteins in the ECM, and was modestly up-regulated in cells cultured on the topography (p<0.05) (Table 5-I, Fig. 5-4). Actin filament capping protein is involved in the modulation of actin stress fibres. It binds to the barbed end of growing F-actin filaments, and prevents the addition of further globular (G)-actin subunits (Wear et al., 2003). The protein appeared to be up-regulated in two independent spots, although this result was not significant due to the relatively large standard deviation between the sample pairs (Fig. 5-4). This is probably an effect of the small number of

replicates, however, and it seems likely that this result may become significant if a greater number of replicates were used. Galectin-1 has multiple functions. It can promote cell migration by altering cell-substrate interactions (Alge et al., 2006; Camby et al., 2002; Camby et al., 2005), and also has a role in pre-mRNA splicing (Vyakarnam et al., 1997; Wang et al., 2006). It has also been shown to alter the selectivity of the G-protein Ras to preferentially interact with Raf-1, rather than phosphoinositide 3-kinase (Elad-Sfadia et al., 2002).

5.3.3.4 Protein Synthesis and Degradation

Eukaryotic translation elongation factor delta (eEFδ) is a guanine nucleotide exchange factor (GEF) for eEF1A, an essential factor for the extension of nascent amino acid chains, and was up-regulated in cells on the topography ($p<0.01$) (Table 5-I, Fig. 5-4). Ubiquitin C-terminal esterase/hydrolase L1 is a deubiquitinase. Addition of a chain of ubiquitin molecules (a process known as ubiquitination) identifies proteins for destruction by targeting them for proteolysis. Deubiquitination (removing ubiquitin from tagged proteins) prevents such proteins being targeted for proteolysis. In addition, ubiquitin serves as an epigenetic histone modification that can affect gene accessibility for transcription (reviewed in (Muratani and Tansey, 2003)).

5.3.4 Integration of Transcriptomic and Proteomic Data

There is some concordance between the differentially abundant proteins noted in Section 5.4.2 and their respective mRNA levels (Table 5-2), with most of the proteins and their respective transcripts appearing to show the same directionality. The transcript and protein abundance appeared most concordant for the *IDH3G* and *LGALS* genes, where a modest increase in mRNA levels appeared to relate to a larger up-regulation at the protein level. As the *p*-values for several transcript abundance levels were not significant (*i.e.* the variation in transcript abundance for those particular genes was too large between arrays to reach a consensus result with the number of arrays used), however, it is difficult to fully evaluate the relationship between the gene and protein levels.

Table 5-II. Comparison between DiGE and microarray data for cells cultured on microgrooved versus planar quartz materials, for the transcripts corresponding to the differentially abundant proteins identified by DiGE. *Data shown for fold change in DiGE data (bold indicates significance at p<0.05), the fold change detected by each individual microarray, and the p-value for the three arrays (bold indicates significance at p<0.05). Note: Transcript data corresponding to prolyl-4-hydroxylase was not available.*

Protein Name/*Gene Name*	Fold Change (DiGE)	Fold Change (μArray)	*p*-value (μArray)
B23 Nucleophosmin/ *NPM1*	**+1.45**	+1.038	6.76×10^{-1}
B23 Nucleophosmin/ *NPM1*	**+1.57**	+1.038	6.76×10^{-1}
Isocitrate Dehydrogenase 3 (NAD^+) gamma isoform a precursor/*IDH3G*	**+1.81**	**+1.278**	$\mathbf{5.5 \times 10^{-3}}$
Proliferating Cell Nuclear Antigen (PCNA)/*PCNA*	+1.57	-1.062	3.03×10^{-1}
Actin Filament Capping Protein/*CAPZA1*	+1.68	+1.102	3.2×10^{-1}
Actin Filament Capping Protein/*CAPZA1*	+1.49	+1.102	3.2×10^{-1}
Galectin-1/*LGALS*	**~ +2.02**	**+1.141**	$\mathbf{5.55 \times 10^{-5}}$
Galectin-1/*LGALS*	> + 2.00	**+1.141**	$\mathbf{5.55 \times 10^{-5}}$
Eukaryotic translation elongation factor delta/*EEF1D*	**+1.30**	+1.142	1.84×10^{-1}
Ubiquitin C-terminal esterase/hydrolase L1/*UCHL1*	**+2.23**	+1.071	3.55×10^{-1}
Annexin V/*ANXA 5*	+1.67	**+1.032**	$\mathbf{2.84 \times 10^{-2}}$
Laminin binding protein/*LOC387867*	**+1.28**	+1.026	7.65×10^{-1}
Enolase I variant/*ENO I*	-1.23	+1.022	4.56×10^{-1}
Enolase I/Calreticulin precursor/*ENO I*/*CALR*	-1.39	+1.022/ **-1.072**	4.56×10^{-1}/ $\mathbf{1.28 \times 10^{-2}}$
Prolyl-4-hydroxylase beta precursor	**-1.55**	-	-

The transcriptomic and proteomic data were combined and submitted for IPA analysis, and the highest scoring pathway is shown in Fig. 5-4. In the network, PCNA was linked with other components of the cell cycle machinery (CDKN1A and cyclin A) and DNA polymerase delta (which was up-regulated at the transcript level). Galectin-1 was implicated in the pathway, with its capacity to inhibit Ras and ERK, and increase transcription from *CDKN1A* (Fischer et al., 2005). Similarly, ANXA5 was included in the pathway due to its ability to regulate Ras, ERK and CDKN1A under certain conditions (Sato et al., 2000). Important contributors to several signalling pathways were implicated in the network (PI3K, NFkB, ERK, ERK 1/2, P38 MAPK, oestrogen receptor), primarily as 'invited' nodes (unchanged expression levels at the applied threshold, but forming important bridges between multiple other nodes). Chromatin remodelling was also highlighted, and the inclusion of HMGA1, which was up-regulated at the transcript level and can modulate expression from many genes, was particularly interesting.

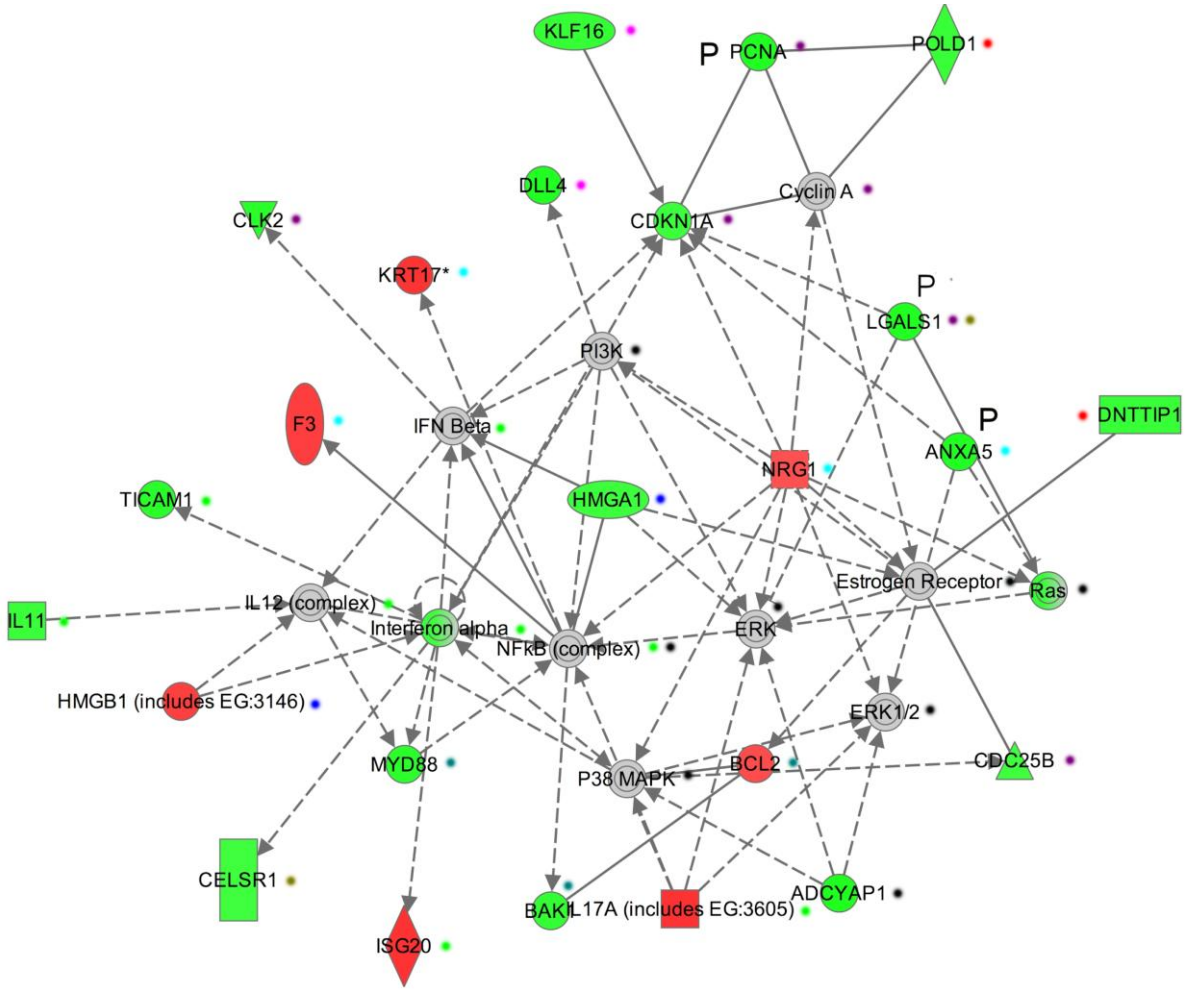

Figure 5-5. IPA network (score 17, 1.3 fold-change threshold, p<0.05) integrating transcriptomic and proteomic data. *Green – up-regulated transcripts/proteins (in cells on the microgrooved substrate), Red – down-regulated transcripts/proteins (in cells on the microgrooved substrate), Grey – unchanged transcript/protein levels relative to controls. Unbroken lines indicate direct interactions (involving physical contact of the molecules), and broken lines indicate indirect interactions (e.g. via the induction of a signalling cascade). Arrowheads indicate the direction of influence. Lines with no arrowhead indicate binding only, and lines with a small perpendicular line at the terminus indicate that the molecule at the start of the line inhibits the molecule at the terminus. 'P' indicates differentially expressed proteins; the remainder are transcripts. The key to potential functions (denoted by coloured dots) is shown below.*

Chromatin remodelling: HMGA1 – high mobility group AT-hook 1, HMGB1 – high mobility group box 1
Transcription factors: DLL4 – Delta-like 4, KLF16 – Kruppel-like factor 16
DNA polymerisation: DNTTIP1 – deoxynucleotidyl transferase, terminal, interacting protein 1, POLD1 – polymerase (DNA directed) delta 1, catalytic subunit, 125 kDa
*Signalling: ADCYAP1 – adenylate cyclase activating polypeptide 1, ERK – extracellular signal-regulated kinase, ERK 1/2 – extracellular signal-regulated kinase 1/2, **Estrogen receptor**, NFκB **(complex)** – nuclear factor kappa B, P38 MAPK – P38 mitogen-activated protein kinase, PI3K - phosphatidylinositol (3, 4, 5)-triphosphate, **Ras***
*Immunity-related: IL11 – interleukin 11, IL **12 (complex)** – interleukin 12, IL17A **(includes EG:3605)** – interleukin 17A, **Interferon alpha**, IFN **Beta** – interferon beta, **ISG20** – interferon-stimulated exonuclease gene 20 kDa, TICAM1-toll-like receptor adapter molecule 1*
*Cell cycle/proliferation-related: CDC25B – cell division cycle 25 homolog B (S. pombe), CDKN1A – cyclin-dependent kinase inhibitor 1A, CLK2 – cell division cycle-like kinase 2, **Cyclin A**, PCNA – proliferating cell nuclear antigen (P), LGALS1 – galectin-1 (P)*
Apoptosis-related: BAK – BCL2-antagonist/killer 1, BCL2 – B-cell lymphoma 2, MYD88 – myeloid differentiation primary response gene (88)
Cell migration/adhesion: CELSR1 – cadherin, EGF LAG seven-pass G-type receptor 1, LGALS1 – galectin-1 (P)
Other: ANXA5 – annexin A5 (unknown, may be involved in Ca^{2+} signalling) (P), KRT17 – keratin 17 (cytoskeletal related), F3 – coagulation factor III (stimulator of platelet aggregation), NRG1 – neuregulin 1

5.4 Discussion

Recently, microarray studies have indicated that the expression levels of a variety of genes in fibroblasts are modulated by topographies including polymer-demixed nanoislands (Dalby et al., 2002b) and microgrooves (Dalby et al., 2003c), both of which resulted in up-regulated transcription of cytoskeletal, ECM-related, transcriptional and proliferative genes, and nanocolumns (Dalby et al., 2005c), which induced a down-regulation of transcription from signalling and proliferative genes. Fluctuations at the mRNA level may give rise to changes at the protein level, but these can have a poor correlation (discussed in (Hegde et al., 2003)). This is probably because microarrays assess the quantity, but not the 'activity' state of particular mRNAs, and additional post-transcriptional events can be involved. Components of the RNA interference machinery can sequester mRNA species away from ribosomes, for example into processing bodies (Jakymiw et al., 2005; Liu et al., 2005a; Sen and Blau, 2005), and the accessibility and turnover of transcripts can affect translation. Protein turnover provides an additional level of post-transcriptional control. Additional information on these variables would increase our understanding of the correlation between the transcript and protein abundance data from this study, and techniques such as ribosome sedimentation microarrays (Melamed et al., 2009) and global analysis of protein translation (Schwanhusser et al., 2009) could be valuable for this purpose. Finally, there are alternative splicing products that may not be detected by the array chip, but can be seen at the protein level as alternative isoforms, and some mRNA expression results were not statistically significant with the number of replicates utilised. Together, these effects could explain why the transcript and protein abundance data were not entirely concordant.

The observation that *LGALS* and *IDH3* were up-regulated at both the transcript and protein levels suggests that there may be a multi-level adaptive response for some genes. For the up-regulated proteins discussed in this chapter, the emphasis seems likely to be on post-transcriptional modulation of abundance, since the magnitude of increase at the protein level appears greater than the more modest up-regulation at the transcript level. This would be beneficial as a rapid response mechanism for the cell, rather than requiring additional time and resources to commence transcription prior to alterations at the protein level. The smaller changes in mRNA abundance could also reflect the initiation of a slower phase of protein modulation, originating from *de novo* transcript synthesis, which could become more important at a later time-point, perhaps to produce a sustained (rather

than initial) response to the mechanostimulus. This is consistent with the data showing that similar functional categories of mRNAs and proteins appeared to be differentially expressed (relating to cytoskeletal turnover, RNA trafficking, cell motility, DNA replication, molecular transport and gene expression), suggesting that the overall response to the topography is concordant. In addition, the IPA analysis integrating the transcript and protein abundance data suggested that there were commonalities between the pathways affected at both levels, and several important signalling molecules (such as ERK) were implicated in the network. Interestingly, many of these signalling molecules were invited nodes, interacting with other components of the network, rather than being directly subject to differential expression. This may be sufficient to engender changes in signalling, if upstream regulators or downstream effectors are modulated, or may be an effect of the early time-point examined in the study, if the changes in these signalling pathways become more prominent with increasing length of culture period.

Increased translation of existing transcripts is likely to have contributed to the observed protein up-regulation. Consistent with this, eEF1δ was up-regulated in cells cultured on the grooved topography. Alternatively, there could be alterations in the proportion of certain proteins being targeted for degradation. The up-regulation of a deubiquinating enzyme (ubiquitin C-terminal esterase L1) in cells on the grooved topography suggests that degradation was being reduced in these cells. This could complement the up-regulation of the accessory translation elongation factor eEF1δ, by both promoting synthesis and reducing degradation, and suggests that cells on the topography may be experiencing (or anticipating) increased demands on their protein production machinery. It is possible that the effects of degradation would be more apparent over longer culture periods, since the turnover rates of different proteins can vary #widely (Doherty et al., 2008).

Interestingly, eEF1A has also been shown to regulate the actin cytoskeleton (Gross and Kinzy, 2005, 2007; Pittman et al., 2009), and the up-regulation of its GEF may be an attempt to improve the turnover rate of GDP to GTP, to generate more active eEF1A to assist in the large structural changes needed for the cells to adapt to the grooved topography. A number of elements of the translational machinery have been shown to interact with the cytoskeleton (reviewed in (Kim and Colulombe, 2010)**),** which appears to be required for efficient protein synthesis. The mechanical alterations induced by the grooved topography may be influencing protein translation, which could be leading to compensatory up-regulation of assistive factors. Cyclic stretch-induced reorganisation of

the cytoskeleton has previously been shown to assist expression of an exogenous reporter gene (Geiger et al., 2006), which could be prevented by use of depolymerising agents. In addition, ribosomal recruitment to focal adhesions is affected by mechanical stretch (Chicurel et al., 1998). It would be anticipated that mRNA and protein transport could also be affected by the topography-induced cytoskeletal reorganisation, particularly since protein shuttles such as galectin-1 and nucleophosmin appear to be up-regulated in cells on the grooved substrate. This also correlated with the altered abundance of transcripts involved in molecular transport and RNA trafficking (Chapter 3).

Up-regulation of nucleophosmin, which shuttles between the nucleolus and cytoplasm, is interesting given the concordant morphological changes described in Chapter 2, and the down-regulation of snoRNAs in cells on the grooved topography (Chapter 3), particularly since nucleophosmin has been implicated in the control of nucleolar plasticity (Martin et al., 2009). Interestingly, lamin B associates with nucleophosmin in nucleoli, and siRNA-mediated knockdown of nucleophosmin led to nucleolar elongation in cells cultured on a planar substrate (Martin et al., 2009), a similar morphological change to that imposed by the grooved topography. Up-regulation of nucleophosmin could be an attempt to compensate for the nucleolar changes induced by the constraints of the topography on the nuclear architecture. In addition, ribosomal protein L5 mRNA was strongly down-regulated (-2.049) in cells on the topography (Chapter 3), and this ribosomal component is dependent on nucleophosmin for export from the nucleus (Yu et al., 2006b). Furthermore, given the architectural changes within the nucleus (Chapter 2) and microarray data indicating differential expression of transcripts relating to molecular transport (Chapter 3), it is interesting that nucleophosmin can regulate the SUMO pathway. SUMOylation has a role in transport of protein between the nucleus and cytoplasm (reviewed in (Pichler and Melchior, 2002), and protein localisation within the nucleus, which could be particularly important in view of the architectural changes in the nucleus. A SUMO precursor (SMT3A protein small ubiquitin-related modifier 3 precursor) was previously shown to be up-regulated in osteoprogenitor cells cultured on microgrooves (Kantawong, 2009). This suggests that post-translational modification, particularly ubiquitination and SUMOylation, is likely to be an important regulatory mechanism in the cellular response to topography. This is consistent with the hypothesis that the protein up-regulation is likely to be occurring primarily at the post-transcriptional level, based on the limited direct concordance between the proteomic and transcriptmic data. Nuclear pores also have a role in protein ubiquitinylation and SUMOylation, and if there are topography-induced

mechanical changes in nuclear pores, these functions may be altered, perhaps necessitating the up-regulation of a deubiquitinase and a regulator of SUMOylation.

The up-regulation of galectin-1, which can promote cell migration, is consistent with the observations from Chapter 2 that cells on the microgrooved substrate adopt a 'motile' bipolar morphology, with fewer, smaller focal adhesions. Interestingly, galectin-1 has been shown to increase the motility of human tumour cells when added to the culture medium, by promoting cytoskeletal reorganisation and transcription of Rho (Camby et al., 2002). This is also consistent with the data from Chapter 3 showing up-regulation of Rho mRNA. Based on the IPA analysis integrating the transcriptomic and proteomic data, it appeared that galectin-1 could inhibit proliferative signals from Ras and ERK (Fischer et al., 2005), while annexin V could modulate the activities of ERK 1/2 and Ras (Sato et al., 2000). Interestingly, galectin-1 could also increase transcription from *CDKN1A*, which regulates G1 progression in the cell cycle (Fischer et al., 2005). Up-regulation of both proteins is likely to be a mechanism contributing to tight control over pro-proliferative signalling, to prevent oncogenesis.

Up-regulation of the precursor to isocitrate dehydrogenase 3 (NAD^+) (gamma isoform a) is suggestive that the cells may have been experiencing or anticipating an increased metabolic demand on the topography, perhaps due to cytoskeletal remodelling and the enforcement of a motile morphology. Down-regulation of the precursor to prolyl-4-hydroxylase suggests that the cells may have been reducing collagen production on the topography. It is possible that this is because the cells exhibited characteristics of more motile cells (bipolar morphology, with protein-level up-regulation of a metabolic enzyme, migratory and actin-regulatory factors) on the grooved substrate, which could promote cell migration over collagen production (more appropriate for cells at confluence laying down the ECM). This is consistent with the up-regulation of transcripts encoding MMPs, including MMP7 (Chapter 3). In light of the protein-level down-regulation of prolyl-4-hydroxylase, this suggests that ECM degradation and remodelling could be predominating over ECM deposition, perhaps to facilitate cell motility on the substrate.

Up-regulation of actin filament capping protein is consistent with the large-scale cytoskeletal reorganisation described in Chapter 2, and the altered levels of cytoskeletal-related transcripts noted in Chapter 3. In addition, actin has been shown to affect nuclear stability in *Xenopus* oocytes (Bohnsack et al., 2006) and nuclear actin appears to function in transcription from class I, II and III genes (Fomproix and Percipalle, 2004; Hofmann et

al., 2004; Hu et al., 2004). Thus, up-regulation of actin filament capping protein could also be contributing to changes at the transcript level. Laminin-binding protein was also modestly up-regulated, however, which suggests the cells may be generating a pool of this pro-adhesive protein, to enable faster turnover of adhesions as cells explore the topography, or promote formation of stronger or more numerous adhesions.

The increase in the abundance of PCNA in cells on the grooved topography is particularly interesting, as this appears to be consistent with the altered lamin B organisation discussed in Chapter 2, with the caveat that the up-regulation was not significant with the number of replicates used. If the changes noted in the nucleoskeleton on the topography contribute to changes in the number or distribution of replication foci, the up-regulation of this replication factor could be acting to offset the alterations in the lamin B network. Such changes may correlate with the altered abundance of transcripts encoding proteins involved in DNA replication (Fig. 5-4 and Chapter 3). IPA analysis incorporating both the transcript and proteomic data suggested that PCNA is likely to be acting as a hub for interactions between the cell cycle and DNA replication machinery.

Galectin-1 was up-regulated in two spots in a previous study of osteoprogenitors cultured on 2 μm depth, 12.5 μm polycaprolactone grooves (Kantawong, 2009). Most interestingly, nucleophosmin, galectin-1, α-enolase, annexin V and the laminin receptor were also up-regulated in osteoprogenitor cells in static culture on a nanodisordered substrate (Kantawong, 2009; Kantawong et al., 2009b), which suggests that these proteins could be common factors involved in the response to multiple topographies. Prolyl-4-hydroxylase was also up-regulated on the nanodisordered surface, but was down-regulated in this study on the microgrooved substrate. This could suggest this metabolic enzyme is responsive to the mechanical changes or demands imposed by topographical substrates, but the precise effect could be cell-type or topography-specific.

5.5 Conclusion

IPA analysis highlighted common links to several important functional pathways, including ERK/MAPK and ERK 1/2 signaling, at both the transcript and protein levels. A number of the up-regulated proteins can modulate other processes, including ribosomal assembly and protein synthesis. The differentially expressed proteins had the potential to affect key processes including cell motility, adhesion, metabolism, DNA replication, ribosomal assembly, RNA production and protein synthesis. Alterations in the abundance

of mediators with the potential to directly influence protein production probably enabled the cells to more effectively respond to the changes in environmental conditions. Concomitant alterations in the abundance of small RNA effectors (Chapter 2) suggests that relatively rapid response mechanisms (*i.e.* protein and RNA direct effectors) may be becoming preferentially activated at this time-point. This could be a strategy to maximise the initial adaptation to the topographical substrate. Together, these results are consistent with a mechanoresponse at the protein level.

6 Discussion

The primary aim of this thesis was to investigate the process of mechanotransduction, using microgrooved topography as a non-invasive mechanostimulus. A multilayered approach was adopted to permit study of the process at different stages, from the receipt and transfer of mechanical stimuli into the nucleus to the induction of gene- and protein-level responses. This necessitated optimisation of protocols for several molecular and cell biological techniques, and generated additional insight into the fundamental biology of mechanotransduction and cell-material interactions.

6.1 Method Development

6.1.1 Structural Analysis

The application of a 3D confocal approach to the study of cellular interactions with microtopography provided additional functional insight into the arrangement of subcellular architecture, improved discrimination between grooves and ridges, and gave a useful starting point to commence investigation of particular structural features in a higher throughput manner. Since a method previously used to stain the nuclear lamina in cells on biomaterials (Dalby et al., 2007b) did not give satisfactory staining in the present study, various methods were appraised to permit the selection of an appropriate protocol (Chapter 2). The approach that emerged as the most reliable and specific, using cold methanol fixation, followed by a lengthy blocking step with a high concentration of BSA (3% (w/v)), has since been successfully applied to the staining of human mesenchymal stem cells cultured on polymeric substrates (M. Tsimbouri, personal communication), indicating its applicability in different human cell types. A method for co-staining of lamin B and vimentin was developed (Chapter 2) that was compatible with epifluorescence microscopy. This staining regime could probably also be utilised in conjunction with high-resolution confocal imaging by using fluorescent dyes with greater spectral separation, negating the requirement for single-track image acquisition, or with some additional modifications to raise the signal intensity.

A protocol was developed for FISH staining of chromosome territories in fibroblasts on quartz substrates using whole-chromosome probes following 24h culture (Chapter 4). This was based on previous work examining fibroblasts on smaller culture

areas with centromeric probes (Dalby et al., 2004g), and whole-chromosome probes after 3 days of culture (Multini, 2007). Use of a different detection kit raised the signal specificity and intensity, and minimised the amount of probe required.

6.1.2 Molecular Biology

A significant challenge to the application of molecular biological techniques to the investigation of cell-biomaterial interactions is in obtaining sufficient biological material from small culture areas. In this study, the difficulty was increased by a requirement for near-monodisperse cell densities, to minimise cell-cell interactions. To overcome this, pooling strategies were employed to generate sufficient RNA for microarray analysis (Chapter 3), and protein for proteomics (Chapter 5). For the proteomic research, DiGEsat was selected as a high-sensitivity approach to permit analysis of lower quantities of protein than the DiGEmin labelling regime would have necessitated. The optimisation of extraction and electrophoretic conditions improved the resolution of the DiGE gels for study of the protein-level response to the mechanostimulus.

6.2 Mechanotransduction

6.2.1 Direct Mechanotransduction – Transfer of Mechanical Stimuli Into the Nucleus

It is interesting to note that a number of elements of the direct mechanotransductive machinery have been shown to be spatially or structurally reorganised in response to the discrete application of mechanical force, including force-induced growth of focal adhesions (Riveline et al., 2001) by assembly of multipartite protein complexes, exposure of binding sites in mechanoresponsive proteins (del Rio et al., 2009), tension-induced recruitment of mRNA and ribosomes to focal adhesions (Chicurel et al., 1998), nucleolar repositioning (Maniotis et al., 1997), and local melting of DNA (DE Ingber, personal communication), with the potential to increase accessibility to transcription factor binding sites. Thus, the cellular organisation appears structurally ‘primed’ for the receipt and interpretation of mechanical signals by this direct route.

Consistent with previous studies, the microgrooved substrate could induce considerable cytoskeletal reorganisation with respect to the control, with alignment of

tubulin, actin and vimentin visible in 2D and 3D (Chapter 2). This was anticipated to induce downstream rearrangement within the nucleus. Indeed, the cytoskeletal changes appeared to result in concordant reorganisation of the nucleoskeletal lamina. Tubule-like structures were diminished in frequency in cells cultured on the microgrooved topography (Chapter 2), which could have affected the transport of nucleic acids or small molecules. Lamin B speckles and tubule-like structures could also be aligned by the grooves, and the tubular features had the capacity to partition the nucleus. These appeared to form physical barriers that were highly likely to contribute to the repositioning of subnuclear objects, particularly when multiple horizontal projections of lamin B were present in a fence-like architecture. It is possible that rearrangement of these structures could alter gene accessibility by creating localised enhancement of mechanical forces at the edges of the nucleus. These could be compressive or tensile, depending on the precise association between the chromosomal and nucleoskeletal elements.

Geiger et al (2006) proposed that the cytoskeleton acts as a mesh to prevent exogenous DNA and particles reaching the nucleus, as the expression of a plasmid reporter construct was increased following nocodazole-induced actin depolymerisation, and stretch-induced actin disorganisation. On the microgrooved substrate utilised in this study, large stress fibres were induced, mostly spanning the length of the cells. In addition, as a result of lateral confinement, the cytoskeletal elements appeared to be in closer proximity, as a tighter, less expansive meshwork, and were generally more aligned along the direction of the topography (Chapter 2). This could potentially reduce the effect of cytoskeletal filtering, perhaps promoting greater exchange between different subcellular compartments and facilitating movement of organelles such as ribosomes, which can be recruited to focal adhesions (Chicurel et al., 1998). This could also be a mechanism for the cells to increase environmental sampling, and adapt to the extracellular locale. Consistent with this, it is interesting to note that the arrangement and frequency of lamin B tubule-like structures was perturbed (Chapter 2), and mRNA for an ABC-type transporter was highly up-regulated in cells on the topography (Chapter 3). Also, RNA trafficking and molecular transport were highlighted as functional categories with a considerable number of differentially expressed genes (Chapter 3).

The alignment of stress fibres, tubulin and vimentin across the nucleus was suggestive of effects within the nucleus (Chapter 2). This was particularly apparent in a cell in which depressions were visible in the underlying vimentin network, due to the tension originating from a very long cellular projection. It is possible that the vimentin

network facilitated dissipation of the tension over a larger area, preventing such acute stress on the nucleus. Consistent with this, tubulin formed a cage-like architecture over the nucleus in cells on the microgrooves, which could also have been acting to shield the nucleus from excessive compression. Dahl et al. proposed that the nucleus is somewhat protected from compressive forces by the restrictions imposed by the nuclear lamina. Using micropipette aspiration, the authors demonstrated a compressibility limit of 25 mN/m, but the nucleus retained an element of elastic deformability, which should accommodate changes in nuclear shape and mechanotransduction (Dahl et al., 2004).

On the topography, nuclei appeared more elongate than on the planar substrate, which was expected to effect changes in subnuclear components. Indeed, nucleoli were generally elongated, aligned and extended in the *z*-direction (Chapter 2 and Fig. 6-1). The topography-induced cell elongation and cytoskeletal rearrangement was strongly suggestive that tensile forces and lateral confinement had promoted the nucleolar alterations. This seems particularly likely since nucleolar alignment was also observed in fibroblasts on the planar substrate that adopted an extended morphology due to intercellular contact (Chapter 2). Nucleoli were also associated with lamin B speckles (Chapter 2), and knockdown of lamin B (but not lamin A/C) has been shown to correlate with alterations in nucleolar morphology (Martin et al., 2009). As nucleoli occupy inter-chromosomal spaces, repositioning of this structure was anticipated to correlate with mechanically mediated alterations in the positioning of chromosomal territories within the nucleus.

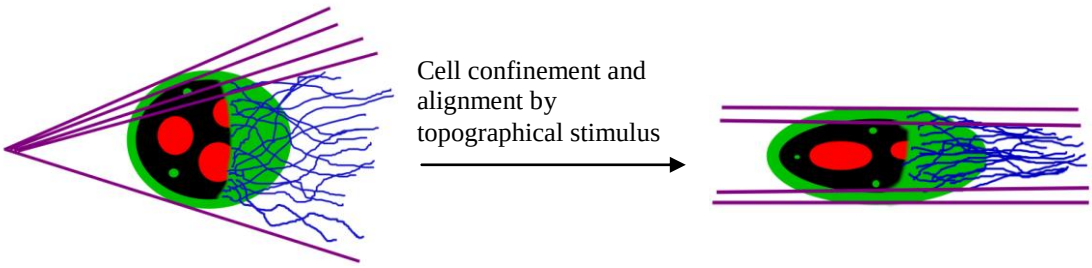

Figure 6-1. Cytoskeletal rearrangement by the microgrooved topography, and downstream mechanostructural effects. *Cytoskeletal filaments, including actin (purple), tubulin and vimentin (blue), were altered from an expansive network to a confined, aligned arrangement on the grooved topography, potentially reducing cytoskeletal 'filtering' effects and promoting subcellular exchange. Nucleoli (red) were aligned and extended in the z-direction, and the nuclear lamina (green) was reshaped, with alignment or reduction in frequency of tubule-like lamin B structures. Certain chromosome territories (located within the black region of the nucleus in diagram), such as Ch1, appeared to be repositioned by the mechanical stimulus, which would be likely to impact upon gene accessibility for transcription and the proximity to transcription factories.*

6.2.2 Contextual Interpretation of Mechanostimuli

In this thesis, microgrooved topography was used as a means to physically confine and align cells, and act as a non-invasive mechanostimulus by promoting cell elongation. The nature and context of the topographical stimulus is likely to be critical to the cellular response. Using rounded or star-shaped adhesive chemical patterns to confine mesenchymal stem cells, Kilian et al. were able to direct adipogenic differentiation in rounded shapes, and osteogenic differentiation in angular patterns (Kilian et al., 2010). The authors concluded that the formation of larger stress fibres with greater tensile strength in the angular moulds promoted osteoinduction, while the smaller adhesions produced in response to the circular shapes reduced cytoskeletal tension and predominantly led to adipogenesis. Together with effect of matrix elasticity on stem cell fate determination (Engler et al., 2006b), and the context-dependency of macrophage alignment to microgrooves (Wojciak-Stothard et al., 1995), this suggests that there is likely to be a threshold effect involved in the differential interpretation of mechanical stimuli, probably mediated through alterations in tension and biochemical signals transferred from focal adhesions to the nucleus.

It seems sensible that the propensity for direct mechanotransduction-mediated gene expression should be context dependent, given that different cell types occupy distinct niches with variant mechanical properties, and the cellular response to these cues will be critically important in directing fate or functionality. The induction of downstream molecular responses will probably be dependent on the magnitude and form of mechanical stimulus required to promote appropriate adaptations for the particular cell type and niche. Local differences in myosin II concentration appeared to correlate with contractility in relation to matrix elasticity (Engler et al., 2006b) and restriction of cell shape (Kilian et al., 2010) in stem cells. In vascular endothelial cells, lowered concentration of myosin II corresponded to a reduction in contractility and cellular branching that conferred directional persistence to the cellular movement (Fischer et al., 2009). On the grooved topography, tropomyosin I and -III transcripts were reduced (Chapter 3), which might contribute to the directional persistence that would most likely be enforced by topographical confinement. The use of apposite topographical stimuli should provide a useful means of guiding cellular responses, probably in part through modulation of focal adhesions, local myosin abundance and cytoskeletal contractility, to affect nuclear elements such as chromosomes.

6.2.3 Chromosomal Effects

Based on the microarray data (Chapter 3), Ch 1 emerged as a hotspot for gene down-regulation in cells on the microgrooved topography, with the fewest gene expression changes on Ch 18, and most up-regulated genes on Ch 19 (Chapter 4). Ch 1 appeared to have become repositioned from a central to a peripheral location in the nucleus, which was suggestive of a move from a more euchromatic site, likely to be enriched in transcription factories, to a more heterochromatic region (discussed in (Felsenfeld and Groudine, 2003)). The presence of an intact nuclear lamina appeared to be required for this repositioning, as the positional disparity in Ch1 localisation between fiborblasts on planar and microgrooved substrata seemed to have been almost completely abrogated in lamin A/C-depleted cells (Chapter 4). Interestingly, Meaburn et al (2007) noted that some chromosome territories in proliferating cells derived from patients with laminopathies occupied positions in the nucleus that more closely approximated their location in quiescent cells (Meaburn et al., 2007). This suggests that the altered forces on the nucleus under conditions of lamin depletion will most likely affect packaging of chromosomes within it, perhaps in part through effects on the tubular structures that might otherwise have contributed to maintaining the resting positions of chromosomes (Chapter 2).

The fewest transcript abundance changes occurred in transcripts encoded in genes on Ch 18, and consistently, this chromosome did not appear to be repositioned in response to the mechanostimulus. Although Ch 19 had the most up-regulated genes, it did not seem to be clearly relocated by the topography. This suggested that there could be a size threshold for mechanical relocation, which was consistent with previous work by Dalby et al (2007) suggesting a reduction in the magnitude of centromeric repositioning with decreasing chromosome size (examining Ch 3, 11 and 16) on a nanotopographical substrate (Dalby et al., 2007a). On Ch 1, the band positions of the differentially expressed genes were spread over a larger area of the chromosome, with a much more localised effect on Ch 19. This suggested that the principle mechanism stimulating differential gene expression could be distinct between the two chromosomes. Mechanical forces were likely to have had the major effect on Ch 1, probably by differences in the accessibility of genes for transcription. The large size of this chromosome, and its position in the nucleus probably make it more susceptible to the tensile forces from the cytoskeleton than the smaller chromosomes. On Ch 19, the band positioning and directionality of transcript-level effects were consistent with local effects, such as looping out of specific loci. This would not have been detectable using whole-chromosome FISH, but may have become

apparent using locus-specific probes. Consistent with this, there were transcript-level effects on chromatin remodeling machines, such as HMGA1 and HMGB1 (Chapter 3), and up-regulation of nucleophosmin at the protein level (Chapter 5), which has also been shown to possess chromatin remodelling activity (Swaminathan et al., 2005).

Nuclear actin could also have acted as a contractile intranuclear network to reposition chromosomal territories in response to the tensile forces experienced at the periphery of the cell. In response to serum starvation of human fibroblasts, chromosome territories could be relocated within 15 minutes, but this could be largely abrogated by inhibition of actin and the motor protein myosin 1β (Mehta et al., 2010). The authors noted that the use of a siRNA directed against myosin 1β could potentially also have depleted other myosins, due to sequence homology. Thus, the down-regulation of tropomyosin transcripts in cells on the topography could also have had effects on chromosome repositioning. Consistent with this, PAK and LIMK, upstream regulators of cofilin, were up-regulated at the transcript level (Chapter 3). Cofilin can facilitate the nuclear import of actin (Pendleton et al., 2003). Depending on the arrangement of actin in the nucleus, there may be a continuous mechanical network transferring stimuli along stress fibres leading from the extracellular environment into the nuclear actin assembly, as the lamina can bind both cytoplasmic and nuclear actin. The topographical mechanostimulus would probably act to directly reposition territories via tensile forces from the cytoskeleton, in conjunction with motor protein-mediated effects. It is possible that the location and conformation of nuclear actin (which may include oligomeric, G-actin or mixed forms, possibly forming a nuclear endoskeleton, as discussed in (Bettinger et al., 2004)) could contribute to the relative mechanosensitivity of different chromosomes and subnuclear sites.

Ch 1 has been shown to be repositioned from the mid-interior to the periphery of proliferating human dermal fibroblast nuclei to the periphery following serum starvation and induction of quiescence (Mehta et al., 2010), while Ch 19 remained in the same position in a central location. It is interesting to note that these positional effects mimic the chromosomal relocation observed in response to the microgrooved substrate. It is possible that the induction of an elongated morphology in cells on the topography could simulate some features of quiescence, if the mechanical constraints of intercellular contact in confluent cultures (including an elongated cell shape in fibroblasts) contribute to contact inhibition and associated quiescence. Mehta et al. commented that the relocation in response to serum starvation did not induce nuclear reshaping, but given that quiescence

was artificially induced by the removal of serum, rather than cell-cell interactions, there may be differences in the mechanism of repositioning. This seems particularly plausible since quiescence has previously been shown to be distinct between confluent cultures and subconfluent serum-starved cultures (Gos et al., 2005). Lateral confinement is likely to have stimulated movement of the chromosome territories in cells on the topography, in addition to acto-myosin interactions, particularly since nucleoli (Chapter 2) and chromosomes (Chapter 4) could be tightly confined by the microgrooves under certain conditions.

6.2.4 Molecular Mechanosignalling

Upon mechanostimulation, both mechanical and molecular mediators contribute to the mechanoresponse. Reduction in number and size of focal adhesions in cells on the grooves suggested that signaling cascades initiating from these mechanosensitive sites would have been altered (Chapter 2). In addition, the topography-induced cytoskeletal reorganisation would be likely to affect the availability of binding sites for cytoskeleton-interacting signaling proteins such as FAK, p130Cas and protein kinase B/Akt (Sawada and Sheetz, 2002b), and the functionality (del Rio et al., 2009; Sawada et al., 2006) or localisation (Zhao et al., 2007) of mechanoresponsive proteins. Many of these interactions were shown to involve the signalling protein Rho, which was up-regulated at the transcript level on the topography (Chapter 2), and can modulate the directional persistence of cell migration (discussed in (Petrie et al., 2009)). Up-regulation of transcripts for Rac and other mediators of Rac signalling suggested that the cells could be compensating for probable topography-mediated restrictions in the directionality of cell migration along the grooves (Chapter 3), as down-regulation of this signalling molecule is associated with persistent movement (Pankov et al., 2005). Cell migration was also highlighted by the up-regulation of galectin-1 (Chapter 5). Protein level up-regulation of annexin V, although not statistically significant, was suggestive of effects on mechanosensitive ion channels (Chapter 5). It is likely that stretch-activated mechanosensitive channels, including members of the TRPV family, would be a major class of molecular contributors to topography-induced mechanotransduction (discussed in (Yin and Kuebler, 2010)).

Up-regulation of transcripts encoding components of actin-mediated signalling (Chapter 3) and proteins involved in cytoskeletal organisation, including eEF1δ and actin filament capping protein, concurred with the observed changes in cytoskeletal organisation (Chapter 2). These factors potentially also contributed to alterations in nuclear actin to

facilitate chromosomal repositioning. Components of important growth factor pathways, including ERK 1/2 signalling, were up-regulated in response to the topography at the early time-point examined (Chapters 3, 5), and it is probable that differential expression in these pathways would have become more prominent with time. The 24 hour culture period was useful to minimise cell-cell interactions and assess the relatively early stage gene expression changes following the interaction of fibroblasts with the topography (following the completion of cell spreading), but would have been too late to examine the first cell responses during the initiation of spreading and initial detection of the topographical features. It is likely, however, that complete adaptation to the substrate (involving the induction of all the appropriate signalling responses) would require more time to become fully established. This seems particularly likely if the response was hierarchical, necessitating multiple interdependent signalling cascades. Later time-point data was not collected in ths study (an inherent difficulty with the application of any costly, non-dynamic (end-point) analytical techniques such as the microarray), but previous research by Dalby et al (2003b) indicated that there had been a reversal from the predominance of gene up-regulation after 24 hours of culture of fibroblasts on micron-scale grooves, to down-regulation after 5 days, which might be consistent with a 'wave' of induction that reached a peak at some time during the 5 day period.

Concurrent with the results of this study, Wnt signalling and ERK 1/2 signalling were modulated in response to substrate elastic modulus (Engler et al., 2006b) and nanotopographical stimuli (Biggs et al., 2009; Kantawong et al., 2009b). There appeared to be tight control over critical processes such as cell growth, by up-regulation of both positive and negative regulators (Chapters 3, 5), presumably to prevent runaway signalling that could lead to oncogenesis or other unwanted consequences. Also, the interaction between components of the transcriptional/translational machinery and the cytoskeleton could be another means of co-regulating these processes in response to mechanical stimulation. Some direct correlation was observed between the abundance of particular transcripts and proteins (Chapter 5), but the overlapping interactions between the gene transcripts and proteins were most apparent following IPA network analysis. One network integrated nodes from several important signalling pathways, including MAPK, ERK1/2 and PI3K signalling, with transcription factors, chromatin remodelling machines, galectin-1, annexin V and cell cycle-related components such as PCNA. This suggests that molecular crosstalk between different pathways may contribute to the integration of multiple effector responses to the mechanostimulus.

6.2.5 PCNA and Nucleophosmin

Nucleophosmin was consistently up-regulated in cells on the microgrooved substrate (Chapter 5), which may have been a mechanism to counteract the nucleolar elongation induced by the topography (Chapter 2). The siRNA-mediated knockdown of lamin B has been shown to increase the abundance of nucleophosmin using 2D electrophoresis, and the interaction between lamin B and nucleophosmin appears to be critical for the maintenance of nucleolar morphology (Martin et al., 2009). Similarly, PCNA, which ensures the procession of DNA replication and interacts with lamin B in discrete nuclear foci, was likely to be up-regulated in response to the structural reorganisation of lamin B (Chapters 2, 5). This was consistent with the differential expression of genes involved in DNA replication (Chapter 3). Interestingly, nucleophosmin can also associate with the nucleoskeleton (Karin et al., 1996), which could be another mechanism by which it is subject to direct mechanoregulation. *PCNA* expression can be co-regulated by nucleophosmin, which interacts with the transcriptional regulator Ying Yang 1 to increase transcription from the *PCNA* promoter (Weng and Yung, 2005), potentially using its capacity to displace histones to facilitate chromatin remodelling. The authors observed that depletion of nucleophosmin also reduced the abundance of PCNA. It seems probable that both of these proteins were subject to topography-induced mechanoregulation, given their associations with the nuclear lamina and nucleoli, both of which were architecturally altered by confinement on the microgrooved topography. A theoretical model for interactions between the lamina, PCNA, nucleophosmin and nucleoli is presented in Fig. 6-2, but additional research would be required to properly evaluate this model.

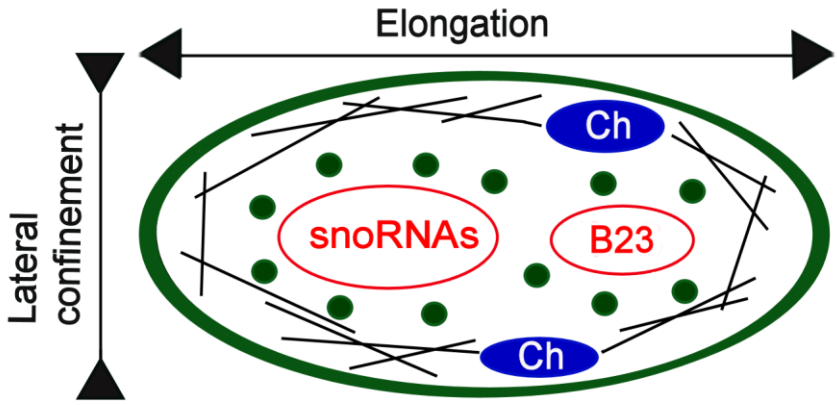

Figure 6-2. Model for interaction between the nuclear lamina, nucleoli and PCNA in cells on the microgrooved topography. *Nuclear reshaping by lateral confinement and tension-mediated horizontal elongation, in conjunction with mechanical lamin B repositioning (green), promotes relocation and elongation of nucleoli (red circles), up-regulation of nucleophosmin (B23) and potentially down-regulation of snoRNAs. Reorganisation of the nucleus and lamina could alter endoskeleton/nuclear actin assembly (black lines), contributing to acto-myosin mediated and direct mechanical repositioning of chromosomes such as Ch 1 (Ch), and altering gene accessibility and proximity to transcription factories. Nucleophosmin could participate in chromatin remodelling. Altered lamin B organisation could lead to compensatory up-regulation of PCNA (co-localised with lamin B; green circles), by increased translation or enhanced PCNA gene transcription, potentially via the nucleophosmin-YY1 interaction. Nucleolar reshaping could alter the production or transport of rRNA, particularly if mechanically mediated changes in lamin B tubule-like structures or nuclear pores altered nucleo-cytoplasmic transport of mRNA and rRNA.*

6.2.6 Small RNAs and Protein Production

Protein production appeared to be modulated at several levels by the topography. Structural nucleolar and lamin B effects were likely to affect production or rRNA and transport of both rRNA and mRNA (Chapter 2), particularly if the nuclear reshaping also had mechanical effects on nuclear pores. Down-regulation of a miRNA targeting proteins including tropomyosin for translational repression (Chapter 3), down-regulation of a number of small RNAs involved in RNA editing (Chapter 3), and up-regulation of proteins directly supporting the synthetic machinery and preventing protein degradation (Chapter 5) were also strongly suggestive of effects on protein abundance.

It is very interesting that multiple small RNAs (including snoRNAs, scaRNAs and a miRNA, *miR-21*) were markedly down-regulated in cells cultured on the microgrooved substrate. Such small RNA direct effectors had not previously been studied in the context of cell interactions with topography. It seems likely that modulation in snoRNA levels could be a response to the altered nucleolar morphology. Resultant modifications might have functional consequences for the translation of edited transcripts, potentially altering the stability or conformation of the target mRNAs. In addition, these small RNAs may also contribute to other processes, since the functions of many snoRNAs and scaRNAs are

not well understood, and the ADAR1 (adenosine deaminase acting on RNA) enzyme, which catalyses RNA editing via the deamination of adenosine to inosine, is involved in RNA editing for the regulation of haematopoetic stem cells (Hartner et al., 2009) and can negatively regulate RNA interference (Hong et al., 2005). A human snoRNA has also been shown to be processed to a miRNA-like ribonucleotide, which may target a chromatin remodelling protein (Ender et al., 2008). The authors also identified several other candidate snoRNAs with scope for conversion to miRNAs, and proposed that some snoRNA and scaRNAs with uncharacterised functions may primarily act as precursors to be processed into miRNAs. It is possible, therefore, that the down-regulation of the sno- and scaRNAs in cells on the microgrooved topography could be another mechanism to modulate gene expression, via changes in post-transcriptional gene silencing, similar to *miR-21*. Post-transcriptional and translational effects on protein regulation are logical targets in the context of mechanostimulation, since both are acting at the level of functional effectors. This is consistent with the promotion of faster response mechanisms at the early time-point examined, perhaps to maximise the initial adaptation to the altered conditions offered by the topography.

6.2.7 Future Research

In view of the structural changes resulting from the topographical mechanostimulus, future research investigating the potential for topography-induced relocation of organelles and ribosomes is likely to be fruitful. Time-lapse imaging of live cells at the interface between the grooved topography and a planar region would be useful to track real-time changes in nuclear and subnuclear architecture using fluorescently tagged proteins. It would be useful to investigate whether the ectopic over-expression of nucleophosmin could be be sufficient to restore nucleolar morphology to the arrangement observed in cells on the planar substrate, and the resultant effects on PCNA and DNA replication. Confirmation of the proteomic and transcriptomic data by additional means, such as Western blotting, antibody arrays or qPCR, would be advantageous. Further research into small RNAs in relation to topographical substrata (and biomaterials in general) has the potential to unveil a new wealth of biological knowledge about cellular interactions with structured substrata.

As there appears to be a mechanical association between the lamina and chromosome positioning, with a probable influence of chromosome size on the magnitude of effect, it would be interesting to examine the contribution of mechanotransductive

changes across additional chromosomes. The use of z-score statistical analysis would be a powerful means of assessing whether particular loci showed more up- or down-regulated genes than would be expected by chance. This approach could be informative about the mechanistic basis (predominantly mechanical alterations in gene accessibility, or local changes in the balance and abundance of transcription factors and components of the transcriptional machinery) of the differential gene expression on each chromosome, depending on the spatial organisation of the up- or down-regulated genes. The study of myosin, particularly acto-myosin interactions in the nucleus, could be informative about the mechanisms of chromosome repositioning on the topography. The use of locus-specific FISH probes would also permit higher resolution analysis of gene-level effects. Further investigation of the contribution of the nuclear lamina, by interference with other elements, such as lamin B and emerin, using siRNA would allow partial uncoupling of chromosomes from the receipt of direct mechanical signals from the nuclear lamina to elucidate additional mechanistic detail. In addition, given that the microgrooved topography appeared to promote tensile strain along the long axis of the cells, it would be beneficial to compare this substrate with other topographical substrata that should alter the internal tension within cells. Deeper microgrooves with the same pitch, for example, should promote increased cell elongation and potentially exaggerate the effects observed in this thesis, perhaps with greater subcellular reorganisation and a 'stronger' (higher magnitude of fold-change, or more rapidly induced) gene- and protein-level response. Conversely, substrata that act to reduce the tensile strain experienced by cells, such as low adhesion hexagonal array of nanopits (Dalby et al., 2007e), would be valuable as a means of contrasting the effects of the microgrooved topography with a substrate that reduces cell spreading and tensile force generated from focal adhesions.

It would also be interesting to examine different cell types in the context of the microgrooved topography and other topographical substrates, to compare the results obtained with fibroblasts. Osteoblasts would be a useful cell type to study, as these cells adopt a polygonal morphology and do not contact align to each other, unlike fibroblasts. This would provide a useful contrasting cell type, as the use of a common non-invasive mechanostimulus would enable any mechanotransductive differences underlying morphological and behavioural distinctions between the two cell types to be investigated in a consistent manner. Following this, it would be useful to probe the response of mesenchymal stem cells to the microgrooved substrate, to investigate whether the stem cells elected to follow a fibroblastic differentiation route, in response to the aligning cues provided by the substrate, or become committed to an alternative lineage. Increased

understanding of the physical cues required to promote stem cell fate decisions would be highly advantageous, particularly for clinical applications, and topography provides a useful platform to probe the mechanotransductive processes that underpin these changes.

6.3 Conclusions – Topography as a Mechanoinducive Stimulus

Topography is a valuable non-invasive stimulus for manipulating cell responses. In this study, culture of human fibroblasts on microgrooved topography induced effects at the chromosome (Chapter 4), small RNA (Chapter 3), mRNA (Chapter 3), protein (Chapter 5) and structural levels (Chapter 2), consistent with the model of multi-layered effects proposed in Chapter 1 (summarised and extended in Fig. 6-3).

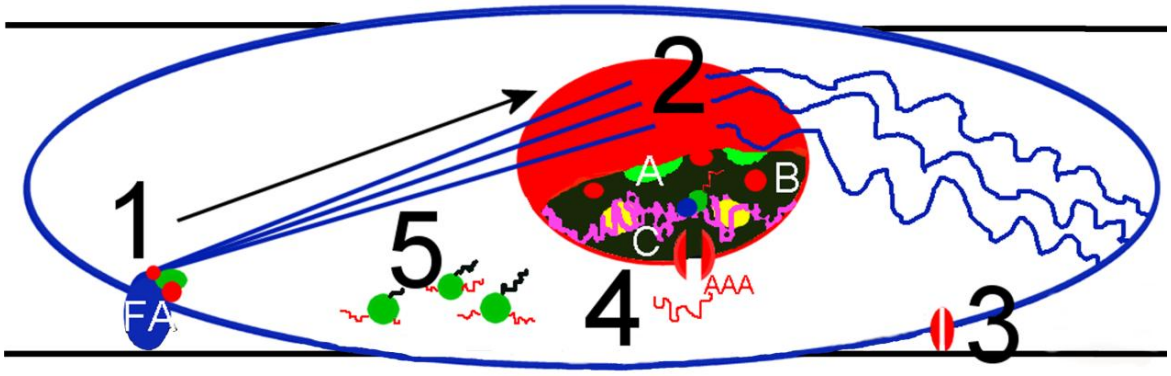

Figure 6-3. Microgrooved topography as a non-invasive mechanoinducer. *Microgrooved topography appeared to modulate focal adhesions (1), cytoskeletal (blue lines) and nucleoskeletal organisation (2), subnuclear components (A - nucleoli, B – lamin B), and gene accessibility or gene proximity to transcription factories (C - via chromosomal repositioning, alterations in chromatin remodelling machinery and differential transcript abundance). Nucleo-cytoplasmic transport and RNA trafficking (4) were likely to be perturbed, based on structural and microarray data, and downstream protein-level effects were observed (5), one of which suggested there may be effects on ion channels (3). Diagram reproduced with modification from McNamara et al. (in press).*

In this thesis, there was a significant challenge in obtaining sufficient biological material to perform molecular biological analysis of cells cultured on the topography. This was circumvented by development of strategies to harvest additional material (such as pooling and amplification), and maximise the data output from the samples generated, by combining high-coverage (transcriptomic) and high-sensitivity (DiGEsat) approaches. Further development of defined topographies that can be readily mass-produced, such as the ordered ‘honeycomb’ substrates fabricated using solvent casting by Wan et al. (Wan et al., 2009), could ease these restrictions, permitting larger culture areas and sample yields.

In addition, increased use of high data yield techniques, such as next generation sequencing (Mardis, 2008), and high-sensitivity approaches, including quantitative PCR with picogram quantities of input RNA (Lang et al., 2009) and μChIP (chromatin immunoprecipitation), a technique for the evaluation of protein interactions with binding sites in DNA in scarce samples (Dahl and Collas, 2008), should facilitate the wider application of molecular tools within the biomaterials community. Furthermore, on-chip microfluidic miniaturisation of processes such as FISH (Sieben et al., 2007) should reduce the quantity of reagents required, decrease the number of cells needed for analysis, and enhance automation, which would also make these techniques more accessible for biomaterials researchers.

The availability of multiple feature types for the non-destructive modulation of cellular architecture, gene expression and functionality should cement the application of topography as a versatile tool for fundamental biological research and translational studies. The use of microgrooved topography as a cue to promote cell guidance and elongation provided additional insight into the multifaceted molecular and structural events occurring following mechanostimulation. Increased understanding of the mechanotransduction underpinning cell-material interactions should facilitate the development of next-generation materials tailored to the direction of favourable cellular responses for research and regenerative medicine.

References

Abad, P.C., Lewis, J., Mian, I.S., Knowles, D.W., Sturgis, J., Badve, S., Xie, J., and Lelievre, S.A. (2007). NuMA influences higher order chromatin organization in human mammary epithelium. Mol Biol Cell *18*, 348-361.

Aebersold, R., and Mann, M. (2003). Mass spectrometry-based proteomics. Nature *422*, 198-207.

Affrossman, S., Henn, G., O'Neill, S.A., Pethrick, R.A., and Stamm, M. (1996). Surface topography and composition of deuterated polystyrene, poly(bromostyrene) blends. Macromolecules *29*, 5010-5016.

Alge, C.S., Priglinger, S.G., Kook, D., Schmid, H., Haritoglou, C., Welge-Lussen, U., and Kampik, A. (2006). Galectin-1 influences migration of retinal pigment epithelial cells. Invest Ophthalmol Vis Sci *47*, 415-426.

Amanchy, R., Kalume, D.E., and Pandey, A. (2005). Stable isotope labeling with amino acids in cell culture (SILAC) for studying dynamics of protein abundance and posttranslational modifications. Sci STKE, p12-.

Arnold, M., Cavalcanti-Adam, E.A., Glass, R., Blummel, J., Eck, W., Kantlehner, M., Kessler, H., and Spatz, J.P. (2004). Activation of integrin function by nanopatterned adhesive interfaces. ChemPhysChem *5*, 383-388.

Båvner, A., Matthews, J., Sanyal, S., Gustafsson, J., and Treuter, E. (2005). EID3 is a novel EID family member and an inhibitor of CBP-dependent co-activation. Nucleic Acids Res *33*, 3561-3569.

Belmont, A.S., Zhai, Y., and Thilenius, A. (1993). Lamin B distribution and association with peripheral chromatin revealed by optical sectioning and electron microscopy tomography. J Cell Biol *123*, 1671-1685.

Beningo, K.A., Dembo, M., Kaverina, I., Small, J.V., and Wang, Y.L. (2001). Nascent focal adhesions are responsible for the generation of strong propulsive forces in migrating fibroblasts. J Cell Biol *153*, 881-888.

Berry, C.C., Campbell, G., Spadiccino, A., Robertson, M., and Curtis, A.S.G.A.S.G. (2004). The influence of microscale topography on fibroblast attachment and motility. Biomaterials *25*, 5781-5788.

Bershadsky, A., Kozlov, M., and Geiger, B. (2006). Adhesion-mediated mechanosensitivity: a time to experiment, and a time to theorize. Current Opinion in Cell Biology *18*, 472-481.

Bettinger, B.T., Gilbert, D.M., and Amberg, D.C. (2004). Actin up in the nucleus. Nat Rev Mol Cell Biol *5*, 410-415.

Biggs, M.J.P., Richards, R.G., Gadegaard, N., Wilkinson, C.D.W., and Dalby, M.J. (2007). Regulation of implant surface cell adhesion: characterization and quantification of S-phase primary osteoblast adhesions on biomimetic nanoscale substrates. Journal of Orthopaedic Research *25*, 273-282.

Biggs, M.J.P., Richards, R.G., Gadegaard, N., Wilkinson, C.D.W., Oreffo, R.O.C., and Dalby, M.J. (2009). The use of nanoscale topography to modulate the dynamics of adhesion formation in primary osteoblasts and ERK/MAPK signalling in STRO-1+ enriched skeletal stem cells. Biomaterials *30*, 5094-5103.

Biggs, M.J.P., Richards, R.G., McFarlane, S., Wilkinson, C.D.W., Oreffo, R.O.C., and Dalby, M.J. (2008). Adhesion formation of primary human osteoblasts and the functional response of mesenchymal stem cells to 330 nm deep microgrooves. Journal of The Royal Society Interface *5*, 1231-1242.

Blumenfeld, R. (2006). Isostaticity and controlled force transmission in the cytoskeleton: a model awaiting experimental evidence. Biophysical Journal *91*, 1970-1983.

Bodas, D., and Khan-Malek, C. (2006). Formation of more stable hydrophilic surfaces of PDMS by plasma and chemical treatments. Microelectronic Engineering *83*, 1277-1279.

Boersema, P.J., Raijmakers, R., Lemeer, S., Mohammed, S., and Heck, A.J.R. (2009). Multiplex peptide stable isotope dimethyl labeling for quantitative proteomics. Nat Protocols *4*, 484-494.

Bohnsack, M.T., Stuven, T., Kuhn, C., Cordes, V.C., and Gorlich, D. (2006). A selective block of nuclear actin export stabilizes the giant nuclei of Xenopus oocytes. Nat Cell Biol *8*, 257-263.

Bolzer, A., Kreth, G., Solovei, I., Koehler, D., Saracoglu, K., Fauth, C., Muller, S., Eils, R., Cremer, C., Speicher, M.R., *et al.* (2005). Three-dimensional maps of all chromosomes in human male fibroblast nuclei and prometaphase rosettes. PLoS biology *3*.

Boyle, S., Gilchrist, S., Bridger, J.M., Mahy, N.L., Ellis, J.A., and Bickmore, W.A. (2001). The spatial organization of human chromosomes within the nuclei of normal and emerin-mutant cells. Hum Mol Genet *10*, 211-219.

Bridger, J.M., Kill, I.R., O'Farrell, M., and Hutchison, C.J. (1993). Internal lamin structures within G1 nuclei of human dermal fibroblasts. J Cell Sci *104*, 297-306.

Britland, S., Morgan, H., Wojiak-Stodart, B., Riehle, M., Curtis, A., and Wilkinson, C. (1996). Synergistic and hierarchical adhesive and topographic guidance of BHK cells. Exp Cell Res *228*, 313-325.

Broers, J.L., Machiels, B.M., van Eys, G.J., Kuijpers, H.J., Manders, E.M., van Driel, R., and Ramaekers, F.C. (1999). Dynamics of the nuclear lamina as monitored by GFP-tagged A-type lamins. J Cell Sci *112*, 3463-3475.

Broustas, C.G., Gokhale, P.C., Rahman, A., Dritschilo, A., Ahmad, I., and Kasid, U. (2004). BRCC2, a novel BH3-like domain-containing protein, induces apoptosis in a caspase-dependent manner. J Biol Chem *279*, 26780-26788.

Brunello, E., Reconditi, M., Elangovan, R., Linari, M., Sun, Y.B., Narayanan, T., Panine, P., Piazzesi, G., Irving, M., and Lombardi, V. (2007). Skeletal muscle resists stretch by rapid binding of the second motor domain of myosin to actin. Proc Natl Acad Sci U S A *104*, 20114-20119.

Camby, I., Belot, N., Lefranc, F., Sadeghi, N., de Launoit, Y., Kaltner, H., Musette, S., Darro, F., Danguy, A., Salmon, I., *et al.* (2002). Galectin-1 modulates human glioblastoma cell migration into the brain through modifications to the actin cytoskeleton and levels of expression of small GTPases. Journal of Neuropathology and Experimental Neurology *61*, 585-596.

Camby, I., Decaestecker, C., Lefranc, F., Kaltner, H., Gabius, H.-J., and Kiss, R. (2005). Galectin-1 knocking down in human U87 glioblastoma cells alters their gene expression pattern. Biochemical and Biophysical Research Communications *335*, 27-35.

Carrette, O., Burkhard, P.R., Sanchez, J.-C., and Hochstrasser, D.F. (2006). State-of-the-art two-dimensional gel electrophoresis: a key tool of proteomics research. Nat Protocols *1*, 812-823.

Chambeyron, S., Da Silva, N.R., Lawson, K.A., and Bickmore, W.A. (2005). Nuclear re-organisation of the Hoxb complex during mouse embryonic development. Development *132*, 2215-2223.

Charest, J.L., Eliason, M.T., GarcÌa, A.J., and King, W.P. (2006). Combined microscale mechanical topography and chemical patterns on polymer cell culture substrates. Biomaterials *27*, 2487-2494.

Chellaiah, M.A., Soga, N., Swanson, S., McAllister, S., Alvarez, U., Wang, D., Dowdy, S.F., and Hruska, K.A. (2000). Rho-A is critical for osteoclast podosome organization, motility and bone resorption. JBC *275*, 11993-12002.

Chen, C., Ridzon, D.A., Broomer, A.J., Zhou, Z., Lee, D.H., Nguyen, J.T., Barbisin, M., Xu, N.L., Mahuvakar, V.R., Andersen, M.R., *et al.* (2005). Real-time quantification of microRNAs by stem–loop RT–PCR. Nucleic Acids Research *33*, e179.

Chen, C.S., Mrksich, M., Huang, S., Whitesides, G.M., and Ingber, D.E. (1997). Geometric control of cell life and death. Science *276*, 1425-1428.

Chicurel, M.E., Singer, R.H., Meyer, C.J., and Ingber, D.E. (1998). Integrin binding and mechanical tension induce movement of mRNA and ribosomes to focal adhesions. Nature *392*, 730-733.

Chou, L., Firth, J.D., Uitto, V.J., and Brunette, D.M. (1995). Substratum surface topography alters cell shape and regulates fibronectin mRNA level, mRNA stability, secretion and assembly in human fibroblasts. J Cell Sci *108*, 1563-1573.

Chubb, J.R. (2009). Gene activation at the edge of the nucleus. Embo J *28*, 2145-2146.

Cichy, J., and Pure, E. (2003). The liberation of CD44. J Cell Biol *161*, 839-843.

Clark, P., Connolly, P., Curtis, A.S., Dow, J.A., and Wilkinson, C.D. (1987). Topographical control of cell behaviour. I. Simple step cues. Development *99*, 439-448.

Clark, P., Connolly, P., Curtis, A.S., Dow, J.A., and Wilkinson, C.D. (1990). Topographical control of cell behaviour: II. Multiple grooved substrata. Development *108*, 635-644.

Cremer, T., and Cremer, C. (2001). Chromosome territories, nuclear architecture and gene regulation in mammalian cells. Nat Rev Genet *2*, 292-301.

Crowe, D.L., and Brown, T.N. (1999). Transcriptional Inhibition of matrix metalloproteinase 9 (MMP-9) Activity by a c-fos/estrogen receptor fusion protein is mediated by the proximal AP-1 site of the MMP-9 promoter and correlates with reduced tumor cell invasion. Neoplasia *1* 368-371.

Curtis, A.S.G., Dalby, M.J., and Gadegaard, N. (2006). Nanoprinting onto cells. Journal of The Royal Society Interface *3*, 393-398.

Dahl, J.A., and Collas, P. (2008). A rapid micro chromatin immunoprecipitation assay (ChIP). Nat Protocols *3*, 1032-1045.

Dahl, K.N., Kahn, S.M., Wilson, K.L., and Discher, D.E. (2004). The nuclear envelope lamina network has elasticity and a compressibility limit suggestive of a molecular shock absorber. J Cell Sci *117*, 4779-4786.

Dalby, M., J. , Gadegaard, N., Herzyk, P., Sutherland, D., Agheli, H., Wilkinson, C., D. W., and Curtis, A., S. G. (2007a). Nanomechanotransduction and interphase nuclear organization influence on genomic control. J Cell Biochem *102*, 1234-1244.

Dalby, M.J., Berry, C.C., Riehle, M.O., Sutherland, D.S., Agheli, H., and Curtis, A.S.G. (2004a). Attempted endocytosis of nano-environment produced by colloidal lithography by human fibroblasts. Exp Cell Res *295*, 387-394.

Dalby, M.J., Biggs, M.J.P., Gadegaard, N., Kalna, G., Wilkinson, C.D.W., and Curtis, A.S.G. (2007b). Nanotopographical stimulation of mechanotransduction and changes in interphase centromere positioning. Journal of Cellular Biochemistry *100*, 326-338.

Dalby, M.J., Childs, S., Riehle, M.O., Johnstone, H.J.H., Affrossman, S., and Curtis, A.S.G. (2003a). Fibroblast reaction to island topography: changes in cytoskeleton and morphology with time. Biomaterials *24*, 927-935.

Dalby, M.J., Gadegaard, N., Herzyk, P., Agheli, H., Sutherland, D.S., and Wilkinson, C.D.W. (2007c). Group analysis of regulation of fibroblast genome on low-adhesion nanostructures. Biomaterials *28*, 1761-1769.

Dalby, M.J., Gadegaard, N., Riehle, M.O., Wilkinson, C.D.W., and Curtis, A.S.G. (2004b/c). Investigating filopodia sensing using arrays of defined nano-pits down to 35 nm diameter in size. Int J Biochem Cell Biol *36*, 2005-2015.

Dalby, M.J., Gadegaard, N., Tare, R., Andar, A., Riehle, M.O., Herzyk, P., Wilkinson, C.D.W., and Oreffo, R.O.C. (2007d). The control of human mesenchymal cell differentiation using nanoscale symmetry and disorder. Nat Mater *6*, 997-1003.

Dalby, M.J., Gadegaard, N., and Wilkinson, C.D.W. (2007e). The response of fibroblasts to hexagonal nanotopography fabricated by electron beam lithography. Journal of Biomedical Materials Research Part A *84A*, 973-979.

Dalby, M.J., Giannaras, D., Riehle, M.O., Gadegaard, N., Affrossman, S., and Curtis, A.S.G. (2004d). Rapid fibroblast adhesion to 27 nm high polymer demixed nano-topography. Biomaterials *25*, 77-83.

Dalby, M.J., Hart, A., and Yarwood, S.J. (2008). The effect of the RACK1 signalling protein on the regulation of cell adhesion and cell contact guidance on nanometric grooves. Biomaterials *29*, 282-289.

Dalby, M.J., Riehle, M.O., Johnstone, H., Affrossman, S., and Curtis, A.S.G. (2004e). Investigating the limits of filopodial sensing: a brief report using SEM to image the interaction between 10 nm high nano-topography and fibroblast filopodia. Cell Biol Int *28*, 229-236.

Dalby, M.J., Riehle, M.O., Sutherland, D.S., Agheli, H., and Curtis, A.S.G. (2004f). Fibroblast response to a controlled nanoenvironment produced by colloidal lithography. Journal of Biomedical Materials Research Part A *69A*, 314-322.

Dalby, M.J., Riehle, M.O., Sutherland, D.S., Agheli, H., and Curtis, A.S.G. (2004g). Use of nanotopography to study mechanotransduction in fibroblasts - methods and perspectives. Eur J Cell Biol *83*, 159-169.

Dalby, M.J., Riehle, M.O., Sutherland, D.S., Agheli, H., and Curtis, A.S.G. (2005a/b/c). Morphological and microarray analysis of human fibroblasts cultured on nanocolumns produced by colloidal lithography. Eur Cell Mater *9*, 1-8; discussion 8.

Dalby, M.J., Riehle, M.O., Yarwood, S.J., Wilkinson, C.D.W., and Curtis, A.S.G. (2003b/c). Nucleus alignment and cell signaling in fibroblasts: response to a micro-grooved topography. Exp Cell Res *284*, 274-282.

Dalby, M.J., Yarwood, S.J., Johnstone, H.J.H., Affrossman, S., and Riehle, M.O. (2002a). Fibroblast signaling events in response to nanotopography: a gene array study. IEEE Trans Nanobioscience *1*, 12-17.

Dalby, M.J., Yarwood, S.J., Riehle, M.O., Johnstone, H.J.H., Affrossman, S., and Curtis, A.S.G. (2002b). Increasing fibroblast response to materials using nanotopography: morphological and genetic measurements of cell response to 13-nm-high polymer demixed islands. Exp Cell Res *276*, 1-9.

Darzacq, X., Jady, B.E., Verheggen, C., Kiss, A.M., Bertrand, E., and Kiss, T. (2002). Cajal body-specific small nuclear RNAs: a novel class of 2[prime]-O-methylation and pseudouridylation guide RNAs. EMBO J *21*, 2746-2756.

Davidson, P., M. , Hayriye, O., Hasirci, V., Reiter, G., and Anselme, K. (2009). Microstructured surfaces cause severe but non-detrimental deformation of the cell nucleus. advanced materials *21*, 3586-3590.

Dayel, M.J., and Mullins, R.D. (2004). Activation of Arp2/3 Complex: Addition of the first subunit of the new filament by a WASP protein triggers rapid ATP hydrolysis on Arp2. PLoS Biology *2*, e91.

del Rio, A., Perez-Jimenez, R., Liu, R., Roca-Cusachs, P., Fernandez, J.M., and Sheetz, M.P. (2009). Stretching single talin rod molecules activates vinculin binding. Science *323*, 638-641.

Deligianni, D.D., Katsala, N., Ladas, S., Sotiropoulou, D., Amedee, J., and Missirlis, Y.F. (2001). Effect of surface roughness of the titanium alloy Ti-6Al-4V on human bone marrow cell response and on protein adsorption. Biomaterials *22*, 1241-1251.

Denis, F.d.r.A., Hanarp, P., Sutherland, D.S., and Dufreyne, Y.F. (2002). Fabrication of nanostructured polymer surfaces using colloidal lithography and spin-coating. Nano Letters *2*, 1419-1425.

DePasquale, J.A., and Izzard, C.E. (1991). Accumulation of talin in nodes at the edge of the lamellipodium and separate incorporation into adhesion plaques at focal contacts in fibroblasts. JCB *113*, 1351-1359.

Derhami, K., Zheng, J., Li, L., Wolfaardt, J.F., and Scott, P.G. (2001). Proteomic analysis of human skin fibroblasts grown on titanium: novel approach to study molecular biocompatibility. J Biomed Mater Res *56*, 234-244.

Ding, Y., Milosavljevic, T., and Alahari, S.K. (2008). Nischarin inhibits LIM kinase to regulate cofilin phosphorylation and cell invasion. Mol Cell Biol *28*, 3742-3756.

Dinnes, D.L., Marcal, H., Mahler, S.M., Santerre, J.P., and Labow, R.S. (2007). Material surfaces affect the protein expression patterns of human macrophages: A proteomics approach. Journal of biomedical materials research *80*, 895-908.

Disanza, A., Mantoani, S., Hertzog, M., Gerboth, S., Frittoli, E., Steffen, A., Berhoerster, K., Kreienkamp, H.-J., Milanesi, F., Fiore, P.P.D., *et al.* (2006). Regulation of cell shape by Cdc42 is mediated by the synergic actin-bundling activity of the Eps8-IRSp53 complex. Nat Cell Biol *8*, 1337-1347.

Doherty, M.K., Hammond, D.E., Clague, M.J., Gaskell, S.J., and Beynon, R.J. (2008). Turnover of the human proteome: determination of protein intracellular stability by dynamic SILAC. J Proteome Res *8*, 104-112.

Du, H., Gu, G., William, C.M., and Chalfie, M. (1996). Extracellular proteins needed for C. elegans mechanosensation. Neuron *16*, 183-194.

Edwards, D.C., Sanders, L.C., Bokoch, G.M., and Gill, G.N. (1999). Activation of LIM-kinase by Pak1 couples Rac/Cdc42 GTPase signalling to actin cytoskeletal dynamics. Nat Cell Biol *1*, 253-259.

Elad-Sfadia, G., Haklai, R., Ballan, E., Gabius, H.-J., and Kloog, Y. (2002). Galectin-1 augments Ras activation and diverts Ras signals to Raf-1 at the expense of phosphoinositide 3-kinase. Journal of Biological Chemistry *277*, 37169-37175.

Elsdale, T.R. (1968). Parallel orientation of fibroblasts in vitro. Exp Cell Res *51*, 439-450.

Ender, C., Krek, A., Friedlander, M.R., Beitzinger, M., Weinmann, L., Chen, W., Pfeffer, S., Rajewsky, N., and Meister, G. (2008). A human snoRNA with microRNA-like functions. *32*.

Engler, A.J., Sen, S., Sweeney, H.L., and Discher, D.E. (2006a/b). Matrix elasticity directs stem cell lineage specification. Cell *126*, 677-689.

Felsenfeld, G., and Groudine, M. (2003). Controlling the double helix. Nature *421*, 448-453.

Filipowicz, W., and Pogacic, V. (2002). Biogenesis of small nucleolar ribonucleoproteins. Current Opinion in Cell Biology *14*, 319-327.

Fischer, C., Sanchez-Ruderisch, H., Welzel, M., Wiedenmann, B., Sakai, T., Andre, S., Gabius, H.-J., Khachigian, L., Detjen, K.M., and Rosewicz, S. (2005). Galectin-1 interacts with the {alpha}5 {beta}1 fibronectin receptor to restrict carcinoma cell growth via induction of p21 and p27. Journal of Biological Chemistry *280*, 37266-37277.

Fischer, R.S., Gardel, M., Ma, X., Adelstein, R.S., and Waterman, C.M. (2009). Local cortical tension by myosin II guides 3D endothelial cell branching. Current Biology *19*, 260-265.

Fomproix, N., and Percipalle, P. (2004). An actin-myosin complex on actively transcribing genes. Exp Cell Res *294*, 140-148.

Formosa, F., Sanchez-Vaquero, V., Rodriguez-Navas, C., Munoz-Noval, A., Tejera-Sanchez, N., Manso Silvan, M., Garcia-Ruiz, J.P., and Marletta, G. (2010). Evaluation of plasma modified polycaprolactone honeycomb scaffolds by human mesenchymal stem cells cultured in vitamin D differentiation medium. Plasma Processes and Polymers *7*, 794-801.

Fricker, M., Hollinshead, M., White, N., and Vaux, D. (1997). Interphase nuclei of many mammalian cell types contain deep, dynamic, tubular membrane-bound invaginations of the nuclear envelope. J Cell Biol *136*, 531-544.

Friedland, J.C., Lee, M.H., and Boettiger, D. (2009). Mechanically activated integrin switch controls {alpha}5{beta}1 function. Science *323*, 642-644.

Gabriely, G., Wurdinger, T., Kesari, S., Esau, C.C., Burchard, J., Linsley, P.S., and Krichevsky, A.M. (2008). MicroRNA 21 promotes glioma invasion by targeting matrix metalloproteinase regulators. Mol Cell Biol *28*, 5369-5380.

Garcia, M., and Knight, M.M. (2010). Cyclic loading opens hemichannels to release ATP as part of a chondrocyte mechanotransduction pathway. Journal of Orthopaedic Research *28*, 510-515.

Geiger, B., Spatz, J.P., and Bershadsky, A.D. (2009). Environmental sensing through focal adhesions. Nat Rev Mol Cell Biol *10*, 21-33.

Geiger, R.C., Taylor, W., Glucksberg, M.R., and Dean, D.A. (2006). Cyclic stretch-induced reorganization of the cytoskeleton and its role in enhanced gene transfer. Gene Ther *13*, 725-731.

Gerashchenko, M.V., Chernoivanenko, I.S., Moldaver, M.V., and Minin, A.A. (2009). Dynein is a motor for nuclear rotation while vimentin IFs is a "brake". Cell Biol Int *33*, 1057-1064.

Gerecht, S., Bettinger, C.J., Zhang, Z., Borenstein, J.T., Vunjak-Novakovic, G., and Langer, R. (2007). The effect of actin disrupting agents on contact guidance of human embryonic stem cells. Biomaterials *28*, 4068-4077.

Goffin, J.M., Pittet, P., Csucs, G., Lussi, J.W., Meister, J.-J., and Hinz, B. (2006). Focal adhesion size controls tension-dependent recruitment of α-smooth muscle actin to stress fibers. JCB *172*, 259-268.

Gos, M., Miloszewska, J., Swoboda, P., Trembacz, H., Skierski, J., and Janik, P. (2005). Cellular quiescence induced by contact inhibition or serum withdrawal in C3H10T1/2 cells. Cell Proliferation *38*, 107-116.

Greengauz-Roberts, O., Stoppler, H., Nomura, S., Yamaguchi, H., Goldenring, J.R., Podolsky, R.H., Lee, J.R., and Dynan, W.S. (2005). Saturation labeling with cysteine-reactive cyanine fluorescent dyes provides increased sensitivity for protein expression profiling of laser-microdissected clinical specimens. Proteomics *5*, 1746-1757.

Gross, S.R., and Kinzy, T.G. (2005). Translation elongation factor 1A is essential for regulation of the actin cytoskeleton and cell morphology. Nat Struct Mol Biol *12*, 772-778.

Gross, S.R., and Kinzy, T.G. (2007). Improper organization of the actin cytoskeleton affects protein synthesis at initiation. Mol Cell Biol *27*, 1974-1989.

Guarda, A., Bolognese, F., Bonapace, I.M., and Badaracco, G. (2009). Interaction between the inner nuclear membrane lamin B receptor and the heterochromatic methyl binding protein, MeCP2. Exp Cell Res *315*, 1895-1903.

Hahne, P., Sechi, A., Benesch, S., and Small, J.V. (2001). Scar/WAVE is localised at the tips of protruding lamellipodia in living cells. FEBS Lett *492*, 215-220.

Haque, F., Lloyd, D.J., Smallwood, D.T., Dent, C.L., Shanahan, C.M., Fry, A.M., Trembath, R.C., and Shackleton, S. (2006). SUN1 interacts with nuclear lamin A and cytoplasmic nesprins to provide a physical connection between the nuclear lamina and the cytoskeleton. Mol Cell Biol *26*, 3738-3751.

Hartner, J.C., Walkley, C.R., Lu, J., and Orkin, S.H. (2009). ADAR1 is essential for the maintenance of hematopoiesis and suppression of interferon signaling. Nat Immunol *10*, 109-115.

Hegde, P.S., White, I.R., and Debouck, C. (2003). Interplay of transcriptomics and proteomics. Current Opinion in Biotechnology *14*, 647-651.

Hennekes, H., and Nigg, E.A. (1994). The role of isoprenylation in membrane attachment of nuclear lamins. A single point mutation prevents proteolytic cleavage of the lamin A precursor and confers membrane binding properties. J Cell Sci *107*, 1019-1029.

Hironori, Y., and Toshizumi, T. (2009). Cell micropatterning on an albumin-based substrate using an inkjet printing technique. Journal of Biomedical Materials Research Part A.

Hofmann, W.A., Stojiljkovic, L., Fuchsova, B., Vargas, G.M., Mavrommatis, E., Philimonenko, V., Kysela, K., Goodrich, J.A., Lessard, J.L., Hope, T.J., *et al.* (2004). Actin is part of pre-initiation complexes and is necessary for transcription by RNA polymerase II. Nat Cell Biol *6*, 1094-1101.

Hong, J., Qian, Z., Shen, S., Min, T., Tan, C., Xu, J., Zhao, Y., and Huang, W. (2005). High doses of siRNAs induce eri-1 and adar-1 gene expression and reduce the efficiency of RNA interference in the mouse. Biochem J *390*, 675-679.

Hsu, J.-L., Huang, S.-Y., Chow, N.-H., and Chen, S.-H. (2003). Stable-isotope dimethyl labeling for quantitative proteomics. Analytical Chemistry *75*, 6843-6852.

Hu, P., Wu, S., and Hernandez, N. (2004). A role for beta-actin in RNA polymerase III transcription. Genes & Development *18*, 3010-3015.

Huang, R., Jiang, W., Yang, J., Mao, Y.Q., Zhang, Y., Yang, W., Yang, D., Burkholder, B., Huang, R.F., and Huang, R.P. (2010). A biotin label-based antibody array for high-content profiling of protein expression. Cancer Genomics Proteomics *7*, 129-141.

Ingber, D.E. (2003a). Tensegrity I. Cell structure and hierarchical systems biology. J Cell Sci *116*, 1157-1173.

Ingber, D.E. (2003b). Tensegrity II. How structural networks influence cellular information processing networks. J Cell Sci *116*, 1397-1408.

Itano, N., Okamoto, S.-i., ZHang, D., Lipton, S.A., and Ruoslahti, E. (2003). Cell spreading controls endoplasmic and nuclear calcium: A physical gene regulation pathway from the cell surface to the nucleus. PNAs *100*, 5181-5186.

Ito, Y., Oike, Y., Yasunaga, K., Hamada, K., Miyata, K., Matsumoto, S., Sugano, S., Tanihara, H., Masuho, Y., and Suda, T. (2003). Inhibition of angiogenesis and vascular leakiness by angiopoietin-related protein 4. Cancer Res *63*, 6651-6657.

Jaalouk, D.E., and Lammerding, J. (2009). Mechanotransduction gone awry. Nat Rev Mol Cell Biol *10*, 63-73.

Jagatheesan, G., Thanumalayan, S., Muralikrishna, B., Rangaraj, N., Karande, A.A., and Parnaik, V.K. (1999). Colocalization of intranuclear lamin foci with RNA splicing factors. J Cell Sci *112 (Pt 24)*, 4651-4661.

Jakymiw, A., Lian, S., Eystathioy, T., Li, S., Satoh, M., Hamel, J.C., Fritzler, M.J., and Chan, E.K.L. (2005). Disruption of GW bodies impairs mammalian RNA interference. Nat Cell Biol *7*, 1267-1274.

Ji, J.Y., Lee, R.T., Vergnes, L., Fong, L.G., Stewart, C.L., Reue, K., Young, S.G., Zhang, Q., Shanahan, C.M., and Lammerding, J. (2007). Cell nuclei spin in the absence of lamin B1. Journal of Biological Chemistry *282*, 20015-20026.

Jopling, H.M., Odell, A.F., Hooper, N.M., Zachary, I.C., Walker, J.H., and Ponnambalam, S. (2009). Rab GTPase regulation of VEGFR2 trafficking and signaling in endothelial cells. Arterioscler Thromb Vasc Biol *29*, 1119-1124.

Kamphoven, J.H., de Ruiter, M.M., Winkel, L.P., Van den Hout, H.M., Bijman, J., De Zeeuw, C.I., Hoeve, H.L., Van Zanten, B.A., Van der Ploeg, A.T., and Reuser, A.J. (2004). Hearing loss in infantile Pompe's disease and determination of underlying pathology in the knockout mouse. Neurobiol Dis *16*, 14-20.

Kantawong, F. (2009). Use of comparative proteomics to study a novel osteogenic nanotopography. In Centre for Cell Engineering (Glasgow, University of Glasgow), pp. 156.

Kantawong, F., Burchmore, R., Gadegaard, N., Oreffo, R.O.C., and Dalby, M.J. (2008). Proteomic analysis of human osteoprogenitor response to disordered nanotopography. Journal of The Royal Society Interface.

Kantawong, F., Burchmore, R., Wilkinson, C.D.W., Oreffo, R.O.C., and Dalby, M.J. (2009a). Differential in-gel electrophoresis (DIGE) analysis of human bone marrow osteoprogenitor cell contact guidance. Acta Biomaterialia *5*, 1137-1146.

Kantawong, F., Burgess, K.E.V., Jayawardena, K., Hart, A., Burchmore, R.J., Gadegaard, N., Oreffo, R.O.C., and Dalby, M.J. (2009b). Whole proteome analysis of osteoprogenitor differentiation induced by disordered nanotopography and mediated by ERK signalling. Biomaterials *30*, 4723-4731.

Karcher, H., Lammerding, J., Huang, H., Lee, R.T., Kamm, R.D., and Kaazempur-Mofrad, M.R. (2003). A three-dimensional viscoelastic model for cell deformation with experimental verification. Biophysical Journal *85*, 3336-3349.

Karin, A.M., Bruno, M.H., Anton, O.M., Luitzen de, J., and Roel van, D. (1996). hnRNP proteins and B23 are the major proteins of the internal nuclear matrix of HeLa S3 cells. J Cell Biochem *62*, 275-289.

Karp, N.A., McCormick, P.S., Russell, M.R., and Lilley, K.S. (2007). Experimental and statistical considerations to avoid false conclusions in proteomics studies using differential in-gel electrophoresis. Mol Cell Proteomics *6*, 1354-1364.

Keller, C., and Krude, T. (2000). Requirement of Cyclin/Cdk2 and protein phosphatase 1 activity for chromatin assembly factor 1-dependent chromatin assembly during DNA synthesis. J Biol Chem *275*, 35512-35521.

Kilian, K.A., Bugarija, B., Lahn, B.T., and Mrksich, M. (2010). Geometric cues for directing the differentiation of mesenchymal stem cells. Proceedings of the National Academy of Sciences *107*, 4872-4877.

Kim, D.-H., Han, K., Gupta, K., Kwon, K.W., Suh, K.-Y., and Levchenko, A. (2009). Mechanosensitivity of fibroblast cell shape and movement to anisotropic substratum topography gradients. Biomaterials *30*, 5433-5444.

Kim, S., and Colulombe, P.A. (2010). Emerging role for the cytoskeleton as an organizer and regulator of translation. Nat Rev Mol Cell Biol *11*, 75-81.

Kim, S., Harris, M., and Varner, J.A. (2000). Regulation of integrin αvβ3-mediated endothelial cell migration and angiogenesis by integrin α5β1 and protein kinase A J Biol Chem *275*, 33920-33928.

Kiss, A.M., Jady, B.E., Bertrand, E., and Kiss, T. (2004). Human box H/ACA pseudouridylation guide RNA machinery. Mol Cell Biol *24*, 5797-5807.

Kivirikko, K.I., Myllyla, R., and Pihlajaniemi, T. (1989). Protein hydroxylation: prolyl 4-hydroxylase, an enzyme with four cosubstrates and a multifunctional subunit. FASEB J *3*, 1609-1617.

Koberna, K., Malinsky, J., Pliss, A., Masata, M., Vecerova, J., Fialova, M., Bednar, J., and Raska, I. (2002). Ribosomal genes in focus: new transcripts label the dense fibrillar components and form clusters indicative of "Christmas trees" in situ. J Cell Biol *157*, 743-748.

Koivunen, E., Gay, D., and Ruoslahti, E. (1993). Selection of peptides binding to the alpha 5 beta 1 integrin from phage display library. J Biol Chem *268*.

Kondo, T., and Hirohashi, S. (2007). Application of highly sensitive fluorescent dyes (CyDye DIGE Fluor saturation dyes) to laser microdissection and two-dimensional difference gel electrophoresis (2D-DIGE) for cancer proteomics. Nat Protocols *1*, 2940-2956.

Kondo, T., Seike, M., Mori, Y., Fujii, K., Yamada, T., and Hirohashi, S. (2003). Application of sensitive fluorescent dyes in linkage of laser microdissection and two-dimensional gel electrophoresis as a cancer proteomic study tool. Proteomics *3*, 1758-1766.

Kubista, H., Hawkins, T.E., Patel, D.R., Haigler, H.T., and Moss, S.E. (1999). Annexin 5 mediates a peroxide-induced Ca2+ influx in B cells. Current Biology *9*, 1403-1408.

Kumaran, R.I., Muralikrishna, B., and Parnaik, V.K. (2002). Lamin A/C speckles mediate spatial organization of splicing factor compartments and RNA polymerase II transcription. J Cell Biol *159*, 783-793.

Kunert-Keil, C., Bisping, F., Kruger, J., and Brinkmeier, H. (2006). Tissue-specific expression of TRP channel genes in the mouse and its variation in three different mouse strains. BMC Genomics *7*.

Kurpinski, K., Chu, J., Hashi, C., and Li, S. (2006). Anisotropic mechanosensing by mesenchymal stem cells. Proceedings of the National Academy of Sciences *103*, 16095-16100.

Lam, M.T., Clem, W.C., and Takayama, S. (2008). Reversible on-demand cell alignment using reconfigurable microtopography. Biomaterials *29*, 1705-1712.
Lammerding, J., Fong, L.G., Ji, J.Y., Reue, K., Stewart, C.L., Young, S.G., and Lee, R.T. (2006). Lamins A and C but not lamin B1 regulate nuclear mechanics. J Biol Chem *281*, 25768-25780.

Lammerding, J., Hsiao, J., Schulze, P.C., Kozlov, S., Stewart, C.L., and Lee, R.T. (2005). Abnormal nuclear shape and impaired mechanotransduction in emerin-deficient cells. J Cell Biol *170*, 781-791.

Lang, J.E., Magbanua, M.J.M., Scott, J.H., Makrigiorgos, G.M., Wang, G., Federman, S., Esserman, L.J., Park, J.W., and Haqq, C.M. (2009). A comparison of RNA amplification techniques at sub-nanogram input concentration. BMC Genomics *10*.

Lehnert, D., Wehrle-Haller, B., David, C., Weiland, U., Ballestrem, C., Imhof, B.A., and Bastmeyer, M. (2004). Cell behaviour on micropatterned substrata: limits of extracellular matrix geometry for spreading and adhesion. J Cell Sci *117*, 41-52.

Lelievre, S.A., Weaver, V.M., Nickerson, J.A., Larabell, C.A., Bhaumik, A., Petersen, O.W., and Bissell, M.J. (1998). Tissue phenotype depends on reciprocal interactions between the extracellular matrix and the structural organization of the nucleus. Proceedings of the National Academy of Sciences of the United States of America *95*, 14711-14716.

Li, S., Butler, P., Wang, Y., Hu, Y., Han, D.C., Usami, S., Guan, J.-L., and Chien, S. (2002). The role of the dynamics of focal adhesion kinase in the mechanotaxis of endothelial cells. Proceedings of the National Academy of Sciences of the United States of America *99*, 3546-3551.

Liang, F., Wu, J., Garami, M., and Gardner, D.G. (1997). Mechanical strain increases expression of the brain natriuretic peptide gene in rat cardiac myocytes. Journal of Biological Chemistry *272*, 28050-28056.

Liedert, A., Kaspar, D., Blakytny, R., Claes, L., and Ignatius, A. (2006). Signal transduction pathways involved in mechanotransduction in bone cells. Biochem Biophys Res Commun *349*, 1-5.

Lin, F., and Worman, H.J. (1993). Structural organization of the human gene encoding nuclear lamin A and nuclear lamin C. Journal of Biological Chemistry *268*, 16321-16326.

Liu, J., Rivas, F.V., Wohlschlegel, J., Yates, J.R., Parker, R., and Hannon, G.J. (2005a). A role for the P-body component GW182 in microRNA function. Nat Cell Biol *7*, 1261-1266.

Liu, J., Valencia-Sanchez, M.A., Hannon, G.J., and Parker, R. (2005b). MicroRNA-dependent localization of targeted mRNAs to mammalian P-bodies. Nat Cell Biol *7*, 719-723.

Lo, W.-S., Gamache, E.R., Henry, K.W., Yang, D., Pillus, L., and Berger, S.L. (2005). Histone H3 phosphorylation can promote TBP recruitment through distinct promoter-specific mechanisms. EMBO J *24*, 997-1008.

Loesberg, W.A., te Riet, J., van Delft, F.C.M.J.M., Schˆn, P., Figdor, C.G., Speller, S., van Loon, J.J.W.A., Walboomers, X.F., and Jansen, J.A. (2007). The threshold at which substrate nanogroove dimensions may influence fibroblast alignment and adhesion. Biomaterials *28*, 3944-3951.

Luderus, M.E., de Graaf, A., Mattia, E., den Blaauwen, J.L., Grande, M.A., de Jong, L., and van Driel, R. (1992). Binding of matrix attachment regions to lamin B1. Cell *70*, 949-959.

Lussi, J.W., Falconnet, D., Hubbell, J.A., Textor, M., and Csucs, G. (2006). Pattern stability under cell culture conditions--a comparative study of patterning methods based on PLL-g-PEG background passivation. Biomaterials *27*, 2534-2541.

Madou, M.J. (2002). Fundamentals of microfabrication: the science of miniaturization, Second Edition edn (Florida, USA, CRC Press).

Maggi, L.B., Jr., Kuchenruether, M., Dadey, D.Y.A., Schwope, R.M., Grisendi, S., Townsend, R.R., Pandolfi, P.P., and Weber, J.D. (2008). Nucleophosmin Serves as a Rate-Limiting Nuclear Export Chaperone for the Mammalian Ribosome. Mol Cell Biol *28*, 7050-7065.

Maingret, F., Fosset, M., Lesage, F., Lazdunski, M., and Honoré, E. (1999). TRAAK is a mammalian neuronal mechano-gated K+ channel. Journal of Biological Chemistry *274*, 1381-1387.

Malhas, A., Lee, C.F., Sanders, R., Saunders, N.J., and Vaux, D.J. (2007). Defects in lamin B1 expression or processing affect interphase chromosome position and gene expression. J Cell Biol *176*, 593-603.

Malmstrom, J., Christensen, B., Jakobsen, H.P., Lovmand, J., Foldbjerg, R., Sorensen, E.S., and Sutherland, D.S. (2010). Large area protein patterning reveals nanoscale control of focal adhesion development. Nano Letters *10*, 686-694.

Mammoto, A., Connor, K.M., Mammoto, T., Yung, C.W., Huh, D., Aderman, C.M., Mostoslavsky, G., Smith, L.E.H., and Ingber, D.E. (2009). A mechanosensitive transcriptional mechanism that controls angiogenesis. Nature *457*, 1103-1108.

Maniotis, A., Chen, C., and Ingber, D. (1997). Demonstration of mechanical connections between integrins, cytoskeletal filaments, and nucleoplasm that stabilize nuclear structure. Proceedings of the National Academy of Sciences of the United States of America *94*, 849-854.

Mardis, E.R. (2008). The impact of next-generation sequencing technology on genetics. Trends in Genetics *24*, 133-141.

Martin, C., Chen, S.B., Maya-Mendoza, A., Lovric, J., Sims, P.F.G., and Jackson, D.A. (2009). Lamin B1 maintains the functional plasticity of nucleoli. J Cell Sci *122*, 1551-1562.

Martinac, B. (2004). Mechanosensitive ion channels: molecules of mechanotransduction. Journal of Cell Sciencce *117*, 2449-2460.

Matarazzo, M.R., Boyle, S., D'Esposito, M., and Bickmore, W.A. (2007). Chromosome territory reorganization in a human disease with altered DNA methylation. PNAS *104*, 16546-16551.

Mazumder, A., and Shivashankar, G.V. (2010). Emergence of a prestressed eukaryotic nucleus during cellular differentiation and development. Journal of The Royal Society Interface *7*, S321-S330.

McNamara, L.E., McMurray, R.J., Biggs, M.J.P., Kantawong, F., Oreffo, R.O.C.O., and Dalby, M.J. (submitted). Nanotopographical control of stem cell differentiation.

McNamara, L.E., McMurray, R.J., Dalby, M.J., and Tsimbouri, P. (in press). Nanostructured surfaces and cell behaviour. In Comprehensive Biomaterials (Elsevier).

McNamara, L.E., Sjostrom, T., Su, B., and Dalby, M.J. (In preparation.). Characterising mesenchymal stem cell responses to titanium nanopillars for orthopaedic applications.

Meaburn, K.J., Cabuy, E., Bonne, G., Levy, N., Morris, G.E., Novelli, G., Kill, I.R., and Bridger, J.M. (2007). Primary laminopathy fibroblasts display altered genome organization and apoptosis. Aging Cell *6*, 139-153.

Mehta, I., Amira, M., Harvey, A., and Bridger, J. (2010). Rapid chromosome territory relocation by nuclear motor activity in response to serum removal in primary human fibroblasts. Genome Biology *11*, 1465-6905.

Melamed, D., Eliyahu, E., and Arav, Y. (2009). Exploring translation regulation by global analysis of ribosomal association. Methods *48*, 301-305.

Mirza, S.P., and Olivier, M. (2008). Methods and approaches for the comprehensive characterization and quantification of cellular proteomes using mass spectrometry. Physiol Genomics *33*, 3-11.

Moazed, D. (2009). Small RNAs in transcriptional gene silencing. Nature *457*, 413-420.
Moir, R.D., Montag-Lowy, M., and Goldman, R.D. (1994). Dynamic properties of nuclear lamins: lamin B is associated with sites of DNA replication. J Cell Biol *125*, 1201-1212.

Moir, R.D., Spann, T.P., Herrmann, H., and Goldman, R.D. (2000a). Disruption of nuclear lamin organization blocks the elongation phase of DNA replication. J Cell Biol *149*, 1179-1192.

Moir, R.D., Yoon, M., Khuon, S., and Goldman, R.D. (2000b). Nuclear lamins A and B1: different pathways of assembly during nuclear envelope formation in living cells. J Cell Biol *151*, 1155-1168.

Morey, C., Kress, C., and Bickmore, W.A. (2009). Lack of bystander activation shows that localization exterior to chromosome territories is not sufficient to up-regulate gene expression. Genome Res *19*, 1184-1194.

Muller, I., Boyle, S., Singer, R.H., Bickmore, W.A., and Chubb, J.R. (2010). Stable morphology, but dynamic internal reorganisation, of interphase human chromosomes in living cells. PLoS ONE *5*, e11560.

Multini, M. (2007). Topographical effects on chromosomal positioning. In Centre for Cell Engineering (Glasgow, University of Glasgow), pp. 34.

Muratani, M., and Tansey, W.P. (2003). How the ubiquitin-proteasome system controls transcription. Nat Rev Mol Cell Biol *4*, 192-201.

Murthy, K.S., Zhou, H., Grider, J.R., and Makhlouf, G.M. (2003). Inhibition of sustained smooth muscle contraction by PKA and PKG preferentially mediated by phosphorylation of RhoA. Am J Physiol Gastrointest Liver Physiol *284*, G1006-1016.

Mutskov, V. (2004). Silencing of transgene transcription precedes methylation of promoter DNA and histone H3 lysine 9. EMBO J *23*, 138-149.

Nagata, K., Duggan, A., Kumar, G., and Garcia-Anoveros, J. (2005). Nociceptor and hair cell transducer properties of TRPA1, a channel for pain and hearing. The Journal of Neuroscience *25*, 4052-4061.

Nakagawa, H., Miki, H., Nozumi, M., Takenawa, T., Miyamoto, S., Wehland, J., and Small, J.V. (2003). IRSp53 is colocalised with WAVE2 at the tips of protruding lamellipodia and filopodia independently of Mena. J Cell Sci *116*, 2577-2583.

Nomizu, M., Weeks, B.S., Weston, C.A., Kim, W.H., Kleinman, H.K., and Yamada, Y. (1995). Structure-activity study of a laminin alpha 1 chain active peptide segment Ile-Lys-Val-Ala-Val (IKVAV). FEBS Lett *365*, 227-231.

Oakley, C., and Brunette, D.M. (1993). The sequence of alignment of microtubules, focal contacts and actin filaments in fibroblasts spreading on smooth and grooved titanium substrata. J Cell Sci *106*, 343-354.

Oh, S., Brammer, K.S., Li, Y.S.J., Teng, D., Engler, A.J., Chien, S., and Jin, S. (2009). Stem cell fate dictated solely by altered nanotube dimension. Proceedings of the National Academy of Sciences *106*, 2130-2135.

Ondrej, V., Lukasova, E., Krejci, J., Matula, P., and Kozubek, S. (2008). Lamin A/C and polymeric actin in genome organisation. Mol Cells *26*, 356-361.

Ong, S.-E., Blagoev, B., Kratchmarova, I., Kristensen, D.B., Steen, H., Pandey, A., and Mann, M. (2002). Stable isotope labeling by amino acids in cell culture, SILAC, as a simple and accurate approach to expression proteomics. Molecular & Cellular Proteomics *1*, 376-386.

Osborne, C.S., Chakalova, L., Brown, K.E., Carter, D., Horton, A., Debrand, E., Goyenechea, B., Mitchell, J.A., Lopes, S., Reik, W., *et al.* (2004). Active genes dynamically colocalize to shared sites of ongoing transcription. Nat Genet *36*, 1065-1071.

Oyer, J.A., Chu, A., Brar, S., and Turker, M.S. (2009). Aberrant epigenetic silencing is triggered by a transient reduction in gene expression. PLoS ONE *4*, 1-11.

Pajerowski, J.D., Dahl, K.N., Zhong, F.L., Sammak, P.J., and Discher, D.E. (2007). Physical plasticity of the nucleus in stem cell differentiation. Proceedings of the National Academy of Sciences *104*, 15619-15624.

Pankov, R., Endo, Y., Even-Ram, S., Araki, M., Clark, K., Cukierman, E., Matsumoto, K., and Yamada, K.M. (2005). A Rac switch regulates random versus directionally persistent cell migration. J Cell Biol *170*, 793-802.

Papini, E., Satin, B., Bucci, C., Telford, J., Manetti, R., Rappuoli, R., Zerial, M., and Montecucco, C. (1997). The small GTP binding protein rab7 is essential for cellular vacuolation induced by Helicobacter pylori cytotoxin. EMBO J *16*, 15-24.

Park, S.A., Kim, I.A., Lee, Y.J., Shin, J.W., Kim, C.-R., Kim, J.K., Yang, Y.-I., and Shin, J.-W. (2006). Biological responses of ligament fibroblasts and gene expression profiling on micropatterned silicone substrates subjected to mechanical stimuli. The Society for Biotechnology, Japan *102*, 402-412.

Pendleton, A., Pope, B., Weeds, A., and Koffer, A. (2003). Latrunculin B or ATP depletion induces cofilin-dependent translocation of actin into nuclei of mast cells. Journal of Biological Chemistry *278*, 14394-14400.

Petrie, R.J., Doyle, A.D., and Yamada, K.M. (2009). Random versus directionally persistent cell migration. Nat Rev Mol Cell Biol *10*, 538-549.

Pichler, A., and Melchior, F. (2002). Ubiquitin-related modifier SUMO1 and nucleocytoplasmic transport. Traffic *3*, 381-387.

Pittman, Y.R., Kandl, K., Lewis, M., Valente, L., and Kinzy, T.G. (2009). Coordination of eukaryotic translation elongation factor 1A (eEF1A) function in actin organization and translation elongation by the guanine nucleotide exchange factor eEF1BŒ±. Journal of Biological Chemistry *284*, 4739-4747.

Pontoglio, M., Pausa, M., Doyen, A., Viollet, B., Yaniv, M., and Tedesco, F. (2001). Hepatocyte nuclear factor 1alpha controls the expression of terminal complement genes. J Exp Med *194*, 1683-1689.

Ramsey, S.A., Knijnenburg, T.A., Kennedy, K.A., Zak, D.E., Gilchrist, M., Gold, E.S., Johnson, C.D., Lampano, A.E., Litvak, V., Navarro, G., *et al.* (2010). Genome-wide histone acetylation data improve prediction of mammalian transcription factor binding sites. Bioinformatics *26*, 2071-2075.

Ranade, S.V., Richard, R.E., and Helmus, M.N. (2005). Styrenic block copolymers for biomaterial and drug delivery applications. Acta Biomaterialia *1*, 137-144.

Reddy, K.L., Zullo, J.M., Bertolino, E., and Singh, H. (2008). Transcriptional repression mediated by repositioning of genes to the nuclear lamina. Nature *452*, 243-247.

Reid, T., Bathoorn, A., Ahmadian, M., and Collard, J. (1999). Identification and characterization of hPEM-2, a guanine nucleotide exchange factor specific for Cdc42. J Biol Chem *247*, 33587-33593.

Reyes-Reyes, M., Mora, N., Zentella, A., and Rosales, C. (2001). Phosphatidylinositol 3-kinase mediates integrin-dependent NF-kB and MAPK activation through separate signaling pathways. J Cell Sci *114*, 1579-1589.

Rid, R., Schiefermeier, N., Grigoriev, I., Small, J.V., and Kaverina, I. (2005). The last but not the least: the origin and significance of trailing adhesions in fibroblastic cells. Cell Motil Cytoskeleton *61*, 161-171.

Riveline, D., Zamir, E., Balaban, N.Q., Schwarz, U.S., Ishizaki, T., Narumiya, S., Kam, Z., Geiger, B., and Bershadsky, A.D. (2001). Focal contacts as mechanosensors: externally applied local mechanical force induces growth of focal contacts by an mDia1-dependent and ROCK-independent mechanism. J Cell Biol *153*, 1175-1186.

Robledo, S., Idol, R.A., Crimmins, D.L., Ladenson, J.H., Mason, P.J., and Bessler, M. (2008). The role of human ribosomal proteins in the maturation of rRNA and ribosome production. RNA *14*, 1918-1929.

Ruxton, G.D. (2006). The unequal variance t-test is an underused alternative to Student's t-test and the Mann-Whitney U test. Behav Ecol *17*, 688-690.

Sasseville, A.M., and Raymond, Y. (1995). Lamin A precursor is localized to intranuclear foci. J Cell Sci *108*, 273-285.

Sato, H., Ogata, H., and De Luca, L.M. (2000). Annexin V inhibits the 12-O-tetradecanoylphorbol-13-acetate-induced activation of Ras/extracellular signal-regulated kinase (ERK) signaling pathway upstream of Shc in MCF-7 cells. Oncogene *19*, 2904-2912.

Sato, Y., Harada, K., Itatsu, K., Ikeda, H., Kakuda, Y., Shimomura, S., Shan Ren, X., Yoneda, N., Sasaki, M., and Nakanuma, Y. (2010). Epithelial-mesenchymal transition induced by transforming growth factor-{beta}1/snail activation aggravates invasive growth of cholangiocarcinoma. Am J Pathol *177*, 141-152.

Sawada, Y., and Sheetz, M.P. (2002a). Force transduction by Triton cytoskeletons. The Journal of Cell Biology *156*, 609-615.

Sawada, Y., and Sheetz, M.P. (2002b). Force transduction by Triton cytoskeletons. J Cell Biol *156*, 609-615.

Sawada, Y., Tamada, M., Dubin-Thaler, B.J., Cherniavskaya, O., Sakai, R., Tanaka, S., and Sheetz, M.P. (2006). Force sensing by mechanical extension of the Src family kinase substrate p130Cas. Cell *127*, 1015-1026.

Schelle, H. (1959). The analysis of variance (New York, Wiley).

Schwanhusser, B., Gossen, M., Dittmar, G., and Selbach, M. (2009). Global analysis of cellular protein translation by pulsed SILAC. Proteomics *9*, 205-209.

Sen, G.L., and Blau, H.M. (2005). Argonaute 2/RISC resides in sites of mammalian mRNA decay known as cytoplasmic bodies. Nat Cell Biol *7*, 633-636.

Shadpour, H., and Allbritton, N.L. (2010). In situ roughening of polymeric microstructures. ACS Appl Mater Interfaces *2*, 1086-1093.

Shiio, Y., and Eisenman, R.N. (2003). Histone sumoylation is associated with transcriptional repression. Proceedings of the National Academy of Sciences of the United States of America *100*, 13225-13230.

Shilatifard, A. (2006). Chromatin modifications by methylation and ubiquination: implications in the regulation of gene expression. Ann Rev Biochem *75*, 243-269.

Sieben, V.J., Debes-Marun, C.S., Pilarski, P.M., Kaigala, G.V., Pilarski, L.M., and Backhouse, C. (2007). FISH and chips: chromosomal analysis on microfluidic platforms. IET Nanobiotechnology *1*, 27-35.

Sillekens, P.T., Beijer, R.P., Habets, W.J., and van Verooij, W.J. (1989). Molecular cloning of the cDNA for the human U2 snRNA-specific A' protein. Nucleic Acids Res *17*, 1893-1906.

Sitek, B., Luttges, J., Marcus, K., Kloppel, G., Schmiegel, W., Meyer, H.E., Hahn, S.A., and Stuhler, K. (2005). Application of fluorescence difference gel electrophoresis saturation labelling for the analysis of microdissected precursor lesions of pancreatic ductal adenocarcinoma. Proteomics *5*, 2665-2679.

Sjostrom, T., Dalby, M.J., Hart, A., Tare, R., Oreffo, R.O.C., and Su, B. (2009). Fabrication of pillar-like titania nanostructures on titanium and their interactions with human skeletal stem cells. Acta Biomaterialia *5*, 1433-1441.

Smith, M.L., Gourdon, D., Little, W.C., Kubow, K.E., Eguiluz, R.A., Luna-Morris, S., and Vogel, V. (2007). Force-induced unfolding of fibronectin in the extracellular matrix of living cells. PLoS biology *5*, e268.

Solovei, I., Kreysing, M., Lanctot, C., Kasem, S., Peichl, L., Cremer, T., Guck, J., and Joffe, B. (2009). Nuclear architecture of rod photoreceptor cells adapts to vision in mammalian evolution. *137*, 356-368.

Swaminathan, V., Kishore, A.H., Febitha, K.K., and Kundu, T.K. (2005). Human histone chaperone nucleophosmin enhances acetylation-dependent chromatin transcription. Mol Cell Biol *25*, 7534-7545.

Tang, C.W., Maya-Mendoza, A., Martin, C., Zeng, K., Chen, S., Feret, D., Wilson, S.A., and Jackson, D.A. (2008). The integrity of a lamin-B1-dependent nucleoskeleton is a fundamental determinant of RNA synthesis in human cells. J Cell Sci *121*, 1014-1024.

Thakar, R.G., Cheng, Q., Patel, S., Chu, J., Nasir, M., Liepmann, D., Komvopoulos, K., and Li, S. (2009). Cell-shape regulation of smooth muscle cell proliferation. Biophysical Journal *96*, 3423-3432.

Thibault, M.M., Hoemann, C.D., and Buschmann, M.D. (2007). Fibronectin, vitronectin, and collagen I induce chemotaxis and haptotaxis of human and rabbit mesenchymal stem cells in a standardized transmembrane assay. Stem Cells Dev *16*, 489-502.
Trinkle-Mulcahy, L., Ajuh, P., Prescott, A., Claverie-Martin, F., Cohen, S., Lamond, A.I., and Cohen, P. (1999). Nuclear organisation of NIPP1, a regulatory subunit of protein phosphatase 1 that associates with pre-mRNA splicing factors. J Cell Sci *112*, 157-168.

Ueda, T., Watanabe-Fukunaga, R., Fukuyama, H., Nagata, S., and Fukunaga, R. (2004). Mnk2 and Mnk1 are essential for constitutive and inducible phosphorylation of eukaryotic initiation factor 4E but not for cell growth or development. Mol Cell Biol *24*, 6539-6549

Ueno, T., Yamada, M., Suzuki, T., Minamikawa, H., Sato, N., Hori, N., Takeuchi, K., Hattori, M., and Ogawa, T. (2010). Enhancement of bone-titanium integration profile with UV-photofunctionalized titanium in a gap healing model. Biomaterials *31*, 1546-1557.

Unlu, M., Morgan, M., E. , Minden, M., Mary, E. , and Minden, J.S. (1997). Difference gel electrophoresis. A single gel method for detecting changes in protein extracts. Electrophoresis *18*, 2071-2077.

Uttayarat, P., Toworfe, G.K., Dietrich, F., Lelkes, P.I., and Composto, R.J. (2005). Topographic guidance of endothelial cells on silicone surfaces with micro- to nanogrooves: Orientation of actin filaments and focal adhesions. Journal of Biomedical Materials Research Part A *75A*, 668-680.

van der Sluisa, M., Vincentc, A., Boumaa, J., Korteland-Van Malea, A., van Goudoevera, J.B., Renesa, I.B., and Van Seuningen, I. (2008). Forkhead box transcription factors Foxa1 and Foxa2 are important regulators of Muc2 mucin expression in intestinal epithelial cells Biochem Biophys Res Commun *369*, 1108-1113.

Vandermoere, F., Yazidi-Belkoura, I.E., Demont, Y., Slomianny, C., Antol, J., Lemoine, J., and Hondermarck, H. (2007). Proteomics exploration reveals that actin is a signaling target of the kinase Akt. Molecular & Cellular Proteomics *6*, 114-124.

Vaughan, O.A., Alvarez-Reyes, M., Bridger, J.M., Broers, J.L.V., Ramaekers, F.C.S., Wehnert, M., Morris, G.E., Whitfield, W.G.F., and Hutchison, C.J. (2001). Both emerin and lamin C depend on lamin A for localization at the nuclear envelope. J Cell Sci *114*, 2577-2590.

Verheggen, C., Lafontaine, D., Samarsky, D., Mouaikel, J., Blanchard, J., Bordonné, R., and Bertrand, E. (2002). Mammalian and yeast U3 snoRNPs are matured in specific and related nuclear compartments. EMBO J *21*, 2736-2745.

Verheggen, C., Mouaikel, J., Thiry, M., Blanchard, J.-M., Tollervey, D., Bordonne, R., Lafontaine, D.L.J., and Bertrand, E. (2001). Box C/D small nucleolar RNA trafficking involves small nucleolar RNP proteins, nucleolar factors and a novel nuclear domain. EMBO J *20*, 5480-5490.

Vieu, C., Carcenac, F., PÈpin, A., Chen, Y., Mejias, M., Lebib, A., Manin-Ferlazzo, L., Couraud, L., and Launois, H. (2000). Electron beam lithography: resolution limits and applications. Applied Surface Science *164*, 111-117.

Vogel, V., and Sheetz, M. (2006). Local force and geometry sensing regulate cell functions. Nat Rev Mol Cell Biol *7*, 265-275.

von Philipsborn, A.C., Lang, S., Bernard, A., Loeschinger, J., David, C., Lehnert, D., Bastmeyer, M., and Bonhoeffer, F. (2006). Microcontact printing of axon guidance molecules for generation of graded patterns. Nat Protocols *1*, 1322-1328.

Vyakarnam, A., Dagher, S.F., Wang, J.L., and Patterson, R.J. (1997). Evidence for a role for galectin-1 in pre-mRNA splicing. Mol Cell Biol *17*, 4730-4737.

Walboomers, X.F., Croes, H.J.E., Ginsel, L.A., and Jansen, J.A. (1998). Growth behavior of fibroblasts on microgrooved polystyrene. Biomaterials *19*, 1861-1868.

Wan, L., Ke, B., Li, X., Meng, X., Zhang, L., and Xu, Z. (2009). Honeycomb-patterned films of polystyrene/poly(ethylene glycol): preparation, surface aggregation and protein adsorption. Science in China Series B: Chemistry *52*, 969-974.

Wang, N., Naruse, K., Stamenovic, D., Fredberg, J.J., Mijailovich, S.M., Tolic-Norrelykke, I.M., Polte, T., Mannix, R., and Ingber, D.E. (2001). Mechanical behavior in living cells consistent with the tensegrity model. Proceedings of the National Academy of Sciences of the United States of America *98*, 7765-7770.

Wang, N., Tytell, J.D., and Ingber, D.E. (2009). Mechanotransduction at a distance: mechanically coupling the extracellular matrix with the nucleus. Nat Rev Mol Cell Biol *10*, 75-82.

Wang, W., Park, J.W., Wang, J.L., and Patterson, R.J. (2006). Immunoprecipitation of spliceosomal RNAs by antisera to galectin-1 and galectin-3. Nucl Acids Res, gkl673.

Wear, M.A., Yamashita, A., Kim, K., MaÈda, Y., and Cooper, J.A. (2003). How capping protein binds the barbed end of the actin filament. Current Biology *13*, 1531-1537.

Wegener, K., and Campbell, I. (2008). Transmembrane and cytoplasmic domains in integrin activation and protein-protein interactions (review). Mol Membr Biol *25*, 376-387.

Weng, J.J., and Yung, B.Y.M. (2005). Nucleophosmin/B23 regulates PCNA promoter through YY1. Biochemical and Biophysical Research Communications *335*, 826-831.

West, A.G., and Fraser, P. (2005). Remote control of gene transcription. Hum Mol Genet *14*, R101-111.

Wiese, S., Reidegeld, K.A., Meyer, H.E., and Warscheid, B. (2007). Protein labeling by iTRAQ: A new tool for quantitative mass spectrometry in proteome research. Proteomics *7*, 340-350.

Wojciak-Stothard, B., Madeja, Z., Korohoda, W., Curtis, A., and Wilkinson, C. (1995). Activation of macrophage-like cells by multiple grooved substrata. Topographical control of cell behaviour. Cell Biol Int *19*, 485-490.

Wojcik, C. (2002). Regulation of apoptosis by the ubiquitin and proteasome pathway. J Cell Mol Med *6*, 25-48.

Wood, M.A., Bagnaninchi, P., and Dalby, M.J. (2008). The [beta] integrins and cytoskeletal nanoimprinting. Exp Cell Res *314*, 927-935.

Wozniak, M.A., and Chen, C.S. (2009). Mechanotransduction in development: a growing role for contractility. Nat Rev Mol Cell Biol *10*, 34-43.

Wright, J.E., Yurasek, G.K., Chen, Y.N., and Rosowsky, A. (2003). Further studies on the interaction of nonpolyglutamatable aminopterin analogs with dihydrofolate reductase and the reduced folate carrier as determinants of in vitro antitumor activity. Biochem Pharmacol *65*, 1427-1433.

Wu, L., Fan, J., and Belasco, J.G. (2006). From the cover: MicroRNAs direct rapid deadenylation of mRNA. Proceedings of the National Academy of Sciences *103*, 4034-4039.

Wu, W., Wang, G., Baek, S.J., and Shen, R. (2005). Comparative study of three proteomic quantitative methods, DIGE, cICAT, and iTRAQ, Using 2D Gel- or LC-MALDI TOF/TOF. J Proteome Res *5*, 651-658.

Xu, J., Khor, K.A., Sui, J., Zhang, J., Lin, T., Wei, T., and Chen, N. (2008). Comparative proteomics profile of osteoblasts cultured on dissimilar hydroxyapatite biomaterials: An iTRAQ-coupled 2-D LC-MS/MS analysis. Proteomics *8*, 4249-4258.

Yang, L., Sheldon, B.W., and Webster, T.J. (2009). The impact of diamond nanocrystallinity on osteoblast functions. Biomaterials *30*, 3458-3465.

Yarwood, S.J., and Woodgett, J.R. (2001). Extracellular matrix composition determines the transcriptional response to epidermal growth factor receptor activation. Proc Natl Acad Sci U S A *98*, 4472-4477.

Yin, J., and Kuebler, W. (2010). Mechanotransduction by TRP channels: general concepts and specific role in the vasculature. Cell Biochemistry and Biophysics *56*.

Yu, Y., Maggi, L., Brady, S., Apicelli, A., Dai, M., Lu, H., and Weber, J. (2006a/b). Nucleophosmin is essential for ribosomal protein L5 nuclear export. Mol Cell Biol *26*, 3798-3809.

Yun, C., Wang, Y., Mukhopadhyay, D., Backlund, P., Kolli, N., Yergey, A., Wilkinson, K.D., and Dasso, M. (2008). Nucleolar protein B23/nucleophosmin regulates the vertebrate SUMO pathway through SENP3 and SENP5 proteases. J Cell Biol *183*, 589-595.

Zhang, Y., and Reinberg, D. (2001). Transcription regulation by histone methylation: interplay between different covalent modifications of the core histone tails. Genes & Development *15*, 2343-2360.

Zhao, X.-H., Laschinger, C., Arora, P., Szaszi, K., Kapus, A., and McCulloch, C.A. (2007). Force activates smooth muscle {alpha}-actin promoter activity through the Rho signaling pathway. J Cell Sci *120*, 1801-1809.

Zhou, G., Li, H., DeCamp, D., Chen, S., Shu, H., Gong, Y., Flaig, M., Gillespie, J.W., Hu, N., Taylor, P.R., *et al.* (2002). 2D differential in-gel electrophoresis for the identification of esophageal scans cell cancer-specific protein markers. Mol Cell Proteomics *1*, 117-123.

Zhu, S., Si, M.-L., Wu, H., and Mo, Y.-Y. (2007a/b). MicroRNA-21 targets the tumor suppressor gene tropomyosin 1 (TPM1). Journal of Biological Chemistry *282*, 14328-14336.

Zhu, S., Wu, H., Wu, F., Nie, D., Sheng, S., and Mo, Y.-Y. (2008). MicroRNA-21 targets tumor suppressor genes in invasion and metastasis. Cell Res *18*, 350-359.

Zhu, W., Smith, J.W., and Huang, C.-M. (2010). Mass spectrometry-based label-free quantitative proteomics. Journal of Biomedicine and Biotechnology *2010*.

Ziegler, N., Alonso, A., Steinberg, T., Woodnutt, D., Kohl, A., Mussig, E., Schulz, S., and Tomakidi, P. (2010). Mechano-transduction in periodontal ligament cells identifies activated states of MAP-kinases p42/44 and p38-stress kinase as a mechanism for MMP-13 expression. BMC Cell Biol *11*.

Zinner, R., Teller, K., Versteeg, R., Cremer, T., and Cremer, M. (2007). Biochemistry meets nuclear architecture: Multicolor immuno-FISH for co-localization analysis of chromosome segments and differentially expressed gene loci with various histone methylations. Advances in Enzyme Regulation *47*, 223-241.